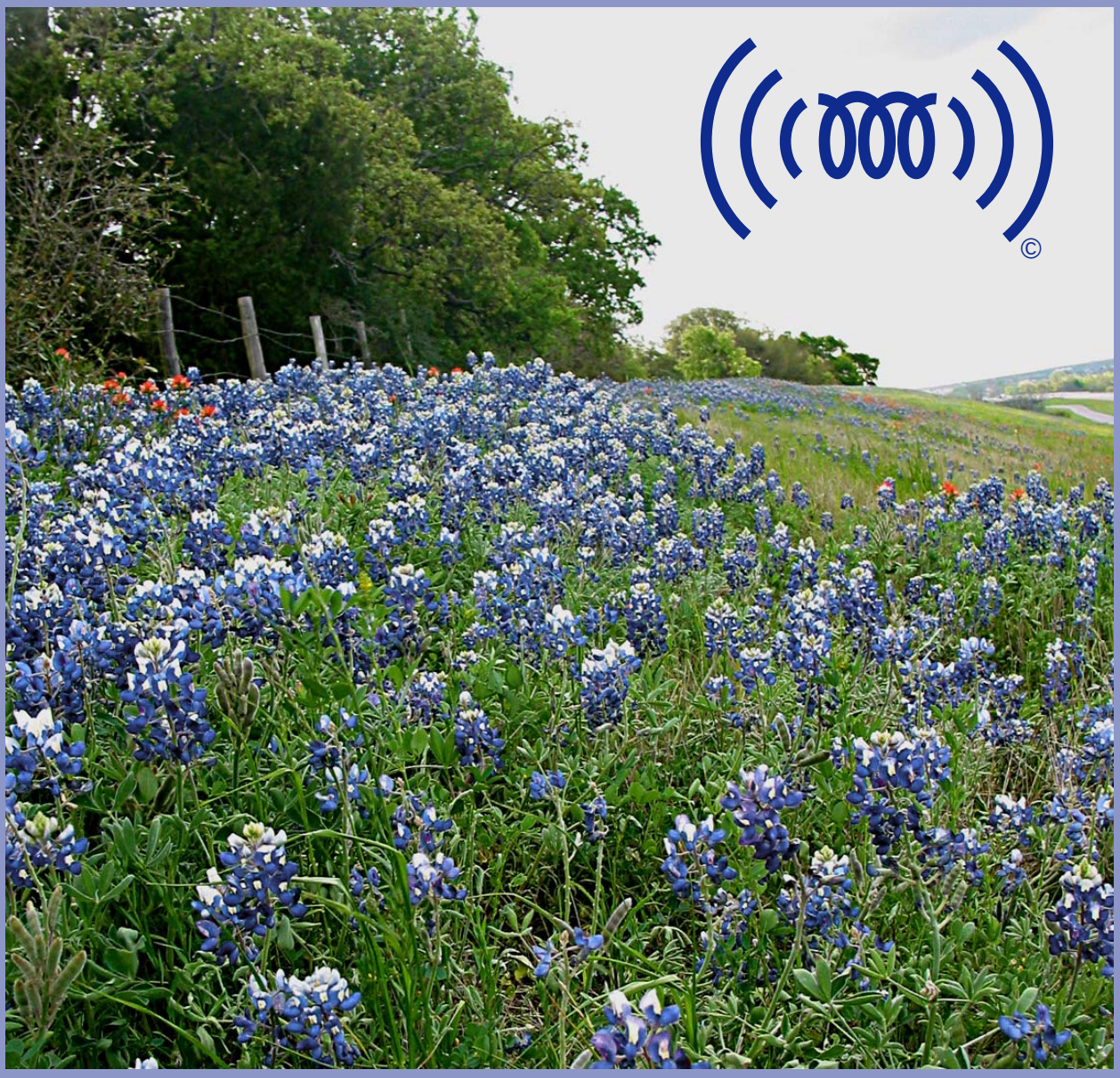

# PROCEEDINGS

of the

# Fourth International Conference on the Ultrasonic Measurement and Imaging of Tissue Elasticity©

**Lake Travis, Austin, Texas, USA**
**October 16 – 19, 2005**

# PROCEEDINGS

of the
Fourth International Conference
on the Ultrasonic Measurement and Imaging
of Tissue Elasticity©

Lake Travis, Austin, Texas, USA
October 16–19, 2005

## Table of Contents



**QUESTIONS OR COMMENTS ARE WELCOME AT ANY TIME AT <elasticity.conference@uth.tmc.edu>**

# Fifth International Conference on the Ultrasonic Measurement and Imaging of Tissue Elasticity©

## Snowbird, Utah, USA
## October 8 – 11, 2006

# FOREWORD

Dear Conference Delegate:

Welcome to the Fourth International Conference on the Ultrasonic Measurement and Imaging of Tissue Elasticity©.

The international participation in this Conference is reflected by delegates from some 20 countries. This year we are continuing to experience a phenomenal growth in the number of abstracts submitted to the Conference as compared to last year; over the last three years since the first Conference, the number of accepted abstracts has increased by some 65%, bringing the total number of abstracts this year to 118. While we were gratified at this continually increasing level of participation, it has created some necessary compromises in the Conference program. We are also seeing a steady increase in the number of clinical papers presented at the Conference, as well as the participation of more research groups from related disciplines and from Industry. We are especially gratified to see an ever-increasing number of students who are participating in the Conference.

Last year's Conference feedback was unanimous in the desire for continuation of the tutorial series. We are pleased that Drs. Joyce McLaughlin (US) and Paul Barbone (US) have jointly agreed to present this year's exciting tutorial on Inverse Methods for Shear Stiffness Imaging on Sunday afternoon. This year we have changed the format of the opening of the Poster Session, where each presenter will have the opportunity to give a brief oral summary of his/her poster, and we thank Dr. Jeff Bamber (UK) for his enthusiastic organization of this event.

We welcome Dr. Youseph Yazdi (US), Corporate Director of Science and Technology in the Johnson & Johnson Corporate Office of Science and Technology (COSAT), who has graciously agreed to deliver our dinner lecture on Monday night. He will share with us his experience and insights through his lecture "*Lessons from the World of Medical Device Commercialization*", which will surely be of great of interest to all those who are working to create new technologies. Dr. Yazdi looks for new scientific breakthroughs that will lead to the medical devices of tomorrow. His technology focuses on MEMS, nanotech, neurotech, energy-based therapeutics and imaging.

We would like to thank all the delegates, the reviewers and the session chairs for their continuing support of the Conference. Special thanks are in order to our enthusiastic support staff that has worked above and beyond in the face of adversity brought upon by Hurricane Rita last September. Ms Manette Price (US) of the Conference Secretariat's office has spent much time and effort handling most of the Conference organizational duties, correspondence and budgets; Ms Karen Ophir (US) volunteered to design and create all the Conference artwork and publications including the Conference Proceedings; Ms Betsy Christiansen (US) has updated and greatly improved the Conference website. Mr. Dario Sosa Cabrera from University of Las Palmas de Gran Canaria, in the Canary Islands, Spain, has kindly agreed to contribute his musical talents for your enjoyment during the Conference Dinner.

This Conference is conducted under the joint auspices of the University of Rochester Center for Biomedical Ultrasound and the Ultrasonics Laboratory in the Department of Diagnostic and Interventional Imaging at the University of Texas Medical School at Houston. However, all funding for the Conference is derived from registration fees alone. With your continued support in abstract submissions and attendance, we hope to continue to improve and expand the Conference in the years to come.

We believe that you will enjoy this year's scientific program as well as the city and countryside of Austin and Lake Travis. We will be looking forward to seeing you again at next year's Fifth Anniversary Conference at the Snowbird Ski and Summer Resort in the Wasatch Mountains of Utah (www.snowbird.com)!

J. Ophir and K.J. Parker
Conference Organizers
October 16, 2005

# CONFERENCE–AT–A–GLANCE

Fourth International Conference on the Ultrasonic Measurement and Imaging of Tissue Elasticity©
Lakeway Inn Conference Resort – Lake Travis, Austin, Texas, USA
October 16–19, 2005

| | | | |
|---|---|---|---|
| **Sunday, October 16** | | **10:00A – 7:30P** | |
| 10:00A – 7:30P | | Registration Desk & Conference Office Open | Rio Grande Foyer |
| 12:00P – 7:30P | **Session EEX:** | Equipment Exhibit *(during breaks)* | Rio Grande II |
| **1:00P – 3:00P** | **Session TUT:** | **Tutorial: Inverse Methods for Shear Stiffness Imaging** | Rio Grande II |
| 3:00P – 3:30P | | *Coffee Break* | Rio Grande Foyer |
| **3:30P – 5:30P** | **Session POS:** | **Poster Session – Live Oral Presentations** | Rio Grande I |
| 5:30P – 7:30P | | *Opening Reception (Proceedings Book Signing)* | Rio Grande I & II |
| **Monday, October 17** | | **7:00A – 10:30P** | |
| 7:00A – 8:00A | | *Group Continental Breakfast* | Rio Grande Foyer |
| 7:00A – 5:30P | | Registration Desk & Conference Office Open | Rio Grande Foyer |
| 8:00A – 5:30P | **Session POS:** | Posters | Rio Grande II |
| 8:00A – 5:30P | **Session EEX:** | Equipment Exhibit | Rio Grande II |
| 7:45A – 8:00A | | Opening Remarks | Rio Grande I |
| **8:00A – 9:45A** | **Session MIP-1:** | **Methods for Imaging Elastic Tissue Properties – I** | Rio Grande I |
| 9:45A – 10:15A | | *Coffee Break* | Rio Grande Foyer |
| **10:15A – 11:30A** | **Session FIP-1:** | **Forward and Inverse Problems – I** | Rio Grande I |
| 11:30A – 1:00P | | *Group Lunch* | Travis Restaurant |
| **1:00P – 2:45P** | **Session CVE:** | **Cardiovascular Elasticity** | Rio Grande I |
| 2:45P – 3:15P | | *Coffee Break* | Rio Grande Foyer |
| **3:15P – 4:15P** | **Session MMA:** | **3D, Multi-Modality & Alternative Applications** | Rio Grande I |
| **4:15P – 5:30P** | **Session SIP-1:** | **Signal and Image Processing – I** | Rio Grande I |
| 5:30P – 7:30P | | *No Conference Activities* | |
| 7:30P – 10:30P | | *Conference Dinner*, Guest Speaker – Youseph Yazdi *(Proceedings Book Signing)* | Rio Grande I |
| **Tuesday, October 18** | | **7:00A – 5:30P** | |
| 7:00A – 8:00A | | *Group Continental Breakfast* | Rio Grande Foyer |
| 7:00A – 5:30P | | Registration Desk & Conference Office Open | Rio Grande Foyer |
| 8:00A – 5:30P | **Session POS:** | Posters | Rio Grande II |
| 8:00A – 5:30P | **Session EEX:** | Equipment Exhibit | Rio Grande II |
| **8:00A – 9:15A** | **Session CAA-1:** | **Clinical and Animal Applications – I** | Rio Grande I |
| **9:15A – 10:00A** | **Session BTM:** | **Biomechanical Tissue Modeling** | Rio Grande I |
| 10:00A – 10:30A | | *Coffee Break* | Rio Grande Foyer |
| **10:30A – 12:00P** | **Session MMT:** | **Mechanical Measurement Techniques for Tissues** | Rio Grande I |
| 12:00P – 1:30P | | *Group Lunch* | Travis Restaurant |
| **1:30P – 3:30P** | **Session MIP-2:** | **Methods for Imaging Elastic Tissue Properties – II** | Rio Grande I |
| 3:30P – 4:00P | | *Coffee Break* | Rio Grande Foyer |
| **4:00P – 4:45P** | **Session PTO:** | **Phantoms and Test Objects** | Rio Grande I |
| **4:45P – 5:30P** | **Session INS:** | **Instrumentation** | Rio Grande I |
| **Wednesday, October 19** | | **7:00A – 9:30P** | |
| 7:00A – 8:00A | | *Group Continental Breakfast* | Rio Grande Foyer |
| 7:00A – 4:00P | | Registration Desk & Conference Office Open | Rio Grande Foyer |
| 8:00A – 4:00P | **Session POS:** | Posters | Rio Grande II |
| 8:00A – 4:00P | **Session EEX:** | Equipment Exhibit | Rio Grande II |
| **8:00A – 9:00A** | **Session SIP-2:** | **Signal and Image Processing – II** | Rio Grande I |
| **9:00A – 10:15A** | **Session FIP-2:** | **Forward and Inverse Problems – II** | Rio Grande I |
| 10:15A – 10:45A | | *Coffee Break* | Rio Grande Foyer |
| **10:45A – 12:15P** | **Session CAA-2:** | **Clinical and Animal Applications – II** | Rio Grande I |
| 12:15P – 1:45P | | *Group Lunch* | Travis Restaurant |
| **1:45P – 3:30P** | **Session MPT:** | **Mechanical Properties of Tissues** | Rio Grande I |
| 3:30P – 4:00P | | *Coffee Break* | Rio Grande Foyer |
| **4:00P – 5:30P** | **Session MIP-3:** | **Methods for Imaging Elastic Tissue Properties – III** | Rio Grande I |
| 5:30P – 6:30P | | *No Conference Activities* | |
| 6:30P – 9:30P | | *Open House* | to be announced |

# PROGRAM

Fourth International Conference
on the Ultrasonic Measurement and Imaging
of Tissue Elasticity©

Lake Travis, Austin, Texas, USA
October 16–19, 2005

## Sunday, October 16 10:00A – 7:30P

**10:00A – 7:30P**
Registration Desk & Conference Office Open — Rio Grande Foyer

**12:00P – 1:00P 3:00P – 3:30P 5:30P – 7:30P**
**Session EEX: Equipment Exhibit** — Rio Grande II

### Sunday 1:00P – 3:00P
### Session TUT: Tutorial: Inverse Methods for Shear Stiffness Imaging

*Chair: JB Weaver, USA* *Co-Chair: MM Doyley, USA* Rio Grande II

**1:00P – 1:45P**
117 IMAGING SHEAR STIFFNESS TISSUE PROPERTIES USING INVERSE METHODS WHEN MEASUREMENTS ARE TIME DEPENDENT.
*JR McLaughlin[1]*.*
[1]Rensselaer Polytechnic Institute, Troy, NY, USA.

**1:45P – 2:00P Discussion**

**2:00P – 2:45P**
116 INFERRING BIOMECHANICAL PROPERTIES FROM QUASISTATIC DEFORMATIONS: AN INTRODUCTION TO ASSOCIATED INVERSE PROBLEMS.
*PE Barbone[1]*.*
[1]Boston University, Boston, MA 02215, USA.

**2:45P – 3:00P Discussion**

**3:00P – 3:30P**
COFFEE BREAK — Rio Grande Foyer

### Sunday 3:30P – 5:30P

(Posters will be open for viewing and Coffee Break Discussion through Wednesday, October 19, 4:00P)

### Session POS: Poster Session – Live Oral Presentations

*Chair: J Bamber, UK* *Co-Chair: TA Krouskop, USA* Rio Grande I

**3:30P – 3:32P**
006 3D SIMULATION MODELS FOR ULTRASOUND ELASTOGRAPHY.
*AV Patil[1,2]*, TA Krouskop[3], J Ophir[1,2], S Srinivasan[2,4].*
[1]University of Houston, Houston, TX, USA; [2]University of Texas Medical School, Houston, TX, USA; [3]Baylor College of Medicine, Houston, TX, USA; [4]Siemens Acuson Ultrasound, Mountain View, CA, USA.

(Session POS continues on next page)

** indicates Presenter*

**3:32P – 3:34P**

012 PRELIMINARY RESULTS OF ELASTICITY IMAGING TO AORTIC PLAQUE.
*T Osaka[1]*, T Matsumura[1], T Mitake[1], S Nakatani[2], T Shiina[3].*
[1]Hitachi Medical Corporation, Chiba, JAPAN; [2]National Cardiovascular Center, Osaka, JAPAN; [3]University of Tsukuba, Ibaraki, JAPAN.

**3:34P – 3:36P**

016 TWO-STEP CROSS-CORRELATION METHOD TO IMPROVE IMAGE QUALITY IN ELASTOGRAPHY.
*H Chen[1]*, H Shi[2], T Varghese[2,3].*
[1,2,3]University of Wisconsin-Madison, Madison, WI, USA.

**3:36P – 3:38P**

021 REGULARIZATION ISSUES IN YOUNG'S MODULUS RECONSTRUCTION.
*J Jiang[1]*, T J Hall[1].*
[1]University of Wisconsin-Madison, Madison, WI, USA.

**3:38P – 3:40P**

022 SIGNIFICANT CLINICAL RESULTS IN THE DIAGNOSIS OF BREAST LESION BY MEANS OF REAL-TIME ELASTOGRAPHY.
*A Thomas[1], S Kümmel[1], H Frey[3]*, G Kristiansen[1], T Fischer[1].*
[1]Charité – CCM, University Berlin, Berlin, GERMANY; [2]Hitachi Medical Systems, Wiesbaden, GERMANY.

**3:40P – 3:42P**

028 SONOELASTOGRAPHY OF THE TESTICLES: PRELIMINARY RESULTS IN THE DIAGNOSIS OF DIFFERENT PATHOLOGICAL PROCESSES.
*L Pallwein[1]*, E Pallwein[1], M Schurich[1], V Fischbach[1], H Steiner[2], F Frauscher[1].*
[1,2]Medical University, Innsbruck, AUSTRIA.

**3:42P – 3:44P**

040 SIMULATION STUDY OF RECONSTRUCTION OF SHEAR MODULUS, DENSITY, POISSON'S RATIO DISTRIBUTIONS – 2nd REPORT.
*C Sumi[1]*.*
[1]Sophia University, Tokyo, JAPAN.

**3:44P – 3:46P**

042 THERMAL PROPERTIES RECONSTRUCTION BASED ON TEMPERATURE MEASUREMENT – 2nd REPORT.
*C Sumi[1]*.*
[1]Sophia University, Tokyo, JAPAN.

**3:46P – 3:48P**

044 REAL-TIME ELASTOGRAPHY FOR PROSTATE CANCER DETECTION: PRELIMINARY EXPERIENCE.
*E Pallwein[1], L Pallwein[1]*, M Schurich[1], W Horninger[2], F Frauscher[1].*
[1,2]Medical University, Innsbruck, AUSTRIA.

**3:48P – 3:50P**

055 AN APPLICATION OF THE LAGRANGIAN SPECKLE MODEL ESTIMATOR TO NON-INVASIVELY CHARACTERIZE THE CAROTID ARTERY: SIMULATION INVESTIGATIONS.
*E Mercure[1]*, RL Maurice[1], G Soulez[2], G Cloutier[1].*
[1,2]University of Montréal Hospital, Montréal, Quebec, CANADA.

**3:50P – 3:52P**

058 NON-RIGID SOFT TISSUE TRACKING WITH THREE-DIMENSIONAL ULTRASOUND.
*P Jordan[1,3]*, T Zickler[1], S Socrate[2], RD Howe[1,3].*
[1]Harvard University, Cambridge, MA, USA; [2]Massachusetts Institute of Technology, Cambridge, MA, USA; [3]Harvard-MIT Division of Health Sciences and Technology, Cambridge, MA, USA.


(Session POS continues on next page)

**3:52P – 3:54P**

060 DETECTION OF NON-DEFORMABLE OBJECTS IN THE BODY USING ULTRASOUND ELASTICITY IMAGING.
*U Bae[1]*, Y Kim[1].*
[1]University of Washington, Seattle, WA USA.

**3:54P – 3:56P**

064 ABSOLUTE ELASTICITY ESTIMATION WITH A NEW ULTRASONIC-MECHANICAL DEVICE.
*T Sato[1], Y Fukuyama[1]*, Y Watanabe[1], S Goka[1], H Sekimoto[1].*
[1]Tokyo Metropolitan University, Tokyo, JAPAN.

**3:56P – 3:58P**

066 THE FEASIBILITY OF USING ELASTOGRAPHIC TECHNIQUES FOR ASSESSING MEAT QUALITY ATTRIBUTES.
*R Righetti[1]*, J Ophir[1], RK Miller[2], TA Krouskop[1,3].*
[1]The University of Texas Health Science Center at Houston, Houston, TX, USA; [2]Texas A&M University, College Station, TX, USA; [3]Baylor College of Medicine, Houston, TX, USA.

**3:58P – 4:00P**

067 NOVEL STRAIN ELASTOGRAPHIC TECHNIQUES.
*R Righetti[1]*, A Thitai Kumar[1,2], S Srinivasan[1,3], J Ophir[1,2], TA Krouskop[1,4].*
[1]The University of Texas Health Science Center at Houston, Houston, TX, USA; [2]University of Houston, Houston, TX, USA; [3]Siemens Acuson Ultrasound, Mountain View, CA, USA; [4]Baylor College of Medicine, Houston, TX, USA.

**4:00P – 4:02P**

070 VISCOELASTIC CHARACTERIZATION OF THERMAL LESIONS IN LIVER.
*MZ Kiss[1]*, T Varghese[1,2].*
[1,2]University of Wisconsin-Madison, Madison, WI, USA.

**4:02P – 4:04P**

076 NOISE REDUCTION IN ELASTOGRAPHIC STRAIN ESTIMATED FROM DISPLACEMENT.
*L Xu[1], JC Bamber[1]*.*
[1]Institute of Cancer Research and Royal Marsden NHS Trust, Sutton, Surrey, England UK.

**4:04P – 4:06P**

078 VIRTUAL ENDOSCOPIC ELASTOGRAPHY – AN INITIAL EXPERIENCE *IN VIVO*.
*PF Zhang[1], X Yi[2], HJ Su[3], M Zhang[1], WQ Chen[1], Y Zhang[1].*
[1]Shandong University Qilu Hospital, Jinan, Shandong Province, CHINA; [2]Chinese Ministry of Education Key Laboratory of Cardiovascular Remodeling and Function Research, Jinan, Shandong Province, CHINA; [3]Shandong University, Jinan, Shandong Province, CHINA.

**4:06P – 4:08P**

079 PLAQUE VOLUME COMPRESSION RATIO – A NEW INDEX IN EVALUATING PLAQUE ELASTICITY PROPERTIES.
*PF Zhang[1], GH Yao[1], M Zhang[1], H Jiang[2], Y Zhang[1].*
[1]Shandong University Qilu Hospital, Jinan, Shandong Province, CHINA; [2]Chinese Ministry of Education Key Laboratory of Cardiovascular Remodeling and Function Research, Jinan, Shandong Province, CHINA.

**4:08P – 4:10P**

082 PHANTOM EXPERIMENTS AND COMPUTER SIMULATION FOR BREAST CANCER ELASTOGRAPY BY WATER BAG PRESSING.
*Y Hayakawa[1]*, K Ishida[1], K Tsuji[1], M Kaitoo[1], M Nakamura[2].*
[1]Toin University of Yokohama, Yokohama, Kanagawa-ken, JAPAN; [2]Yokohama General Hospital, Yokohama, Kanagawa-ken, JAPAN.

(Session POS continues on next page)

**4:10P – 4:12P**

088 PRELIMINARY CLINICAL STUDY OF SEMI-QUANTITATIVE FREEHAND ELASTOGRAPHY FOR THE ASSESSMENT OF RADIATION INDUCED BREAST FIBROSIS.

*NL Bush[1], JC Bamber[1]*, PE Barbone[3], JR Yarnold[2].*

[1,2]Institute of Cancer Research and Royal Marsden NHS Trust, Sutton, Surrey, England, UK; [3]Boston University, Boston, MA, USA.

**4:12P – 4:14P**

090 PROGRESS IN QUANTITATIVE BIOMECHANICAL IMAGING.

*NH Gokhale[1], MS Richards[2], C Rivas Aroni[1], R Leiderman[1], AA Oberai[1], PE Barbone[1]*.*

[1,2]Boston University, Boston, MA, USA.

**4:14P – 4:16P**

099 TISSUE MOTION AND ELASTICITY IMAGING EVALUATED BY ULTRASOUND IN A TISSUE-MIMICKING PHANTOM.

*AAO Carneiro[1]*, H Chen[2], T Varghese[2], TJ Hall[2], JA Zagzebski[2].*

[1]Universidade de São Paulo, Ribeirão Preto, São Paulo, BRAZIL; [2]University of Wisconsin-Madison, Madison, WI, USA.

**4:16P – 4:18P**

101 COMPARISON BETWEEN AXIAL ELASTOGRAMS OF A CONNECTED AND DISCONNECTED INCLUSION IN HOMOGENEOUS BACKGROUND: A SIMULATION STUDY.

*A Thitai Kumar[1,2]*, J Ophir[1,2], TA Krouskop[1,3].*

[1]The University of Texas Medical School, Houston, TX, USA; [2]University of Houston, Houston, TX, USA; [3]Baylor College of Medicine, Houston, TX, USA.

**4:18P – 4:20P**

106 THEORETICAL AND SIMULATION STUDY OF WAVE GENERATION AND ITS EFFECT ON LESION DETECTION IN SONOELASTOGRAPHY.

*JM Park[1], SJ Kwon[1], MK Jeong[1]*, MH Bae[2].*

[1]Daejin University, Pocheon, Kyeonggi, KOREA; [2]Hallym University, Chuncheon, Kangwon, KOREA.

**4:20P – 4:22P**

109 ULTRASOUND CHARACTERIZATION OF MECHANICAL PROPERTIES OF SILICONE TUBE WALLS.

*E Haeggstrom[1]*, A Wallin[1], M Leppänen[3].*

[1]Helsinki University, Helsinki, FINLAND.

**4:22P – 4:24P**

114 ELASTICITY AND PATHOLOGY IMAGING CORRELATION OF BREAST TUMOURS.

*WE Svensson[1]*, A Usupbaeva[1], S Shousha[2], S McLaggan[1], A Al-Kufaishi[3], PTR Thiruchelvam[3], JSK Lewis[3], HD Sinnett[3], J Malin[5], C Lowery[4].*

[1,2,3]Charing Cross Hospital, London, England, UK; [4]Siemens Medical Solutions Ultrasound Group, Issaquah, WA, USA.

**4:24P – 4:26P**

118 EFFECTS OF VISCOELASTICITY IN SHEAR WAVE SPEED RECONSTRUCTION.

*J Klein[1]*, JR McLaughlin[1].*

[1]Rensselaer Polytechnic Institute, Troy, NY, USA.

**4:26P – 4:28P**

119 VISCOELASTIC CHARACTERIZATION OF SOFT MATERIALS THROUGH CREEP TEST EXPERIMENTS.

*JJ Ammann[1,2]*, R Rivera[1], J Ophir[3].*

[1]Universidad de Santiago de Chile, Santiago, CHILE; [2]CIMAT, Santiago, CHILE; [3]The University of Texas Health Science Center at Houston, Houston, TX, USA.

**4:28P – 5:30P Discussion**

** indicates Presenter*

**Sunday 5:30P – 7:30P**
**Opening Reception** *Proceedings Book Signing* Rio Grande I & II

## Monday, October 17 7:00A – 10:30P

**7:00A – 8:00A**
GROUP CONTINENTAL BREAKFAST Rio Grande Foyer
**7:00A – 5:30P**
Registration Desk & Conference Office Open Rio Grande Foyer
**8:00A – 5:30P** **Session POS: Posters** Rio Grande II
**Session EEX: Equipment Exhibit** Rio Grande II

## Monday 7:45A – 8:00A
## OPENING REMARKS
*KJ Parker, J Ophir* Rio Grande I

## Monday 8:00A – 9:45A
## Session MIP-1: Methods for Imaging Elastic Tissue Properties – I
*Chair: A Sarvazyan, USA* *Co-Chair: R Rohling, Canada* Rio Grande I

**8:00A – 8:15A**
003 FROM STATIC TO DYNAMIC ELASTOGRAPHY: THE UNIFIED RANGE OF ELASTIC RESPONSE.
*KJ Parker[1]*, LS Taylor[1], SM Gracewski[2], DJ Rubens[3].*
[1,2,3]University of Rochester, Rochester, NY USA.

**8:15A – 8:30A**
009 ULTRASONIC TRACKING OF ACOUSTIC RADIATION FORCE-INDUCED DISPLACEMENT IN HOMOGENEOUS MEDIA.
*ML Palmeri[1]*, SA McAleavey[2], GE Trahey[1], KR Nightingale[1].*
[1]Duke University, Durham, NC, USA; [2]University of Rochester, Rochester, NY, USA.

**8:30A – 8:45A**
013 THE IMPACT OF PHYSIOLOGICAL MOTION ON ABDOMINAL ACOUSTIC RADIATION FORCE IMPULSE IMAGING.
*BJ Fahey[1]*, ML Palmeri[1], GE Trahey[1].*
[1]Duke University, Durham, NC, USA.

**8:45A – 9:00A**
017 RADIOFREQUENCY ABLATION ELECTRODE DISPLACEMENT ELASTOGRAPHY – A PHANTOM STUDY.
*S Bharat[1,2], EL Madsen[1], JA Zagzebski[1], T Varghese[1,3]*.*
[1,2,3]University of Wisconsin – Madison, Madison, WI, USA.

**9:00A – 9:15A**
053 *IN-VITRO* DEMONSTRATION OF REAL TIME MONITORING OF REGIONAL TISSUE ELASTICITY DURING FOCUSED ULTRASOUND THERAPY USING HARMONIC MOTION IMAGING.
*C Maleke[1]*, M Pernot[1], EE Konofagou[1].*
[1]Columbia University, New York, NY, USA.

**9:15A – 9:30A**
019 NORMAL AND SHEAR STRAIN ESTIMATION AND ANGULAR COMPOUNDING USING BEAM STEERING ON LINEAR ARRAY TRANSDUCERS.
*M Rao[1]*, Q Chen[1], H Shi[1], EL Madsen[1], JA Zagzebski[1], T Varghese[1].*
[1]University of Wisconsin-Madison, Madison, WI, USA.

(Session MIP-1 continues on next page)

**9:30A – 9:45A**

071 DESIGN OF A HAND-HELD PROBE FOR IMAGING TISSUE ELASTICITY.
*H Rivaz[1]*, R Rohling[1].*
[1]University of British Columbia, Vancouver, BC, CANADA.

**9:45A – 10:15A**

COFFEE BREAK — Rio Grande Foyer

## Monday 10:15A – 11:30A
## Session FIP-1: Forward and Inverse Problems – I

*Chair: T Varghese, USA* *Co-Chair: T Mitake, Japan* — Rio Grande I

**10:15A – 10:30A**

049 SHEAR MODULUS RECONSTRUCTION USING DIRECT FINITE ELEMENT INVERSION ALGORITHM IN TRANSIENT ELASTOGRAPHY.
*E Park[1]*, AM Maniatty[1].*
[1]Rensselaer Polytechnic Institute, Troy, NY, USA.

**10:30A – 10:45A**

023 FINITE ELEMENT ANALYSIS AND YOUNG'S MODULUS RECONSTRUCTION FOR ELASTICITY IMAGING WITH DEFORMATION BY A RADIOFREQUENCY ABLATION ELECTRODE.
*J Jiang[1]*, T Varghese[1], TJ Hall[1], Q Chen[1], JA Zagzebski[1].*
[1]University of Wisconsin-Madison, Madison, WI, USA.

**10:45A – 11:00A**

086 THREE DIMENSIONAL ULTRASOUND IMAGE REGISTRATION AND SHEAR ELASTIC MODULUS RECONSTRUCTION.
*MS Richards[1]*, NH Gokhale[2], AA Oberai[2], PE Barbone[2].*
[1,2]Boston University, Boston, MA, USA.

**11:00A – 11:15A**

089 ZERO MEMORY GAUSS-NEWTON METHOD FOR THE DETECTION OF SMALL INCLUSIONS.
*J Fehrenbach[1]*, M Masmoudi[1], R Souchon[2], P Trompette[2].*
[1]Laboratoire MIP, Toulouse, FRANCE; [2]INSERM UMR 556, Lyon, FRANCE.

**11:15A – 11:30A**

092 THE INFLUENCE OF CAUSALITY ON THE RECONSTRUCTION OF SHEAR MODULUS FOR DYNAMIC ELASTOGRAPHY.
*B Robert[1]*, R Sinkus[1], J Bercoff[1], M Tanter[1], M Fink[1].*
[1]Laboratoire Ondes et Acoustique, ESPCI, Paris, FRANCE.

**11:30P – 1:00P**

GROUP LUNCH — Travis Restaurant

## Monday 1:00P – 2:45P
## Session CVE: Cardiovascular Elasticity

*Chair: SY Emelianov, USA* *Co-Chair: HM Langevin, USA* — Rio Grande I

**1:00P – 1:15P**

007 MOTION COMPENSATION FOR INTRAVASCULAR ULTRASOUND PALPOGRAPHY FOR *IN VIVO* VULNERABLE PLAQUE DETECTION.
*KYE Leung[1], RA Baldewsing[1], F Mastik[1], MG Danilouchkine[1], JA Schaar[1], A Gisolf[2], AFW van der Steen[1,3]*.*
[1]Erasmus MC, Rotterdam, The NETHERLANDS; [2]Delft University of Technology, The NETHERLANDS; [3]Interuniversity Cardiology Institute of the Netherlands, Utrecht, The NETHERLANDS.

**1:15P – 1:30P**

005 A COMPOUNDING METHOD FOR RECONSTRUCTING THE HETEROGENEOUS YOUNG'S MODULUS DISTRIBUTION OF ATHEROSCLEROTIC PLAQUES FROM THEIR RADIAL STRAIN.
*RA Baldewsing[1]*, F Mastik[1], JA Schaar[1], AFW van der Steen[1,2].*
[1]Erasmus MC, Rotterdam, The NETHERLANDS; [2]Interuniversity Cardiology Institute of the Netherlands, Utrecht, The NETHERLANDS.

**1:30P – 1:45P**

025 AN INTEGRATED ULTRASOUND-BASED INTRAVASCULAR IMAGING OF ATHEROSCLEROSIS.
*S Sethuraman[1]*, SR Aglyamov[1], JH Amirian[2], RW Smalling[2], SY Emelianov[1].*
[1]The University of Texas at Austin, Austin, TX, USA; [2]University of Texas Health Science Center Houston, Houston, TX, USA.

**1:45P – 2:00P**

054 ELECTROMECHANICAL MAPPING OF THE NORMAL AND ISCHEMIC MYOCARDIUM.
*M Pernot[1], SD Fung-Kee-Fung[1], EE Konofagou[1]*.*
[1]Columbia University, New York, NY, USA.

**2:00P – 2:15P**

056 ANGLE INDEPENDENT STRAIN ESTIMATION IN MYOCARDIAL ELASTOGRAPHY.
*SD Fung-Kee-Fung[1]*, EE Konofagou[1].*
[1]Columbia University, New York, NY, USA.

**2:15P – 2:30P**

063 NON-INVASIVE VASCULAR ELASTOGRAPHY FOR CAROTID ARTERY PLAQUE CHARACTERIZATION: *IN VIVO* FEASIBILITY STUDY.
*RL Maurice[1]*, G Cloutier[1], M-F Giroux[2], S Lanthier[3], G Soulez[2].*
[1,2,3]University of Montréal Hospital, Montréal, CANADA.

**2:30P – 2:45P**

068 A 3D SIMULATION MODEL FOR PERFORMANCE ASSESSMENT OF 2D MYOCARDIAL ELASTOGRAPHY.
*WN Lee[1]*, CP Ingrassia[1], EE Konofagou[1].*
[1]Columbia University, New York, NY, USA.

**2:45P – 3:15P**

COFFEE BREAK — Rio Grande Foyer

## Monday 3:15P – 4:15P
## Session MMA: 3D, Multi-Modality & Alternative Applications

*Chair: KJ Parker, USA* *Co-Chair: JC Bamber, UK* — Rio Grande I

**3:15P – 3:30P**

008 FRAME FILTERING FOR IMPROVED FREEHAND 3D ULTRASOUND ELASTOGRAPHY.
*JE Lindop[1]*, GM Treece[1], AH Gee[1], RW Prager[1].*
[1]University of Cambridge, Cambridge, England, UK.

**3:30P – 3:45P**

057 AN INVERSE DEFORMATION METHOD FOR THE VISUALIZATION OF REAL-TIME 3D LUNG DYNAMICS.
*AP Santhanam[1]*, JP Rolland[2].*
[1,2]University of Central Florida, Orlando FL, USA.

**3:45P – 4:00P**

091 COMPARISON OF THREE NON-AXIAL STRAIN ESTIMATION TECHNIQUES FOR 3D STRAIN ESTIMATION IN ELASTIC MATERIALS AND TISSUES.
*RGP Lopata[1]*, MM Nillesen[1], IH Gerrits[1], JM Thijssen[1], L Kapusta[2], CL de Korte[1].*
[1,2]Radboud University Medical Center, Nijmegen, The NETHERLANDS.

(Session MMA continues on next page)

** indicates Presenter*

**4:00P – 4:15P**

102 STEADY-STATE HARMONIC ELASTOGRAPHY: VISUALIZING THE VISCOELASTIC PROPERTIES WITHIN SOFT TISSUES.
*MM Doyley[1, 2]*, Q Feng[2], JB Weaver[1,2], FE Kennedy[2], KD Paulsen[2].*
[1]Dartmouth Medical School, Hanover, NH, USA; [2]Dartmouth College, Hanover, NH, USA.

## Monday 4:15P – 5:30P
## Session SIP-1: Signal and Image Processing – I

*Chair: TJ Hall, USA* *Co-Chair: T Shiina, Japan* Rio Grande I

**4:15P – 4:30P**

059 ANGULAR STRAIN METHOD FOR STRAIN ESTIMATION IN ULTRASOUND ELASTICITY IMAGING.
*U Bae[1]*, Y Kim[1].*
[1]University of Washington, Seattle, WA, USA.

**4:30P – 4:45P**

037 MULTIDIMENSIONAL AUTOCORRELATION AND DOPPLER METHODS VERSUS CROSS-SPECTRUM PHASE GRADIENT METHOD.
*C Sumi[1]*.*
[1]Sophia University, Tokyo, JAPAN.

**4:45P – 5:00P**

087 HIGH RESOLUTION TIME OF FLIGHT MEASUREMENTS WITH THE PULSED PHASE LOCKED LOOP.
*T Lynch[1]*, JS Heyman[1], D Blaker[2].*
[1]Luna Innovations Inc., Hampton, VA, USA; [2]Luna Innovations Inc., Blacksburg, VA, USA.

**5:00P – 5:15P**

093 EFFECTS OF PHYSIOLOGICAL TISSUE MOTION STATISTICS ON PREDICTED ELASTOGRAPHIC IMAGE QUALITY *IN VIVO*.
*R Chandrasekhar[1,2]*, J Ophir[1,2], T Krouskop[3], K Ophir[4].*
[1]The University of Texas Medical School, Houston, TX, USA; [2]University of Houston, Houston, TX, USA; [3]Baylor College of Medicine, Houston, TX, USA.; [4]Austin, TX, USA.

**5:15P – 5:30P**

052 ELASTICITY IMAGING USING ULTRAFAST VS. CONVENTIONAL ULTRASOUND IMAGING.
*S Park[1]*, SR Aglyamov[1], J Shah[1], WG Scott[2], SY Emelianov[1].*
[1]University of Texas at Austin, Austin, TX, USA; [2]Winprobe Corporation, North Palm Beach, FL, USA.

5:30P – 7:30P *No Conference Activities*

## Monday 7:30P – 10:30P
## Conference Dinner *Proceedings Book Signing* Rio Grande I

**7:30P – 10:30P**

*Chair: J Ophir, USA*

000 LESSONS FROM THE WORLD OF MEDICAL DEVICE COMMERCIALIZATION.
*Y Yazdi[1]*.*
[1]Corporate Office of Science and Technology, Johnson & Johnson, New Brunswick, NJ, USA.

*Violin selections performed by Dario Sosa Cabrera, Canary Islands, SPAIN.*

## Tuesday, October 18 7:00A – 5:30P

**7:00A – 8:00A**
GROUP CONTINENTAL BREAKFAST — Rio Grande Foyer

**7:00A – 5:30P**
Registration Desk & Conference Office Open — Rio Grande Foyer

**8:00A – 5:30P** **Session POS: Posters** — Rio Grande II
**Session EEX: Equipment Exhibit** — Rio Grande II

## Tuesday 8:00A – 9:15A
## Session CAA-1: Clinical and Animal Applications – I

*Chair: JM Rubin, USA* *Co-Chair: BS Garra, USA* Rio Grande I

**8:00A – 8:15A**
104 ARTERIAL ELASTIC MODULUS RECONSTRUCTION FROM *IN-VIVO* STRAIN IMAGING AND PWV.
*WF Weitzel[1]*, K Kim[2], H Xie[2], JM Rubin[3], C Jia[2], M O'Donnell[2].*
[1,2,3]University of Michigan, Ann Arbor, MI, USA.

**8:15A – 8:30A**
074 COMPUTER AIDED DIAGNOSIS OF BREAST CANCER BASED ON ELASTICITY IMAGES.
*T Shiina[1]*, M Yamakawa[1], A Itoh[2], E Tohno[2], E Ueno[2], T Matsumura[3], T Mitake[3].*
[1,2]University of Tsukuba, Tsukuba, JAPAN; [3]Hitachi Medical Corporation, Kashiwa, JAPAN.

**8:30A – 8:45A**
033 DIAGNOSIS OF LIVER FIBROSIS IN CHILDREN USING FIBROSCAN®.
*L Sandrin[1]*, V Miette[1], C Fournier[1], T Lamireau[2], V de Lédinghen[3].*
[1]Echosens, Paris, FRANCE; [2]Hôpital Pellegrin, Bordeaux, FRANCE; [2]Hôpital Haut Lévêque, Pessac, FRANCE.

**8:45A – 9:00A**
112 CLINICAL EVALUATION OF THYROID TUMOR WITH REAL-TIME TISSUE ELASTOGRAPHY.
*K Tanaka[1], N Fukunari[2], H Akasu[1], W Kitagawa[1], K Shimizu[2], K Ito[2], T Mitake[3]*.*
[1]Nippon Medical School, Tokyo, JAPAN; [2]Ito Hospital, Tokyo, JAPAN; [3]Hitachi Medical Corporation, Tokyo, JAPAN.

**9:00A – 9:15A**
115 ELASTICITY IMAGING OF 67 CANCERS AND 167 BENIGN BREAST LESIONS SHOWS THAT IT COULD HALVE BIOPSY RATES OF BENIGN LESIONS.
*WE Svensson[1]*, D Amiras[3], S Shousha[2], A Rattansingh[1], D Chopra[1], HD Sinnett[3], TJ Hall[4], Y Zhu[5], J Malin[6], C Lowery[6].*
[1,2,3]Charing Cross Hospital, London, England, UK; [4]University of Wisconsin-Madison, Madison, WI, USA; [5]University of Kansas Medical Center, Kansas City, KS, USA; [6]Siemens Medical Solutions Ultrasound Group, Issaquah, WA, USA.

## Tuesday 9:15A – 10:00A
## Session BTM: Biomechanical Tissue Modeling

*Chair: WF Weitzel, USA* *Co-Chair: E Mazza, Switzerland* Rio Grande I

**9:15A – 9:30A**
031 THE ROLE OF ANISOTROPIC ELASTICITY AND VISCOSITY IN SKELETAL MUSCLE IMAGING.
*SF Levinson[1]*, S Catheline[2], M Fink[2], RL Ehman[3].*
[1]Wayne State University, Detroit, MI, USA; [2]Laboratoire Onde et Acoustique, ESPCI, Paris, FRANCE; [3]Mayo Clinic Department of Radiology, Rochester, MN, USA.

(Session BTM continues on next page)

**9:30A – 9:45A**

094 MICROMECHANICAL ANALYSIS OF DENTIN ELASTIC ANISOTROPY.
*A Misra[1]*, P Spencer[2], O Marangos[1], Y Wang[2], M Walker[2], JL Katz[1,2].*
[1,2]University of Missouri-Kansas-City, Kansas City, MO, USA.

**9:45A – 10:00A**

095 CALIBRATING SCANNING ACOUSTIC MICROSCOPY FOR MICROMECHANICAL PROPERTY QUANTIFICATION.
*O Marangos[1]*, A Misra[1], JL Katz[1,2], Y Wang[2], P Spencer[2].*
[1,2]University of Missouri-Kansas City, Kansas City, MO, USA.

**10:00A – 10:30A**

COFFEE BREAK — Rio Grande Foyer

## Tuesday 10:30A – 12:00P
## Session MMT: Mechanical Measurement Techniques for Tissues

*Chair: GE Trahey, USA* *Co-Chair: L Sandrin, France* Rio Grande I

**10:30A – 10:45A**

001 AVERAGE "GRAIN-SIZE" ESTIMATION IN LIQUID OR SOLID CHANNELS.
*D Hazony[1], Y Hazony[2], JL Katz[1,3]*.*
[1]Case Western Reserve University, Cleveland, OH, USA; [2]Boston University, Boston, MA, USA; [3]University of Missouri-Kansas City, Kansas City, MO, USA.

**10:45A – 11:00A**

002 STUDY OF THE EFFECT OF BOUNDARY CONDITIONS AND INCLUSION'S POSITION ON THE CONTRAST TRANSFER EFFICIENCY IN ELASTOGRAPHY**.**
*D Sosa Cabrera[1,2]*, J Ophir[1,3], T Krouskop[4], A Thitai Kumar[1,3], J Ruiz-Alzola[2].*
[1]The University of Texas Medical School, Houston, TX, USA; [2]University of Las Palmas de Gran Canaria, Las Palmas de Gran Canaria, Canary Islands, SPAIN; [3]University of Houston, Houston, TX, USA; [4]Baylor College of Medicine, Houston, TX, USA.

**11:00A – 11:15A**

026 *IN VIVO* MECHANICAL BEHAVIOR OF HUMAN LIVER.
*E Mazza[1]*, A Nava[1], D Hahnloser[2], W Jochum[3], M Bajka[4].*
[1]Swiss Federal Institute of Technology, Zurich, SWITZERLAND; [2,3,4]University Hospital, Zurich, SWITZERLAND.

**11:15A – 11:30A**

027 MECHANICAL CHARACTERIZATION OF SOFT TISSUE: COMPARISON OF DIFFERENT EXPERIMENTAL TECHNIQUES ON SYNTHETIC MATERIALS.
*D Valtorta[1]*, M Hollenstein[1], A Nava[1], V Luboz[2], MH Lu[3], A Choi[3], E Mazza[1], YP Zheng[3], SM Cotin[2].*
[1]Swiss Federal Institute of Technology, Zürich, SWITZERLAND; [2]Massachusetts General Hospital, Boston, MA, USA; [3]The Hong Kong Polytechnic University, Hong Kong, CHINA.

**11:30A – 11:45A**

039 SHEAR MODULUS RECONSTRUCTION USING ULTRASONICALLY MEASURED STRAIN RATIO.
*C Sumi[1]*.*
[1]Sophia University, Tokyo, JAPAN.

**11:45A – 12:00P**

081 NONINVASIVE INTRAMUSCULAR PRESSURE MEASUREMENTS THROUGH HARMONIC ANALYSIS OF ARTERIAL PULSATIONS.
*T Lynch[1]*, T Ueno[2], AD Cutuk[2], JM Wiemann[2], BR Macias[2], AR Hargens[2].*
[1]Luna Innovations Inc., Hampton, VA, USA; [2]University of California San Diego, San Diego, CA, USA.

**12:00P – 1:30P**
GROUP LUNCH Travis Restaurant

## Tuesday 1:30P – 3:30P
## Session MIP-2: Methods for Imaging Elastic Tissue Properties – II
*Chair: R Sinkus, France* *Co-Chair: JL Katz, USA* Rio Grande I

**1:30P – 1:45P**
061 THE SPATIO-TEMPORAL VARIATION OF THE STRAIN FIELD INSIDE COMPRESSED POROELASTIC MATERIALS.
*GP Berry[1]*, JC Bamber[1], NL Bush[1], NR Miller[1].*
[1]Institute of Cancer Research, Sutton, Surrey, England, UK.

**1:45P – 2:00P**
065 A NEW COMPRESSION METHOD FOR GENERATING POROELASTOGRAMS IN INHERENTLY NOISY APPLICATIONS.
*R Righetti[1]*, J Ophir[1], BS Garra[2], TA Krouskop[1,3].*
[1]The University of Texas Health Science Center at Houston, Houston, TX, USA; [2]The University of Vermont College of Medicine, Burlington, VT, USA; [3]Baylor College of Medicine, Houston, TX, USA.

**2:00P – 2:15P**
018 MAXIMUM STRAIN ACCUMULATION FOR *IN VIVO* TISSUE.
*AM Sommer[1]*, TJ Hall[1], J Jiang[1].*
[1]University of Wisconsin – Madison, Madison, WI, USA.

**2:15P – 2:30P**
032 DOPPLER MYOGRAPHY—DETECTING AND IMAGING INTRINSIC MUSCLE SOUNDS.
*SF Levinson[1]*, H Kanai[2], H Hasegawa[2].*
[1]Wayne State University, Detroit, MI, USA; [2]Tohoku University, Sendai, JAPAN.

**2:30P – 2:45P**
029 TRANSIENT ULTRASOUND ELASTOGRAPHY USING IMPULSIVE ULTRASOUND RADIATION FORCE.
*D Melodelima[1], JC Bamber[1]*, F Duck[2], S Shipley[2].*
[1]Royal Marsden NHS Trust and Institute of Cancer Research, Sutton, Surrey, England, UK; [2]Royal United Hospital NHS Trust, Bath, England, UK.

**2:45P – 3:00P**
080 AN *IN VIVO* COMPARATIVE ASSESSMENT OF ADAPTIVE ELASTOGRAPHIC TECHNIQUES.
*K Hoyt[1,2], F Forsberg[2]*, CRB Merritt[2], JB Liu[2], J Ophir[3].*
[1]Drexel University, Philadelphia, PA, USA; [2]Thomas Jefferson University, Philadelphia, PA, USA; [3]University of Texas Medical School, Houston, TX, USA.

**3:00P – 3:15P**
043 DISPLACEMENT OF A SOLID SPHERE IN A VISCOELASTIC MEDIUM IN RESPONSE TO AN ACOUSTIC RADIATION FORCE: THEORETICAL ANALYSIS AND EXPERIMENTAL VERIFICATION.
*SR Aglyamov[1]*, AB Karpiouk[1], YA Ilinskii[2], EA Zabolotskaya[2], SY Emelianov[1].*
[1,2]The University of Texas at Austin, Austin, TX, USA.

**3:15P – 3:30P**
050 ELASTOGRAPIC IMAGING OF UTERINE TISSUE.
*MA Hobson[1]*, MZ Kiss[1], H Shi[1], T Varghese[1,2], MA Kliewer[3], JA Zagzebski[1], TJ Hall[1], J Harter[4], EM Hartenbach[5], EL Madsen[1].*
[1,2,3,4,5]University of Wisconsin-Madison, Madison, WI, USA.

**3:30P – 4:00P**
COFFEE BREAK Rio Grande Foyer

** indicates Presenter*

## Tuesday 4:00P – 4:45P
## Session PTO: Phantoms and Test Objects

*Chair: AFW van der Steen, The Netherlands Co-Chair: TA Krouskop, USA* Rio Grande I

**4:00P – 4:15P**

045 PVA PROSTATE PHANTOM FOR ULTRASOUND AND MR ELASTOGRAPHY.
*W Khaled[1]*, T Neumann[1], J Stapf[1], H Ermert[1].*
[1]Institute of High Frequency Engineering, Ruhr-University, Bochum, GERMANY.

**4:15P – 4:30P**

046 A NOVEL 3D HAPTIC SENSOR SYSTEM BASED ON ULTRASOUND ELASTOGRAPHY.
*W Khaled[1]*, S Reichling[2], OT Bruhns[2], A Lorenz[3], A Pesavento[3], H Ermert[1].*
[1,2]Ruhr-University, Bochum, GERMANY; [3]LP-IT Innovative Technologies GmbH, Bochum, GERMANY.

**4:30P – 4:45P**

048 TISSUE MIMICKING MATERIALS AND PHANTOMS FOR ELASTICITY IMAGING.
*J Beck[1]*, S Sethuraman[1], S Mallidi[1], AB Karpiouk[1], SR Aglyamov[1], SY Emelianov[1].*
[1]The University of Texas at Austin, Austin, TX, USA.

## Tuesday 4:45P – 5:30P
## Session INS: Instrumentation

*Chair: GJ Streekstra, The Netherlands Co-Chair: AM Maniatty, USA* Rio Grande I

**4:45P – 5:00P**

035 DEVELOPMENT OF AN *IN VIVO* TISSUE INDENTATION SYSTEM USING AN ELECTROMAGNETIC SPATIAL LOCATING SENSOR.
*YP Zheng[1]*, MH Lu[1], QH Huang[1], W Yu[1], GHY Lo[1].*
[1]The Hong Kong Polytechnic University, Hong Kong, CHINA.

**5:00P – 5:15P**

036 DEVELOPMENT OF A SOFTWARE PLATFORM FOR ULTRASOUND MEASUREMENT OF MOTION AND ELASTICITY (UMME).
*YP Zheng[1]*, J Shi[1], QH Huang[1], X Chen[1].*
[1]The Hong Kong Polytechnic University, Hong Kong, CHINA.

**5:15P – 5:30P**

084 MEASURING STIFFNESS OF BREAST TISSUE *EX-VIVO*.
*A Iqbal[1]*, T Frank[1], D McLean[1], A Thompson[1], A Cuschieri[1].*
[1]Ninewells Hospital and Medical School, University of Dundee, Dundee, Scotland, UK.

## Wednesday, October 19 7:00A – 9:30P

**7:00A – 8:00A**
GROUP CONTINENTAL BREAKFAST Rio Grande Foyer

**7:00A – 4:00P**
Registration Desk & Conference Office Open Rio Grande Foyer

**8:00A – 4:00P** **Session POS: Posters** Rio Grande II
**Session EEX: Equipment Exhibit** Rio Grande II

## Wednesday 8:00A – 9:00A
## Session SIP-2: Signal and Image Processing – II

*Chair: F Forsberg, USA* *Co-Chair: EE Konofagou, USA* Rio Grande I

**8:00A – 8:15A**

098 2D STRAIN ESTIMATION BASED ON A NEWTON CONSTRAINED MINIMIZATION STRATEGY: APPLICATION TO EXPERIMENTAL DATA.
*E Brusseau[1], JF Déprez[1]*, G Said[1], O Basset[1].*
[1]CREATIS UMR CNRS 5515 INSERM U630, Lyon, FRANCE.

**8:15A – 8:30A**

083 STRAIN ESTIMATION WITH PULSE SHAPING.
*R Souchon[1]*, S Vassant[1], J-C Béra[1], J-Y Chapelon[1].*
[1]INSERM UMR 556, Lyon, FRANCE.

**8:30A – 8:45A**

100 SIGNAL-TO-NOISE RATIO UPPER-BOUND IN SHEAR STRAIN ELASTOGRAMS.
*A Thitai Kumar[1,2]*, J Ophir[1,2] and TA Krouskop[1,3].*
[1]The University of Texas Medical School, Houston, TX, USA; [2]University of Houston, Houston, TX, USA; [3]Baylor College of Medicine, Houston, TX, USA.

**8:45A – 9:00A**

041 REGULARIZATION FOR STRAIN MEASUREMENT AND SHEAR MODULUS RECONSTRUCTION.
*C Sumi[1]*.*
[1]Sophia University, Tokyo, JAPAN.

## Wednesday 9:00A – 10:15A
## Session FIP-2: Forward and Inverse Problems – II

*Chair: JR McLaughlin, USA* *Co-Chair: R Souchon, France* Rio Grande I

**9:00A – 9:15A**

107 2D AND 3D ELASTICITY AND VISCOSITY IMAGING USING NEW RECONSTRUCTION STRATEGIES IN DYNAMIC ELASTOGRAPHY.
*J Bercoff[1], R Sinkus[1]*, M Tanter[1], M Fink[1].*
[1]Laboratoire Ondes et Acoustique, ESPCI, Paris, FRANCE.

**9:15A – 9:30A**

097 AN ANALYTICAL MODEL FOR 3D LONGITUDINAL WAVE PROPAGATION IN A VISCOELASTIC CYLINDER: APPLICATIONS TO MR ELASTOGRAPHY.
*GJ Streekstra[1]*, P van Horssen[1], DMJ van den Berg[1], JGG Dobbe[2], J Strackee[1].*
[1,2]Academic Medical Center, Amsterdam, The NETHERLANDS.

**9:30A – 9:45A**

103 A BAYESIAN IMAGE RECONSTRUCTION APPROACH FOR MODEL-BASED ELASTOGRAPHY.
*MM Doyley[1,3]*, S Srinivasan[2], E Dimidenko[1], N Soni[3], J Ophir[2].*
[1]Dartmouth Medical School, Hanover, NH, USA; [2]University of Texas Medical School, Houston, TX, USA; [3]Dartmouth College, Hanover, NH, USA.

**9:45A – 10:00A**

077 IMAGING ANISOTROPIC ELASTICITY USING SUPERSONIC RADIATION FORCE EXCITATION.
*JR Yoon[1]*, D Renzi[2], JR McLaughlin[2].*
[1]Clemson University, Clemson, SC, USA; [2]Rensselaer Polytechnic Institute, Troy, NY, USA.

**10:00A – 10:15A**

113 FAST INVERSION TECHNIQUES FOR 3D ELASTICITY IMAGING.
*BB Guzina[1]*, AI Madyarov[1], I Chikichev[1].*
[1]Univiersity of Minnesota, Minneapolis, MN, USA.

**10:15A – 10:45A**
COFFEE BREAK Rio Grande Foyer

## Wednesday 10:45A – 12:15P
## Session CAA-2: Clinical and Animal Applications – II
*Chair: WE Svensson, UK* *Co-Chair: RL Maurice, Canada* Rio Grande I

**10:45A – 11:00A**
004 ULTRASOUND ELASTICITY IMAGING FOR AGING DEEP VENOUS THROMBOSIS IN HUMANS.
*JM Rubin[1]*, H Xie[1], K Kim[1], WF Weitzel[1], SY Emelianov[2], S Aglyammov[2], TW Wakefield[1], M O'Donnell[1].*
[1]University of Michigan, Ann Arbor, MI, USA; [2]University of Texas at Austin, Austin, TX, USA.

**11:00A – 11:15A**
030 A NOVEL PERFORMANCE DESCRIPTOR FOR ULTRASONIC STRAIN IMAGING: A PRELIMINARY STUDY.
*J Jiang[1]*, TJ Hall[1], AM Sommer[1].*
[1]University of Wisconsin-Madison, Madison, WI, USA.

**11:15A – 11:30A**
111 A COMPARISON OF REAL-TIME AND POST-PROCESSED ELASTOGRAPHY WITH SURGICAL FINDINGS FOR INTRA-OPERATIVE DETECTION OF BRAIN TUMOURS.
*A Chakraborty[1]*, JC Bamber[2], NL Dorward[1].*
[1]Royal Free Hospital, London, England, UK; [2]Institute of Cancer Research and Royal Marsden NHS Trust, Sutton, Surrey, England, UK.

**11:30A – 11:45A**
051 SOFT TISSUE BIOMECHANCIAL BEHAVIOR DURING ROBOTIC ACUPUNCTURE IN LOW BACK PAIN USING ULTRASOUND ELASTICITY IMAGING.
*HM Langevin[1]*, EE Konofagou[2], J Wu[3], JR Fox[4] and JC Iatridis[5].*
[1,3,4,5]University of Vermont, Burlington, VT, USA; [2]Columbia University, New York, NY, USA.

**11:45A – 12:00P**
110 REALTIME SONOELASTOGRAPHY OF 156 BREAST LESIONS IN A PROSPECTIVE CLINICAL SETTING.
*S Weber[1], S Wojcinski[1], K Ertan[1], K Remberger[2], U Stein[2], R Ohlinger [3], A Thomas[4], W Schmidt[1].*
[1,2]University of Saarland, Homburg, Saar, GERMANY; [3]Ernst-Moritz-Arndt University, Greifswald, GERMANY; [4]Charité – CCM, University Berlin, Berlin, GERMANY.

**12:00P – 12:15P**
075 ULTRASOUND ELASTOGRAPHY OF SKIN UNDER SURFACE EXTENSIVE LOADING.
*L Coutts[1], JC Bamber[1]*, NR Miller[1].*
[1]Institute of Cancer Research, Sutton, Surrey, England, UK.

**12:15P – 1:45P**
GROUP LUNCH Travis Restaurant

## Wednesday 1:45P – 3:30P
## Session MPT: Mechanical Properties of Tissues
*Chair: SF Levinson, USA* *Co-Chair: C Sumi, Japan* Rio Grande I

**1:45P – 2:00P**
047 DIFFERENTIATING MECHANICAL PROPERTIES OF CORNEAL PHANTOMS USING AN ULTRASOUND METHOD.
*J Liu[1]*, CJ Roberts[1], X He[1].*
[1]The Ohio State University, Columbus, OH, USA.

**2:00P – 2:15P**

010 ACOUSTOELASTICTY TO BIOLOGICAL TISSUES: MEASUREMENT OF REFLECTION COEFFICIENT CHANGE IN TENDONS UNDER DIFFERENT TENSILE STRAINS.
*H Kobayashi[1], A Oza[1]*, R Vanderby[1].*
[1]University of Wisconsin-Madison, Madison, WI, USA.

**2:15P – 2:30P**

011 ACOUSTOELASTICTY IN BIOLOGICAL TISSUES: ULTRASOUND WAVE VELOCITY CHANGE IN COMPRESSED TISSUES.
*H Kobayashi[1]*, A Oza[1], MS Cooper[2], R Vanderby[1].*
[1]University of Wisconsin-Madison, Madison, WI, USA; [2]Portage Veterinary Clinic, Portage, WI, USA.

**2:30P – 2:45P**

034 NONCONTACT ULTRASOUND INDENTATION SYSTEM FOR ASSESSING BONE-TENDON JUNCTION TISSUES: PRELIMINARY RESULTS.
*MH Lu[1], YP Zheng[1]*, HB Lu[2], QH Huang[1], L Qin[2].*
[1]The Hong Kong Polytechnic University, Hong Kong, CHINA; [2]Chinese University of Hong Kong, Hong Kong, CHINA.

**2:45P – 3:00P**

062 MECHANICAL MEASUREMENT OF ELASTIC PROPERTIES OF BOVINE LIVER AND HUMAN PROSTATE UNDER COMPRESSION.
*M Zhang[1]*, ZC Wu[1], DJ Rubens[2], KJ Parker[1].*
[1,2]University of Rochester, Rochester, NY, USA.

**3:00P – 3:15P**

069 VISCOELASTIC AND ULTRASONIC PROPERTIES OF THE UTERUS.
*MZ Kiss[1]*, T Varghese[1,2], MA Hobson[1], MA Kliewer[3], J Harter[4], EM Hartenbach[5].*
[1,2,3,4,5]University of Wisconsin-Madison, Madison, WI, USA.

**3:15P – 3:30P**

105 EVALUATION OF ANISOTROPY IN THE NORMAL PLANTAR SOFT TISSUES: SHEAR MODULUS FOR SHEARING DEFORMATION AND COMPRESSIVE DEFORMATION.
*JB Weaver[1]*, TB Miller[2], MM Doyley[1], PR Perrinez[2], H Wang[2], YY Cheung[1], JS Wrobel[3,4], FE Kennedy[2], KD Paulsen[2].*
[1]Dartmouth-Hitchcock Medical Center, Lebanon, NH, USA; [2]Dartmouth College, Hanover, NH, USA; [3]VA Medical Center, WRJ, VT, USA; [4]Dartmouth Medical School, Hanover, NH, USA.

**3:30P – 4:00P**

COFFEE BREAK — Rio Grande Foyer

## Wednesday 4:00P – 5:30P

## Session MIP-3: Methods for Imaging Elastic Tissue Properties – III

*Chair: YP Zheng, China* *Co-Chair: J Liu, USA* — Rio Grande I

**4:00P – 4:15P**

085 DIRECT INVERSION METHOD FOR SHEAR WAVE SPEED RECONSTRUCTION IN ELASTOGRAPHY.
*K Lin[1]*, JR McLaughlin[1].*
[1]Rensselaer Polytechnic Institute, Troy, NY, USA.

**4:15P – 4:30P**

015 ISSUES IN REAL-TIME ACOUSTIC RADIATION FORCE IMPULSE IMAGING.
*GE Trahey[1]*, GF Pinton[1], ML Palmeri[1], RR Bouchard[1], JJ Dahl[1].*
[1]Duke University, Durham, NC, USA.

(Session MIP-3 continues on next page)

**4:30P – 4:45P**

073 *IN VITRO* MEASUREMENT AND IMAGING OF THE STRAIN AT THE BOVINE ACL-BONE INSERTION.
*EE Konofagou[1]*, JP Spalazzi[1], SD Fung-kee-Fung[1], HL Lu[1].*
[1]Columbia University, New York, NY 10027, USA.

**4:45P – 5:00P**

096 FFT ANALYSIS OF THE PERIODIC STRUCTURES IN HAVERSIAN BONE BASED ON SCANNING ACOUSTIC MICROSCOPY (SAM).
*JL Katz[1,2]*, A Misra[2], O Marangos[2], Y Wang[1], P Spencer[1].*
[1,2]University of Missouri-Kansas City, Kansas City, MO, USA.

**5:00P – 5:15P**

108 SHEAR STIFFNESS IDENTIFICATION USING MOVING INTERFERENCE PATTERNS IN SONOELASTOGRAPHY.
*JR McLaughlin[1], D Renzi[2]*.*
[1,2]Rensselaer Polytechnic Institute, Troy, NY, USA.

**5:15P – 5:30P**

014 ASSESSMENT OF MECHANICAL PROPERTIES OF PVA-C WITH FOUR DIFFERENT ELASTOGRAPHIC METHODS.
*JL Gennisson[1]*, J Fromageau[1], C Schmitt[1], RL Maurice[1], R Mongrain[2], G Cloutier[1].*
[1]University of Montréal Hospital, Montréal, Québec, CANADA; [2]McGill University, Montréal, Québec, CANADA.

## Session EEX: Equipment Exhibit

Rio Grande II

*Hitachi Medical Corporation.*
Kashiwa, JAPAN.

*Siemens Medical Solutions Ultrasound Group.*
Issaquah, WA, USA.

*Ultrasonix Medical Corporation*
Burnaby, BC, CANADA.

5:30P – 6:30P *No Conference Activities*

## Wednesday 6:30P – 9:30P

## Open House

*Proceedings Book Signing*

# AUTHOR INDEX

# AUTHOR INDEX

# ABSTRACTS

Fourth International Conference
on the Ultrasonic Measurement and Imaging
of Tissue Elasticity©

Lake Travis, Austin, Texas, USA
October 16–19, 2005

## Guest Lecture

000 **LESSONS FROM THE WORLD OF MEDICAL DEVICE COMMERCIALIZATION.**

*Youseph Yazdi*[1]*.

[1]Corporate Office of Science & Technology, Johnson & Johnson, 410 George Street, New Brunswick, NJ 08901, USA.

Considerable time and money have been spent on healthcare-related research funded by public and private sources. We live in a time that is rich with new scientific discoveries and technological advances, but the translation of these developments into clinically useful therapies is arguably lagging.

This presentation will focus on the trials and tribulations of moving great ideas from a glimmer in the mind of the inventor to the hands of the physicians. Along the way, some lessons learned for those eager to see their ideas put to practical use will be described.

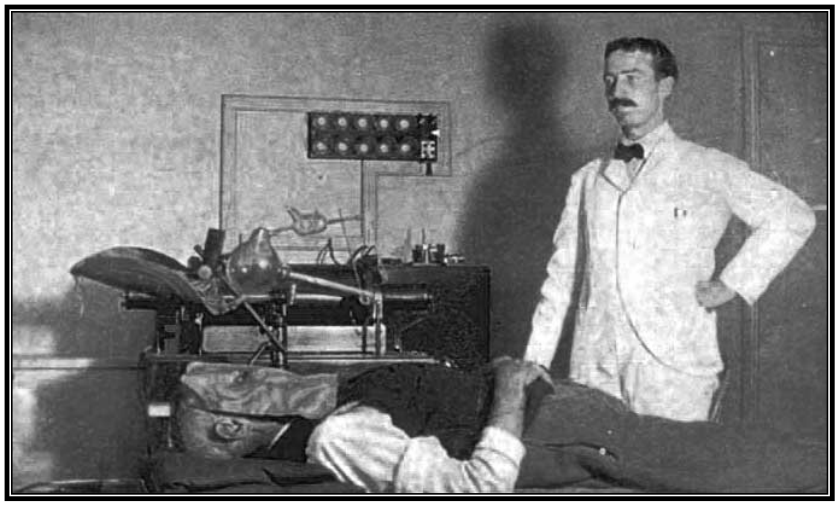

*Youseph Yazdi, Ph.D., is currently Director, Science & Technology, in the Johnson & Johnson Corporate Office of Science & Technology (COSAT). Dr. Yazdi looks for new scientific and technological breakthroughs that will lead to the medical devices of tomorrow. His technology focuses are on MEMS, nanotech, neurotech, energy-based therapeutics and imaging. He is also a member of the Tech Transfer & Academic Relations team working to improve Johnson & Johnson's outreach to academic/clinician scientists and inventors. Other duties include promoting scientific excellence and collaboration within the corporation and identifying new growth areas for J&J. Prior to joining COSAT, Dr. Yazdi held positions in R&D and Business Development at Johnson & Johnson's Ethicon Endo-Surgery division. Dr. Yazdi graduated from Rice University with the B.S. in Electrical and Computer Engineering and earned his M.S. and Ph.D. degrees from The University of Texas at Austin. His academic research interests were mainly in Optical and Ultrasonic Tissue Characterization.*

117 **IMAGING SHEAR STIFFNESS TISSUE PROPERTIES USING INVERSE METHODS WHEN MEASUREMENTS ARE TIME DEPENDENT.**

*Joyce R. McLaughlin*[1]*.
[1]Rensselaer Polytechnic Institute, 110 8th Street, Troy, NY 12180, USA.

The goal of this tutorial is to present an overview of inverse methods that can be used to image soft tissue shear stiffness from time dependent tissue displacements. The targeted experiments include supersonic imaging, transient elastography, 'crawling' and 'holographic' waves in sonoelasticity, and single frequency wave motion measured with ultrasound or MR. In all of these experiments, images of the amplitude of the wave can be made; this imaging technique does not utilize inverse methods and can provide a reasonable image when the change in biomechanical properties or the region over which the change occurs is large. The use of inverse methods enables us to take shear stiffness imaging 'to the next level' targeting specific stiffness properties as well as small, either in amplitude or size, biomechanical changes; the methods can be applied to phantom, *in vitro* and *in vivo* data sets.

There are a number of distinct parts of an inverse method:
(1) the first is that a mathematical model or equation is formulated so that the measured data can reasonably be predicted as the solution of the equation;
(2) some of the functions in the model, such as the elastic Lamé parameters, Young's modulus, or the shear wave speed are unknown; at least one of these quantities is targeted to be imaged;
(3) after determining that the data set, or sometimes even a subset of the data set, is rich enough to determine all the targeted quantities, then algorithms are developed that most effectively utilize the data (sub)set and that are stable when noise is present in the data.

This is a major challenge. For the time-dependent data sets targeted in this tutorial we review:
(a) Methods that utilize the propagating front of a wave or the phase to determine shear wave or phase wave speed. We include the mathematical model and descriptions of how correlation and optimization methods can be used to find the front positions, or lines of constant phase: we also describe direct methods and the arrival time algorithm to determine the wave speed in each case.
(b) Methods that utilize the time Fourier Transform of the data. This procedure divides the data set by its frequency content where sometimes multiple frequency contents are significant enough to be used in an inverse algorithm. A broad set of algorithms have been implemented here including direct methods, methods based on finite element formulations and methods that utilize statistical methods. In all cases, derivatives of data must be taken, and we include discussion about stable methods for these calculations.

**Acknowledgments:** McLaughlin directs IPRPI, the Inverse Problems Center at RPI. She and her collaborators and working group members are funded by NIH, ONR and NSF.

116 **INFERRING BIOMECHANICAL PROPERTIES FROM QUASISTATIC DEFORMATIONS: AN INTRODUCTION TO ASSOCIATED INVERSE PROBLEMS.**

*Paul E. Barbone*[1]*.
[1]Boston University, Boston, MA 02215, USA.

We consider the problem of quantifying biomechanical properties of soft tissues from ultrasound measurements of quasistatic deformation. Techniques developed in the context of elastography allow the measurement *in vivo* of tissue deformations. Given these measured deformations, then, an inverse problem to determine the biomechanical properties of the tissue can be formulated.

This tutorial addresses the "What, when, how and who" of this inverse problem in the context of quasistatic deformation.

**What is the problem to be solved?** The inverse problem depends on the mathematical model used to predict the deformation of tissue being observed. For example, one researcher might use a one-dimensional nonlinear uniaxial stress model; another might use a linear plane-stress model. In the first part of this tutorial, we discuss which basic physical assumptions underlie each mathematical model. This knowledge makes clear which physical phenomena are captured and ignored by the various models considered.

**When can the problem be solved?** Depending upon the complexity of the mathematical model chosen to represent the tissue behavior, there may not be enough information in the measured deformation field to determine all the parameters in the model (i.e. the answer is nonunique). On the other hand, it may be the case that the measured deformation field has too much inconsistent information, so that no set of material properties explains all the observations (i.e. no answer exists). The second part of this tutorial discusses the conditions under which different inverse problems resulting from different mathematical models can give reliable solutions.

**How can the problem be solved?** The third part of the tutorial discusses algorithms and methods to solve the inverse problem. The typical iterative approach requires three steps:

(1) computing a predicted displacement,
(2) checking similarity between measured and predicted displacements,
(3) updating the material properties, and then iterating.

All three of these steps deserve careful attention in practice, and we discuss the considerations in each case.

**Who has solved the inverse problem so far?** In the fourth part of the tutorial, we shall review approaches taken by several researchers in the field and attempt to draw lessons from their collected experience.

**Acknowledgments:** It is a pleasure to acknowledge the tutelage and collaboration of Dr. Jeffrey C Bamber, Professor Assad Oberai, and the BU Biomechanical Imaging Team: Michael Richards, Nachiket Gokhale, Ricardo Leiderman and Carlos Rivas. This work has been supported in part by CenSSIS (The Center for Subsurface Sensing and Imaging Systems) under the Engineering Research Centers Program of the National Science Foundation (Award No. EEC-9986821) and the Department of Defense Breast Cancer Research Program (Award No. W81XWh-04-1-0763).

006 **3D SIMULATION MODELS FOR ULTRASOUND ELASTOGRAPHY.**

*A. V. Patil[1,2]*, T. A. Krouskop[3], J. Ophir[1,2], S. Srinivasan[2,4].*
[1]University of Houston, Electrical Engineering Department, Houston, TX, USA; [2]University of Texas Medical School, Diagnostic and Interventional Imaging Department, Houston, TX, USA; [3]Baylor College of Medicine, Houston, TX, USA; [4]Siemens Acuson, Mountain View, CA, USA.

**Aim:** Previously reported work evaluated the performance of ultrasound elastography using 1D and 2D simulation models. However, elastography is inherently a 3D problem. This implies that the nature of the ultrasound pulse used to image the tissue and the tissue motion, which results from the application of the external compression, is three-dimensional. This work evaluates the elastographic image quality using realistic 3D geometry and 3D motion conditions.

**Background:** 2D simulation models lead to over optimistic estimation of elastographic image quality (signal-to-noise ratio ($SNR_e$), contrast-to-noise ratio ($CNR_e$), and spatial resolution). The 2D models (elevationally narrow ultrasound beam and cylindrical inclusions) and assumptions like plane strain conditions are inadequate to model the realistic 3D conditions. For homogeneous, isotropic, and incompressible tissue, the elevational motion due to the external compression results in approximately one fourth of the axial motion. Coupled with the factor of an unknown elevational beam width this elevational motion results in a subsequent degradation of the axial elastographic image quality. The elevational motion increases as one traverses away from the scan plane symmetry, which leads to a further degradation in the image quality. This means that the strain filter and consequently the $CNR_e$ filter are non-stationary in the elevational direction as they are in the lateral and the axial directions. However, the non-stationarity is expected to be more pronounced in the elevational direction than the in axial and the lateral directions due to the sampling limitations in the elevational direction.

**Methods:** Simulations were performed using 2D and 3D acoustical and mechanical models. A sphere was used to model the inclusion in 3D, whereas a 2D inclusion was modeled as a cross-section of a cylinder. The enclosing matrix in 2D was a rectangle (40x40 $mm^2$), whereas in 3D it was a cube (40x40x40 $mm^3$). The inclusions, in both the 2D and 3D cases, had a cross-sectional radius of 2.5 mm. The simulations were performed at a 5 MHz center frequency and sampling frequency of 48 MHz. The RF data were modeled as a 3D convolution of the impulse response of the tissue scatterer function (TSF) and the system point spread function (PSF). The TSF was modeled as a random normal distribution of the point scatterers. The PSF was modeled as a Gaussian modulated cosine pulse with 50% fractional bandwidth. A two-stage hybrid (adaptive displacement + staggered strain) estimator was used to generate elastograms. The elastograms obtained from the 2D and 3D models were compared using established image quality factors such as, $SNR_e$, $CNR_e$ and spatial resolution.

**Results:** The elastograms obtained from the 3D models had poorer image quality than the elastograms obtained from the 2D models, for an applied strain range of 0.7- 8%. The $CNR_e$ and the $SNR_e$ curves obtained from the 3D models were statistically lower than those obtained from the 2D models for an applied strain range of 0.7-8%. Also, the difference between the $CNR_e$ curves of the 2D and 3D models increased as the modulus contrast ratio between the inclusion and the background decreased from 10-1.5. The elastographic image quality degraded as the scan plane shifted away from the axes of the elevational symmetry. The degradation in image quality with increasing elevational shift was nonlinear. The detectability of the inclusion was poorer in the 3D model elastograms than in the 2D model elastograms. On an average (50 realizations), the inclusions of same size looked smaller in 3D than 2D model elastograms. The effect can be attributed to the averaging effect of the elevational beamwidth, which is not incorporated in 2D simulations. The estimated axial and the lateral resolutions of the 2D and the 3D model elastograms were statistically similar. However, at larger beam-ratios (elevational to the lateral beamwidth), the estimated axial and the lateral resolutions of the 3D model elastograms were significantly worse than those of the 2D model elastograms.

**Conclusions:** 2D simulations make overoptimistic estimation of the elastographic image quality and, hence, it may not be appropriate to use 2D simulation models to evaluate the performance of ultrasound elastography for interesting cases of small (< 1.5 mm) and low contrast targets (modulus contrast < 2).

**Acknowledgement:** Supported by NIH Program Project Grant PO1-CA64597-12 to the University of Texas.

012 **PRELIMINARY RESULTS OF ELASTICITY IMAGING TO AORTIC PLAQUE.**

*Takashi Osaka[1]*, Takeshi Matsumura[1], Tsuyoshi Mitake[1], Satoshi Nakatani[2], Tsuyoshi Shiina[3].*
[1]Research and Development Center, Hitachi Medical Corporation, Chiba, JAPAN; [2]Cardiology Division, National Cardiovascular Center, Osaka, JAPAN; [3]Graduate School of Systems and Information Engineering, University of Tsukuba, Ibaraki, JAPAN.

**Background and Aims:** In general, it is well known that cancer tissue becomes harder compared with other normal tissues. Our group has developed a real-time tissue elastography imaging system and continued to evaluate its clinical usefulness for application to organs such as the mammary gland, the prostate, the thyroid and other areas. In this paper, we report preliminary clinical results for aortic plaque.

**Methods:** RF image frames are transferred from the ultrasound scanner to an external PC, and these data frames are reconstructed into elasticity (strain) images with about 12 fps throughput on the PC. Additional signal and image processing is also accomplished in the PC in off-line mode. Strain images are obtained by differentiating displacements between neighboring frames. A special feature of the reconstruction algorithm that we use is based upon the "Combined Autocorrelation Method", that is, inter-frame displacements greater than a wavelength are estimated by envelope correlation in addition to the usual precise autocorrelation method to detect change of phase [1].

For application to the aorta, a transesophageal echocardiography probe (TEE) is used to get RF image frames via the esophagus, and the variation of aortic blood pressure is used as the compression force without the need for any external compression devices.

The color-coded elasticity (strain) images are overlaid on the usual B-mode images in a translucent style. Here, harder areas are depicted in blue and softer areas in red, with intermediate hardness displayed in green.

System details:
- Ultrasound Scanner System: Hitachi EUB-8500
- External PC: Dell PowerEdge SC1420(3.2GHz Xeon Dual CPU Type)
- Probe: EUP-ES52M (Central Frequency 5.0MHz)

**Preliminary Results:** The patient was a 71 year old male. The plaque is about 2-3mm thick and is confined in the arrowed region in the transverse-axis B-mode TEE image. The corresponding tissue strain image obtained using our elastography system shows blue color in the arrowed region. This result suggests that the plaque might be a hard plaque and doesn't have potential for abrupt separation. This result encourages us to apply our system to more clinical study and also extend its application to other arterial diseases, e.g., arterial sclerosis.

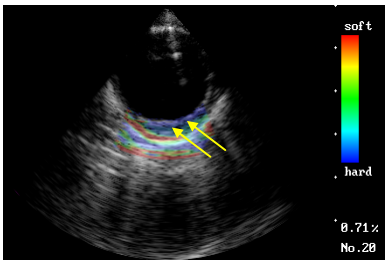


Figure1: Strain Imaging of Aortic Plaque

**Reference:**

[1] T. Shiina, M.M. Doyley, J.C. Bamber, "Strain Imaging Using Combined RF and Envelope Autocorrelation Processing", Proc. of 1996 IEEE Ultrasonics Symp. 1331-1336, 1997.

016 **TWO-STEP CROSS-CORRELATION METHOD TO IMPROVE IMAGE QUALITY IN ELASTOGRAPHY.**

*Hao Chen[1]*, Hairong Shi[2], Tomy Varghese[2,3].*
[1]Electrical and Computer Engineering, [2]Medical Physics, [3]Biomedical Engineering Departments, University of Wisconsin-Madison, 1300 University Avenue, 1530 MSC, Madison, WI 53706, USA.

**Aims:** We propose a new approach that enables the use of window lengths on the order of 1-2 wavelengths that provide strain estimates with similar noise properties as to those obtained with a 10-wavelength window using a two-step technique.

**Background:** Traditional cross-correlation based strain estimation methods require a window length of at least 10 wavelengths to obtain reliable strain estimates. Shorter window lengths generally incur more signal decorrelation with the subsequent strain estimates more contaminated with noise artifacts.

**Methods:** The first processing step utilizes a window length on the order of 10-20 wavelengths to obtain coarse displacement estimates between the pre- and post- compression radio frequency data frames. This coarse displacement is then interpolated and utilized as the initial guess-estimate for the second processing step in the strain estimation. During the second step of the cross-correlation estimation, the post- compression window segment length on the order of 1-2 wavelengths is shifted to the initial coarse displacement position, and a final displacement estimate obtained.

**Results:** Our results demonstrate that we can easily reduce the window length during the second step of the processing down to 1~2 wavelengths (about 0.2~0.4 mm for 7.5 MHz transducer), without incurring significant errors in the strain estimates. Signal-to-noise and contrast-to-noise ratio estimates are also significantly improved at the smaller window lengths with the two-step processing when compared to the use of a similar sized window in the traditional method. The selection of first step window length also does not have a major impact on the results.

**Conclusions:** The new processing method provides a significant improvement in the axial resolution of the strain estimates in the elastograms due to the small window lengths utilized and the potential of obtaining closely spaced strain estimates.

**Acknowledgements:** This work was supported by NIH grant R21 EB003853.

021 **REGULARIZATION ISSUES IN YOUNG'S MODULUS RECONSTRUCTION.**

*J Jiang[1]*, T J Hall[1].*
[1]Medical Physics Department, University of Wisconsin-Madison, Madison, WI, USA.

**Aims:** This investigation compares three well-known regularization approaches, namely total variation regularization [1], Laplacian smoothing regularization [2] and Tikhonov regularization [3], in the framework of inverse elasticity problems. The mathematical nature of regularization, bias and variance of results, and computational efficiency were also analyzed.

**Background:** Tissue modulus imaging reveals intrinsic tissue properties that are otherwise unavailable thereby aiding analysis of tissue during the pathological evolution of disease and treatment. Unfortunately, Young's (or shear) modulus reconstruction is a nonlinear inverse problem that may be ill-posed. The goal of regularization is to use constraints on the computational problem to obtain a physically meaningful solution for ill-posed problems.

**Methods:** Three regularization methods were implemented in conjunction with an iterative modulus reconstruction approach. In this study, a direct inversion method based on the finite element method (FEM) [4] was used as an extreme case to demonstrate the effect of no regularization. Experiments with a computer-simulation phantom are reported to demonstrate the importance of regularization and selection of the regularization parameters. Specifically, we utilized simulated displacement data from a two-dimensional finite element model, where a cluster of four circular inclusions (6mm in diameter) were embedded into a uniform background (40mm square), with an additive displacement noise. The elasticity contrast between the inclusions and background was 3:1.

**Results:** Preliminary results demonstrate that the appropriate regularization is important to obtain good quality modulus estimates. For instance, Zhu et al.'s approach [4] appears to be more efficient and accurate when the displacement estimates have very high signal-to-noise ratio (SNR, e.g. >50dB). However, iterative regularized modulus reconstruction methods are necessary to obtain good results with lower SNR (e.g. <20dB). In addition, the total variation regularization is robust to noise and improves resolution in modulus images by preserving sharp boundaries.

**Conclusions:** Results suggest that the total variation regularization is superior to the Tikhonov and Laplacian regularization methods for the data investigated. The bias error and variance in modulus estimates are small compared to typical elasticity contrast (e.g. >3:1).

**Acknowledgements:** We are grateful for the support from the USAMRMC (DAMD17-00-1-0596), the NIH (CA100373), and the University of Wisconsin.

**References:**

[1] C. R. Vogel and M. E. Oman, "Fast, robust total variation-based reconstruction of noisy, blurred images," *IEEE Transactions on Image Processing*, vol. 7, pp. 813-824, 1998.
[2] A. A. Oberai, N. H. Gokhale, and G. R. Feijoo, "Solution of inverse problems in elasticity imaging using the adjoint method," *Inverse Problems*, vol. 19, pp. 297-313, 2003.
[3] F. Kallel and M. Bertrand, "Tissue elasticity reconstruction using linear perturbation method," *IEEE Transactions on Medical Imaging*, vol. 15, pp. 299-313, 1996.
[4] Y. Zhu, T. J. Hall, and J. Jiang, "A finite-element approach for Young's modulus reconstruction," *IEEE Transactions on Medical Imaging*, vol. 22, pp. 890-901, 2003.

022 **SIGNIFICANT CLINICAL RESULTS IN THE DIAGNOSIS OF BREAST LESION BY MEANS OF REAL–TIME ELASTOGRAPHY.**

*Anke Thomas[1], Sherko Kümmel[1], Holger Frey[2]*, Glen Kristiansen[1], Thomas Fischer[1].*
[1]Charité – CCM, University Berlin, Berlin, GERMANY; [2]Hitachi Medical Systems, Wiesbaden, GERMANY.

**Aims:** The goal of the study consisted of testing the suitability of the method for breast tumour diagnosis in clinical practice.

**Background:** Real-time elastography was carried out in 108 candidate patients with histologically confirmed findings as a new, non-invasive method for the diagnosis of mammary carcinoma.

**Methods:** Differences between normal and tumour tissue were visualised by measurements of elasticity properties, based on the elastic deformability of tissue after probe pressure. The study contained 108 female potential breast cancer patients with histologically confirmed focal signs (58 benign, 50 malignant) in the age range of 16 to 84 years old. Evaluation was made with the real-time elastography method (Hitachi EUB 8500) and was colour-coded and superimposed on the ultrasound scan in brightness mode (B-mode). The results were compared with the data of previous ultrasound investigations and histology and were statistically assessed with the aid of matrices and ROC curves. The ultrasound classification was based on BIRADS and input from Ei Ueno, MD. A second examiner was employed, in order to evaluate the objectivity of the method.

**Results:** The study showed that the correspondence between elastography and ultrasound in the BIRADS classification of mammary carcinoma was good. Assessment in McNemar's Test gave a weighted kappa of 0.5565 – 0.7751. Benign tissues were recognised with certainty, although malignant findings resulted in significant differences compared to the histological results which were moreover dependent on the examiner ($p = 0.008/0.012$). Overall, elastography possesses a sensitivity of 91% and a specificity of 83%. The area under the curve (AUC) gave 0.93 for ultrasound and 0.87 for the elastography. Both methods together showed in the ROC curve a greater AUC (0.94), but it is not significant.

**Conclusions:** The conclusion is that measurement of tissue elasticity by means of real-time elastography combined with the familiar B image improves diagnosis of breast lesions. Additionally, the method can be integrated easily into daily clinical practice.

028 **SONOELASTOGRAPHY OF THE TESTICLES: PRELIMINARY RESULTS IN THE DIAGNOSIS OF DIFFERENT PATHOLOGICAL PROCESSES.**

*L Pallwein[1]*, E Pallwein[1], M Schurich[1], V Fischbach[1], H Steiner[2], F Frauscher[1].*
[1]Radiology, [2]Urology Departments, Medical University, Innsbruck, AUSTRIA.

**Aims:** To assess the value of sonoelastography in the differential diagnosis of inflammatory and neoplastic disease of the testicles.

**Background:** In a patient with acute scrotal pain and swelling, the differentiation of neoplastic from inflammatory processes in the testicles can be difficult and usually a biopsy is required. Elastography of the testicles may improve the detection of areas with increased stiffness which are suspicious for neoplastic changes and, therefore, may also improve the differentiaton between neoplastic and inflammatory processes.

**Methods:** In 15 patients suffering from scrotal pain and swelling, a routine US examination (B-mode and color Doppler US) was performed (Acuson Sequoia, Mountainview, Ca, USA). All patients underwent an additional qualitative measurement of tissue elasticity by using sonoelastography (Hitachi EUB-8500). These exams were performed by a different uroradiologist, who was blinded to the results of routine sonography. The stiffness of the lesion was displayed from red (soft) to blue (hard). Hard lesions were considered as malignant. The diagnostic outcome of the two examinations was compared in each patient.

**Results:** In 7 patients, routine US was able to detect testicular masses of different size, which were histologically proven to be neoplastic lesions of different types (germ cell tumor, seminoma, teratoma, mixed tumors and sarcoma of the tunica albuginea in one case). Elastography was able to detect all these lesions and enabled the detection of two additional lesions that were not well circumscribed in a patient suspected to have tumor recurrence in a single testis. Elastography was also able to differentiate between inflammatory changes and testicular swelling in a patient suspected of diffuse lymphomatous infiltration based on the differences in tissue stiffness. Inflammatory processes of the testicles showed normal to decreased tissue stiffness in the suspected areas.

**Conclusions:** Our preliminary findings showed that in patients with diffuse scrotal swelling and pain, the sonoelastography improved the detection of testicular masses and allow the differentiation of inflammatory changes from other pathological processes based on the differences in tissue elasticity.

040 **SIMULATION STUDY OF RECONSTRUCTION OF SHEAR MODULUS, DENSITY, POISSON'S RATIO DISTRIBUTIONS – 2ND REPORT.**

*Chikayoshi Sumi[1]*.*
[1]Sophia University, 7-1 Kioicho, Chiyodaku, Tokyo 102-8554, JAPAN.

**Aims:** Previously, we proposed 3D and 2D methods to reconstruct the Poisson's ratio distribution as well as shear modulus [1]. Furthermore, we proposed to reconstruct density distribution as well to allow dealing with dynamic deformation [1]. However, due to tissue incompressibility, reconstruction of shear modulus, Poisson's ratio, and density become unstable. In this report, to stabilize these reconstructions, we report a new reconstruction method using mean normal stress as the unknown [2]. This method also allows stable reconstruction of shear modulus and density under the condition that Poisson's ratio remains unknown. The effectiveness is verified through 3D simulations.

**Methods:** By measuring the acceleration vector $\alpha_i$ (i = 1-3) and the strain tensor $\varepsilon_{ij}$ (i,j = 1-3) throughout the 3D ROI, motion equations are dealt with as the simultaneous first order partial differential equations for unknown distributions of the Lame's constants of $\lambda$ and shear modulus $\mu$ and density $\rho$, i.e.,

$$\rho\alpha_i = (\varepsilon_{\alpha\alpha}\lambda)_{,j}\,\delta_{ij} + 2\varepsilon_{ij}\mu_{,j} + 2\varepsilon_{ij,j}\mu \qquad \text{(Equation 1)}$$

Provided that the reference values of the Lame's constants are given in the ROI, this reconstruction problem becomes an initial-values problem for the unknown Lame's constants and density distributions. To yield the reference value of $\lambda$, the reference value of the Poisson's ratio $\nu$ can be set in the ROI.

However, since almost soft tissues are considered to be incompressible ($\nu\rightarrow0.5$; $\varepsilon_{\alpha\alpha}\rightarrow0$), volume strain $\varepsilon_{\alpha\alpha}$ generated in soft tissues is very small. This causes reconstruction of Lame's constants to be unstable. Thus, by dealing with the mean normal stress $p(=\varepsilon_{\alpha\alpha}\lambda)$ as unknown in Equation 1 instead of $\lambda$, we realize stable reconstruction of shear modulus, $\mu$. In this new method, the reference (initial) values might be set for both of shear modulus and mean normal stress (reference is needless for density). However, since it is difficult to directly measure the mean normal stress, when reference region is incompressible ($\nu\rightarrow0.5$; $\lambda\rightarrow\infty$), the reference value of mean normal stress p cannot be set. Furthermore, neither Poisson's ratio nor mean normal stress might be reconstruction targets. In these cases, we determine only shear modulus under the condition that the mean normal stress remains unknown. As we utilize the iterative method (specifically, conjugate gradient method) to solve this problem for shear modulus and mean normal stress, by setting only reference shear moduli we stably obtain a unique shear modulus reconstruction and biased mean normal stress reconstruction (dependent on the initial distribution (value) used for the iterative method). If homogeneous region of $\lambda$ exists in the ROI, reference region of $\lambda$ can be set into the region, and the reference value set at an arbitrary value and volume strain are also used. When the tissue is not incompressible and Poisson's ratio $\nu$ (or $\lambda$) is target as well, reference of Poisson's ratio need to be set. Reference density can also be used instead of reference shear modulus [2]. In order to cope with occurrence of the improper configurations and noise-contamination, regularization is performed respective for unknown mechanical properties distributions.

**Results:** The cubic phantom (50mm sides) includes a spherical inclusion (radius 5mm) at the center (depth 25.0mm) having twice as high a shear modulus as that of the surrounding medium, i.e., 2.0H105N/m$^2$ vs. 1.0H105N/m$^2$. The Poisson's ratio of the inclusion is 0.4, while the value of the surrounding medium is 0.47. Density is uniformly 1.0g/cm$^3$. Noise-filled measurement data of displacement vector were simulated by adding white noise to the calculated raw displacement vector data. Regularization yields stable quantitative reconstructions. Figures 1a and 1b respectively show regularized and non-regularized shear modulus reconstructions obtained (i) without reference value of mean normal stress (mean values at central square region (5.0mmH5.0mm), 1.76 vs. 1.84), while Figures 1c and 1d respectively show regularized and non-regularized Poisson's ratio reconstructions obtained (ii) with reference value of mean normal stress (mean values, 0.416 vs. 0.396) (density omitted).

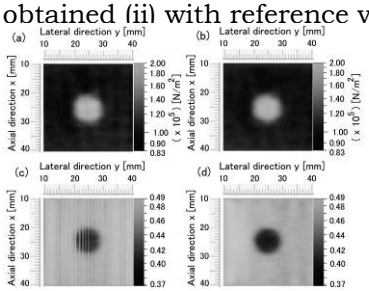

Figure 1: Reconstructions

**Conclusions:** The developed method realizes stable reconstruction.

**References:**

[1] Sumi, "Simulation study of reconstruction of shear modulus, density, Poisson's ratio distributions," Proc. 3rd Int. Conf. Ultrason. Meas. Imag. Tissue Elasticity, p. 88, 2004.
[2] Sumi, "Reconstruction of shear modulus distribution together with Poisson's ratio distribution and Density Distribution," Proc. of IEEE EMBS Conf (CD-ROM), Sep 2005.

* *indicates Presenter*

042 **THERMAL PROPERTIES RECONSTRUCTION BASED ON TEMPERATURE MEASUREMENT - 2ND REPORT.**

*Chikayoshi Sumi[1]*.*
[1]Sophia University, 7-1 Kioicho, Chiyodaku, Tokyo 102-8554, JAPAN.

**Aims:** At the last conference, we reported methods to reconstruct thermal properties such as conductivity, capacity and diffusivity in addition to the mechanical properties for diagnosis and treatment (planning). Temperature distribution can be measured by ultrasonic imaging and MRI. Provided that the reference values of thermal properties are given in the ROI as initial conditions, by solving the simultaneous first order partial differential equations (heat transfer equations) having the heat flux field as inhomogeneous coefficients, we can determine the thermal properties distributions. In this report, we focus on non-steady case, in which respective thermal properties distributions are regularized using different regularization parameters. To verify the feasibility of the method, simulations and ultrasonic phantom experiments were conducted [1].

**Methods and Results:**

*(1) Simulations*: Our 3D techniques were evaluated using a cubic phantom (50.0mm sides) containing a central spherical region (diameter=5.0mm) which had twice as high conductivity and specific heat as those of the surrounding medium, i.e., 1.0 vs. 0.5W/(mK), and 8,400 vs. 4,200J/(KKg). The uniform density was 1,000 kg/m$^3$. A cubic ROI (30.0mm sides) was set at the center of the phantom. The phantom temperature was a uniform 36.0ºC. One surface was fixed at 36.0ºC, and the temperature of the opposite surface was heated with 46.0ºC stepwise. The following two cases were dealt with.

(Case 1) Figure 1 shows the reconstructed conductivity, capacity, diffusivity (bird's eye views of z = 25.0mm) obtained using two pairs of subsequent temperature distributions (1,000sec and 2,000sec, surface of x = 0.0mm was heated). The proper reference region was set at the surface of the ROI having higher temperatures. As shown, the thermal properties were stably reconstructed.

(Case 2) Reconstructions were stably obtained using two paired subsequent temperature distributions generated by different heat source positions, i.e., temperatures having opposite heat fluxes generated by respectively heating opposite surfaces (surfaces of x = 0.0mm and x = 50.0mm). The reference region was set at the surface of the ROI, i.e., x = 10.0mm.

Table I summarizes means of the conductivity, capacity, and diffusivity evaluated at the central square region (5.0H5.0mm) of the spherical region. In both cases, the thermal properties were quantitatively evaluated.

*(2) Phantom experiments:* An agar phantom (height=50mm) was used (3.87%). A cylindrical inhomogeneous region (diameter=15mm) was made at the depth of 25mm using small amount of copper powder. The phantom was heated by hot water from the under side. Temperature was measured using our previously developed phase matching method by measuring generated strains due to thermal effect. In Figure 2, (a) B-mode image, (b) measured temperature (strain), (c) conductivity, (d) capacity, (e) diffusivity are shown. The inhomogeneous region was detected in these images (mean value of square region of 6.5H5.8mm vs. reference value: conductivity, 0.700 vs. 0.625W/(mK); capacity, 3.18 vs. 4.20H10$^6$J/(m$^3$K); diffusivity, 2.20 vs. 1.49H10$^{-7}$m$^2$/s).

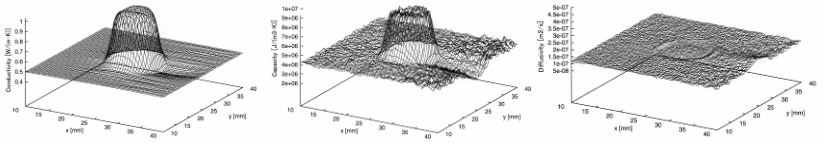

Figure 1: Reconstructions of Thermal Conductivity, Capacity, Diffusivity (Case 1)

| Case | $k$ $[W/(m \cdot K)]$ | $\rho c$ $(\times 10^6)$ $[J/(m^3 \cdot K)]$ | $k/\rho c$ $(\times 10^{-7})$ $[m^2/s]$ |
|---|---|---|---|
| Original | 1.00 | 8.40 | 1.19 |
| 1 | 1.01 | 8.59 | 1.18 |
| 2 | 1.05 | 9.01 | 1.17 |

Table I: Mean Values of Thermal Conductivity $k$, Capacity ρc, Diffusivity k/ρc.

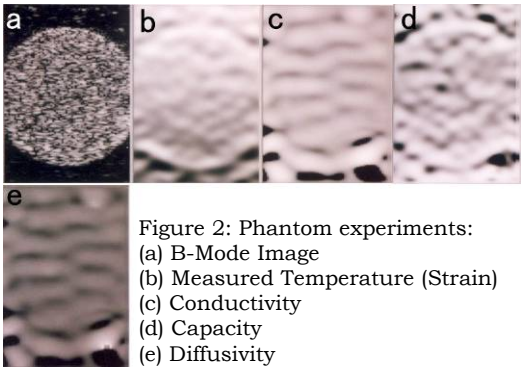


Figure 2: Phantom experiments:
(a) B-Mode Image
(b) Measured Temperature (Strain)
(c) Conductivity
(d) Capacity
(e) Diffusivity

**Conclusions:** These thermal properties were quantitatively reconstructed for agar phantoms as well as simulated phantoms. *In vivo* data will be reported soon.

**References:** [1] Sumi, "Reconstruction of thermal peoperty distributions," Proc of IEEE EMBS Conf (CD-ROM), Sep 2005.

044 **REAL-TIME ELASTOGRAPHY FOR PROSTATE CANCER DETECTION: PRELIMINARY EXPERIENCE.**

*Eva Pallwein[1], Leo Pallwein[1]*, Matthias Schurich[1], Wolfgang Horninger[2], Ferdinand Frauscher[1].*
[1]Radiology 2, [2]Urology Departments, Medical University, Innsbruck, AUSTRIA.

**Aims:** For the first time, we used real-time elastography for the detection of prostate cancer.

**Background:** Since most solid tumors differ with regard with their consistency from the deriving tissue, elastography may offer a new tool for cancer detection.

**Methods:** We examined 15 patients (mean age: 56 ± 6.2 years; range: 46 - 71 years). All patients had the diagnosis of biopsy proven prostate cancer with a mean PSA of 4.6 (range, 1.4 - 16.1). All patients were scheduled for radical prostatectomy. We used a Voluson 730 (GE Ultrasound) US system with a 7.5 MHz transrectal transducer. The US examinations were performed by two investigators and interpreted in consensus. Cancer location and size was determined in the elastography mode. A single pathologist performed pathological classification of tumor localization, grade and stage. The real-time elastography findings were compared with pathological findings.

**Results:** Radical prostatectomy was performed in all cases without major complications. All patients had a pT2 tumor on pathohistological examination. The Gleason score of our patients varied between 5 and 9. The tumor size varied from 0.2 to 3.5 cm (mean: 1.1 cm). Thirty-two foci of prostate cancer were present at pathologic evaluation. Multiple foci of cancer were found in 13 of the 15 glands (87%). Real-time elastography detected 28 of 32 cancer foci (sensitivity: 88%). Four sites were false-positive with no pathological abnormality. The patient by patient analysis demonstrated that real-time elastography detected at least one cancer foci in each of the 15 patients. The limitations of our study were: a relatively small number of patients and the lack of data on inter- and intra-observer variability. The elastographic findings were evaluated for the presence of cancer only, and so we had no data about elastographic findings in BPH or other benign diseases.

**Conclusions:** Our data demonstrate that real-time elastography allows for detection of prostate cancer and estimation of tumor localization and size. Real-time elastography has shown to be capable for visualizing differences in tissue elasticity. Four sites with false positive findings on elastography and no pathohistological correlation were found in our study only. These findings were obtained in our first 5 patients (learning curve!). In summary, real-time elastography of the prostate is a unique imaging modality with a great potential for the detection of prostate cancer.

055 **AN APPLICATION OF THE LAGRANGIAN SPECKLE MODEL ESTIMATOR TO NON-INVASIVELY CHARACTERIZE THE CAROTID ARTERY: SIMULATION INVESTIGATIONS.**

*Elizabeth Mercure[1]*, Roch L. Maurice[1], Gilles Soulez[2], Guy Cloutier[1].*
[1]Laboratory of Biorheology and Medical Ultrasonics, [2]Department of Radiology, University of Montréal Hospital, Montréal, Quebec, CANADA.

**Aims:** Atherosclerosis is a disease that often leads to plaque rupture. It has been suggested that this event is initiated by an alteration of the arterial wall elastic properties, and it was shown that these properties can be assessed by measuring the strain within the arterial wall. Ultrasound elastography techniques have been developed to assess the mechanical properties of soft tissue using measurements of strains. A model based on the Lagrangian description of speckle motion, known as the Lagrangian Speckle Model Estimator (LSME), allows the computation of the strain distribution inside the vessel wall using radio-frequency (RF) data acquired non-invasively. However, these RF images are rarely obtained under optimal scanning conditions. For the characterization of the carotid arterial wall, the positioning of the probe is impeded by the restricted area of the neck, and since this artery is often tortuous, this leads to errors in the estimation of the strain. Therefore, the motivation of this study was first to demonstrate the effectiveness of the LSME, using simulated RF data, for the case of an ideal probe and vessel position. A second motivation was to evaluate the errors of estimation coming from an off-axis probe position or when the vessel axis is inclined in the image.

**Methods:** The modeling was achieved with realistic parameters corresponding to the specifications of the ES500RP (Ultrasonix, Vancouver, Canada) ultrasound system equipped with a 7 MHz linear array probe. The kinetics and geometry of a three-dimensional model of a homogenous common carotid artery were simulated using a commercial finite element software (Ansys, release 8.1). To validate the method, theoretical elastograms (axial strain distributions) obtained with Ansys were compared to those computed with the LSME on longitudinal sections of the simulated artery. These longitudinal sections were taken at the mid-plane of the straight 3D model, off its axis and at the mid-plane of an inclined version of the same model.

**Results:** The results showed an underestimation of the mean axial strain by around 3% under ideal scan conditions. Such an underestimation is, at least, partly explained by the image-formation model used to simulate RF data and by the windowing process required by the LSME. In the case of the images simulating an off-axis probe position, the out-of-plane motion causes the strain to be underestimated with the error increasing with distance away from the longitudinal axis. In the case when the vessel is rotated, the axial strain is also underestimated with the error increasing with the angle of rotation according to a simple trigonometric function.

**Conclusions:** Overall, the LSME showed promising results for the characterization of vascular tissues. However, in order to avoid any significant errors in the estimation of the axial strain due to the inclination of the vessel, one should be able to correct the strain results using the measured angle in the image, as it is done with Doppler ultrasound.

058 **NON-RIGID SOFT TISSUE TRACKING WITH THREE-DIMENSIONAL ULTRASOUND.**

*P Jordan[1,3]*, T Zickler[1], S Socrate[2], RD Howe[1,3].*

[1]Harvard University, Division of Engineering and Applied Sciences, Cambridge, MA, USA; [2]Massachusetts Institute of Technology, Departmant of Mechanical Engineering, Cambridge, MA, USA; [3]Harvard-MIT Division of Health Sciences and Technology, Cambridge, MA, USA.

**Aims:** The primary focus of our research efforts is modeling the mechanical behavior of soft tissues for surgical simulation and virtual surgical environments. Our current tissue characterization approach combines traditional indentation testing with three-dimensional ultrasonic imaging. Estimates of complete deformation fields obtained through imaging are incorporated into an iterative finite-element modeling (FEM) scheme [1] to identify tissue-specific parameters of a physically based nonlinear poro-viscoelastic constitutive law [2, 3]. Our preliminary work suggests that deformation fields obtained from traditional optical flow techniques [4, 5] suffer from prohibitively high levels of noise present in ultrasound images. To address this, we present a non-rigid motion tracking technique that combines local optical flow measurements with a deforming finite-element model to improve motion estimates in noisy datasets.

**Methods:** Characteristic force displacement relationships are obtained from an indentation of porcine liver while imaging with 3D ultrasound (Philips SONOS 7500 Live 3D Echo, Philips Medical Systems, Andover, MA, USA), providing the ability to estimate the complete three-dimensional deformation field of the sample under indentation. Since good textural information is required for differential optical flow techniques, principal component analysis is used to quantify local textural content and provide confidence values associated with local motion estimates. A sparse set of local estimates of optical flow is computed in regions with high confidence values by a modified version of the Lucas-Kanade algorithm [5]. A finite-element model, reflecting tissue sample geometry, boundary conditions, and predetermined constitutive law parameters, is registered to the ultrasound volume and used to properly constrain and interpolate the sparse optical flow estimates. The resulting non-rigid tracking method relies on optical flow estimates in regions of significant texture and on displacement estimates from FEM in regions without trackable features. In future work, we plan to implement the proposed approach in an iterative framework where the computed deformation fields are used to refine the estimates of the FEM constitutive parameters.

**Results:** We present preliminary results comparing deformation fields obtained from traditional optical flow methods of Horn and Schunck [4] and Lucas-Kanade [5] to those obtained from FEM-constrained optical flow. Tracking accuracy is evaluated on an indentation trial of porcine liver with embedded markers and synthetically generated motion scenes with varying levels of image noise. We demonstrate robustness of motion estimates in noisy datasets and reduced levels of multi-frame flow accumulation error.

**Acknowledgments:** This work is supported by the U.S. Army Medical Materials Acquisition Research Command, contract number DAMD 17-01-1-0677.

**References:**

[1] Kerdok AE, Jordan P, Liu Y, Wellman PS, Socrate S, Howe RD. Identification of Nonlinear Constitutive Law Parameters of Breast Tissue. Proc. of the 2005 Summer Bioengineering Conference, ASME, 2005.

[2] Socrate S, Boyce MC. A constitutive model for the large strain behavior of cartilage. In Proceedings of 2001 Bioengineering Conference, volume 50, pages 597-598. ASME, 2001.

[3] Febvay S, Socrate S. Biomechanical modeling of cervical tissue: a quantitative investigation of cervical funneling. In ASME Int. Mechanical Engineering Congress and Exposition (IMECE), 2003.

[4] Horn BPK, Schunck BG. Determining optical flow. Art. Intelligence, 16(1-3):186–203, August 1981.

[5] Lucas BD, Kanade T. An iterative image registration technique with an application to stereo vision. Proc. of the 7th Inter. Joint Conf. on Artificial Intelligence (IJCAI '81), pages 674–679, April 1981.

** indicates Presenter*

060 **DETECTION OF NON-DEFORMABLE OBJECTS IN THE BODY USING ULTRASOUND ELASTICITY IMAGING.**

*Unmin Bae[1]* and Yongmin Kim[1].*

[1]Electrical Engineering and Bioengineering Departments, University of Washington, Seattle, WA, USA.

**Background:** Ultrasound elasticity imaging has focused on differentiating among soft tissues with different elasticity moduli, such as detecting relatively hard cancerous breast tissue and analyzing the composition of atherosclerotic plaques. While the Young's modulus of soft tissue falls in the range of kPa, bone, calcifications and many implanted objects, such as brachytherapy seeds, have a much higher Young's modulus, e.g., above 1 MPa. Since these objects are hardly compressed with the small force applied in ultrasound elasticity imaging, they may be considered as non-deformable objects in ultrasound elasticity imaging. Detection of these objects is clinically important for the diagnosis and treatment of pathologies, such as determining the type of an atherosclerotic plaque and evaluating the efficacy of a brachytherapy procedure compared to the pre-implant plan. Using ultrasound, these non-deformable objects usually appear hyperechoic in B-mode images. However, they may be confused by bright speckles and/or strong echo spots, such as those caused by air bubbles introduced during brachytherapy. Since elasticity imaging is based on stiffness rather than echogenicity, it may be useful for detection of the non-deformable objects, such as brachytherapy seeds [1].

**Methods:** We have conducted simulation and experiments to evaluate ultrasound elasticity imaging for detecting the non-deformable objects, specifically calcifications and brachytherapy seeds. Since the atherosclerotic calcification process is similar to bone formation and one of the main components of atherosclerotic calcifications is calcium hydroxyapatite [2], we embedded bone fractions and precipitates of calcium hydroxyapatite with a volume of several $mm^3$ into agar phantoms. The cylindrical brachytherapy seeds with a length of 4.5 mm and a diameter of 0.8 mm were embedded in agar phantoms and in an *ex vivo* porcine prostate gland with about 5 mm space between seeds. In experiments, ultrasound data were acquired by a Hitachi EUB-6000 ultrasound system (Hitachi Medical Corp., Japan) with a 7.5 MHz linear array transducer. In simulation, an object having a hard inclusion with a diameter of 1 mm was generated, and the elasticity modulus contrast between the inclusion and the background was varied up to 1000 to accommodate the modulus contrast between soft tissue and the non-deformable objects. For elasticity imaging, axial compression was applied and the angular strain method [3] estimated the resulting strain.

**Results:** In simulation, increasing the modulus contrast between the inclusion and the background increases the strain contrast to noise ratio although the slope of the increment is quickly reduced as the modulus contrast increases beyond 10. The improved strain contrast with a high modulus contrast helped the visual recognition of the 1 mm inclusion. In experiments, the bone fractions and precipitates of calcium hydroxyapatite in the agar phantoms were clearly visible in the strain images. The longitudinal and cross sections of brachytherapy seeds in agar phantoms showed the reverberation effect and the dimension of seeds in the axial direction appears larger than the actual dimension in both B-mode and strain images, making seed detection easier. The brachytherapy seeds embedded in the porcine prostate did not show the strong reverberation effect seen with the seeds in agar phantoms, but were still readily detectable in the strain images.

**Conclusions:** The results from simulation and experiments indicate the feasibility of ultrasound elasticity imaging for detecting non-deformable objects in the body. Ultrasound elasticity imaging would provide complementary information to B-mode imaging, helping identification of the non-deformable objects. The capability to image both soft tissue and non-deformable objects could make ultrasound imaging more attractive for diagnosis and treatments.

**References:**

[1] Rossignol G, Souchon R, Angel YC, and Chapelon JY. Using elastography to detect brachytherapy seeds: a feasibility study. The 1st International Conference on the Ultrasonic Measurement and Imaging of Tissue Elasticity, Ontario, Canada, 2002.

[2] Wexler L, Brundage B, Crouse J, Detrano R, Fuster V, Maddahi J, Rumberger J, Stanford W, White R, and Taubert K. Coronary artery calcification: pathophysiology, epidemiology, imaging methods, and clinical implications. A statement for health professionals from the American Heart Association. Circulation, 94:1175-1192, 1996.

[3] Bae U and Kim Y. Angular strain method for strain estimation in ultrasound elasticity imaging. The 4th International Conference on the Ultrasonic Measurement and Imaging of Tissue Elasticity, Austin, Texas, USA, 2005.

064 **ABSOLUTE ELASTICITY ESTIMATION WITH A NEW ULTRASONIC-MECHANICAL DEVICE.**

*T. Sato[1], Y. Fukuyama[1]*, Y. Watanabe[1], S. Goka[1], H. Sekimoto[1].*
[1]Faculty of Urban Liberal Arts, Tokyo Metropolitan University, Tokyo, JAPAN.

**Aims:** Absolute measurement of tissue elastic modulus is extremely important for assessing tissue properties, and is a goal of sonography. In this study, as the first step in absolute measurement of tissue elastic modulus, we have developed a device that estimates the absolute elastic modulus of layered tissue by obtaining strain images from pre- and post-compression datasets and accurately detecting the compression force to the complex tissue.

**Background:** Relative elasticity reconstruction of complex tissue has been successful using the technique of static elastography [1], but estimating the absolute elasticity of each of various layers or units in actual biological tissue is still difficult. Here we develop an original device, which measures the absolute elasticity of complex tissue by combining the static measuring method of Young's modulus with a technique of the ultrasonic strain imaging.

**Methods:** An experimental device was developed based on the understanding that absolute estimation can be accomplished by adding a mechanical approach to static elastography. The device measures the loaded force F with a compression board attatched to a microbalance, and obtains sonograms with a transducer placed in the center of the compression board. In the sonograms of a rectangular-shaped two-layered phantom with known dimensions, the device detected the boundaries between the layers and the displacements in each layer, where the absolute Young's modulus E was estimated with with the following equation:

$$E = (Fg/S) / (\Delta L/L)$$

where F is the value on the balance, g is the acceleration of gravity, S is the area of the top and the bottom of the phantom, L is the height of the phantom, and $\Delta L$ is the compression stroke controlled with a motorized stage.

**Results:** Experiments comfirmed the effectiveness of this device. Two-layered cylindrical phantoms with radii of 22 mm were used. Each phantom had an upper layer with a thickness of 6.3 mm and a Young's modulus of 93.3 kPa and a lower layer with a thickness of 4.0 mm and a Young's modulus of 46.8 kPa. The thickness and Young's modulus estimated by our device, 6.2 mm and 90.3 kPa at the upper layer and 4.0 mm and 49.0 kPa at the lower layer, corresponded with the known values.

**Conclusions:** The next steps in absolute measurement of tissue elasticity *in situ* should be directly attaching the compression board and the transducer to the microbalance and performing structural analysis of various geometries of complex tissues obtained from sonograms.

**Reference:**

[1] A. R. Skovoroda, S. Y. Emelianov and M. O'Donnell: Tissue Elasticity Reconstruction Based on Ultrasonic Displacement and Strain Images, IEEE. Trans. Ultrason., Ferroelect., Freq., Cont., Vol.42, No.4, 747-765, 1995.

** indicates Presenter*

066 **THE FEASIBILITY OF USING ELASTOGRAPHIC TECHNIQUES FOR ASSESSING MEAT QUALITY ATTRIBUTES.**

*Raffaella Righetti[1]*, Jonathan Ophir[1], Rhonda K. Miller[2], Thomas A. Krouskop[1,3].*

[1]The University of Texas Health Science Center at Houston, 6431 Fannin St., Houston, TX 77030, USA; [2]Texas A&M University, College of Agriculture and Life Sciences, 2471 TAMU, College Station, TX 77843, USA; [3]Baylor College of Medicine, One Baylor Plaza, Houston, TX 77030, USA.

**Aim:** To study the feasibility of using elastographic methods for assessing meat quality as reflected in the stiffness, water holding capacity and the amount of unbound water that characterize different meat samples.

**Background:** Currently, beef carcasses are graded by human subjective evaluation. Because the grading process is based on expected differences in palatability, which include physiological age and marbling, high variations exist within a quality grade. In the last several years, many efforts have been made to find objective technologies for assessing meat quality that could replace the human subjective evaluations. In this paper, we investigated the feasibility of using elastographic techniques for predicting some porcine meat quality attributes.

**Methods:** Data were acquired from porcine skeletal muscles harvested from meat that was characterized by one of the most important porcine meat quality-defect conditions: PSE (Pale, Soft and Exudative), a condition that is characterized by a pale color, a soft texture and a low water holding capacity; and DFD (Dark, Firm and Dry), a condition that is characterized by a darker than normal color, a stiff texture and a high water-holding capacity. For comparison, elastographic experiments were also performed on ovine livers, which are known to be more homogeneous and isotropic tissues. Optical images, sonograms, axial strain elastograms, strain ratio elastograms, poroelastograms and strain ratio time constant elastograms were generated from the three types of tissues. Statistical analyses were carried out to compare the spatial and temporal elastic and poroelastic distributions observed for the various tissue samples.

**Results:** The preliminary results of this study suggest different spatial and temporal behaviors in the three types of tissues that were investigated. In the spatial domain, all porcine muscle tissues appear to behave as spatially complex structures, with some areas characterized by different elastic and compressibility properties. Distinct spatial elastic features were consistently observed in the elastograms obtained from the porcine muscle samples. These spatial features appeared to follow the general direction of the anisotropic muscle fiber orientation and are to be contrasted with the lack of such features in the elastograms obtained from the liver samples. The liver tissue appeared to be more homogeneously elastic, isotropic and nearly incompressible. Similarly, in the temporal domain, each of the tissues showed a different behavior. Figure 1 shows the histograms of the strain ratio distributions for the three different types of tissue with time. Observe that the two PSE histograms exhibit a time-dependent increase in skewness towards lower strain ratios, while both the two DFD histograms and the two liver histograms were found not to have statistically significant differences in their means, medians, or modes and their strain ratio distributions appeared nearly constant with time. It is hypothesized that these temporal behaviors are related to the different tissue elastic properties, permeability and unbound water contents.

**Conclusions:** These preliminary results suggest that elastographic techniques may have significant potential for predicting meat quality attributes based on the tissue stiffness, water content and water motility. However, larger statistical studies as well as independent mechanical measurements of the elastic and poroelastic properties of the tested tissues are required to confirm these expectations.

**Acknowledgements:**
This work was supported by NCI Program Project PO1-CA64597. The porcine muscle samples used for the study were courtesy of Texas A&M University.

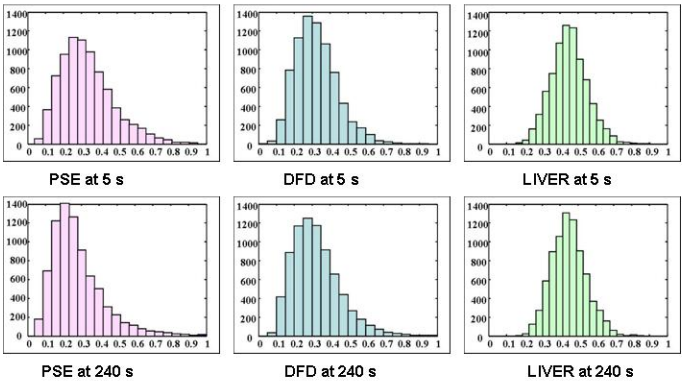


Figure 1

067 **NOVEL STRAIN ELASTOGRAPHIC TECHNIQUES.**

*Raffaella Righetti[1]*, Arun Thitai Kumar[1,2], Seshadri Srinivasan[1,2,3], Jonathan Ophir[1,2], Thomas A. Krouskop[1,4].*

[1]The University of Texas Health Science Center at Houston, 6431 Fannin St., Houston, TX 77030, USA; [2]University of Houston Cullen College of Engineering, 4800 Calhoun Rd., Houston, TX 77204, USA; [3]Siemens Acuson Ultrasound, 1230 Shorebird W., Mountain View, CA 94043, USA; [4]Baylor College of Medicine, One Baylor Plaza, Houston, TX 77030, USA.

**Aim:** To report on the novel elastographic image methodologies that have been developed in our laboratory during the last few years and elucidate the information contained in the various types of strain elastograms about the corresponding mechanical properties of the imaged material.

**Background:** Initial work in the field of elastography was exclusively based on the estimation of local axial tissue displacements and strains [1]. Later, elastographic methods were also extended to estimate the additional parameters of local lateral and elevational displacements and strains [2]. These parameters, combined with further studies, opened the way for the generation of new types of elastograms, which have been referred to as the Poisson's ratio elastogram, the shear strain elastogram, the poroelastogram, the Poisson's ratio time constant elastogram and the permeability elastogram. This report summarizes the elastographic imaging methodologies that have been developed to create the various types of strain elastograms, with particular emphasis on the recently developed techniques, which allowed generation of these newer types of elastograms. This study also investigates the connections between the various elastographic images and the underlying mechanical properties of the material that is imaged.

**Methods:** Simulations, phantom experiments and statistical analyses were performed to explain the procedures that allow generation of axial strain, lateral strain, Poisson's ratio, shear strain, Poisson's ratio time constant and permeability elastograms and poroelastograms and investigate how these elastograms relate to the corresponding ideal strain and mechanical property distributions, such as elastic modulus, Poisson's ratio, permeability and connectivity.

**Results:** The results obtained from the recent studies carried out in our laboratory suggest that, under a range of conditions of clinical interest, there exists good correlations between:

1) axial strain elastograms and the corresponding elastic modulus distribution;
2) Poisson's ratio elastograms and the corresponding Poisson's ratio distribution;
3) Poisson's ratio time constant elastograms and the corresponding permeability distribution; and
4) shear strain elastograms and the corresponding internal connectedness of the materials.

**Conclusions:** We have summarized our recent developments in the elastographic field, which yield new types of strain elastograms, and we have shown that there is a relationship between the several types of elastograms and the corresponding underlying mechanical properties of the material. The good correlation between the various elastographic images and the corresponding mechanical distributions suggests the potential of elastography to convey complementary information on the mechanical properties that govern the behavior of the material that is imaged. It is expected that the combined information derived from these different elastographic techniques will provide a powerful tool to understand the local mechanical behavior of a material.

**Acknowledgements:** This work was supported by NCI Program Project PO1-CA64597-12.

**References:**

[1] Ophir J, Cespedes EI, Ponnekanti H, Yazdi Y, Li X. Elastography: a quantitative method for imaging the elasticity of biological tissues. Ultrasonic Imaging, 1991; 13:111-134.

[2] Konofagou EE, Ophir J. A new elastographic method for estimation and imaging of lateral displacements, lateral strains, corrected axial strains and Poisson's ratios in tissues. Ultrasound in Medicine and Biology. 1998. 24: 1183-1199.

** indicates Presenter*

070 **VISCOELASTIC CHARACTERIZATION OF THERMAL LESIONS IN LIVER.**

*M.Z. Kiss[1]*, T. Varghese[1,2].*
[1]Medical Physics, [2]Biomedical Engineering Departments, 1300 University Ave., Room 1530, University of Wisconsin-Madison, Madison, WI, USA.

**Aims:** The viscoelastic properties of thermal lesions in animal liver have been investigated. The success of elastography depends in part on the modulus contrast in the image, which in turn depends on accurate determination of the tissue's modulus. The stiffness properties of thermal lesions created in the liver may provide a certain means to ascertain whether the ablation procedure was successful in inducing complete thermal necrosis of cancerous tissue.

**Background:** Manual palpation is used extensively to detect lesions in organs such as the liver. This is due to the fact that pathologic and stiffness changes in the body are generally well correlated. Elastography has shown some utility in imaging lesions, which may be too deep in the body or otherwise transparent to conventional ultrasound. The elastogram can be used to study the variations in the stiffness of thermal lesions in tissue as a function of lesion temperature. The success of elastography depends in part on the modulus contrast in the image, which in turn depends on accurate determination of the tissue's modulus.

**Methods:** Normal tissue from canine and porcine livers were excised from bulk tissue and cut to a useful geometry (typically cylindrical 20 mm in diameter and 3 – 6 mm in height). Lesions were prepared either through double immersion boiling or radio frequency ablation at several temperatures from 60°C – 90°C and placed in Bose/Enduratec ELF 3220, a dynamic testing device. The complex modulus was determined by applying a periodic strain amplitude of 1% (with a precompression strain of 1%), and a frequency from 0.1 – 50 Hz, and then measuring the force response at the load cell.

**Results:** Experiments show that the complex modulus for both normal tissue and thermal lesions generally increased with increasing frequency from 4 kPa at 0.1 Hz for normal tissue to more than 100 kPa at 50 Hz for thermal lesions. The phase of the modulus generally increased from 0.1 to 0.5 over the same frequency range, for all tissue types. When the modulus is plotted as a function of the lesion temperature, a distinct peak exists around 70°C. Depending on the animal type and method of lesion preparation, the modulus above 70°C will drop and then increase or drop without increasing. These results suggest that image contrast in elastograms may be optimized at lower temperatures, and issues such as blood coagulation or tissue desiccation may be avoided.

**Conclusions:** Characterization of the viscoelastic properties of *in vitro* liver specimens may provide some insight to the expected elastographic image contrast and eventually lead to improved elastographic methods of monitoring the treatment of certain liver diseases.

**Acknowledgements:** This research is supported in part by NIH grant T32CA09206, and the Whitaker Foundation grant RG-02-0457.

076 **NOISE REDUCTION IN ELASTOGRAPHIC STRAIN ESTIMATED FROM DISPLACEMENT.**

*Lijun Xu[1], Jeffrey C. Bamber[1]*.*
[1]Joint Department of Physics, Institute of Cancer Research and Royal Marsden NHS Trust, Downs Road, Sutton, Surrey SM2 5PT, England, UK.

**Aim:** The aim of this work was to demonstrate and evaluate the potential of a new wavelet transform-based approach to strain noise reduction that, it was hoped, would not compromise resolution.

**Background:** Elastography is an established method for imaging soft tissue relative strain. Traditional methods for strain estimation first measure tissue displacement via cross-correlation and then calculate the strain as the gradient of the displacement. Trade-off exists between the axial resolution and the signal-to-noise ratio (SNR) [1]. Calculating the gradient amplifies the noise in the measured displacement. Published methods have tended to reduce this by averaging the gradient over time (using many compressions) or space (from a fitted equation, e.g., the least-square (LSQ) method), trading temporal or spatial resolution for improved strain SNR and CNR. We are investigating the use of the wavelet transform to reduce the noise level in the measured displacement and hence that in the estimated strain while still retaining strain transition details. We evaluate whether it offers improved spatial and contrast resolution.

**Methods:** In the new approach to elastogram generation discussed here, the displacement image was decomposed using the wavelet transform into octave sub-bands (i.e., different scales) consisting of one "approximate sub-band" and several "detail sub-bands". Each sub-image obtained in a detail sub-band contains information from the original displacement image at the corresponding scale. If a suitable wavelet is selected, the wavelet coefficients in a detail sub-band associated with the discontinuities in the image have larger values than the other coefficients associated with noise. Wavelet coefficient thresholding was implemented by removing the (noise) coefficients of smaller absolute value. A de-noised displacement image was then reconstructed from the thresholded detail sub-images and the untreated approximate sub-image. Finally, a strain image was obtained by applying the direct gradient operator to the de-noised displacement image. In this approach, the gradient operator amplified only a small amount of the noise, i.e. that present in the approximate sub-band, while most of noise in the other detail sub-bands was cancelled. Since the discontinuous details of the original image were retained while reducing the noise level, the spatial resolution in the estimated strain was hardly affected. This new approach offers potential for smaller data segment windows to be used for cross-correlation tracking and strain estimation, enabling a better spatial resolution to be obtained while retaining high strain SNR and CNR.

**Results:** Zero mean white noise was added to a simulated displacement image obtained by integrating the strain in a homogeneous soft background containing a stiff inclusion of circular cross-section. The strain values in the background and the inclusion were 0.02 and 0.015. Strain images obtained using the direct gradient, LSQ and new estimators were compared. The LSQ estimator (window size 5) produced SNR and CNR values (18.4dB and 9.8) smaller than those obtained using the new estimator (19.0dB and 11.3), and both were substantially better than values obtained with the direct gradient estimator (16.3dB and 8.5). The new estimator, however, retained many of the sharp boundary details of the inclusion that were blurred by the LSQ estimator. Similar observations have been made from tests using real echo data, obtained whilst straining gelatine phantoms that contain stiff spherical inclusions. All implementations used Matlab™ built-in functions without speed optimisation, but the wavelet method was much faster than the LSQ method (×2 for a 100×100 image and ×13 for a 500×100 image).

**Conclusions:** Wavelet transform-based noise reduction methods in strain estimation appear to hold potential for enhancing contrast, spatial or temporal resolution in elastography. Further work is required to explore alternative approaches to taking advantages of the properties of the wavelet transform, and to determine whether potential concerns, e.g., those arising from noise retained at sharp boundaries, represent disadvantages.

**Acknowledgements:** We are grateful to the EPSRC for supporting this work.

**References:**

[1] S. Srinivasan, R. Righetti and J. Ophir, "Trade-offs between the axial resolution and the signal-to-noise ratio in elastography," Ultrasound in Med. & Biol., vol. 29, no. 6, pp.847-866, 2003.

** indicates Presenter*

078 **VIRTUAL ENDOSCOPIC ELASTOGRAPHY – AN INITIAL EXPERIENCE *IN VIVO*.**

*Peng-Fei Zhang[1], Xin Yi[2], Hai-Jun Su[3], Mei Zhang[1], Wen-Qiang Chen[1], Yun Zhang[1].*
[1]Shandong University Qilu Hospital, No107 Wenhuaxi Road, Jinan, Shandong Province, 250012, CHINA; [2]Chinese Ministry of Education Key Laboratory of Cardiovascular Remodeling and Function Research, No107 Wenhuaxi Road, Jinan, Shandong Province, 250012, CHINA; [3]Shandong University, No 27 Shandanan Road, Jinan, Shandong Province, 250014, CHINA.

**Aims:** To develop virtual endoscopic elastography (VE-IVUSE) via a combination of virtual endoscopy (VE) technique and intravascular ultrasound elastography (IVUSE) technique. To validate the feasibility of *in vivo* application of VE-IVUSE on animal models.

**Background:** Although the important role of two-dimensional intravascular elastography (IVUSE) in plaque components characterization has been demonstrated on animal models and human femoral or coronary arteries *in vitro*, it failed to reveal the spatial information which is of critical value in the localization of atherosclerotic plaques and thorough understanding of their geometric shape. The virtual endoscopy (VE) technique holds the feature of convenient human-computer interaction and dynamic navigator [1]. We hypothesized that the combination of IVUSE and VE techniques could provide more accurate spatial elastic information of local and global arterial intima.

**Methods:** Software for VE-IVUSE was developed using the Microsoft® C++ computer language. Six Chinese experimental mini pigs were fed a diet with 4% cholesterol for 40 weeks. For each animal, the endothelia on one of the two renal arteries were injured with a Forgaty balloon while the other renal artery was left as a control. The IVUS images of both renal arteries were acquired and then processed with the VE-IVUSE software. With the VE-IVUSE images, high-strain spots [2] were identified, and the number of the spots in each of the arteries was counted.

**Results:** With a Galaxy intravascular ultrasound system (Boston Scientific Inc. USA), IVUS images were obtained from 12 renal arteries and were processed with a self-made software program. With the view observing the intima from the lumen side, which could be illustrated in Figure 1, high strain concentrated at the shoulders of the plaques and from the shoulders to the fibrous caps, the strain values decreased gradually. Moreover, the high-strain spots could be counted clearly. Significant difference existed between the numbers of high-strain spots in the injured arteries and those in the non-injured arteries (5.0±0.3 and 0.8±0.2, respectively, $P<0.05$).

**Conclusions:** VE-IVUSE can be achieved with off-line image-processing techniques and spatial elastic information of the intima can be demonstrated accurately with this new elastography technique.

**References:**

[1] Wahle, A, Mitchell SC, Ramaswamy SD, et al. Visualization of human coronary arteries with quantification results from 3-D and 4-D computational hemodynamics based upon virtual endoscopy. Int Congr Ser, 2001, 1230: 923-929.

[2] Schaar JA, Regar E, Mastik F, et al. Incidence of high-strain patterns in human coronary arteries-assessment with three-dimensional intravascular palpography and correlation with clinical presentation. Circulation. 2004, 109: 2716-2719.

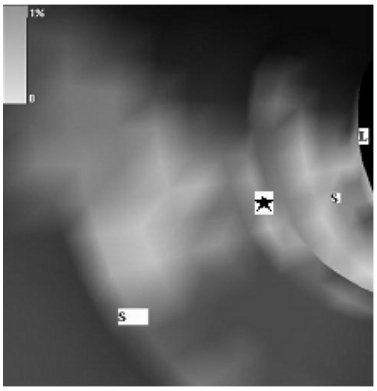


Figure 1: VE-IVUSE image of the renal artery acquired from atherosclerotic mini pigs. L-lumen, S-shoulder of plaques, ★ indicates the fibrous cap of plaques.

** indicates Presenter*

079 **PLAQUE VOLUME COMPRESSION RATIO – A NEW INDEX IN EVALUATING PLAQUE ELASTICITY PROPERTIES.**

*Peng-Fei Zhang[1], Gui-Hua Yao[1], Mei Zhang[1], Hong Jiang[2], Yun Zhang[1].*
[1]Shandong University Qilu Hospital, No107 Wenhuaxi Road, Jinan, Shandong Province, 250012, CHINA; [2]Chinese Ministry of Education Key Laboratory of Cardiovascular Remodeling and Function Research, No107 Wenhuaxi Road, Jinan, Shandong Province, 250012, CHINA.

**Aims:** To validate a new method for quantitative assessment of plaque volume by real-time 3-D echo imaging (RT-3DE) on phantoms. To develop and elucidate a new index – plaque volume compression ratio (Rpv), for use in carotid arterial plaque elasticity evaluation.

**Background:** A series of indices such as stiffness index (β), pressure-strain modulus (Ep), etc, have been documented to demonstrate the elastic characteristics of carotid arteries. Mainly, 1-D or 2-D parameters are involved in these equations [1, 2]. However, plaque volume should be a more accurate index for evaluating the pathological process of atherosclerosis because during this process, plaques grow not only along the short axis, but also along the long and the circumferential axes, of involved arteries [3]. Plaque volumes change periodically because of the pulsation of blood pressure, and the extent of such changing is different according to the elastic characteristics of plaques. That is, tissues with bigger elastic moduli tend to deform less and vice versa. So, plaque compression ratio (Rpv), calculated as Rpv = (Plaque volume at end diastole-Plaque volume at end systole)/Plaque volume at end diastole, could be a more accurate index to evaluate the elasticity. RT-3DE, a newly developed technique, has been shedding light on real-time plaque volume quantification. Compared with the massive cardiac application, few publications have been about the application of RT-3DE on carotid artery imaging. In the present study, the feasibility of plaque volume quantification via RT-3DE was first validated on vessel-mimicking phantoms and then the real-time carotid arterial plaque volumes were measured to calculated Rpv. The clinical value of Rpv index was elucidated also.

**Methods:** Thirty-two carotid artery-mimicking phantoms were made from the mixture of gelatin, agar and silicon carbide. The diameter of the phantom lumen was 10.0±1.0mm and the maximum thickness of plaques was 1.40±0.20mm. The RT-3DE data sets, acquired with frame rate of 30f/s, were transferred into a TomTec 4D Cardio-View workstation, and plaque volume was measured using 8 cut planes. Two experienced sonographers measured each plaque volume in a double-blind way, and one sonographer repeated the same measurement one month later. Twenty patients were randomly selected for this study and divided into 3 groups: patients with hypertension (HTN), non-hypertension patients with myocardial infarction or cerebral infarction (VE) and normal controls (NC). There were no significant differences in risk factors such as age, smoking history, etc. In total, 30 plaques were detected and for each group, n=13, 11 and 6, respectively. The acoustic properties of the plaques were determined with an acoustic densitometry (AD) technique. According to the AD ratio of plaque to vessel adventitia, plaques were classified as lipid, fibrous and calcified plaques.

**Results:** Good correlations were obtained between the real phantom plaque volume and the estimated plaque volume. There was no significant intra- and inter-observer difference between measurements. With a mean plaque volume ranging from 500mm$^3$ to 1,300mm$^3$, the coefficient of variance varied from 2.0% to 9.7%. Rpv values differed significantly in lipid, fibrous and calcified plaques (43.80%±6.99%, 22.54%±6.88% and 11.63%±9.09%, respectively, $P$<0.01). As for lipid plaques, the Rpv values (47.63%±4.25%) in the HTN group was highest compared to those in the VE group (37.15±3.89) and the NC group (36.03±3.94) with $P$<0.05. As for fibrous and calcified plaques, there were no significant differences in Rpv values among groups.

**Conclusions:** RT-3DE provides a reliable and reproducible approach to the quantitative assessment of carotid arterial plaque volume. Rpv, as a new index, provides a non-invasive method to evaluate the difference of elastic characteristics of carotid arterial atherosclerotic plaques.

**References:**

[1] Fenster A, Landry A, Downey DB, et al. 3D ultrasound imaging of the carotid arteries. Curr Drug Targets Cardiovasc Haematol Disord, 2004, 4(2):161-175.
[2] Riley WA, Barnes RW, Evans GW, et al. Ultrasonic measurement of the elastic modulus of the common carotid artery: the atherosclerosis risk in communities (ARIC) study. Stroke. 1992, 23: 952-956.
[3] Landry A, Spence JD, Fenster A. Measurement of carotid plaque volume by 3-dimensional ultrasound. Stroke. 2004, 35(4): 864-869.

082 **PHANTOM EXPERIMENTS AND COMPUTER SIMULATION FOR BREAST CANCER ELASTOGRAPY BY WATER BAG PRESSING.**

*Y Hayakawa[1]*, K Ishida[1], K Tsuji[1], M Kaitoo[1], M Nakamura[2].*
[1]Toin University of Yokohama, Yokohama, Kanagawa-ken, JAPAN; [2]Yokohama General Hospital, Yokohama, Kanagawa-ken, JAPAN.

**Aims:** The present work aims to obtain the modulus of elasticity of lesions in the breast. As breast cancer has a higher elasticity modulus [1], this may lead to discrimination of cancer from benign lesions [2, 3]. Although the apparatus for elastography of the breast is commercially available [e.g. Hitachi], the resultant image is rather qualitative. The present work aims to obtain more quantitative information by simplifying the force delivered to the breast by water bag pressing as schematically shown in the figure below.

**Background:** The existing commercially available apparatus for elastography applies force by planar pressing. The stress inside the breast is too complex to obtain the modulus of elasticity quantitatively. We simplify the pressure distribution by using a water bag to exert the pressure, in which case the pressure is nearly uniform across the whole surface of the water-breast interface.

**Methods:** A phantom of 10% by weight gelatin, width 8cm, height 4cm, and length 10cm, containing a Plexiglas rod of 1cm in diameter, centered at 1.5cm and 2.5cm depth from the upper and the lower surface, was created. Pressure was applied to the phantom using a water bag and ranged from 1.0kPa to 2.3kPa. The deformation of the phantom was observed using an 11MHz ultrasound echo technique.

**Results:** As the water pressure increased, the curvature of the water-gelatin surface was greater when the Plexiglas rod was nearer to the water-gelatin surface. These observations were simulated using Finite Element Methods (ANSYS9.0) and the elasticity modulus of the gelatin was estimated to be between 5500Pa and 6500Pa under the assumption of Poisson's ratio being 0.49. Another experiment using a 5cmH5cmH8cm gelatin block with weight upon it was analyzed by Finite Element Method and gave an elasticity modulus of 5800Pa.

**Conclusions:** Our preliminary study shows the qualitative and quantitative coincidence of the phantom experiments and computer simulation using Finite Element Method. A more realistic phantom experiment using a softer cancer model than a Plexiglas rod is under development, where the elasticity modulus of a cancer model is to be determined.

**References:**

[1] Krouskop TA, Wheeler TM, Kallel K et al., Ultrasonic Imaging 26(1998)260-274.
[2] J Ophir, I Cespedes, H Ponnekanti et al., Ultrasonic Imaging 13(1991) 111-134.
[3] M Yamakawa, N Nitta, T Shiina, et al., Jpn.J.Appl.Phys. 42(2003)3265-327.

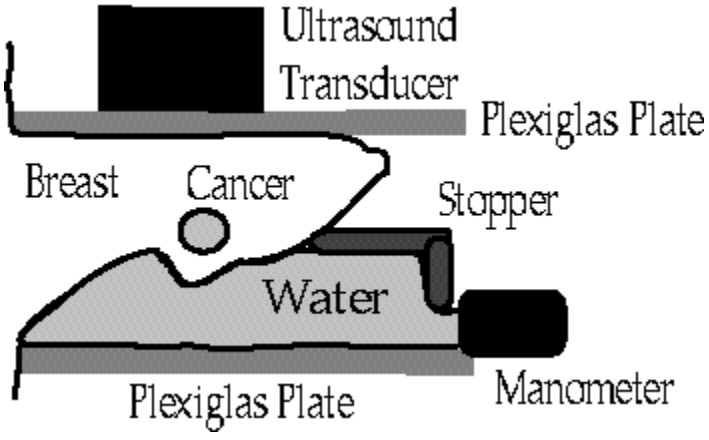

088 **PRELIMINARY CLINICAL STUDY OF SEMI-QUANTITATIVE FREEHAND ELASTOGRAPHY FOR THE ASSESSMENT OF RADIATION INDUCED BREAST FIBROSIS.**

*Nigel L. Bush[1], Jeffrey C. Bamber[1]*, Paul E. Barbone[3], John R. Yarnold[2].*
[1]Joint Department of Physics and [2]Section of Radiotherapy, Institute of Cancer Research and Royal Marsden NHS Trust, Downs Road, Sutton, Surrey, SM2 5PT, England, UK; [3]Department of Aerospace and Mechanical Engineering, Boston University, Boston, MA 02215, USA.

**Aims:** We report on a small clinical pilot study designed to investigate the potential use of pseudo-static freehand ultrasound elastography as a tool for assessing diffuse tissue stiffness, as applied to gain further understanding of radiation-induced fibrosis of the breast, and in monitoring its severity and treatment. A compliant elastic standoff pad of known elastic modulus, placed between the compressor and breast, provides a measure of the applied axial stress profile at the tissue surface, allowing a simple first-order correction of the strain data to produce relative strain (stiffness) images.

**Background:** Following radiotherapy treatment for early breast cancer, some women will develop disabling tissue hardness in the breast and shoulder girdle, with consequent compression of the lymphatic, vascular and nerve sheaths, leading to devastating disabilities. Radiation fibrosis can render tissue palpably and measurably stiffer than normal [1], and is primarily assessed and monitored clinically using subjective palpation methods. Physician assessment of radiation-induced induration is, however, unreliable [2] and unable to provide specific information concerning the distribution of radiation-altered mechanical properties amongst the component tissues of the breast. Thus, there is a need for an alternative objective non-invasive imaging method for assessing breast fibrosis. Although we are working towards a solution to this problem using inverse reconstruction methods, we decided, as a preliminary step, to gain some clinical experience of a simple calibrated strain imaging technique.

**Methods:** Acquisitions were performed as part of a routine ultrasound examination using freehand contact scanning. The ultrasound imaging probe was manually guided to gently palpate the breast through a compliant gel pad of known, tissue-equivalent elastic modulus. The ultrasound scanner (Acuson XP10, 7.5MHz) provided radio frequency (RF) frame sequences corresponding to a compression palpation cycle. Off-line processing, using cross-correlation techniques, was applied to the RF frame sequence data to generate strain images for scan planes distributed radially (with respect to the nipple) around each treated breast, and for scan planes corresponding to contra-lateral sites on each untreated breast. Normalized strain images, referenced to the strain in the standoff, were generated using regional standoff strain values, where the reference regions were drawn on the strain images with the aid of registered B-mode images. A similar method was used to draw regions on the strain images within the breast, with the intention of separately evaluating any effect of fibrosis on tissue elasticity in regions classified as skin, adipose and fibro-glandular tissue.

**Results:** Results for three patients are reported. In all three cases, the method demonstrated an increased stiffness in the irradiated breast relative to the unirradiated breast, for all tissue types, although the adipose tissue appeared to show the greatest contrast between the treated and untreated breasts.

**Conclusions:** Increases in tissue stiffness due to radiation-induced fibrosis of the breast are detectable by comparing the palpation-induced strain in the breast to that produced simultaneously in an overlying standoff pad. Therefore, it would appear worthwhile developing and evaluating methods that offer a further improved degree of quantification, especially to compensate for the stress distribution within the breast, with a view to reducing variability of the measurement and confirming whether the fibrosis really does affect the adipose tissue more than other parts of the breast.

**Acknowledgements:** This work is supported by funding from the EPSRC.

**References:**

[1] Zheng YP, Leung SF, Mak AFT. Assessment of neck tissue fibrosis using an ultrasound palpation system: a feasibility study. Medical and Biological Engineering and Computing, 38:497-502, 2000.
[2] Gothard L et al, Double-blind placebo-controlled randomized trial of Vitamin E and pentoxifylline in patients with chronic arm lymphoedema and fibrosis after surgery and radiotherapy for breast cancer Radiotherapy and oncology, 73:133-139, 2004.

** indicates Presenter*

090 **PROGRESS IN QUANTITATIVE BIOMECHANICAL IMAGING.**

*Nachiket H. Gokhale[1], Michael S. Richards[2], Carlos Rivas Aroni[1], Ricardo Leiderman[1], Assad A. Oberai[1], Paul E. Barbone[1]*.*

[1]Aerospace & Mechanical Engineering, [2]Biomedical Engineering, Boston University, Boston, MA, USA.

**Aims:** To noninvasively measure and thereby image *in vivo* distributions of biomechanical properties of soft tissues. The intended application of our work is in the detection and diagnosis of breast cancer and other soft tissue pathologies. This poster reviews our team's progress in this direction. The efforts described include the development and computational implementation of mathematical models to describe soft tissue behavior, the development of techniques to accurately measure vector displacements of tissue deformation, the analysis of inverse problems associated with the quantitative inference of material properties from measured displacements, and the development of algorithms to solve those inverse problems.

**Background and Methods:** It is widely recognized that soft tissue pathologies often change the tissue's biomechanical properties. The inference of biomechanical properties from a measured deformation field requires a mathematical model that accurately describes tissue deformation. The parameters that go into the mathematical model may then be recovered by comparing the predictions of the model to the observed tissue deformations. Sometimes there is enough information in the observed deformation to confidently determine the desired tissue properties; sometimes there is not. In the latter case, additional information must be supplied in order to determine the tissue properties. To solve the inverse problem, we typically use an adjoint based gradient descent algorithm to determine the parameter values that minimize the difference between observed and predicted deformations.

**Results:** We present progress in several areas: novel methods in displacement estimation, advanced mathematical models of tissue deformation, and analysis and solution of their associated inverse problems. In the first category, we present novel methods to improve displacement estimates via image registration. The measured deformation is interpolated on a finite element mesh. The flexibility inherent in the FEM interpolation provides a basis suitable to explore advanced techniques to accurately determine non-axial displacements. These techniques include regularization, physical constraints, and novel ultrasound data collections strategies. In the second category of effort, we present our experience with several different mathematical models for tissue behavior suitable for different experimental conditions. Some of these models are motivated by microstructural considerations. The models include both two and three dimensional deformations, and linear and nonlinear deformations. Finally, mechanical property reconstructions derived from our novel adjoint-based gradient descent quasi-Newton algorithm are presented. Where possible, these are compared to values determined by independent mechanical testing.

**Conclusions:** Suitable mathematical models of tissue deformation, coupled with precise and accurate observations of tissue behavior can be used to determine many different biomechanical properties of soft tissue, including but not limited to shear elastic modulus. We demonstrate this on both phantom and simulated data. We also show that the measurement of displacement and strain itself can be improved by imposing physics-based mathematical constraints on the measured displacements. Of course, if the mathematical model fails to accurately represent the real physical situation, then the displacement measurement will be incorrectly biased. Overall, the breadth of possibilities for biomechanical imaging is quite exciting.

**Acknowledgements:** This work has been supported in part by CenSSIS (The Center for Subsurface Sensing and Imaging Systems) under the Engineering Research Centers Program of the National Science Foundation (Award No. EEC-9986821) and the Department of Defense Breast Cancer Research Program (Award No. W81XWh-04-1-0763).

099 **TISSUE MOTION AND ELASTICITY IMAGING EVALUATED BY ULTRASOUND IN A TISSUE-MIMICKING PHANTOM.**

*AAO Carneiro[1]*, H Chen[2], T Varghese[2], TJ Hall[2], JA Zagzebski[2].*

[1]Departamento de Física e Matemática, FFCLRP, Universidade de São Paulo, Ribeirão Preto, São Paulo, BRAZIL; [2]Departament of Medical Physics, University of Wisconsin-Madison, 1300 University Avenue, 1530 MSC, Madison, WI 53706, USA.

**Aims:** This work provides a comparison of low frequency compressions in the range of 0.5-10 cycles/sec for elasticity imaging. Tissue stiffness increases in some tumors, as they form and grow because of a dense cellular reaction, specifically in malignant breast lesions with highly cross-linked collagenous fibers. The development of elasticity imaging is driven, in part, by the need to improve the detection and differentiation of early malignant disease.

**Background:** Elastography or elasticity imaging is a new imaging modality where elastic tissue parameters related to the structural organization of normal and pathological tissues are imaged [1]. Both static and dynamic techniques have been utilized for measuring tissue elastic properties. In quasi-static elastography, radiofrequency (RF) signals acquired before and after a small amount of compression are compared. Dynamic methods, on the other hand, image local vibrations within tissues or structures induced by externally applied oscillations using transducers or acoustic radiation force at low frequencies [2].

**Methods:** In this work, we apply a quasi-static compression to tissue-mimicking phantoms using a motorized system with controlled compression frequency. The 8cm cubic phantom was positioned between two aluminum plates. The top plate was fixed and also contained a rectangular slot to hold the transducer, while the bottom plate is moved up-down in a sinusoidal fashion by the motor. Loops of RF echo frames were acquired that were not synchronized to the compression. The compression frequency varied from 0.5 cycles/sec to 10 cycles/sec and the maximum deformation was 5%. Displacement and strain maps were evaluated using cross-correlation techniques between the pre- and post-compressed RF frames. Strain images were then obtained from the derivative of the displacement data. RF data were acquired using an ultrasound machine with a research interface, the Ultrasonix 500RP, with a linear array transducer.

**Results:** Experiments were conducted on both uniformly elastic and inclusion phantoms. We observed increased viscoelastic contributions with an increase in the compression frequency. The use of sinusoidal compressions enable the averaging of data obtained at similar compression increments, thereby improving the noise properties of the strain images.

**Conclusions:** Strain images obtained using different compression frequencies were compared. We observed viscoelastic contributions to the elastogram as the compression frequency increases. Variations in the signal-to-noise ratios and contrast-to-noise ratios in the phantom are presented.

**Acknowledgements:** This work is supported in part by the University of Wisconsin-Madison and the University of São Paulo.

**References:**

[1] Ophir J, Cespedes I, Ponnekanti H, Yazdi Y and Li X 1991. Elastography: a quantitative method for imaging the elasticity of biological tissues, Ultrason. Imaging 13: 111–34.

[2] Hall TJ, Zhu YN, Spalding CS 2003. *In vivo* real-time freehand palpation imaging; Ultrasound in Medicine and Biology 29 (3): 427-435.

** indicates Presenter*

101 **COMPARISON BETWEEN AXIAL ELASTOGRAMS OF A CONNECTED AND DISCONNECTED INCLUSION IN HOMOGENEOUS BACKGROUND: A SIMULATION STUDY.**

*A Thitai Kumar[1,2]*, J Ophir[1,2] and TA Krouskop[1,3].*
[1]The University of Texas Medical School, Houston, TX, USA;[2]University of Houston, Houston, TX, USA; [3]Baylor College of Medicine, Houston, TX, USA.

**Introduction:** When a material is compressed, there are several parameters that affect the stress distribution, and, hence, the strain distribution in the material. The coefficient of friction of an inclusion to the background material is a critical parameter. Current algorithms used to solve the inverse elasticity problem assume a fully connected interface between the inclusion and the background. This assumption may be applicable in some circumstances but not in general. In this poster, we perform a parametric study using simulations to compare the observed strain contrast and contrast-to-noise ratio (CNR) in the axial elastograms of material models with either a connected or a disconnected elastic cylindrical inclusion in a homogeneous, elastic background.

**Methods:** We considered a 2D plane strain problem with a circular inclusion in a square region of interest. The assumptions for the material properties and external boundary conditions were taken to be

1) both the inclusion and background are incompressible elastic materials (Poisson's ratio =0.495) and
2) there was no-slip at the center point in the bottom plane.

We compared the axial elastograms obtained for a circular inclusion with varying degrees of coefficient of friction with respect to the background (modeled as the coefficient of friction at the interface between the inclusion and background). The effects of applied axial strain and modulus contrast between the inclusion and the background were also compared for the cases of a fully connected inclusion and a completely disconnected inclusion.

**Results:** The results indicate that the observed strain contrast for a disconnected inclusion is significantly higher than that of the connected inclusion at all applied axial strains (Figure 1). There is also a significant difference between the observed strain contrasts in these two cases at higher modulus contrasts (Figure 2). In addition, the degree of friction causes significant differences in the observed strain contrast (Figure 3).

**Conclusions:** We conclude from this study that at typical elastographic compression levels used in practice and at different modulus contrasts, there are significant differences between the axial elastograms of the two cases, completely disconnected and fully connected inclusion, in terms of the observed contrast and the CNRe. This indicates that care must be exercised in interpreting the information conveyed in an axial elastogram and also in using axial elastogram data to solve the inverse problem since the friction can change the ratio of the stiffnesses used in the calculations. In addition, we also conclude that shear strain elastograms can be explored for information about the degree of internal friction (Figure 4), and this may often be useful in solving the inverse problem.

**Acknowledgement:** Supported by NIH Program Project P01-CA64597-12 to the University of Texas

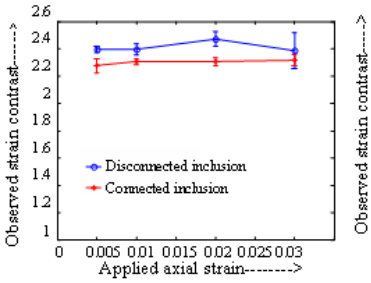


Figure 1

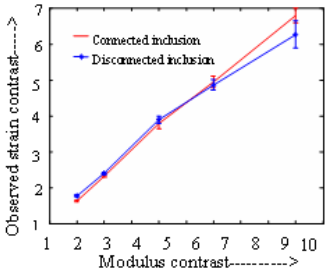


Figure 2

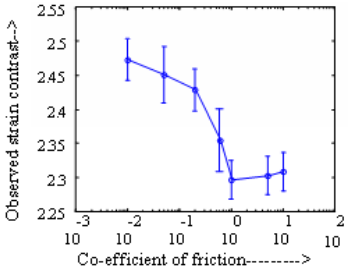


Figure 3

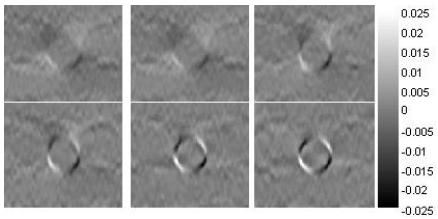

Figure 4: SSE at various coefficients of friction from 5 (top left) to 0.01 (bottom right).

* *indicates Presenter*

106 **THEORETICAL AND SIMULATION STUDY OF WAVE GENERATION AND ITS EFFECT ON LESION DETECTABILITY IN SONOELASTOGRAPHY.**

*JM Park[1], SJ Kwon[1], MK Jeong[1]*, MH Bae[2].*
[1]Daejin University, Pocheon, Kyeonggi, 487-711, KOREA; [2]Hallym University, Chuncheon, Kangwon, 200-702, KOREA.

**Aims:** In order to implement a sonoelastographic imaging modality in a medical diagnostic ultrasonic imaging system, in this paper we have investigated wave generation characteristics in soft tissue due to a surface vibrator and the effects of vibration patterns within tissue on lesion detectability.

**Background:** Sonoelastography is an ultrasound-based technique that visualizes the elastic properties of soft tissues by measuring the tissue motion generated by an externally applied vibration [1], [2]. Requiring the use of separate vibrators, this method may be cumbersome to apply to the human body compared to the static method, but is advantageous in that it can deliver vibrational forces to deep-lying lesions to which it is difficult to apply pressure, and thus obtain images of the resulting vibrational amplitude.

**Methods:** Theoretical expressions were derived for the wave generated by a vibration source applied perpendicularly to the surface of a semi-infinite solid, as well as an infinite plate, and were numerically evaluated to determine vibration patterns inside tissue subjected to an external vibration force. We also simulated the vibration pattern in a finite-sized inhomogeneous tissue embedded with hard lesions using FEM.

**Results:** We found that the wave generation in soft tissue due to a surface vibrator is characterized by a shear wave propagating predominantly in particular directions. The directions in which the maximum energy of the shear wave propagates depend on the vibrator frequency and the distance from it. The maximum angles increase with decreasing distance and frequency, implying that the wave generation characteristic inside tissue cannot be accurately represented by the far-field approximation. When the shear wave frequency is increased such that the shear wavelength becomes shorter than the vibrator width, the number of shear lobes, which are separated into different regions, is found to increase. Based on vibrational amplitude images, we explain that the reflected wave from a boundary in a finite-sized tissue deforms the wave pattern emitted from the vibrator. The degree to which the wave pattern is deformed by interference was found to be large at low frequencies where attenuation is low, but turned out to be small at high frequencies where attenuation is high, resulting in nearly the same wave generation characteristic as observed in half space.

**Conclusions:** We found it difficult to relate quantitatively the vibrational amplitude itself to tissue stiffness because lesion detectability from vibrational amplitude images varies greatly depending on the lesion location and vibrator frequency. We showed, however, that by contrast, strain imaging is less sensitive to the variation of modal patterns. Therefore, we conclude that if we obtain strain images using sonoelastography in a proper manner, they can be considered as a fairly quantitative measure of representing tissue stiffness, as is the case in static elastography.

**Acknowledgements:** This work was supported by a research grant from Medison.

**References:**

[1] L Gao, KJ Parker, SK Alam, "Sonoelasticity imaging: Theory and experimental verification," J. Acoust. Soc. Am, vol. 97, no. 6, pp.3875-3886, 1995.
[2] KJ Parker, D Fu, SM Gracewski, F Yeung, SF Levinson, "Vibration sonoelasticity and the detectability of lesions," Ultrasound in Med. Biol., vol. 24, no. 9, pp. 1437-1447, 1998.

109 **ULTRASOUND CHARACTERIZATION OF MECHANICAL PROPERTIES OF SILICONE TUBE WALLS.**

*Edward Haeggstrom[1]*, Anders Wallin[1] and Mikko Leppänen[1].*
[1]Helsinki University, Vaino Auerin katu 11, Helsinki, Uusimaa, FINLAND.

**Aims:** An acoustic method to estimate mechanical characteristics of the wall of an air-filled, freely suspended, non-porous silicone tube is being developed.

**Background:** This method is based on our earlier work on thin plastic foils [1].

**Methods:** A 1-cycle, 23 kHz, acoustic signal is excited into the tube wall (Tygone 3350 1/32 x 3/32) with a piezoceramic actuator and received with an inductive pickup (sensitivity 14.1±0.1 μV/nm). This kind of actuation-detection scheme can be used for radial and axial wave excitation and detection. By measuring the time of flight (TOF) at different actuator-receiver separations, the sound wave velocity in the tube wall was determined from a least-squares-fit. The corresponding elastic modulus was calculated.

**Results:** The results were verified with a laser Doppler interferometer. Our next step will be to determine the sensitivity of the method to detect changes in the tube wall stiffness and thickness by monitoring the dispersion of the propagating modes.

**Conclusions:** We hope that being able to determine mechanical tube wall parameters might carry interest with e.g. a) experimental verification of tube models used to predict vascular pathologies [2], b) acoustic wave devices for sensing based on propagating tube waves [3], and c) noise reduction in the intake system of an engine where the acoustic wall impedance of the inlet hose must be measured [4].

**References:**

[1] Leppänen, M., et al., 2005, "Plastic Foam Porosity Characterization by Air-Borne Ultrasound", 32 Annual Review of Progress in Quantitative Nondestructive Evaluation 2005, 31.7- 5.8, Maine, USA.
[2] Smye, S. W. and Bloor, M. I. G., 1995, “Prediction of reactive hyperaemia in vascular pathologies using elastic porous tube model", Medical & Biological Engineering & Computing. 33(2), p. 185-9.
[3] Xing-Li et al. ,1996, “Ultrasonic thin-walled tube wave structure for sensing devices”, IEEE Trans. on Ultrasonics, Ferroelectrics and Frequency Control, 43(2), p. 331-6.
[4] Chul-Min-Park. Et al., 2003, “Inverse estimation of the acoustic impedance of a porous woven hose from measured transmission coefficients”, Journal of the Acoustical Society of America 113(1), p.128-38.

114 **ELASTICITY AND PATHOLOGY IMAGING CORRELATION OF BREAST TUMOURS – INITIAL RESULTS.**

*William E Svensson[1]*, Asel Usupbaeva[1], Sami Shousha[2], Sheena McLaggan[1], A Al-Kufaishi[3], PTR Thiruchelvam[3], Jackie SK Lewis[3], H Dudley Sinnett[3], Joe Malin[4], Carol Lowery[4].*

[1]Radiology, [2]Pathology and [3]Surgery Departments, Charing Cross Hospital, London, England, UK; [4]Siemens Medical Solutions Ultrasound Group, Issaquah, WA, USA.

**Aims:** To determine how accurately freehand elasticity images and measurements correlate to the pathological appearances and dimensions of breast cancers.

**Background:** Earlier work done in our centre has suggested that freehand compression elasticity imaging is more accurate than conventional B-mode ultrasound for the assessment of breast tumour extent. Reported series show re-operation rates of as high as 50% when wide local excision is based on conventional breast imaging techniques.

**Methods:** Freehand elasticity images were obtained at regular intervals through tumour the day before surgery. The skin of the breast was marked to allow orientation sutures to be placed on the tumour specimen as it was excised. Histology sections were made in the same plane as the imaging planes at right angles to the greatest diameters of the B-mode tumour appearance. The edges of the specimen were examined to ensure tumour margin extent was accurately measured. The skin marking at imaging, and specimen marking at surgery, allowed ultrasound and specimen image correlation.

**Results:** One of nine cases of elasticity imaging underestimated maximum tumour diameter. B-mode underestimated in seven cases. Seven cases of elasticity imaging had closer correlation to pathology diameters than B-mode imaging. On average, B-mode underestimated by 20% while elasticity imaging overestimated by 14%. The elasticity image of Case 1 extended to the edge of the strain box, which could explain the underestimation.

**Conclusions:** Initial results suggest that elasticity imaging may provide a more reliable method of assessing tumour extent.

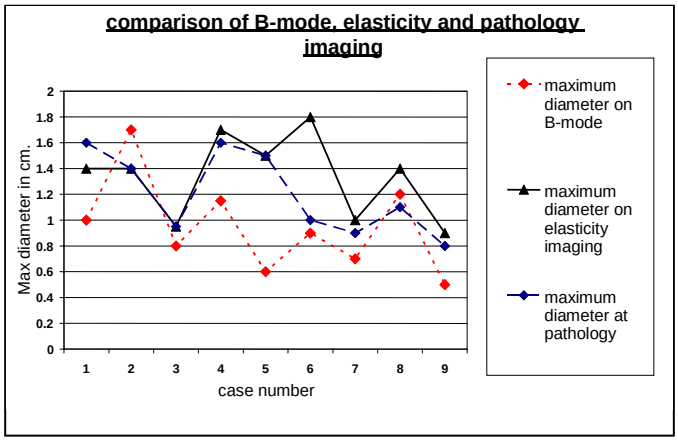


Table 1: Results of all nine cases

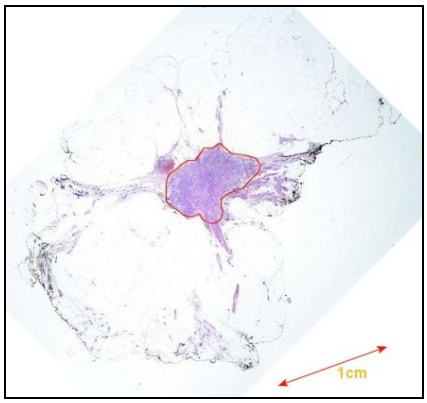


Figure 1: Histology

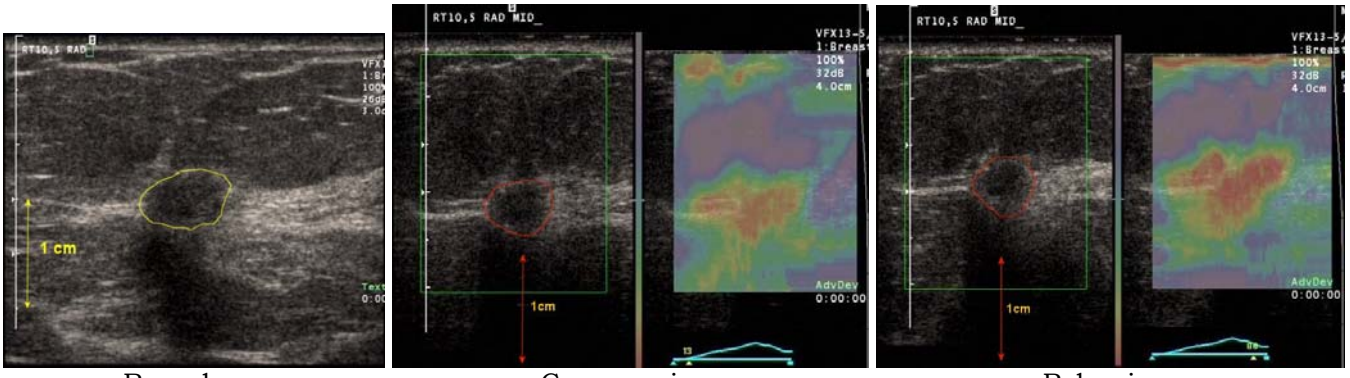


B-mode Compressing Releasing

Figure 2: Case 6 centre of tumour at right angles to longest diameter, images all same scale and orientation.

* *indicates Presenter*

118 **EFFECTS OF VISCOELASTICITY IN SHEAR WAVE SPEED RECONSTRUCTION.**

*J Klein[1]*, JR McLaughlin[1].*
[1]Rensselaer Polytechnic Institute, 110 8th Street, Troy, NY, USA.

**Aims:** In this report, we will show viscoelastic effects in transient elastography data and outline an approach to cope with these effects based on the idea of propagating wave fronts [1].

**Background:** The talk is based on phantom and *in vivo* data gathered by Mathias Fink's group [2].

**Methods:** The estimation of the arrival time of the wave front is improved by taking the spreading of the wave, caused by the viscoelastic effects, into account.

**Results:** The reconstruction of the shear wave speed is clearly improved by incorporating a simple model for viscoelasticity. This can be observed for the phantom as well as the *in vivo* data.

**Conclusions:** The improvement in reconstruction quality is promising considering the use of a very simple model. This approach allows, for the first time, the reconstruction of *in vivo* data in good quality for the technique using the arrival time of wave fronts. Therefore, further studies regarding viscoelastic effects seem very worthwhile.

**Acknowledgements:** This work has been supported by the NIH.

**References:**

[1] Ji L, McLaughlin J R, Renzi D, Yoon J R: Interior elastodynamics inverse problems: shear wave speed reconstruction in transient elastography, Inverse Problems, Vol. 19, No. 6, pp. s1-s29, 2003.
[2] Bercoff J, Chaffai S, Tanter M, Sandrin L, Catheline S, Fink M, Gennisson J L, Meunier M: *In vivo* breast tumor detection using transient elastography, Ultrasound in Med. & Biol., Vol. 29, No. 10, pp. 1387-1396, 2003.

119 **VISCOELASTIC CHARACTERIZATION OF SOFT MATERIALS THROUGH CREEP TEST EXPERIMENTS.**

*Jean Jacques Ammann[1,2]*, Ricardo Rivera[1], Jonathan Ophir[3].*
[1]Universidad de Santiago de Chile, Physics Department, Santiago, CHILE; [2]CIMAT, Santiago, CHILE; [3]The University of Texas Health Science Center at Houston, Houston, TX, USA.

**Aims:** As previously shown by Righetti et al. through stress relaxation experiments [1], imaging and characterizing the time dependency of tissue elastic constants open a new field to elastography-based diagnostics. We present here a method based on a composed Standard Anelastic Solid model [2], for a full characterization of the viscoelastic behavior of biomimetic materials. This is achieved through a creep test experiment and extracts a set of five rheological parameters from 1-D RF signals.

**Methods:** The method consists in determining the material viscoelastic parameters by interpreting time-dependant elastographic data through a 2 Voigt cell rheological model.

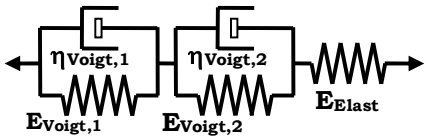


The experiment consists in applying a constant force on the specimen and the time-dependant behavior is recorded as a series of RF traces along the compression axis, acquired at increasing time intervals.

To process the acquired data, a windowed cross-correlation is performed between each pair of the successive traces. The Hilbert transform and a peak envelope detection routine allow the determination of the local displacement increment along the compression axis. The slope of the displacement curves vs. time corresponds to the strain increment. Integrating the slope from the application of the load to time-t yields the real strain vs. time curve.

The interpretation of the time-dependent strain is based on a 2 Voigt cell rheological model (see inset) accounting for five parameters: three elastic moduli $\mathbf{E_{Elast}}$, $\mathbf{E_{Voigt,1}}$ and $\mathbf{E_{Voigt,2}}$ and two viscosity coefficients $\boldsymbol{\eta}_{\mathbf{Voigt,1}}$ and $\boldsymbol{\eta}_{\mathbf{Voigt,2}}$. The time dependant strain equation for this model becomes:

$$\varepsilon(t) = \sigma_0 \left[ \frac{1}{E_{Voigt,1}} \left(1 - e^{\frac{-E_{Voigt,1}}{\eta_{Voigt,1}} t}\right) + \frac{1}{E_{Voigt,2}} \left(1 - e^{\frac{-E_{Voigt,2}}{\eta_{Voigt,2}} t}\right) + \frac{1}{E_{Elast}} \right]$$

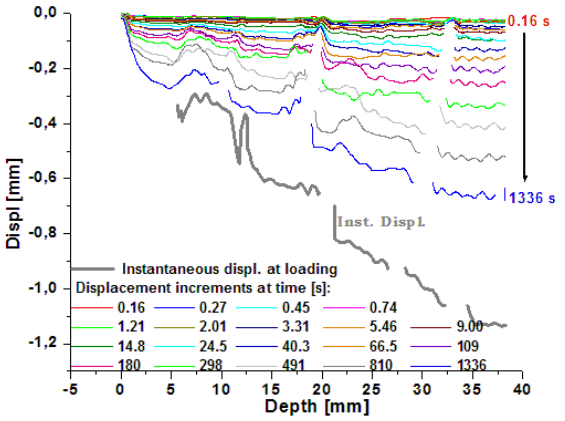


**Results:** The method is applied in a temperature-controlled water bath to a sample of fresh white cheese of 50mm diameter and 37mm height. The experiment consists in applying a pre-compression load through a polymer disc of size larger than the specimen to the cylindrical specimen. The disc holds in its center a 2.2MHz broadband transducer, which is directly in contact with the specimen. After the acquisition of four control RF traces, an additional force (brass ring: 187g) is applied to the top of the polymer disk. A series of 20 transducer traces is then recorded, subtracting the transducer ring-down previously acquired. The time delay between each acquisition is increased exponentially for a total acquisition time of 22 minutes. After processing, the viscoelastic parameters are obtained from the fit of the strain vs. time plot according to the equation above, yielding the following values:

| Parameter | Value |
|---|---|
| $\sigma_0$ | **-94.54 Pa** |
| $E_{Elast}$ | **3.376 kPa** |
| $E_{Voigt,1}$ | **1.15 kPa** |
| $\eta_{Voigt,1}$ | **1.3 MPa·s** |
| $E_{Voigt,2}$ | **5.05 kPa** |
| $\eta_{Voigt,2}$ | **0.2 MPa·s** |

**Conclusions:** A rheological model with two Voigt cells tracks consistently with the experimental behavior of a viscoelastic materials observed through a creep test experiment. The creep test experiment is expected to be readily implemented for tissue viscoelastic characterization.

**Acknowledgements:** This work is supported by Fondecyt project No. 1040206, Chile, ECOS-Conicyt project No C01E01(Chile-France), Fondap project No. 11980002 and Dicyt/USACH, Chile.

**References:**

[1] R. Righetti, J. Ophir, and T. A. Krouskop, Ultrasound in Med. & Biol., Vol. 31, No. 6, pp. 803–816, 2005.
[2] A. S. Novick and B. S. Berry, Anelastic Relaxation in Crystalline Solids, Academic Press, New York, 1972.

* *indicates Presenter*

003 **FROM STATIC TO DYNAMIC ELASTOGRAPHY: THE UNIFIED RANGE OF ELASTIC RESPONSE.**

*KJ Parker[1]*, LS Taylor[1], SM Gracewski[2], DJ Rubens[3].*
[1]Electrical and Computer Engineering, [2]Mechanical Engineering, [3]Radiology Departments, University of Rochester, Rochester, NY, USA.

**Background:** New approaches to imaging the elastic properties of tissue have been developed over the last 20 years, using either ultrasound or MRI to image the tissue response to some stimulus. Researchers have evaluated a wide range of stimuli, including heat, water jets, vibration shear waves, compression, and quasi-static compression, using single or multiple steps or low-frequency (<10 Hz) cyclic excitation. These appear to produce distinctly different types of information and images.

**Discussion:** In this presentation, we focus on the major classes of excitation stimuli, demonstrating that they produce responses that fall within a common range of elastic behavior. Within this range, the major classes of excitation include step compression, cyclic quasi-static compression, harmonic shear wave excitation, and transient shear wave excitation. The information that these different techniques reveal about the unknown elastic distribution within an imaging region of interest are shown to be fundamentally related because the tissue responses are governed by the same equation. The examples use simple geometry to emphasize the commonality of the approaches, providing a unified overview of elastic responses.

**Acknowledgement:** This work was supported in part by NIH 5 R01AG16317-03, "3D sonoelastography imaging for prostate cancer."

009 **ULTRASONIC TRACKING OF ACOUSTIC RADIATION FORCE-INDUCED DISPLACEMENT IN HOMOGENEOUS MEDIA.**

*ML Palmeri[1]*, SA McAleavey[2], GE Trahey[1], and KR Nightingale[1].*
[1]Duke University, Durham, NC, USA; [2]University of Rochester, Rochester, NY, USA.

**Aims:** Tracking tissue deformation generated by impulsive acoustic radiation force using ultrasonic methods, as is done in Acoustic Radiation Force Impulse (ARFI) imaging, is subject to jitter and displacement underestimation (bias). The purpose of these studies is to study the impact of acoustic material properties, excitation focal configuration, and tracking parameters on the bias and jitter in dynamic ultrasonic displacement estimates performed during ARFI imaging.

**Background:** Studies by McAleavey *et al.* [1] have demonstrated that steady-state, Gaussian displacement fields in the focal zone of the tracking beams are subject to bias and jitter due to scatterer shearing in the lateral and elevation dimensions of the point spread function (PSF) of the tracking beams. These studies expand upon those findings to quantify the displacement estimate bias and jitter for realistic, dynamic 3D displacement fields generated by ARFI excitations.

**Methods:** Models have been developed using Finite Element Methods and Field II [2], a linear acoustic field simulation package, to study the impact of focal configuration, frequency and material properties on the accuracy of ultrasonic tracking tissue deformation generated by acoustic radiation force excitation. Field II was used to simulate the acoustic radiation force field generated during ARFI imaging, while LS-DYNA3D was used to solve the equations of motion to determine the resulting dynamic 3D displacement fields in materials of varying stiffness [3]. Those displacement fields were then used to translate 3D distributions of randomly positioned, uniform amplitude acoustic scatterers, and Field II was used to simulate different transducer configurations and their impact on tracking the displacement fields through time.

**Results:** Displacement underestimation can be as great as 50% and jitter can be as great as +/- 2 μm immediately after excitation in an 8.5 kPa medium. Both displacement underestimation and jitter improve with time after excitation as shear wave propagation away from the region of excitation reduces scatterer shearing within the tracking PSF in the lateral and elevation dimensions. The use of a broader excitation configuration (greater F/#) compared with the tracking beams can reduce shearing in the lateral dimension of a 1D array. The use of higher tracking frequencies in broadband transducers leads to decreased jitter levels and more accurate displacement tracking. Relative displacement underestimation remains constant and jitter increases as a function of displacement magnitude (i.e., applied force). Underdeveloped speckle (SNR < 1.91) leads to greater jitter and peak displacement underestimation immediately after ARFI excitation. Axial shearing over the tracking kernel lengths used in ARFI imaging does not impact ARFI displacement estimation.

**Conclusions:** These models demonstrate that lateral and elevation shearing underneath the PSF of the tracking beam leads to displacement underestimation in the focal zone that can be reduced by using tracking beams that are confined within the extent of the displacement fields. Dynamic displacement estimate bias and jitter are dependent on material stiffness. The use of higher tracking frequencies with broadband transducers and multi-dimensional arrays should improve bias and jitter in displacement estimates. This model will allow for the impact of other factors on displacement tracking, such as physiologic motion, to be evaluated in ARFI imaging.

**Acknowledgements:** The authors would like to thank Dr. Jeremy Dahl and Gianmarco Pinton for their insights, and Joshua Baker-LePain for his technical assistance.

**References:**

[1] S.A. McAleavey, K.R. Nightingale, and G.E. Trahey. “Estimates of echo correlation and measurement bias in acoustic radiation force impulse imaging,” IEEE Trans. Ultrason., Ferroelec., Freq. Contr., 50(6): 631-641, 2003.

[2] J.A. Jensen and N.B. Svendsen. “Calculation of pressure fields from arbitrarily shaped, apodized, and excited ultrasound transducers,” IEEE Trans. Ultrason., Ferroelec., Freq. Contr., 39(2): 262-267, 1992.

[3] M.L. Palmeri, A.C. Sharma, R.R. Bouchard, R.W. Nightingale, and K.R. Nightingale. “A finite element method model of soft tissue response to impulsive acoustic radiation force,” IEEE Trans. Ultrason., Ferroelec., Freq. Contr., in press.

** indicates Presenter*

013 **THE IMPACT OF PHYSIOLOGICAL MOTION ON ABDOMINAL ACOUSTIC RADIATION FORCE IMPULSE IMAGING.**

*BJ Fahey[1]*, ML Palmeri[1], GE Trahey[1].*
[1]Duke University, Department of Biomedical Engineering, 136 Hudson Hall, Durham, NC, USA.

**Aims:** To assess the impact of physiological motion in organs such as the liver on abdominal acoustic radiation force impulse (ARFI) imaging and suggest strategies for minimizing the prevalence of motion artifacts in images.

**Background:** The presence of physiological motion in target tissues during ARFI imaging has two major consequences. First, significant motion can decorrelate speckle patterns, decreasing the effectiveness of correlation-based methods used for motion tracking. Secondly, axial components of physiologic motion will add biases to displacement estimates. Previous work has demonstrated the feasibility of acquiring ARFI images of the human abdomen that are free of significant motion artifacts [1], and Kolen et al. [2] have investigated physiological motion in the liver for the application of elasticity imaging. The current research builds upon these previous studies to quantify the tolerance for physiological motion in radiation force-based imaging methods (which generally have different methods and timescales for data acquisition compared to elastography) and assess the implications this has on imaging parameters such as line density, which govern the time window needed for data acquisition.

**Methods:** A multi-axis linear translation stage with programmable velocity and acceleration settings was used to simulate single and multi-axis physiologic motion while imaging a uniform tissue-mimicking phantom. Velocity and acceleration values were chosen to cover ranges presented in [2]. Statistical methods were used to quantitatively assess the effects of motion in terms of speckle decorrelation and displacement bias. Finite Element Method (FEM) mechanical models were also used in conjunction with synthetic RF data to model the effects of physiological motion at a range of velocities, accelerations, and transmit frequencies. Experimental results and models were compared to theoretical predictions of speckle decorrelation and measurement bias. In addition, during *in vivo* ARFI imaging of human volunteers and of RF ablation procedures in ovine livers, images were acquired with and without implementing ECG-triggering and motion-correcting filters.

**Results:** Motion of target tissues in ARFI imaging leads to speckle decorrelation artifacts if it is significant during the time period over which a single data line is sampled (1 – 3 ms). Therefore, in many ARFI imaging applications, motion artifacts are manifested mainly in the form of an added displacement bias to data. However, decorrelation artifacts will persist in ARFI images if large (e.g. respiratory) or high-velocity (e.g. imaging near large vessel) tissue motions are encountered. Although linear motion filters can be used to remove biases introduced by tissue motion, these filters become less effective as velocities increase and ineffective (and technically invalid) when significant tissue acceleration is present during acquisition. *In vivo* results from both human volunteers and animal models indicate that ECG-triggered data acquisitions with appropriately selected trigger delays can be used to effectively eliminate the presence of motion artifacts in many abdominal imaging applications.

**Conclusions:** Physiological motion of target tissues can degrade the quality of ARFI images if it is of significant velocity or magnitude. Imaging parameters, such as line density, field-of-view, and the temporal window over which displacements are monitored, must be chosen carefully in order to maximize trade-offs between image quality and acquisition time. ECG-triggered data acquisitions used in conjunction with linear motion filters are effective at eliminating many artifacts in ARFI images associated with abdominal physiological motion.

**Acknowledgements:** This work is supported by NIH grant #1R01CA114093-01.

**References:**

[1] Fahey, Brian J., et al. "Acoustic Radiation Force Impulse Imaging of the Abdomen: Demonstration of Feasibility and Utility." Ultrasound in Medicine and Biology, *in press*, 2005.
[2] Kolen, Alexander F. et al. "Characterization of Cardiovascular Liver Motion for the Eventual Application of Elasticity Imaging to the Liver *In Vivo*." Physics in Medicine and Biology, 49: 4187-4206, 2004.

017 **RADIO FREQUENCY ABLATION ELECTRODE DISPLACEMENT ELASTOGRAPHY – A PHANTOM STUDY.**

*Shyam Bharat[1,2], Ernest L. Madsen[1], James A. Zagzebski[1], Tomy Varghese[1,3]*.*
[1]Medical Physics; [2]Electrical and Computer Engineering; [3]Biomedical Engineering Departments, University of Wisconsin – Madison, 1300 University Avenue, 1530 MSC, Madison, WI, 53706, USA.

**Aims:** We describe a phantom-based validation study of a novel method of tissue perturbation for the elastographic visualization of radio frequency (RF) ablation-induced thermal lesions. This method involves the use of the RF ablation electrode as a controlled compression or displacement device. This method of inducing tissue displacement has previously been reported for *in vivo* experiments on porcine liver [1]. It provides localized compression in the region of interest. This phantom-based study seeks to quantify various aspects of this tissue displacement technique in terms of parameters such as inclusion size, contrast or strain ratio, contrast-to-noise ratio ($CNR_e$) and signal-to-noise ratio ($SNR_e$).

**Background:** Various techniques such as external plate compression, diaphragmatic motion resulting from respiration and cardiovascular motion have been employed to induce *in vivo* compressions in the liver for elastographic imaging. Early *in vivo* uses of RF ablation electrode displacement elastography resulted in good quality elastograms for small electrode displacements, on the order of 0.05 – 0.1 mm. Problems such as excessive lateral and elevational motions (which are commonplace in external plate compression) are not expected to be encountered in this tissue displacement method.

**Methods:** Initial studies have been performed on a single spherical inclusion phantom, with the inclusion being approximately 5 times stiffer than the background. Stepper motor controlled displacement was applied to an electrode with a U-shaped tip embedded in the inclusion, and raw ultrasound RF data was acquired with the ultrasound transducer positioned adjacent to the electrode stem. Data were acquired for different stages of electrode displacement away from the ultrasound transducer and towards the transducer (after an initial pre-compression of 0.25 mm). Ten independent data sets were acquired in each case. The inclusion width, height and area (as seen on the elastograms) were compared with known values. The contrast, $CNR_e$ and $SNR_e$ were also evaluated.

**Results:** The elastographic inclusion width estimates are close to the actual value, although in this version of the phantom the height and area measures were consistently underestimated. The contrast is greater than expected, likely because of perturbation mode that provides the localized deformation. The $CNR_e$ and $SNR_e$ are fairly consistent over all stages of displacement.

**Conclusions:** The RF ablation electrode displacement method for elastography offers the advantages of localized compression in the region of interest and results in good quality elastograms for extremely small displacements. It also causes little or no non-axial tissue motion and reduces lateral slippage, both of which, if present, are factors in reducing elastographic image quality. In an *in vivo* RF ablation procedure, this method offers the possibility of integrating the processes of RF ablation and elastography.

**Acknowledgements:** This work is supported by the Whitaker Foundation grant RG-02-0457.

**References:**

[1] Varghese T, Zagzebski JA, Lee FT Jr. Elastographic imaging of thermal lesions in the liver *in vivo* following radiofrequency ablation: preliminary results. Ultrasound Med Biol 2002; 28(11/12):1467-1473.

** indicates Presenter*

053 ***IN-VITRO* DEMONSTRATION OF REAL TIME MONITORING OF REGIONAL TISSUE ELASTICITY DURING FOCUSED ULTRASOUND THERAPY USING HARMONIC MOTION IMAGING.**

*Caroline Maleke[1]*, Mathieu Pernot[1], Elisa E. Konofagou[1].*
[1]Columbia University, Department of Biomedical Engineering, 1210 Amsterdam Avenue, New York, NY 10027, USA.

**Aims:** In this study, we discuss a new Harmonic Motion Imaging technique (HMI) that estimates tissue displacements produced by harmonic radiation force excitation using a single focused element in *in-vitro* tissue.

**Background:** Previously, we demonstrated the feasibility of a technique for simultaneous monitoring of ultrasound therapy treatment using two separate focused ultrasound transducer elements [1]. First, wave propagation simulation models were used to compare the use of one Amplitude-Modulated (AM) focused beam versus two overlapping focused beams as previously implemented for HMI [1]. Simulation results indicated that, in unlike the two-beam configuration, the AM beam produced a consistent, stable focus for the applied harmonic radiation force. The AM beam thus offered the unique advantage of sustaining the application of the radiation force on the same tissue region.

**Methods:** Experiments were then performed on tissue mimicking phantom and *in-vitro* tissues. The radiation force was generated by a 4.68 MHz focused transducer using a low-frequency Amplitude-Modulated (AM) Radio Frequency signal (RF). A 7.5 MHz single element, diagnostic transducer was placed through the center of the focused transducer so that the diagnostic and focused beams were properly aligned. A bandpass analog filter was used to remove the spectrum of the focused beam. Consecutive RF signals were acquired with a Pulse Repetition Frequency (PRF) of 5 kHz and the displacements were estimated using a classical cross-correlation algorithm.

**Results:** The intensity of the focused beam was varied from 26.34 W/cm$^2$ to 421.44 W/cm$^2$ with the AM frequency at 5 Hz allowing us to detect tissue displacements before and after tissue ablation. Tissue displacements before and after ablation were found up to 131 µm and up to 101 µm respectively. The local elastic properties were reconstructed using a Voigt model [2], and the regional elastic moduli before and after ablation were found to be 1.4 kPa and 1.8 kPa respectively. Furthermore, taking advantage of the real-time capability of our method, the change in the elastic properties was monitored during focused ultrasound (FUS) ablation of tissue mimicking phantom. In this experiment, the intensity of the focused ultrasound beam was 948.23 W/cm$^2$ at the focus, in order to simultaneously generate the harmonic radiation force and the tissue temperature variation and ablation. A decreasing slope of the oscillatory displacements was observed with time due to the change in the speed of sound vs. temperature. Based on the harmonic displacements and the calculated acoustic radiation force, the local elastic modulus was determined.

**Conclusions:** In conclusion, the feasibility of using an AM radiation force for harmonic motion imaging for simultaneous monitoring of tissue elasticity variation during ultrasound therapy was demonstrated in tissue mimicking phantoms and *in-vitro* tissues. Further study of this method will include stiffness and temperature mapping, *ex-vivo* and *in-vivo*.

**Acknowledgements:** This study was supported by a Special Development Award from the Whitaker Foundation. The authors also wish to acknowledge the Riverside Research Institute for providing the transducers used for this study.

**References:**

[1] Konofagou EE, Hynynen K., Ultras Med Biol; 29(10), 1405-1413 (2003).
[2] Krouskop, T., et al., Ultrasonic Imaging 20, 260-274 (1998).

019 **NORMAL AND SHEAR STRAIN ESTIMATION AND ANGULAR COMPOUNDING USING BEAM STEERING ON LINEAR ARRAY TRANSDUCERS.**

*Min Rao[1]*, Quan Chen[1], Hairong Shi[1], E.L. Madsen[1], J.A. Zagzebski[1], Tomy Varghese[1].*
[1]University of Wisconsin-Madison, 1530 Medical Science Center, 1300 University Ave., Madison, WI, USA.

**Aims:** In elastographic imaging, all components of the strain tensor are required to characterize the displacement following a compression since the resultant tissue motion inevitably occurs in three dimensions. Techavipoo et al. [1] recently proposed a method to estimate components of a displacement vector using RF echo signal data acquired along multiple angular insonification directions. In this study, we use this technique for estimating displacement vectors and strain tensor components using beam steering on a linear array transducer. We also investigate the performance of spatial angular compounding for elastography using the angular elastograms obtained.

**Background:** Previous research for the estimation tissue displacement vectors for strain imaging has been reported [2, 3]. Lubinski et al. [2] obtained lateral displacements for strain imaging utilizing assumptions of tissue incompressibility. However, the incompressibility assumption may not hold in some tissues, and the Poisson's ratio may not be a constant. Konofagou and Ophir [3] proposed the simultaneous estimation of both axial and lateral displacements and strains using a precision tracking algorithm. However, the extensive interpolation and recorrelation steps required increases the computational complexity. Spatial-angular compounding for elastography was also recently discussed [4].

**Methods:** Single and multiple inclusion phantoms with different boundary conditions between the inclusion and background material were imaged. Phantoms were scanned using an Ultrasonix 500RP machine with a 5 MHz linear-array transducer having an approximately 60% band width. A compression plate with a rectangular slot fitted with the transducer was mounted on a stage driven by a stepper motor. Data was collected using an automated beam-steering and RF echo data acquisition algorithm implemented on the Ultrasonix system. Pre-compression data along specified angles (-15º to 15º) at 0.75º increments are acquired, following which, the stepper motor is activated to compress the phantom. Following the compression, post-compression RF data are acquired along the same angles. Displacements were then measured along each beam direction. Axial (parallel to the compression direction) and lateral components of the displacement vector were estimated from the angular displacement data using a least squares solution. Strain tensor components are then estimated from the axial and lateral displacements. For spatial angular compounding the angular elastograms estimated at different angles are appropriately weighted and then averaged to generate a compounded elastogram.

**Results:** Axial-strain elastograms using this technique have higher image quality than traditional strain images. Lateral strain images have a lower signal to noise ratio (SNR) than axial strain images. Inclusions are clearly visible in both lateral and axial strain elastograms as well as in the estimated shear strain elastograms. Different patterns are observed in shear strain images of a mobile inclusion than in images of fixed inclusions. Improvements in the signal-to-noise ($SNR_e$) of 5dB for maximum angles in the range of 9 to 15º and contrast-to-noise ratios ($CNR_e$) of around 8 to 16dB, with the maximum angles ranging from 9 to 12º are obtained with by angular compounding for the single inclusion phantom.

**Conclusions:** Angular RF echo signals synchronized to the mechanical, uniaxial compressions using beam steering on a linear array transducer are acquired. These were used to generate axial, lateral, and shear strain images. Compounded elastograms also can be generated from angular elastograms to reduce noise artifacts. Experimental results suggest that shear strain images have a role in differentiating fixed from mobile lesions in the breast. The compounded elastograms demonstrate significant improvement in the $SNR_e$ and $CNR_e$ obtained by angular compounding.

**Acknowledgements:** This work is supported in part by NIH grant R21 EB003853 and R01EB000459.

**References:**

[1] Techavipoo, U., et al., IEEE Trans. Med. Imag., 2004. 23(12): p. 1479-1489.
[2] Lubinski, M.A., et al., IEEE Trans. Ultrason. Ferroel. Freq Cont., 1996. 43(2): p. 247-256.
[3] Konofagou, E., and J. Ophir, Ultrason. Med Biol., 1998. 24(8): p. 1183-1199.
[4] Techavipoo, U., et al., IEEE Trans. Ultrason. Ferroel. Freq Cont., 2004. 51(5): p. 510-520.

** indicates Presenter*

071 **DESIGN OF A HAND-HELD PROBE FOR IMAGING TISSUE ELASTICITY.**

*Hassan Rivaz[1]*, Robert Rohling[1].*
[1]Department of Electrical and Computer Engineering, University of British Columbia, Vancouver, BC, CANADA.

**Aims:** This paper describes a hand-held probe with a combined vibration source and ultrasound transducer to measure the motion. A multi-frequency excitation is used together with a recently developed vibro-elastography (VE) [1] method for extracting the tissue properties. Since the hand-held device is light, reaction forces from the tissue induce large amplitude vibrations of the user's hand. Therefore, the design uses a vibration absorption system to counter-balance the reaction forces from contact with the tissue.

**Background:** VE identifies the mechanical properties of tissue by measuring tissue motion in response to an external multi-frequency vibration, followed by system identification techniques to estimate the tissue properties. Previous research on VE showed the possibility of measuring the tissue properties by solving 1D equations of motion of a tissue model, or plotting the transfer function of motion between two points.

**Methods:** Four different methods for reducing vibration are well known: vibration isolation, passive vibration absorption, semi-active vibration absorption and active vibration absorption. An active dynamic vibration absorption (DVA) technique called the Delayed Resonator (DR-DVA) [2] is exploited in this design. Figure 1(a) shows a model of an active dynamic vibration absorber attached to the primary system, the hand-held device. In this picture, $F_e$, $F_c$, $m_a$, $b_a$ and $k_a$ are the excitation forces that vibrate tissue, the vibration absorption control force, absorber mass, absorber damping and absorber stiffness respectively. In order for DR to cancel the vibrations of the hand-held device at the excitation frequency of $\omega_e$, the feedback force, $F_c$, should be applied such that the absorber system mimics a resonator at the frequency of $\omega_e$ [2].

**Results:** Figure 1(b) shows the design of the hand-held device. The main parts of the probe are two linear voice-coil actuators (one for excitation, one for DR-DVA), a faceplate, an absorber mass and an accelerometer. The probe is designed for a desired frequency range of 5-25 Hz to cover a significant bandwidth of the tissue response. Different ranges are possible by tuning the system. Several experiments were then carried out on the probe to show the effectiveness of the DR-DVA. In Figure 1(c), the probe is held by a human operator on the forearm of a human subject. In this experiment, the DR-DVA starts at t=0.8 s, and decreases the peak-to-peak motion from 1.28 mm to 0.13 mm. A B-mode image obtained from a three layered phantom is shown in Figure 1(d). The middle layer of the phantom is stiffer than the other layers but exhibits the same acoustic properties; therefore is not visible in the B-mode image. Figures 1(e) and 1(f) show two vibro-elastograms obtained with the hand-held device using a 5 Hz excitation without and with DR-DVA respectively. The time domain cross-correlation with prior estimates [3] is used for motion tracking. The motion tracking accuracy is reduced by probe vibration, resulting in a poor vibro-elastogram (Figure 1(e)). A vibro-elastogram obtained with the hand-held device using a 1 Hz excitation is shown in Figure 1(g). The use of such low frequency excitations requires a new control algorithm that is operational from 0-25 Hz. We are currently developing such a new algorithm based on proportional-integral control. Future research will therefore continue to focus on two main goals: reduce probe vibration as a way to increase the accuracy of VE, and reduce user fatigue.

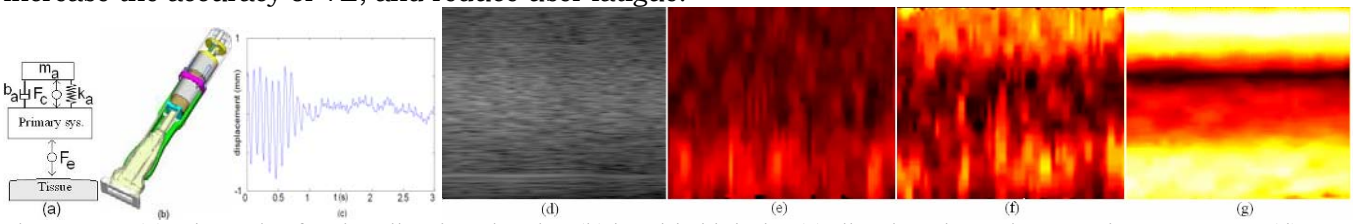


Figure 1: (a) schematic of active vibration absorber (b) hand-held device (c) vibration absorption experiment at 10 Hz (d) B-mode image (e) elastogram without DVA (f) elastogram with DVA (g) elastogram at 1 Hz.

**References:**

[1] E. Turgay, S. MacIntosh, R. Rohling and S. Salcudean. Parameter identification of tissue lumped models based on sequences of ultrasonic train images. Second Intl. Conf. on Ultrasonic Measurement and Imaging of Tissue Elasticity. pp. 29, Corpus Christi, Texas, Oct. 2003.

[2] N. Olgac, Holm-Hansen. A novel active vibration absorption technique: delayed resonator. J. of Sound and Vibration Vol. 176 pp 93-104, 1994.

[3] R. Zahiri, S. E. Salcudean. Time domain cross correlation with prior estimates. Third Intl. Conf. on Ultrasound Measurement and Imaging of Tissue Elasticity. Lake Windermere, Cumbria, UK, Oct. 2004.

049 **SHEAR MODULUS RECONSTRUCTION USING DIRECT FINITE ELEMENT INVERSION ALGORITHM IN TRANSIENT ELASTOGRAPHY.**

*Eunyoung Park[1]*, Antoinette M. Maniatty[1].*
[1]Rensselaer Polytechnic Institute, Jonsson Engineering Center 2049, 110 8th Street, Troy, NY, USA.

**Aims:** The goal of this work is to reconstruct the shear modulus field in tissue from discrete measurements of the displacement field in space and time resulting from an interior or exterior, transient, dynamic excitation. A robust, fast algorithm that considers the complete equations of isotropic, linear, elasto-dynamics is sought.

**Background:** Reconstruction of tissue elastic properties, in particular shear modulus which characterizes elastic resistance to shape change, holds great promise as a diagnostic tool because of the close relationship between the elastic shear modulus and the underlying structure of tissue. The shear modulus is also closely related to the shear wave speed; thus, observation of shear waves traveling through tissue can provide a rich dataset for recovering the shear modulus. Based on this premise, ultrasound [1] and MRI [2] techniques have been developed for measuring the displacement field in tissue resulting from a single frequency pulse excitation in order to observe propagating shear waves. Using such data, several researchers have presented methods for reconstructing the shear modulus field. In order to simplify the inversion algorithm, most researchers assume the equations for elasto-dynamics can be approximated by the Helmholz equation. To make this simplification, the gradients of the pressure and shear modulus fields are neglected. In this work, the complete equations for elasto-dynamics are considered and the effect of these simplifying assumptions investigated.

**Methods:** A space-time finite element method is used as a basis for the inversion algorithm. This approach is chosen because it reduces the highest order derivatives in space and time from two to one, which reduces sensitivity to noise, and allows for the general equations of elasto-dynamics to be considered. A mixed formulation, with interpolation of both the displacement and pressure field, is used in order to handle the relatively, nearly incompressible behavior of tissue. A direct inversion approach is used for solving for the shear modulus field because it does not overweight the boundary data and is quick since it does not require iterations nor forward solution of the governing equations. In addition, it can be applied on local subdomains, which also reduces the computation time as well as allows for straightforward parallelization of the algorithm. In this approach, the pressure as well as the shear modulus are reconstructed.

**Results:** The shear modulus distribution is reconstructed quantitatively from numerical and experimental data. The effect of neglecting the pressure gradient is considered. The effect of the time window of the data chosen to be used in the reconstruction for a given region of interest is also investigated. This choice of window is important because sufficient data is needed for a unique reconstruction, and the data with the most information, i.e. data with a high signal to noise ratio, should be chosen.

**Conclusions:** The primary advantages of this algorithm are: it considers the complete equations for isotropic, linear elasto-dynamics; it is extendible to more complex constitutive models, such as considering anisotropy and viscoelastic effects, provided sufficient data is available; does not overweight boundary data; and is fast relative to other finite element based methods. Since this method requires the reconstruction of the pressure distribution, which depends on both space and time, there is the potential to have too many unknowns. An appropriate choice for the window in the time domain is needed to ensure that the number of equations will be more than that of unknowns.

**Acknowledgements:** This work has been supported by the National Science Foundation through grant DMS-0101458 and by the National Institutes of Health through grant 5 R21 EB003000-02. The authors thank J. McLaughlin, J-R. Yoon, and D. Renzi at Rensselaer for many valuable discussions.

**References:**

[1] J. Bercoff, M. Tanter, and M. Fink, "Supersonic Shear Imaging: a new technique for soft tissues elasticity mapping," IEEE Trans. Ultrason., Ferroelec., Freq. Contr. 51 (4), 374-409, 2004.
[2] P.J. McCracken, A. Manduca, J. Felmlee, R.L. Ehman, "Mechanical transient-based magnetic resonance elastography," Magn. Reson. Med., 53 (3), 628-639, 2005.

** indicates Presenter*

023 **FINITE ELEMENT ANALYSIS AND YOUNG'S MODULUS RECONSTRUCTION FOR ELASTICITY IMAGING WITH DEFORMATION BY A RADIOFREQUENCY ABLATION ELECTRODE.**

*J Jiang[1]*, T Varghese[1], TJ Hall[1], Q Chen[1] and JA Zagzebski[1].*
[1]Medical Physics Department, University of Wisconsin-Madison, Madison, WI, USA.

**Background:** Recent results (e.g. [2]) indicate changes in tissue stiffness following RF ablation correlate with the ablation temperature. Hence, elasticity imaging might be a means to monitor tissue status during the RF ablation process. Previous work by our group [1] demonstrated that tissue deformation obtained by moving the ablation electrode during radiofrequency (RF) ablation was controllable and reproducible and yielded clinically acceptable elastograms. This presentation will summarize our recent advances in modulus imaging for monitoring RF ablation.

**Aims:** The aims of this study were to understand the mechanics of tissue deformation with the RF ablation electrode using finite element analysis (FEA) and to develop a computer model to reconstruct Young's modulus from simulated ultrasound data. One of the challenges that must be met in this effort stems from the fact that a typical RF needle electrode and the tissue interactions are three dimensional and nonlinear. Even modeling the biomechanical contact between the needle electrode (cylindrical geometry) and thermal lesion (spherical or oval objects) with FEA is a computationally demanding task. We have developed a new approach under which the reconstruction problem for this geometry is simplified to a two-dimensional problem. This simplification relaxes computational demands typically required for full three-dimensional finite element analysis (FEA) based modulus reconstruction.

**Methods:** Forward FEA was used to investigate the feasibility of reconstructing the Young's modulus distribution resulting from RF ablation. Specifically, assuming that the RF electrode is always bound to the treated tissue but is not attached to the untreated tissue, realistic tissue deformations were simulated from a 3D rigorous finite element model where tissue was deformed by displacing the RF ablation electrode. The simulated tissue deformation patterns were then employed to deform an assumed numerical phantom. A frequency-domain ultrasound simulation program [4] was employed to compute images of the numerical phantom and to obtain pre- and post-deformation RF echo data. Lastly, an iterative Young modulus reconstruction with total variation regularization [3] was used to obtain tissue modulus with axial displacements estimated from the numerical phantom.

**Results:** The effect of this 2-D simplification on modulus reconstruction was evaluated by comparing the axial displacement field to that of its corresponding rigorous three-dimensional FEA model. The absolute difference between the axial displacement images obtained using the 3-D model and the 2-D simplified model provides a quantitative measure of the errors incurred for the simplification. The absolute peak difference was 12% for the plane stress condition and 25% for the plane strain condition, while the average absolute differences were 7% and 17%, respectively. The plane stress condition, therefore, provides the best approximation to the 3-D model. Preliminary results, obtained using the ultrasound simulation program [4], suggest that high contrast modulus images can be reconstructed. The estimated Young's moduli for thermally-introduced lesions were underestimated by about 10%, while the size of thermal lesions was underestimated by 15-20% along the direction perpendicular to the needle displacement direction on modulus images.

**Conclusions:** FEA of tissue deformation with the RF ablation electrode is an important step toward understanding this biomechanical system *in vivo*. Using numerical phantoms based on FEA computed tissue deformations, we found that it is feasible to reconstruct the Young's modulus distribution following measurements of tissue deformation with a RF ablation electrode. The underestimation of lesion size and the large error variance in modulus estimates are due to the 2D simplified model; this topic requires further attention.

**Acknowledgements:** This work is supported in part by grants from CDMRP DAMD17-00-1-0596, NIH-R01CA100373, NIH-R21-EB002722, Whitaker Foundation RG-02-0457, and the UW-Madison.

**References:**

[1] T. Varghese, J. A. Zagzebski, and F. T. Lee, "Elastographic imaging of thermal lesions in the liver *in vivo* following radiofrequency ablation: preliminary results," *Ultrasound Med Biol*, 28, pp. 1467-73, 2002.
[2] S. Bharat *et al.*, "Monitoring stiffness changes in lesions after radiofrequency ablation at different temperatures and durations of ablation," *Ultrasound in Med Biol*, 31, pp. 415-422, 2005.
[3] C. R. Vogel and M. E. Oman, "Fast, robust total variation-based reconstruction of noisy, blurred images," *IEEE Transactions on Image Processing*, 7, pp. 813-824, 1998.
[4] Y. Li and J. A. Zagzebski, "Frequency domain model for generating B-mode images with array transducers," *IEEE Transactions on UFFC*, 46, pp. 690-699, 1999.

086 **THREE DIMENSIONAL ULTRASOUND IMAGE REGISTRATION AND SHEAR ELASTIC MODULUS RECONSTRUCTION.**

*Michael S Richards[1]*, Nachiket H Gokhale[2], Assad A Oberai[2], Paul E Barbone[2].*
[1]Biomedical Engineering, [2]Aerospace and Mechanical Engineering Departments, Boston University, 110 Cummington Street, Boston, MA 02215, USA.

**Aims:** To develop and evaluate an ultrasound technique to quantitatively measure and image the mechanical properties of soft tissues in 3D. The intended application of our work is in the detection and diagnosis of breast cancer and other soft tissue pathologies. The specific goal of this project is the accurate measurement of the elastic shear modulus distribution of a tissue mimicking ultrasound phantom, using a 3D ultrasound imaging system. This requires the design and characterization of algorithms to provide 3D motion estimates and to solve the 3D inverse problem to recover shear elastic modulus.

**Background:** Ultrasound elastography typically utilizes quasistatic compression of tissues. The deformation is observed via 2D (plane) ultrasound. It is measured by cross-correlation block image matching, and interpreted via the strain field. These methods are simple to apply clinically, computationally inexpensive, easy to interpret, and have demonstrated clinical benefit in several studies. Nevertheless, they have some drawbacks; the elimination of which may further improve clinical performance. For example, though the observation is 2D, the deformation field *in vivo* may be expected to violate 2D assumptions. In addition, in noisy situations, block-matching tends to produce noisy displacement estimates. We have developed two methods by which we reconstruct a 3D modulus image from the ultrasound data. In both cases, the measured deformation is interpolated on a 3D finite element mesh, which effectively provides local and optimal "companding". The first method uses a sum-squared intensity difference objective function, which is minimized to produce displacements. These displacements are then used in an inverse algorithm which minimizes the difference in displacement from those measured, to those predicted given a shear modulus distribution and the equations of linear elasticity. The adjoint method combined with a gradient based, quasi-Newton inversion algorithm is used to find the modulus distribution which minimizes this equation. The second is a constrained optimization algorithm which minimizes the sum-squared image intensity difference with respect to the shear modulus distribution directly. The adjoint method and a gradient based, quasi-Newton inversion algorithm is also used to find this modulus distribution.

**Methods:** To acquire our 3D ultrasound images, we mechanically translate a linear ultrasound array in the elevation direction to obtain multiple images. We use a 10-12 MHz linear array driven by our Analogic Ultrasound Engine (AN 2300) which allows us access to the preprocessed RF data. The modulus inversion algorithms require the input of either the displacement or traction boundary conditions of the image domain. This data can either be calculated from the images or known experimentally. The algorithms can also calculate modulus distributions from multiple sets of images, or multiple displacements, if they are necessary to ensure the uniqueness of the solution.

**Results:** Results are presented of displacement measurements and shear modulus inversions which were calculated from the ultrasound phantom created and imaged in our lab. The exact dimensions and contrast of the resulting shear modulus image are compared with the actual phantom dimensions and independently calibrated mechanical properties. A comparison of the shear modulus inversion from displacement measurements and inversion directly from ultrasound image pairs is shown. The effect of the boundary conditions and regularization methods on the reconstructed modulus images and the uniqueness of the solution are also discussed.

**Conclusions:** Our algorithms for shear modulus reconstructions may improve the detection and diagnostic power of standard mammography practices. The resulting modulus images are quantitative and can provide an accurate representation of the mechanical properties and spatial distributions of soft tissue. Our image acquisition and computational costs are high due to the size of the 3D images and problem calculations. The nature of this algorithm makes it well suited for applications in mammography, where the mechanical behavior of the tissue is well controlled. This algorithm also has the potential to be applied to a broad spectrum of imaging modalities, including Ultrasound, X-ray tomosynthesis, and MRI.

**Acknowledgements:** This work is supported in part by CenSSIS (The Center for Subsurface Sensing and Imaging Systems) under the Engineering Research Centers Program of the National Science Foundation (Award No. EEC-9986821) and the Department of Defense Breast Cancer Research Program (Award No. W81XWh-04-1-0763).

** indicates Presenter*

089 **ZERO MEMORY GAUSS-NEWTON METHOD FOR THE DETECTION OF SMALL INCLUSIONS.**

*J Fehrenbach[1]*, M Masmoudi[1], R Souchon[2], P Trompette[2].*
[1]Laboratoire MIP, Toulouse, FRANCE; [2]INSERM UMR 556, Lyon, FRANCE.

**Aims:** Elastography is an emerging imaging technique that provides a strain image of an elastic tissue under a small compression. Here, we address the problem of Young's modulus estimation from an elastogram. A Gauss-Newton algorithm was applied to elastography under known boundary conditions in [1] and [2], but this algorithm has a heavy computational cost. Our first contribution is to identify the boundary conditions. We also propose an implementation of Gauss-Newton algorithm that requires little memory (only one stiffness matrix is stored) and few computations. This algorithm was applied to experimental data.

**Background:** Numerous reports and methods have been published on the estimation of Young's modulus. In [3], the strain-based and model-based modulus elastography were compared, and it was shown that model-based elastography provides a better estimation of modulus contrast.

**Methods:** In this contribution, we implemented a Gauss-Newton algorithm that uses both direct and reverse modes of algorithmic differentiation [4]. This implementation was applied to two consecutive inverse problems. The first one was to estimate the forces on the boundaries, since measured data are only radial strain. The second inverse problem is the Young's modulus reconstruction itself.

**Results:** Our algorithm was applied to data obtained from a gelatin phantom [5]. The estimation of the boundary conditions was satisfactory, at least qualitatively, since with our experimental data, 4 small inclusions out of 6 were detectable. The Young's modulus reconstruction showed the 4 inclusions, as expected. All these computations were performed on a standard desktop computer. However, the true value of the Young's modulus was not checked against an independent method.

**Conclusions:** The Gauss-Newton implementation presented here allowed working on fine meshes for solving the Young's modulus inverse problem. This allowed finding small inclusions in an elastic medium. Further studies have to be conducted to compare the measured contrast to the true contrast.

**Acknowledgements:** This work was supported in part by the National Cancer Institute (USA) Program Project Grant P01-64597 to the University of Texas Medical School at Houston; and by the ACINIM CNRS Project (France)

**References:**

[1] F Kallel, M Bertrand, Tissue Elasticity Reconstruction Using Linear Perturbation Method, IEEE Trans.Med.Imag. 15(3), 299-313 (1996).
[2] M Doyley, P Meaney, J Bamber, Evaluation of an Iterative Reconstruction Method for Quantitative Elastography, Phys.Med.Biol. 45(6), 1521-1540 (2000).
[3] M Doyley, S Srinivasan, S Pendergrass, Z Wu, J Ophir, Comparative Evaluation of Strain-Based and Model-Based Modulus Elastography, Ultrasound Med.Biol.31(6), 787-802 (2005).
[4] A Griewank, Evaluating Derivatives, Principles and Techniques of Algorithmic Differentiation, Frontiers in Applied Mathematics, SIAM (2000).
[5] R Souchon, O Soualmi, M Bertrand, JY Chapelon, F Kallel, J Ophir, Ultrasonic Elastography Using Sector Scan Imaging and a Radial Compression, Ultrasonics 40(1-8) 867-871 (2002).

092 **THE INFLUENCE OF CAUSALITY ON THE RECONSTRUCTION OF SHEAR MODULUS FOR DYNAMIC ELASTOGRAPHY.**

*Benjamin Robert[1]*, Ralph Sinkus[1], Jeremy Bercoff[1], Mickael Tanter[1], Mathias Fink[1].*
[1]Laboratoire Ondes et Acoustique, ESPCI, 10 rue Vauquelin, 75005 Paris, FRANCE.

**Aims:** The principle of causality (Kramers-Kronig relations) imposes an underlying relationship between the loss modulus $G_l$ and the dynamic modulus $G_d$. Thereby, the shear modulus - as reconstructed by the classical Voigt model - does not represent the elasticity at zero frequency ($\mu_0$). Aim of this analysis is to present a technique leading to a reduced bias for the reconstruction of the shear modulus in case of dynamic elastography.

**Background:** Many analyses suggest that attenuation of acoustic waves obeys a power law dependence on frequency [1]. This leads the loss modulus to the general form $G_l=b|\omega|^{\alpha}$. Utilization of the Kramers-Kronig relations yields the corresponding expression for the dynamic modulus $G_d=\mu_0+ctg(\alpha\,\pi/2)*G_l$ [2]. Reconstruction is typically done utilizing the classical wave equations [3], i.e.:

$$-\rho\omega^2\mathbf{q} = G_d\Delta\mathbf{q} + iG_l\Delta\mathbf{q}, \qquad \mathbf{q}=\mathrm{curl}(\mathbf{u}), \qquad \mathbf{u} = \text{displacement vector.} \qquad \text{Equation (1)}$$

Thus, if the material obeys a linear power law (i.e. $\alpha=1$), reconstruction of the dynamic modulus $G_d$ provides the desired information $\mu_0$. There is, however, strong evidence that tissue does not obey a linear power law [4, 5] leading to difficulties to properly interpret $G_d$. In steady-state mono-frequent elastography, the assessment of the power $\alpha$ is not possible. Moreover, due to the utilization of compressional waves for mechanical excitation, it is observed that the reconstruction of the loss modulus $G_l$ yields negative values within tumors. This is caused by the fact that tumors act as sources of shear waves due to strong internal mode conversion. Thus, a malignant absorbing tumor might appear soft in the image of $G_d$ (Figure1).

**Methods:** $G_d$ and $G_l$ correspond to the material parameters of the classical Voigt model ($\mu^{Voigt}=G_l$, $\eta^{Voigt}=G_l/\omega$). Thus, the bias for the estimation of $\mu_0$ is determined by $\Delta\mu^{Voigt}= ctg(\alpha\,\pi/2)*G_l$ which can vary depending on the sign of $G_l$. If we choose to reconstruct the data not with the classical Voigt model but rather with the Maxwell model (spring and dashpot are here in series), we find the following equation:

$$-\rho\omega^2\mathbf{q} = -i\omega\eta^{Max}\Delta\mathbf{q} - i\rho\omega^3\eta^{Max}/\mu^{Max}\mathbf{q}. \qquad \text{Equation (2)}$$

This equation can be rewritten such that it resembles the form of Equation (1) providing:

$$\Delta\mu^{Max} = \Delta\mu^{Voigt} + (G_l)^2/G_d. \qquad \text{Equation (3)}$$

The second term in Equation (3) does not depend upon the sign of the loss modulus and counteracts the first term. It can be shown that the bias on $\mu^{Max}$ is greatly diminished for those cases were $G_l$ is negative. Whenever $G_l$ is positive, the Voigt model is the one providing less bias.

**Results & Conclusions:** *In-vivo* results from breast lesions indicate the necessity to take the sign of $G_l$ into account for reconstruction of $G_d$. Furthermore, it is demonstrated that the power dependence of the loss modulus is not linear within breast lesions since otherwise the maps of $G_d$ would show the tumors.

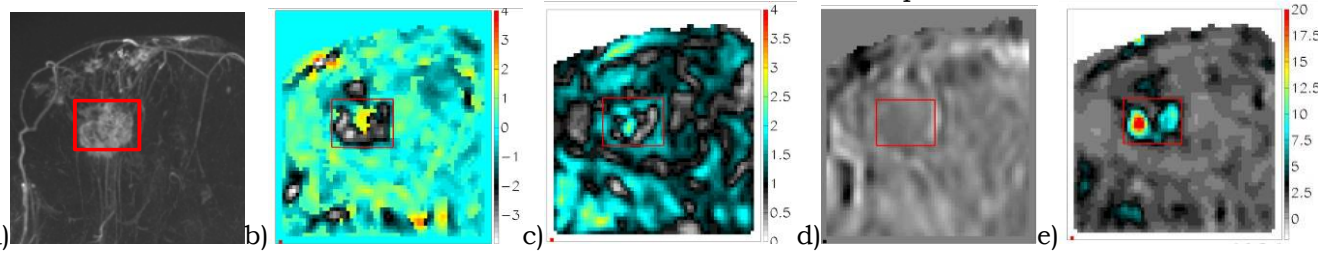


Figure 1: a) MR-subtraction image indicating the location of the tumor. b) Map of reconstructed lost modulus $\eta^{Voigt}=G_l/\omega$ [Pa*s]. Strongly negative values are recorded at the location of the tumor. c) Map of reconstructed dynamic modulus $G_d=\mu^{Voigt}$ [kPa]. The tumor does not appear as a hard entity although the change in wavelength is clearly visible in the map of $q_y=\mathrm{curl}(\mathbf{u})_y$ (see d). e) the tumors are well visualized. Here, both values, $\mu^{Voigt}$ and $\mu^{Maxwell}$, are mixed according to the sign of $G_l$.

**References:**
[1] Szabo, J. Acoustic Soc. Am. **96** (1) July (1994) 491-500.
[2] Pritz, Applied Acoustics **65** (2004) 1027-1036.
[3] Sinkus et. el, MRI **23** (2) February (2005) 159-165.
[4] Mason et. al., J. Rheol. **44** (4) July/August (2000) 917-928.
[5] Kiss et al., Phys. Med. Biol. **49** (2004) 2307-4218.

* *indicates Presenter*

007 **MOTION COMPENSATION FOR INTRAVASCULAR ULTRASOUND PALPOGRAPHY FOR *IN VIVO* VULNERABLE PLAQUE DETECTION.**

*K. Y. Esther Leung[1], Radj A. Baldewsing[1], Frits Mastik[1], Mikhail G. Danilouchkine[1], Johannes A. Schaar[1], Andries Gisolf[2] , and Antonius F. W. van der Steen[1,3]*.*
[1]Biomedical Engineering, Thorax Centre, Erasmus MC, Rotterdam, The NETHERLANDS; [2]Acoustical Imaging and Sound Control, Faculty of Applied Sciences, Delft University of Technology, The NETHERLANDS; [3]Interuniversity Cardiology Institute of The Netherlands, Utrecht, The NETHERLANDS.

**Background:** Intravascular ultrasound palpography can assess the mechanical properties of coronary arteries *in vivo* by radial strain measurements. Validation studies of this technique, previously reported at this conference, have revealed a clear association between high-strain patterns and the number of vulnerable plaques. The strain is measured by cross-correlating RF signals acquired at different systemic pressures. However, catheter motion due to cardiac activity causes misalignment of these signals, so that fewer strain estimates are obtained.

**Aims:** This study reports motion compensation methods to correct for in-plane catheter rotation and translation.

**Methods:** Four motion compensation methods, all based on block matching, were devised. The global rotation block matching (GRBM) and contour mapping (CMAP) methods measured catheter rotation, while local block matching (LBM) and catheter rotation and translation (CRT) estimated displacements of local tissue regions. The methods were validated on nine *in vivo* pullback acquisitions, acquired with a 20 MHz 64 element phased-array transducer (Volcano Corp.) at 30 frames/s. Each frame consisted of 512 circumferential RF lines and 1024 radial samples, which were sampled at 100 MHz. The motion compensation methods were used to align the RF signals of consecutive diastolic frames before strain calculation. The resulting strain images, i.e. partial palpograms, were aligned and averaged per heart cycle to produce more accurate and robust compounded palpograms. To assess the performance of each method, the number of valid strain estimates in the partial and compounded palpograms was compared with the number without motion compensation. The validity of a strain estimate was determined from the theoretical relationship between strain and decorrelation of the signals: if the decorrelation did not fit the expected value as predicted by the measured strain within a certain bandwidth, the strain estimate was considered invalid.

**Results:** We found that all four methods significantly increase the number of valid strain estimates in the partial and compounded palpograms ($P<0.004$). For the GRBM, CMAP, LBM, and CRT methods, the average increase in the partial palpograms amounted to 8.1%, 7.0%, 17%, and 11%, while the increase in the compounded palpograms was 5.9%, 4.8%, 15% and 9.3% respectively.

**Conclusions:** The Local Block Matching method is the best of the four methods. Application of the motion compensation methods leads to palpograms with more strain estimates, which will improve the information coming from intravascular ultrasound palpography.

**Acknowledgements:** We wish to thank the Dutch Technology Foundation (STW) and Volcano Corp. (Rancho Cordova, CA) for their support.

005 **A COMPOUNDING METHOD FOR RECONSTRUCTING THE HETEROGENEOUS YOUNG'S MODULUS DISTRIBUTION OF ATHEROSCLEROTIC PLAQUES FROM THEIR RADIAL STRAIN.**

*Radj A. Baldewsing[1]*, Frits Mastik[1], Johannes A. Schaar[1], and Antonius F. W. van der Steen[1,2].*
[1]Biomedical Engineering, Thorax centre, Erasmus MC, Rotterdam, The NETHERLANDS; [2]Interuniversity Cardiology Institute of the Netherlands, Utrecht, The NETHERLANDS.

**Background:** Rupture of vulnerable atherosclerotic plaques, with subsequent thrombosis, is the main cause of stroke and myocardial infarction. Pharmaceutical treatments aim at stabilizing a plaque by reducing or stiffening its atheroma. Stabilization can be quantitatively monitored by imaging the Young's Modulus (YM). Since a radial strain elastogram can be reliably measured *in vivo* using intravascular ultrasound (IVUS) elastography, a YM image can be obtained from it by solving the inverse problem.

**Aims:** A compounding method for solving the inverse problem for arbitrary atherosclerotic plaques is described. It is an extension of a previous YM reconstruction framework [1] that was mainly suited for reconstruction of thin-cap fibroatheromas (i.e., plaques with a large lipid pool covered by a thin fibrous cap). To allow YM reconstruction of an arbitrary plaque, the following adaptations are made to the existing framework: (1) use of deformable Bezier curves to parameterize arbitrary geometries of plaque components, (2) use of the strain elastogram to define initial YM distributions and (3) use of a compounding method to obtain a heterogeneous YM distribution from individual YM reconstructions.

**Methods:** An individual YM reconstruction is obtained from a measured strain elastogram, as follows: an optimization algorithm adjusts the morphology and stiffness parameters of a Plaque Finite Element Model (PFEM), to maximize the similarity (in terms of root mean squared error) between the simulated and measured strain elastograms. The PFEM's morphology parameters are the control-points of two deformable Bezier curves, one curve delineates the lipid pool, the other the cap; each of these plaque components is homogenous and its stiffness is characterized by a YM. The inner and outer PFEM boundaries are detected from the IVUS echogram.
Each individual YM reconstruction was started from a PFEM Initial State (IS) (i.e., initial values for the PFEM morphology and stiffness parameters). IS were automatically created, as follows: (a) each high strain (>~0.7%) region produced an IS by placing the PFEM lipid pool tightly around it and the PFEM cap in front of it, and (b) at the area of maximum wall-thickening a large PFEM lipid pool was placed with the PFEM cap in front of it. The initial YM of the plaque components were estimated from their mean strain according to a theoretical "YM-strain" relationship for a pressurized axisymmetric homogeneous tube.
Finally, each reconstructed YM image was compounded into a final YM image. This was done by locally weighting each reconstruction with the inverse of the local difference between simulated and measured strain elastogram. The method was applied to five FE-simulated radial strain elastograms (e.g., Figure A) obtained from histology-traced YM distributions [2] (e.g., Figure B) of five atherosclerotic human coronaries.

**Results:** For the studied arteries, the compounded YM image (e.g., Figure C) showed much resemblance with the histology-traced YM (e.g., Figure B). However, not all soft regions were (correctly) identified. Probable causes are: (a) not every soft region gives rise to high strain and vice versa, consequently, no IS was placed, or (b) there was too much strain decay from inner to outer wall-border as a result of natural stress decay caused by the circumferential geometry of the vessel wall.

**Conclusions:** Our fully automatic method reconstructs the heterogeneous YM distribution of arbitrary atherosclerotic plaques from their radial strain elastogram. It may be used for *in vivo* tissue characterization to quantify pharmaceutical induced plaque stabilization. The method can be generalized to other arteries/organs where one or more strain-tensor components are measurable. More validation is needed using measured strain elastograms and corresponding arterial histology to quantify its accuracy.

**Acknowledgements:** STW, NWO and Volcano Corporation.

**References:**

[1] Baldewsing et al., IEEE TMI, 24(4), 514-28, 2005.
[2] Baldewsing et al., Ultrasound Med. Biol., 30(6), 803-13, 2004.

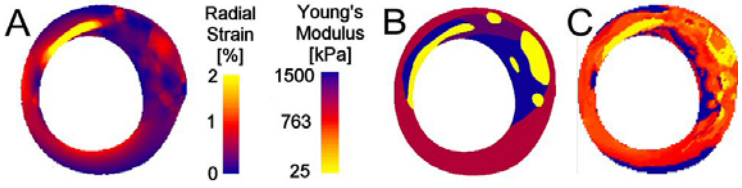


* *indicates Presenter*

025 **AN INTEGRATED ULTRASOUND-BASED INTRAVASCULAR IMAGING OF ATHEROSCLEROSIS.**

*Shriram Sethuraman[1]*, Salavat R. Aglyamov[1], James H. Amirian[2], Richard W. Smalling[2], and Stanislav Y. Emelianov[1].*

[1]Department of Biomedical Engineering, University of Texas at Austin, Austin, TX 78712, USA; [2]Division of Cardiology, University of Texas Health Science Center Houston, Houston, TX 77030, USA.

**Aims:** In this work we investigate the possibility of combining intravascular ultrasound (IVUS), photoacoustic (IVPA) and elasticity imaging to detect and differentiate vulnerable coronary plaques. Our aim is to utilize many synergistic features of these imaging techniques and to develop an integrated intravascular imaging system capable of direct assessment of morphological, functional and biomechanical properties of atherosclerotic plaques of coronary arteries.

**Background:** Cardiovascular diseases continue to be the leading cause of death and disability in the United States. High mortality rates result from the rupture of plaques that is considered insignificant on a coronary angiographic evaluation. Unfortunately, all clinical imaging procedures lack the specificity and sensitivity to effectively guide coronary interventions. Indeed, most of the clinical imaging systems can identify luminal diameter, stenosis, wall thickness and plaque volume; however, none can reliably characterize plaque composition and therefore identify vulnerable plaques. To address these limitations, we introduce combined intravascular imaging approach based on photoacoustic imaging augmented by ultrasound and elasticity imaging. Intravascular photoacoustic (IVPA) imaging involves the detection of pressure transients generated by a laser induced optical excitation of the tissue. Primary contrast mechanism for IVPA imaging is the presence of structures (hemoglobin, fat, fibrous tissue, etc.) with different optical absorption. Therefore, starting with IVUS images of tissue morphology, plaque composition can be identified using IVPA. In addition, significant changes in the mechanical properties of atherosclerotic lesions can be assessed using intravascular elasticity imaging. As a result, the combination of these ultrasound-based imaging techniques could aid in determining the morphology and composition of coronary plaques.

**Methods:** To evaluate the performance of the combined IVUS, IVPA and intravascular elasticity imaging system, the studies were performed using vessel mimicking phantoms made out of polyvinyl alcohol (PVA). Inclusions with optical contrast (0.08% graphite particles) and elastic contrast were embedded in the vascular phantom (8% PVA and 0.4% silica scatterers for ultrasonic contrast). Single element high frequency IVUS imaging catheters (20 MHz and 40 MHz) were used to image the modeled vessel with atherosclerotic plaques. Laser excitation required for IVPA imaging was provided by an Nd:YAG (532 nm) pulsed laser system. Simultaneous acquisition of ultrasound and photoacoustic signals allowed automatic registration of intravascular images. For intravascular elasticity imaging, the phantom was deformed using intravascular pressures. A high speed acquisition system was used to collect a large number of IVUS frames during the deformation of the phantom. Multiple IVUS frames acquired at different pressures were post-processed to obtain intravascular strain images.

**Results:** The integration of IVUS imaging with intravascular elasticity and IVPA imaging was successful without any major modifications to IVUS imaging. The combined imaging procedure was capable of identifying the inclusions not necessarily visible in the IVUS image alone. For example, images of radial strain revealed less than 2 mm diameter inclusion in the vessel wall based on the mechanical contrast between inclusion and surrounding medium. The inclusion was further identified in the IVPA image due to elevated optical absorption. These results demonstrate that both IVPA and elasticity imaging can provide additional information complementary to IVUS imaging.

**Conclusions:** A combined IVUS, IVPA and intravascular elasticity imaging is possible and could provide a much needed comprehensive imaging solution to detect and differentiate atherosclerotic plaques based on anatomic and functional properties.

**Acknowledgements:** This research was supported by The University of Texas Center for Biomedical Engineering seed grant. We thank Boston Scientific, Inc. for supplying IVUS imaging catheters.

054 **ELECTROMECHANICAL MAPPING OF THE NORMAL AND ISCHEMIC MYOCARDIUM.**

*Mathieu Pernot[1], Simon D. Fung-Kee-Fung[1], Elisa E. Konofagou[1]*.*
[1]Department of Biomedical Engineering, Columbia University, New York, NY, USA.

**Aims:** The heart is a complex electromechanical pump. Therefore, accurate and complete diagnosis of heart diseases should entail quantitative analysis of the electromechanical mechanisms. However, this is currently limited by the lack of noninvasive imaging techniques of the global electromechanical function. We propose here an ultrasound based method for measuring and imaging the electromechanical regional function of the myocardium.

**Background:** The propagation of electrical waves through the cardiac muscle induces contraction of the myocardium that results in the propagation of a strong mechanical wave. Since this wave results from coupling of the electrical excitation and the mechanical response of the tissue, it is hereby named "electromechanical wave".

**Methods:** Our method is based on imaging and analyzing the delay in small tissue displacements resulting from the propagation of the electrical excitation. *In-vivo* experiments were performed in anesthetized open chested dogs. A 2.5MHz phased array transducer (Terason 2000, Teratech, Inc.) was placed over the anterior wall in order to obtain a short-axis view of the left ventricle. Sequences of approximately three cardiac cycles were acquired at a frame rate of 56 images/s. The 2D displacement maps were estimated using a cross-correlation algorithm between two successive frames (window size: 5mm, 90% overlap). Temporary regional ischemia was then induced by a 90% flow constriction of the left anterior descending (LAD) coronary artery.

**Results:** The displacement maps clearly showed the propagation of several mechanical waves along the circumference of the myocardium (Figure 1). The wave velocity was found to be approximately 0.6m/s in the posterior wall. After the induction of ischemia, the mechanical wave completely disappeared in the ischemic region. These results were corroborated through invasive electrophysiological measurements using a matrix of electrodes on a proximal site.

**Conclusions:** These results demonstrate the feasibility of imaging the electromechanical activity of the myocardium *in vivo*. Since the electromechanical wave speed is a function of both electrical and mechanical properties of the myocardium, i.e., the electrical conductivity and the shear modulus, this method could potentially be used for early, noninvasive and simultaneous detection of electrical and mechanical dysfunctions in the heart and monitoring of treatment such as resynchronization therapy.

**Acknowledgements:** This study was supported by a Scientist Development Grant from the American Heart Association and a Special Developmental Award from the Whitaker Foundation.

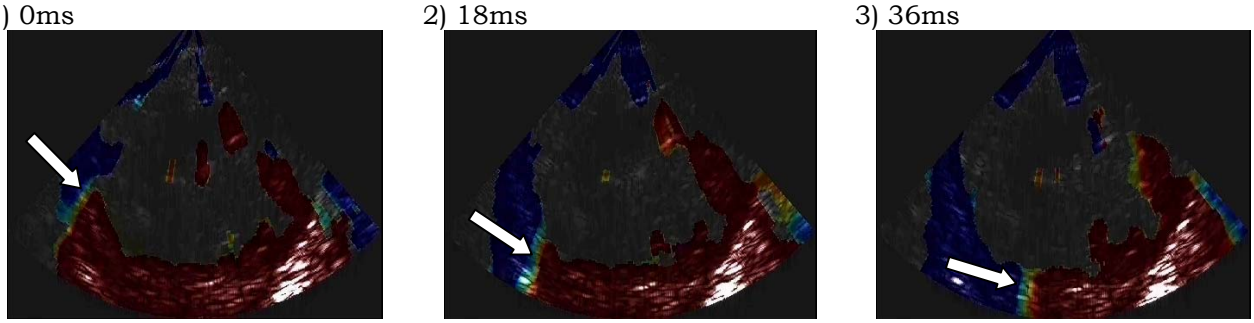


Figure 1: Propagation of the electromechanical wave in the dog myocardium. The displacement maps in color are superimposed on the grayscale ultrasound image. The white arrows show the position of the wavefront of the electromechanical wave.

056 **ANGLE INDEPENDENT STRAIN ESTIMATION IN MYOCARDIAL ELASTOGRAPHY.**

*Simon D. Fung-Kee-Fung[1]*, Elisa E. Konofagou[1].*
[1]Columbia University, Department of Biomedical Engineering, 1210 Amsterdam Avenue, New York, NY 10027, USA.

**Aims:** To remove the dependence of current strain estimations on the position and angle of the transducer, by converting them to strain estimates with respect to the heart's geometry.

**Background:** Current methods for the detection and measurement of ischemia and related heart diseases involve human visual observation and other qualitative methods of assessing wall motion and wall thickening of the myocardium. Myocardial Elastography has been previously proposed as a new method to quantify and visualize muscle abnormalities by measuring regional axial displacements and strains [1]. However, these measurements are dependent on transducer location and the angle of the ultrasound beam relative to the direction of motion of the muscle. In order to make these measurements useful and more relevant to cardiologists, in a step towards the development of this technique as a clinical tool, this paper describes a method for the removal of the aforementioned angle-dependence and transforms strains measured in (x, y, z) with respect to the beam of the transducer to strains that could be displayed to the cardiologist as radial, circumferential and longitudinal, i.e. with respect to the heart's geometry.

**Methods:** A 2D simulation model was created for testing the hypothesis. Temporal displacement measurements of motion in the short axis (SA) plane of a canine left ventricle (LV) were generated at a frame rate comparable to that achieved with a standard echocardiography machine. This simplified 2D model simulated basic wall motion of the left ventricle by including radial expansion and contraction, circumferential twisting and wall thickening and thinning. These displacements were generated using the same configuration as that of current elastography techniques (i.e. axially and laterally with respect to the transducer). Full representation of the strain tensor was obtained by calculating the gradient of each displacement map in both axial and lateral directions. It has been previously shown that eigenvalue decomposition of the complete strain tensor yields the principal strains (eigenvalues) that match the corresponding regional strains in the radial, circumferential and longitudinal directions in an axisymmetric configuration [2]. Model complexities were also introduced, by simulating non-homogeneous areas of strain, areas of ischemia through decreased regional motion, and phase delays to simulate the propagation of the electromechanical wave of muscle stimulation around the myocardium.

**Results:** During mid-diastole, the model was given an incremental radial strain of 2.20% without any circumferential strain. Axial and lateral strain values were calculated from displacement maps at the same phase of the heart cycle. Axial and lateral strains varied around the myocardium in the homogeneous case, with average values of 1.3% ± 0.7% and 1.3% ± 0.7% respectively. After eigenvalue decomposition, the average value of the principal strain found in the myocardium was 2.17%. The principal strain was found to be homogeneous across the entire muscle, and, therefore, angle-independent. Similar good results were found throughout all phases of the cardiac cycle.

**Conclusions:** An analytic, homogeneous strain model was created. Using this simple model we have shown a robust method of converting strain values from an arbitrary coordinate space with respect to the transducer beam to values with respect to left-ventricular geometry; a more reliable method for the accurate depiction of myocardial properties during freehand, echocardiographic scanning.

**Acknowledgements:** This study was supported by a Scientist Development Grant from the American Heart Association and a Special Developmental Award from the Whitaker Foundation.

**References:**

[1] Konofagou E, D'hooge J, Ophir J. Myocardial Elastography – A Feasibility Study *In Vivo*. Ultrasound in Med. & Biol., Vol. 28, No. 4, pp. 475–482, 2002.
[2] Waldman L, Fung Y, Covell J. Transmural Myocardial Deformation in the Canine Left Ventricle. Circ Res 57: 152-163, 1985.

063 **NON-INVASIVE VASCULAR ELASTOGRAPHY FOR CAROTID ARTERY PLAQUE CHARACTERIZATION: *IN VIVO* FEASIBILITY STUDY.**

*Roch L. Maurice[1]*, Guy Cloutier[1], Marie-France Giroux[2], Sylvain Lanthier[3], and Gilles Soulez[2].*
[1]Laboratory of Biorheology and Medical Ultrasonics, Research Center, [2]Radiology, [3]Neurology Departments, University of Montreal Hospital, Montreal, CANADA.

**Aims:** A fatal complication of carotid artery atherosclerosis is thrombosis, a consequence to plaque rupture or fissure. Plaque rupture is a complicated mechanical process, correlated with plaque morphology, composition, mechanical properties and with the blood pressure and its long term repetitive cycle. Extracting information on the plaque local mechanical properties and on the surrounding tissues may thus reveal relevant features about plaque vulnerability. This paper presents preliminary *in vivo* results for two healthy subjects and one patient.

**Background:** Our group recently developed a new approach to characterize mechanical properties of arteries by non-invasively assessing the strain within the vascular wall (non-invasive vascular elastography, NIVE) [1, 2]. For this purpose, the ultrasound transducer is placed on the neck over the carotid artery, whereas the vessel wall is compressed (dilated) by the normal cardiac pulsation. In NIVE, the elastograms are computed from the assessment of the vascular tissue kinetics using the Lagrangian Speckle Model Estimator (LSME). The LSME is a model-based estimator that considers the speckle as a material property [3].

**Methods:** Ultrasound radio-frequency (RF) data were acquired with an ES500RP system (Ultrasonix, Vancouver, Canada) equipped with a 7 MHz linear array transducer. Two healthy subjects and one patient were investigated. For each of them, elastograms were computed from longitudinal segments of the common and proximal internal carotid arteries (CCA and PICA, respectively).

**Results:** For the healthy subjects, comparisons were made for the NIVE elastograms computed from the RF data collected by two radiologists over the left and right carotid arteries. For each healthy segment (CCA and PICA), strain values around 1% were estimated. Considering the recorded cardiac pulsation, the instrumentation parameters along with the LSME implementation, that is around 300 kPa of elastic modulus for the healthy carotid arteries. These results also showed good similarities between the left and right carotid arteries as well as between the two radiologists. Regarding the pathologic subject, very low strain values (<<1%) were observed in areas where B-mode images revealed the presence of an atherosclerotic plaque.

**Conclusions:** This study allowed differentiating normal vessel walls from a plaque non-invasively based on the strain patterns. Similarities between mechanical properties of the left and right carotids were observed. The reproducibility of the process was also addressed and confirmed by two radiologists. In summary, these results suggest that NIVE could be a potential clinical tool for carotid artery investigations. Whereas small wall thickness of such arteries may be a limitation, our group currently conducts a Phase 1 clinical investigation to fully investigate the potential of NIVE. This clinical protocol will be introduced and some preliminary results will be discussed.

**References:**

[1] Roch L. Maurice, Jacques Ohayon, Yves Frétigny, Michel Bertrand, Gilles Soulez, Guy Cloutier, *Non-invasive Vascular Elastography: Theoretical Framework*, IEEE – Transactions on Medical Imaging, Vol. 23, No 2, pp. 164-180, February 2004.
[2] Roch L. Maurice, Michel Daronat, Jacques Ohayon, Ékatherina Stoyanova, Stuart Foster, Guy Cloutier, *Non-Invasive High-frequency Vascular Ultrasound Elastography*, Physics in Medicine & Biology, Vol. 50, pp. 1611-1628, 2005.
[3] Roch L. Maurice, Michel Bertrand, *Lagrangian Speckle Model and Tissue Motion Estimation - Theory*, IEEE – Transactions on Medical Imaging, Vol. 18, No 7, pp. 593-603, July 1999.

** indicates Presenter*

068 **A 3D SIMULATION MODEL FOR PERFORMANCE ASSESSMENT OF 2D MYOCARDIAL ELASTOGRAPHY.**

*Wei-Ning Lee[1]*, Christopher Ingrassia[1], Elisa E Konofagou[1].*
[1]Columbia University, Department of Biomedical Engineering, 1210 Amsterdam Avenue, New York, NY 10027, USA.

**Aims:** The main purpose of this paper is to fundamentally characterize the performance of Myocardial Elastography in 2D and identify the optimal parameters to be used for the more reliable detection of ischemia or infarction.

**Background:** A complete representation of the left-ventricular function throughout an entire cardiac cycle was previously demonstrated through the use of a 3D finite-element analysis (FEA) model [1]. This FEA model together with an ultrasound image formation model is used here in order to test the performance of 2D Myocardial Elastography at distinct phases of the cardiac cycle and at different states of myocardium, i.e., normal and ischemic, based on *in vivo* canine data [1].

**Methods:** A previously developed 3D finite-element analysis (FEA) model of a normal canine left ventricle with 40 nodes and 16 elements was first used to simulate the passive filling phase. The finite-element model [1] was defined in prolate coordinates ($\lambda$, $\mu$, $\theta$) while the RF images were generated in Cartesian coordinates ($x$, $y$, $z$). Short-axis displacement and strain maps were computed using the FEA model at several slices (i.e., $\mu$ = 0 – 120) starting with an undeformed representation (0 mmHg) and passively inflating the model up to 1.875 mmHg. Second, to simulate the ischemic case, a 3D regionally (i.e. posterior lateral wall) ischemic model, LCx (left circumflex) occlusion canine model was used and evaluated at two different end systolic pressures, which started from 111 mmHg to 75 mmHg with a constant level of contractility (constant elastance). The model in this case contained 48 nodes and 24 elements. A convolutional image formation model was employed to generate the corresponding 2D short axis RF images in both normal and ischemic cases. The axial and lateral displacements within multiple image (x-y) planes across the left-ventricular volume were iteratively calculated and corrected to reduce the decorrelated noise [2]. Thus, the displacement in each strain component is corrected in the direction perpendicular to that calculated, i.e., the post-deformation RF signals are corrected for the lateral displacement previous to the axial strain estimation.

**Results:** The iterative correction method successfully obtained high quality axial and lateral displacement images as well as elastograms of normal and shear strain components with a very good agreement between the radial FEA and elastographic estimates, in both normal and ischemic simulations. The strains measured were found to be within an error of 5% in the normal and 2% in the ischemic case on the average. The ischemic region was most visible on the elastogram at high pressure gradients during systole.

**Conclusions:** The performance of Myocardial Elastography was evaluated using a previously established left-ventricular FEA model. Given the excellent agreement between the FEA solution and the elastographic strains measured in the axial and lateral directions, Myocardial Elastography proves to be a reliable technique for the accurate assessment of the myocardial deformation in 2D at distinct phases of the cardiac cycle as well as detection of ischemia.

**Acknowledgements:** This study was supported by the American Heart Association.

**References:**

[1] Usyk T.P., LeGrice I.J., McCulloch A.D., Computational model of three-dimensional cardiac electromechanics, Comput Visual Sci 4: 249–257, 2002.
[2] Konofagou E.E. and Ophir J., 'A new elastographic method for estimation and imaging of lateral displacements, lateral strains, corrected axial strains and Poisson's ratios in tissues', Ultrasound in Med. & Biol., Vol. 24, No. 8, pp.1183-1199, 1998.

008 **FRAME FILTERING FOR IMPROVED FREEHAND 3D ULTRASOUND ELASTOGRAPHY.**

*JE Lindop[1]*, GM Treece[1], AH Gee[1], RW Prager[1].*
[1]University of Cambridge, Cambridge, England, UK.

**Aims:** 2D elastograms produced from freehand scans are of unreliable quality. Frame filtering has been investigated as a means of improving the contrast-to-noise ratio (CNR) in 3D elastograms. This enhances the freehand 3D elastography system outlined in a previous article [1], which to our knowledge remains the only such system to have been reported in the literature.

**Background:** To record a 3D elastogram, the probe is swept across a volume of several centimetres in length over the course of up to ten seconds. Strain estimates are calculated by tracking speckle between consecutive ultrasound frames, using an adaptation of the efficient, high-accuracy algorithm described by Pesavento *et al.* [2]. Each 2D elastogram is normalised according to a min-max strain scale, and these are stacked together to form a 3D data set, using the position sensing and software of an existing freehand 3D ultrasound system [3]. The problem with freehand scanning is that excessive non-axial motion often causes too much signal decorrelation for successful strain estimation. The high frame acquisition rate (>30 Hz) reduces the level of motion, but this means that some strains are too small to record. Frame filtering can be used to discard data where the correlation or the strain is too low.

**Methods:** A phantom was constructed simulating a stiff inclusion in soft tissue (olive/gelatin). A freehand scan was processed offline: A-lines were analysed using 60 windows at 85% overlap between neighbours; a least squares strain estimator of length 2, 3 or 5 windows produced the final estimates. A reslice plane (Figure 1) was defined perpendicular to the scan plane, incorporating data from all the 308 2D elastograms. In every resultant 3D elastogram the olive/gelatin CNR was evaluated to measure performance, using a segmentation based on B-scans not elastograms.

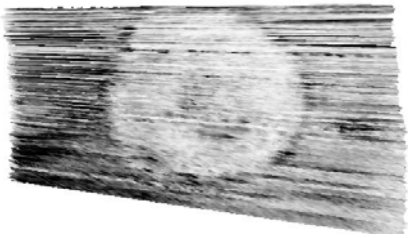

Figure 1: Unfiltered Elastogram Reslice.

**Results:** Figure 2 shows the effect on reslice CNR of discarding 2D elastograms whose mean strain is below a threshold. 0.04% gave the highest CNR, so Figure 3 shows the results for mean correlation thresholds which were applied in addition to a 0.04% strain threshold. Up to a correlation threshold of 0.87, this produced considerably improved 3D elastograms regardless of the length of the least squares filter that was used. Higher thresholds discarded too much data, however, and the sparse distributions of retained data became insufficient for accurate representation of the strain field.

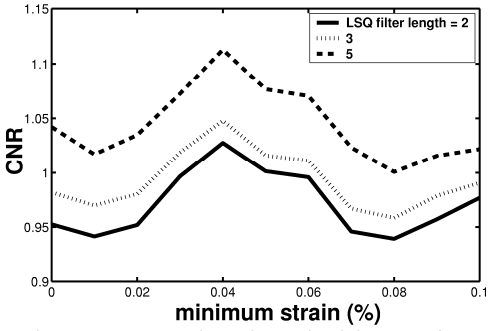


Figure 2: Strain Threshold Results.

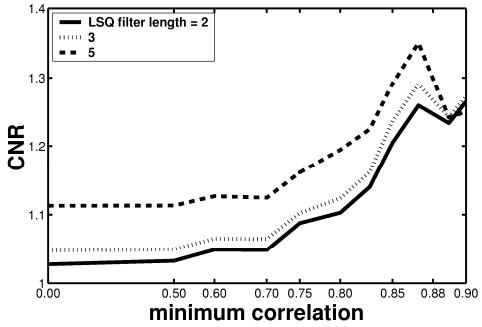


Figure 3: Correlation Threshold Results.

**Conclusions:** Frame filtering offers a simple, computationally inexpensive means of significantly boosting the quality of freehand 3D elastograms. There remains scope for introducing more sophisticated measures of elastogram quality, which are likely to yield further improvements.

**References:**

[1] JE Lindop, GM Treece, AH Gee, and RW Prager. 3D elastography using freehand ultrasound. In Medical Image Computing and Computer-Assisted Intervention — MICCAI'04(2): 1103–1104, 2004.
[2] A Pesavento, C Perrey, M Krueger, and H Ermert. A time efficient and accurate strain estimation concept for ultrasonic elastography using iterative phase zero estimation. IEEE T. Ultrason. Ferr., 46(5): 1057–1067, 1999.
[3] GM Treece, AH Gee, RW Prager, CJC Cash, and L Berman: High definition freehand 3D ultrasound. Ultrasound Med. Biol. 29: 529–546, 2003.

** indicates Presenter*

057 **AN INVERSE DEFORMATION METHOD FOR THE VISUALIZATION OF REAL-TIME 3D LUNG DYNAMICS.**

*Anand P Santhanam[1]*, Jannick P Rolland[1,2].*
[1]School of Computer Science, [2]College of Optics and Photonics (CREOL/FPCE), University of Central Florida, 4000 Central Florida Blvd, Orlando, FL 32816, USA.

**Aims:** Physically accurate simulation of 3D lung dynamics is an effective tool for guidance in clinical maneuvers. Technical advances in medical imaging techniques have led to the availability of 3D high-resolution lung models. The main focus of our research is to simulate a patient's normal and patho-physical lung dynamics using physically based deformation methods. However, for accuracy and smoothness in simulation, physically based deformation methods are required to deform lungs using human subject specific elastic parameters. Such estimations may also be an early indicator for patients' disease states such as COPD and tumor. The focus of this paper is on the estimation of elastic tissue properties of a normal human subject's lungs from a sequence of high-resolution 3D lung models. Such estimation would facilitate accurate simulations of the 3D lung dynamics. The approach adopted for such estimation is to use a deformation algorithm that can account for the morphological changes from one 3D model to another during breathing.

**Background:** The method previously used for lung deformations was based on Finite Element Methods (FEM), NURBS, and Green's Formulation (GF) [1]. While the FEM is computationally expensive, NURBS is not a physically based deformation method. Thus, in this paper, we use a GF based deformation for modeling lung dynamics which is a convolution of the force applied on each node and a transfer matrix traditionally referred to as either transfer function or operator. The force applied on each node represents the air-flow and is based on the distance from the resting surface (due to gravity) [2]. This paper presents a method for inverse analysis using spectral decomposition of a GF based deformation using spherical harmonic (SH) transformations. A key property of the transfer matrix is that the row of this matrix forms a converging sequence. Thus, the SH coefficients of every row also form a converging sequence which can be approximated using Dirichlet integrals [3]. The usage of this approximation allows us to simplify the GF.

**Methods:** For mathematical analysis the GF is represented in a continuous domain. A polar coordinate representation is used for representing each node in the Green's Formulation. The displacement of every node is taken as input from the CT data. The force applied on each node is estimated for a supine position. They are then re-represented in frequency space using SH transformations and plugged into the GF. The SH coefficients of the deformation are now represented as a direct product of the SH coefficients of the applied force and a summation of a set of SH coefficients of the transfer matrix's row which can be computed for a known applied force and displacement. The individual SH coefficients of this summation are then estimated using Dirichlet integrals as shown in [3]. Thus, for a known applied force the SH coefficients of the transfer function can be computed, and the original transfer function can be estimated.

**Results:** The proposed method is used for a sequence of 3D lung models obtained from a 4D HRCT [4]. The number of 16 SH coefficients is used for the analysis. An initial estimation of the transfer matrix shows that the actual deformation from a 3D model to another and the re-simulated deformation match closely with less than 1% RMS error.

**Conclusions:** The method presented in this paper allows us to estimate the elasticity of high-resolution 3D lung models of normal human subjects. The average range of elasticity of human lungs can be estimated for set of patients.

**Acknowledgements:** This work is funded by CREOL/FPCE.

**References:**

[1] Santhanam, A., Fidopiastis, C., Hamza-Lup, F., Rolland, J.P., and Imielinska, C., "Physically-based Deformation of High-resolution 3D lung models for Augmented Reality based Medical Visualization. "Medical Image Computing and Computer Aided Intervention, AMI-ARCS. Rennes,St-Malo Lecture Notes on Computer Science (2004). pp. 21-32.
[2] Fan, L., Chen, C.-W., Hoffman, E.A., and Reinhardt, J.M., "Evaluation and application of 3D lung warping and registration model using HRCT images."Proc. SPIE Conf. Medical Imaging. San Diego,CA (2001). pp. 234-243.
[3] MacRobert and Murray, T., Spherical Harmonics an elementary treatise on harmonic functions with applications. International series of monographs in pure and applied mathematics. New York: Oxford Pergamon Press (1967).
[4] Segars, W.P., "Development of a new dynamic NURBS-based cardiac-torso (NCAT) phantom." 2002, University of North Carolina Chapel-Hill.

091 **COMPARISON OF THREE NON-AXIAL STRAIN ESTIMATION TECHNIQUES FOR 3D STRAIN ESTIMATION IN ELASTIC MATERIALS AND TISSUES.**

*Richard G.P. Lopata[1]*, Maartje M. Nillesen[1], Inge H. Gerrits[1], Johan M. Thijssen[1], Livia Kapusta[2], Chris L. de Korte[1].*

[1]Clinical Physics Laboratory, [2]Children's Heart Center, Radboud University Medical Center, Nijmegen, The NETHERLANDS.

**Aims:** In this study, a framework is set for future 3D anisotropic strain imaging in a complex structure as the human heart, by determining the strain in 3 orthogonal directions.

**Background:** Imaging of 2D elastic properties of human tissue has been proven to be a useful tool in the clinical setting. In previous studies, capturing radio-frequency data (RF) of 2D ultrasonic datasets has enabled estimation of axial and lateral strain. Complex structures like the human heart require 3D imaging techniques to fully capture the strains in different directions involved in active contraction and relaxation during a single heart cycle. Also, the orientation of the muscle fibers is not confined to one single plane. With the availability of 3D ultrasound, new techniques are available for assessing strain in all dimensions.

**Methods:** Using a Philips SONOS 7500, equipped with a 4MHz 3D transducer and a RF-interface, raw ultrasound data were acquired. The non-axial displacement was estimated using three different algorithms.

I. The axial displacement is estimated using cross-correlation analysis of the RF-data and subsequently, the non-axial displacement is assessed using cross-correlation analysis of the envelope. The axial displacement was used as an offset for non-axial displacement measurements. Interpolation was performed in axial (32 times) and in non-axial direction (16 times).
II. A 2D RF-based displacement tracking algorithm was implemented using the 2D cross-correlation function. Five post-deformation lines were compared to five pre-deformation lines.
III. An integrated algorithm was implemented. The axial and non-axial displacements were measured using the previous algorithm (I). The obtained axial displacements were used to calculate the local axial strain, which was used to stretch the data in axial direction. This iterative procedure was performed using the RF-data. After optimizing the axial strain, the lateral displacement was measured, using the axial displacement and strain as input.

All methods were validated using simulations (uniform axial compression of 1% and 0.5% non-axial compression (to simulate a material with a Poisson-ratio of 0.5) and phantom (10% PVA or 10% gelatin, 15µm SiC-scatterers) experiments. *In vivo* the algorithms were further evaluated using a volunteer's biceps and calf muscle during passive compression with the transducer and active compression by means of muscle contraction.

**Results:** The simulation revealed that using the first two algorithms a bias in the lateral displacement is introduced by axial decorrelation due to an axial strain component. This decorrelation cannot be corrected for by extensive interpolation. The third algorithm (using axial stretching) significantly improved the lateral displacement measurements (no additional improvement in the axial strain after 3 iterations). Using stretching, the standard deviation of the strain estimate in axial direction decreased with a factor 15 whereas 5 times better strain estimates were found in non-axial direction.

The phantom experiments revealed similar results. 2D interpolation (Method II) performed better than the two-step approach (Method I). Stretching (Method III) had similar results as 2D interpolation. A possible explanation is the limited accuracy of the used local axial strain estimates. Global stretching wasn't used in this study, since it is often not applicable for cardiac strain imaging. The *in vivo* experiment revealed different strain values in lateral and elevational direction due to the anisotropy of the muscle tissue.

**Conclusions:** 3D strain estimation is feasible using a real-time 3D scanner. Additional validation studies in anisotropic phantoms are required to fully validate the technique.

**Acknowledgements:** The financial support of the Dutch Technology Foundation (STW) is acknowledged.

** indicates Presenter*

102 **STEADY-STATE HARMONIC ELASTOGRAPHY: VISUALIZING THE VISCOELASTIC PROPERTIES WITHIN SOFT TISSUES.**

*Marvin M. Doyley[1,2]*, Qin Feng[2], John B. Weaver[1,2], Francis E. Kennedy[2], Keith D. Paulsen[2].*
[1]Department of Radiology, Dartmouth Medical School, Hanover, NH 03755, USA; [2]Thayer School of Engineering, Dartmouth College, Hanover NH 03755, USA.

**Aims:** The primary objective of this paper is to report the results of experiments conducted on viscoelastic phantoms and volunteer breast cancer patients to validate the performance of viscoelastic image reconstruction procedure.

**Background:** Magnetic resonance elastography (MRE) is an emerging imaging modality that derives intrinsic tissue mechanical property images from MR measured induced internal tissue displacements based on the premise that soft tissues exhibit linear isotropic elastic behavior. Although these assumptions have proven to be a good approximation for some tissues, it is inappropriate for tissues that exhibit considerable viscoelastic tendencies, such as the breast. Consequently, an enhanced inverse image reconstruction technique has been developed based on a viscoelastic formulation of shear wave propagation.

**Methods:** The governing partial differential equations (PDEs) that describes the propagation of shear waves in a linear isotropic viscoelastic medium is given by $\nabla\bullet\mu\nabla\bar{\mathbf{u}}+\nabla(\lambda+\mu)\nabla\bullet\bar{\mathbf{u}}=(i\omega\alpha-\rho\omega^2)\bar{\mathbf{u}}$, where $\bar{\mathbf{u}}$ is the spatially varying complex-valued displacement vector **u**, μ and λ are Lamé constants, α is the damping coefficient and ρ is the density of the medium, which in this study was assumed to be equivalent of water (≈1000kg/m$^3$). Information regarding shear wave propagation obtained by employing contrast enhanced MRI is generally in the form of phase and harmonic amplitude maps. However, this information was transformed to frequency domain Viz. $\mathbf{u}(x,y,z,t)=\mathrm{Re}\{\bar{\mathbf{u}}(x,y,z)e^{i\omega t}\}$ to facilitate image reconstruction. The dominant mechanical parameters (i.e. shear modulus, μ, and the damping coefficient, α) were estimated from the complex-valued displacements by employing an overlapping subzone inversion strategy that we have recently developed based on the equations of motions for a viscoelastic medium.

**Results**. Figure 1 shows representative examples of contrast enhanced T2 weighted MR images, and shear modulus elastograms that were obtained from a breast cancer patient with a locally advanced malignancy. The tumor that is visualized in the contrast enhanced MR images has a highly localized region of low intensity, which corresponds to an area of high shear modulus (mean shear modulus = 11 ± 2kPa; shear modulus contrast ≈14.8dB (5:1)) in the shear modulus elastogram. Figure 2 shows a montage of damping coefficient elastograms corresponding to the images shown in Figure 1. The inclusion is not discernible in damping coefficient elastograms, which suggests that globally both tissue types (inclusion and surrounding tissues) exhibit similar viscoelastic behavior. It is apparent from the images shown in Figure 1 and the damping coefficient images shown in Figure 2, that there is a strong correlation between regions of high contrast uptakes and regions of low damping (as well with regions of high shear modulus); however, not all regions with high contrast uptakes correspond to regions of low damping. We believe that the regions where low damping correlates with areas of high shear modulus correspond to areas where the fibrous encapsulation of the malignancy is intact. Further investigations are currently being conducted to corroborate this hypothesis.

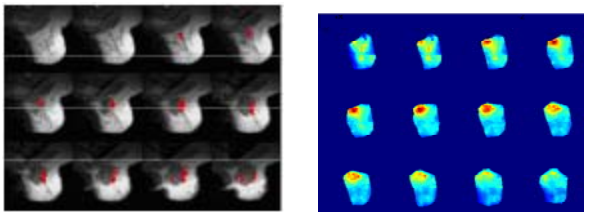

Figure 1: Montage of contrast enhanced T2 weighted MR images (left) and shear modulus elastograms (right) obtained from a patient with a locally advanced malignancy. The red arrows indicate areas of contrast enhancement.

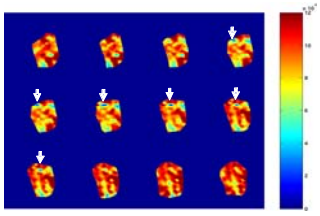

Figure 2: Montage of damping coefficient elastograms corresponding to the modulus elastograms and MR images shown in Figure 1. Arrows denotes areas of increased damping coefficient.

**Conclusions:** The preliminary results reported in this article demonstrate that taking proper account of viscoelastic effects in breast tissues will not only provide a new contrast mechanism that could aid the differential diagnosis of breast cancer but should also improve the statistical accuracy of shear modulus elastograms.

059 **ANGULAR STRAIN METHOD FOR STRAIN ESTIMATION IN ULTRASOUND ELASTICITY IMAGING.**

*Unmin Bae[1]* and Yongmin Kim[1].*
[1]Electrical Engineering and Bioengineering Departments, University of Washington, Seattle, WA, USA.

**Aim:** Our aim is to develop an accurate and computationally efficient strain estimation method to accelerate and/or enable the use of ultrasound elasticity imaging in various clinical applications.

**Background:** Traditional ultrasonic strain estimators derive tissue displacements before and after compression, and then compute the strain from a spatial derivative of the displacement. For typical ultrasonic strain estimation, such as the imaging depth of several cm and a sub-mm strain sample length, a displacement can be as large as a hundred times of the displacement difference. For example, when 1% compression is applied to a 3 cm elastically homogeneous object and the strain sample length is 200 μm, a displacement can be up to 300 μm, which is 150 times larger than the displacement difference of 2 μm. Thus, if strain is computed from large displacements, any error in displacement estimation can be magnified in strain computation.

**Methods:** We have developed a phase-based direct strain estimator called angular strain method (ASM). It computes temporal and spatial correlation between the correlated ultrasound signals from pre- and post-compression frames. The phase of temporal and spatial correlation is defined as angular strain, which leads to strain after normalization. Before estimating the angular strain, a motion-vector estimation technique, such as the crosscorrelation method, is utilized to find the correlated signals from different frames where the distance between the correlated signals (in samples) is defined as a gross motion vector.

**Results:** We have found in simulation that our phase-based direct strain estimator improves the strain signal to noise ratio (SNR) and the dynamic range of strain SNR, compared to the conventional strain estimator using crosscorrelation with interpolation. For example, using ASM, strain SNR is improved to about 3 times for the strain ranging from 0.1% to 3% when the correlation window of 0.49 mm and the strain sample length of 0.23 mm were used. If an ideal gross motion vector is used (instead of an estimated one), the dynamic range of the strain SNR curve is further improved, indicating that strain SNR for large compression is limited by the gross motion vector estimation using the crosscorrelation method, rather than the subsequent phase-based strain estimation. In experiments with gelatin-based phantoms, the hard inclusions with diameter ranging from 0.8 cm to 1.1 cm can be delineated in the ASM-based strain images for large compressions, such as 3%, whereas noise due to large compression dominates the strain images derived from the strain estimator using crosscorrelation with interpolation.

**Conclusions:** A new strain estimator has been developed for ultrasound elasticity imaging. It improves the accuracy and strain SNR by directly estimating strain from the phase of temporal and spatial correlation between the correlated ultrasound signals from different frames. In addition, the proposed strain estimator is computationally efficient. The computational burden of traditional strain estimation is usually very high due to computer-intensive processing methods, such as accurate interpolation processing, or a large amount of data to be processed arising from a high sampling frequency and/or a high frame rate. Since our phase-based strain estimator does not require interpolation, a high frame rate or a high sampling frequency, it can be implemented in commercial ultrasound machines to provide real-time ultrasound elasticity imaging, which we have demonstrated.

037 **MULTIDIMENSIONAL AUTOCORRELATION AND DOPPLER METHODS VERSUS CROSS-SPECTRUM PHASE GRADIENT METHOD.**

*Chikayoshi Sumi[1]*.*
[1]Sophia University, 7-1 Kioicho, Chiyodaku, Tokyo 102-8554, JAPAN.

**Aims:** Two new methods of measuring a multidimensional displacement vector using an instantaneous ultrasound signal phase are reported, i.e., the multidimensional autocorrelation method [1, 2] and the multidimensional Doppler method [1, 2]. High measurement accuracy is achieved by combining either method with our developed lateral Gaussian envelope cosine modulation method (LGECMM) [2]. Compared with our previously developed multidimensional cross-spectrum phase gradient method (CSPGM) [3], as shown, both methods yield accurate measurements, require less computational time, and provide real-time measurement. Both methods can be applied to the measurement of tissue strain, blood flow, sonar data, and other target motions.

**Results:** 2D displacement vector measurements are simulated, assuming that LGECMM is used (ultrasound frequency fx = lateral modulation frequency, fy = 3.5MHz, $\sigma_x = \sigma_y = 0.4$mm, speed of sound =1,500m/s). The distribution of a displacement vector (0.01mm, 0.01mm) is evaluated. First, the usefulness of LGECM was verified for our previously developed phase matching [2] using CSPGM. When laterally modulating, the axial and lateral estimation converged to 2 iterations, i.e., by one phase matching. However, non-modulation resulted in their slow convergence. Nine iterations do not allow the lateral measurement accuracy to reach that of modulation case. Utilization of LGECMM realizes rapid convergence.

Next, measurement accuracy (SNR) is evaluated for multidimensional autocorrelation and Doppler methods by changing fy and $\sigma_y$. White noise is added to the pre- and post-echo data. SNR versus lateral modulation wavelength was evaluated when moving average width is set at 64H64 points (3.2mmH3.2mm) for calculating the phase and spatial derivatives, i.e., instantaneous frequencies (echo data SNRs of 20dB and ∞dB (no noise)). Here, we should keep in mind that the phase of the autocorrelation signal evaluated from the moving-averaged real and imaginary components yields a more accurate displacement vector measurement than the moving-averaged phase [1]. The accuracy of axial displacement measurement is sufficiently high regardless of fy. However, when the lateral modulation wavelength is longer than half the ultrasound wavelength ($\lambda_{axial}/2$), the accuracy of lateral displacement measurement decreases compared with that of axial displacement measurement. Also, if the echo is not laterally modulated (wavelength = ∞), then, in the absence of noise, the accuracy of lateral displacement measurement is quite high (>40dB). However, the accuracy is considerably lower at a low echo data SNR. If the moving average width is set to a smaller value, all measurement accuracies decrease. These two methods allow more accurate measurement than CSPGM using a window having the same size as that of moving average (Figure 1, 64H64). When $\sigma_y$ is changed from 0.4mm to a larger value under a constant echo data SNR (20dB), the accuracies of the axial and lateral displacement measurements decrease slightly in a similar manner (omitted).

**Conclusions:** To realize high measurement accuracy, lateral modulation frequency and ultrasound frequency should be set higher at the same echo data SNR. Moreover, beam width and pulse length should be narrower and shorter, respectively. These conditions also yield high spatial resolution. A large moving average width stabilizes the measurement at a trade off with spatial resolution. However, phase matching [3] and echo compression/stretching allows heightening the spatial resolution. Moreover, we previously confirmed that the regularization method is effective in increasing the measurement stability and accuracy of the CSPGM [4]. Future work will be directed at evaluating the effectiveness of the regularization method for the application to both instantaneous phase methods. Measurement accuracies of strains will also be compared.

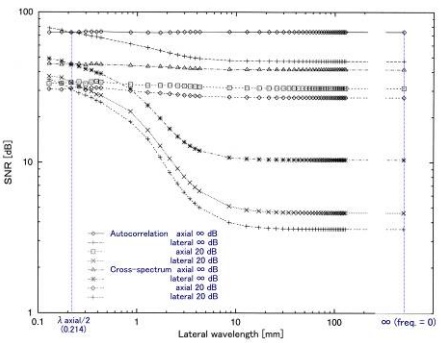

Figure 1: Multidimensional Autocorrelation Method vs. CSPGM.

**References:**

[1] Sumi, Technical report of Japan Soc of Ultrason in Med, **102**, no. 4, pp. 37-40, Dec 2002 (in Japanese).
[2] Sumi, "Multidimensional displacement vector measurement methods utilizing instantaneous phase," Proc. of IEEE EMBS Conf. (CD-ROM), Sep 2005.
[3] Sumi, IEEE Trans. UFFC, **46**, pp. 158-166, 1999.
[4] Sumi, Technical report of Japan Soc of Ultrason in Med, **101**, no. 4, pp. 31-41, Dec 2001 (in Japanese).

** indicates Presenter*

087 **HIGH RESOLUTION TIME OF FLIGHT MEASUREMENTS WITH THE PULSED PHASE LOCKED LOOP.**

*Ted Lynch[1]*, Joe S. Heyman[1], David Blaker[2].*
[1]Luna Innovations, Inc., 130 Research Dr., Hampton, VA 23666, USA; 2Luna Innovations, Inc., 2851 Commerce Street, Blacksburg, VA 24060, USA.

**Aims:** This report compares the resolution of the ultrasonic pulsed phase locked loop (PPLL), FFT-based phase measurements, and cross-correlation time-shift analysis for assessing tissue motion in elasticity studies.

**Background:** The PPLL was invented in the 1980's at NASA Langley Research Center and has been used extensively in materials characterization studies, demonstrating the ability to detect changes in the time of flight of an ultrasonic tone-burst with parts-in-ten-million resolution [1-5]. For ultrasonic measurements in the MHz frequency range with a 10 microsecond path length, this translates to the ability to resolve changes in the time of flight in the picosecond range. Recently, Luna has begun testing medical applications of the PPLL, particularly for the noninvasive assessment of intracranial pressure and intramuscular pressure. We are currently updating the processing architecture of the PPLL so that it can provide absolute measurements of the time-of-flight with equal resolution to the derivative measurements already demonstrated using analog signal processing.

**Methods:** Computer simulations were performed comparing the PPLL with the cross-correlation time-shift algorithm and FFT-based phase measurements. For the PPLL and FFT-based measurements, the simulation employed a 10-cycle, 1 MHz ultrasonic tone-burst with 20 dB of random noise added; for cross-correlation, a single-cycle 1 MHz return echo with 20 dB of random noise added was used. For each algorithm, the simulated signal was converted to a 16-bit signal and sampled at 48 MHz and the time delay was computed using digital signal processing.

**Results:** The PPLL was able to resolve phase shifts down to 0.001°, equivalent to a 2 picosecond time shift, better than twice the resolution of FFT-based phase measurements and several orders of magnitude better than cross-correlation analysis. We have also found that the PPLL phase detection algorithm is more robust than FFT-based measurements in the presence of frequency dispersion, interference or noise.

**Conclusions:** PPLL-based phase measurements provide superior time resolution than comparable techniques used in tissue motion analysis and are particularly useful in applications where the use of 5-10 cycle tonebursts will provide adequate depth resolution of tissue boundaries.

**Acknowledgements:** Portions of this work was funded through a U.S. Army Phase II SBIR contract.

**References:**

[1] J.S. Heyman. "A CW Ultrasonic Bolt Strain Monitor," SESA Experimental Mechanics, 17 (1977) 183.
[2] J.S. Heyman and E.J. Chern. "Characterization of Heat Treatment in Aluminum Based on Ultrasonic Determination of the Second and Third Order Elastic Constants," proceedings of the 1981 IEEE Ultrasonics Symposium. 1981 (936-939).
[3] J.S. Heyman, S.G. Allison and K. Salama. "The Effect of Carbon Concentration and Plastic Deformation on Ultrasonic Higher Order Elastic Properties of Steel," Ultrasonics International. 1985 (786).
[4] J.S. Heyman, S.G. Allison and K. Salama. "Temperature Dependence of Ultrasonic Velocity in Carbon Steels," proceedings of the 1983 IEEE Ultrasonics Symposium, Atlanta, GA, October 31-Novermber 2, 1983.
[5] Ueno T, Macias BR, Hargens AR and Yost WT. "Pulsed Phase Lock Loop Technique to Measure Intracranial Pressure Noninvasively." Proceedings 2003 IEEE Ultrasonics Symposium, October 5-8, 2003, Honolulu, Hawaii.
[6] JE Lynch, JS Heyman and AR Hargens. "Ultrasonic Device for the Noninvasive Diagnosis of Compartment Syndrome." Physiological Measurement, 25(1), N1-N9.

** indicates Presenter*

093 **EFFECTS OF PHYSIOLOGICAL TISSUE MOTION STATISTICS ON PREDICTED ELASTOGRAPHIC IMAGE QUALITY *IN VIVO*.**

*R. Chandrasekhar[1,2]*, J. Ophir[1,2], T. Krouskop[3] and K. Ophir[4].*
[1]The University of Texas Medical School, Houston, TX, USA; [2]University of Houston, Houston, TX, USA; [3]Baylor College of Medicine, Houston, TX, USA.; [4]Austin, TX, USA.

**Introduction:** In elastography, the time elapsed between the pre- and the post-compression frame is referred to as the inter-frame interval. For *in vivo* elastography, the inter-frame interval is critical because uncontrolled physiological motion, such as heartbeat, muscle motion, respiration and blood flow, introduce inter-frame decorrelation that reduces the quality of elastograms [1]. To obtain a measure of this decorrelation, *in vivo* experimental data (from human livers and thyroids) at various inter-frame intervals were obtained from twenty healthy subjects. In order to further examine the effect of the different inter-frame intervals on the elastographic image quality, the experimental data were also used in combination with elastographic simulation data.

**Methods:** RF data from liver and thyroid were obtained from twenty healthy subjects using a Philips HDI-1000 ultrasound scanner and a digital motion controller (DMC). The transducer was placed in the region of interest using the DMC to ensure a controlled experimental setup to remove undesired effects such as operator and out of plane motion. Ten exams (each with twenty frames of data) were performed at the maximum frame rate possible by the apparatus. The post-compression step was skipped as only uncontrolled *in-vivo* motion was of interest. The decorrelation (noise) introduced due to uncontrolled motion was obtained at various inter-frame intervals from these data (Figure 1). An exponential curve fit was employed to obtain a noise measure at various inter-frame intervals which was then used to compute the combined SNR used in simulations. The deterioration of elastographic image quality was objectively evaluated by computing the area under the strain filter (SF) at a given resolution [2]. The variation of the area Q under the SF with inter-frame interval is shown in Figure 2.

**Results:** The results of this study demonstrate a statistical exponential behavior of the temporal decay of the echo signal cross-correlations from tissues *in vivo* due to uncontrollable motion. The results also indicate that the dynamic range and height of the SF at a given resolution are reduced at increased inter-frame intervals, suggesting that in elastographic applications, good objective image quality may be achieved only when a high frame rate is maintained.

**Conclusions:** The study indicates that elastography can be used successfully *in vivo* on homogeneous regions when the inter-frame interval meets the minimum requirements for a specific image quality. Processing extra data without significant improvement in the quality might affect system performance in real time elastography, and the results may help in understanding the (nonlinear) tradeoff between the frame rate and the image quality in real time elastography.

**References:**

[1] Souchon, R., Ophir, J, Srinivasan, S., Chapelon, J.: Prostate Elastography: Causes of decorrelation *in-vivo*, First International Conference on the Ultrasonic Measurement and Imaging of Tissue Elasticity, Niagara Falls, Ontario, Canada, p. 86, October 20-23, 2002.

[2] Varghese, T. and Ophir, J.: A theoretical framework for the performance characterization of elastography: The Stain Filter, IEEE Transactions on Ultrasonics, Ferroelectrics, and Frequency Control Society, Vol. 44 (1), pp. 164 - 172, 1997a.

**Acknowledgement:** Supported by NIH Program Project P01-CA64597-10 to the University of Texas.

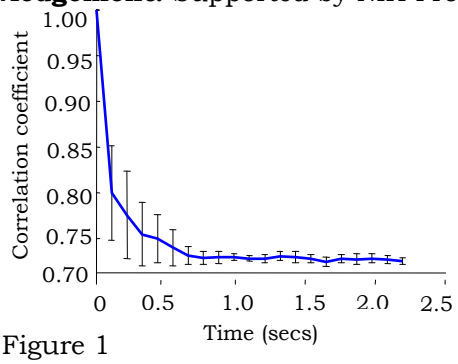


Figure 1

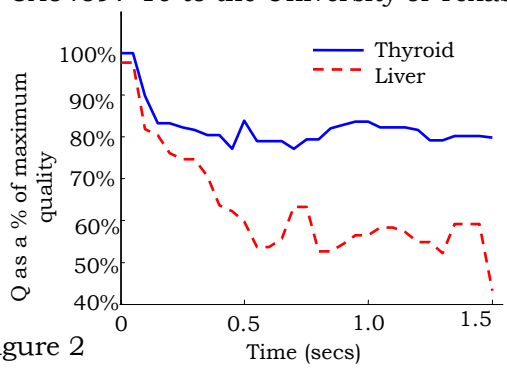


Figure 2

052 **ELASTICITY IMAGING USING ULTRAFAST VS. CONVENTIONAL ULTRASOUND IMAGING.**

*Suhyun Park[1]*, Salavat R. Aglyamov[1], Jignesh Shah[1], W. Guy Scott[2], Stanislav Y. Emelianov[1].*
[1]Department of Biomedical Engineering, University of Texas at Austin, Austin, TX 78712, USA; [2]Winprobe Corporation, North Palm Beach, FL 33408, USA.

**Aims:** In elasticity imaging, conventional and ultrafast ultrasound imaging approaches have been used. Each one has advantages and limitations including image quality and frame rate. The goal of this study is to quantitatively compare the performance of elasticity imaging based on each of these imaging techniques and combination of both.

**Background:** In elasticity imaging, ultrasound images are acquired during externally or internally applied motion/deformation of the tissue. If the motion or the deformation rate is small (e.g., breast or prostate imaging), the conventional ultrasound imaging can be used. Here each ultrasound beam is tightly focused on transmit and dynamically focused on receive to form high quality ultrasound images. However, if the motion or deformation rate is high (e.g., shear wave or cardiac strain rate imaging), the severe decorrelation between the neighboring conventional ultrasound images requires alternative high frame rate imaging techniques such as ultrafast ultrasound imaging. Indeed, in ultrafast ultrasound imaging, the transmitted broad and unfocused ultrasound beam interrogates the entire volume and the backscattered signal is received on all elements of the array transducer at once and is dynamically focused at every depth to produce an image. Compared to conventional imaging, ultrafast ultrasound imaging has the advantage of the higher frame rate, but image quality is reduced. In this paper, we quantitatively compare elasticity images obtained with conventional and ultrafast ultrasound imaging methods. Much of the work in elasticity imaging has been focused on ultrafast or conventional imaging separately, however very little simulation and experimental data are available for both.

**Methods:** The performance of elasticity imaging based on ultrafast and conventional imaging techniques was evaluated using simulated data. Both ultrafast and conventional ultrasound images were obtained from tissue phantoms measuring 40-mm laterally and 50-mm axially. Specifically, a homogeneous phantom and a phantom with a single hard inclusion were imaged using 128-element transducer operating at 5 MHz. To produce either conventional or ultrafast ultrasound images of the entire phantom, the custom simulations using linear acoustic propagation were performed where backscattered ultrasound signals from necessary transmit-receive combinations of elements were digitized at 40 MHz, base-banded, interpolated and appropriately added. Surface deformations of the phantoms, applied in increments of 0.30%, were calculated using analytical solutions of the equations of equilibrium. After ultrafast and conventional images of the phantom were obtained, the 2-D cross-correlation based speckle motion tracking was performed to evaluate displacement vector and strain tensor components. Based on *a priori* known size of the inclusion and displacement and strain values, the signal-to-noise ratio (SNR), contrast-to-noise ratio (CNR) and spatial resolution of the resulting images were estimated.

**Results:** The simulated ultrafast and conventional ultrasound images clearly indicated the expected difference in ultrasound image quality – these differences were also apparent in the displacement and strain images. For example, at the focal region of the conventional imaging, the SNR, CNR and lateral resolution of axial displacement and strain images were generally greater compared to that of the ultrafast imaging. The differences of the maximum strain SNR and CNR between conventional and ultrafast imaging were no more than 16% and 12%, respectively. These differences, however, rapidly tapered off away from the focal region. For ultrafast imaging, the displacement/strain SNR and CNR did not vary significantly throughout the entire image. There were also similarities between both imaging methods. For instance, as the applied strain increases, strain SNR and CNR in both imaging modes reached maximum values around 3-5% of the axial strain. Finally, the axial resolution was comparable in all images.

**Conclusions:** The results of the study suggests that the ultrafast ultrasound imaging can be reliably used for the elasticity imaging if frame rate is critical to capture the fast motion or high-rate deformation of the tissue. The displacement and strain estimates obtained using ultrafast ultrasound imaging has tolerable levels of SNR, CNR and axial resolution. The quality of the displacement and strain images can be improved with averaging since ultrafast imaging frame rate is faster compared to conventional images. In addition, different implementations of motion tracking algorithms are possible with ultrafast imaging. However, further experimental studies are needed to support these observations.

**Acknowledgements:** Support in part by National Institutes of Health under grants CA110079 and CA96018 is acknowledged.

* *indicates Presenter*

104 **ARTERIAL ELASTIC MODULUS RECONSTRUCTION FROM *IN-VIVO* STRAIN IMAGING AND PWV.**

*W.F. Weitzel[1]*, Kang Kim[2], Hua Xie[2], J.M. Rubin[3], Congxian Jia[2], M. O'Donnell[2].*
[1]Internal Medicine, [2]Biomedical Engineering, and [3]Radiology Departments, University of Michigan, Ann Arbor, MI 48109, USA.

**Aims:** Using a simple arterial model, we determined the arterial wall elastic modulus independently from strain and pulse wave velocity (PWV) measurements and compared these results with each other.

**Background:** Arterial compliance is an important indicator of vascular disease. Stiffening of the arterial wall lowers the strain in the vessel wall and increases the PWV.

**Methods:** For both strain and PWV measurements, an ultrasound correlation-based, phase-sensitive, speckle-tracking algorithm was employed for data collection. For the elastic modulus reconstruction from strain image, a simple model was used in which elastic modulus, $E_1$, of the artery wall is related to elastic modulus, $E_2$, of surrounding tissue by

$$E_1 + K_2 E_2 = K_1 \left[ \frac{\Delta p}{\Delta \varepsilon} \right]$$

where $K_1$ and $K_2$ are geometric factors, $\Delta p$ is pulse pressure and $\Delta \varepsilon$ is inter-cardiac strain (i.e., change in strain from systole to diastole). Within an offset proportional to $E_2$, it is possible to reconstruct the arterial elastic modulus as a function of mean arterial strain from the ratio $[\Delta p/\Delta \varepsilon]$. To reconstruct elastic modulus from PWV, Moens-Kotewerg equation for tethered elastic tube was employed. In both cases, artery geometrical factors, including inner and outer radius, were obtained from B-scan images and speckle tracking correlation images. For the PWV case, the density of the arterial wall was assumed to be in the range of 1071-1100kg/m$^3$. Incompressibility was also assumed for both cases. A non-invasive free-hand ultrasound scanning procedure was performed to measure both strain and PWV. Using a commercial ultrasound probe, a transverse scan was performed for strain estimation and a longitudinal scan was performed at the same location for the PWV measurement. Using a 5.8 MHz linear transducer, the scanhead was applied over the brachial artery of a 43 year old healthy volunteer. A pressure equalization procedure, previously evaluated in our lab, was used to lower the transmural arterial pressure and resulting vessel wall strain and PWV.

**Results:** Using arterial mean pressure equalization, the reconstructed elastic modulus of the brachial artery (inner and outer radii were 1.3mm and 2.0mm) from a measured pulse pressure induced strain of 30.0% was 30.0kPa. The longitudinal PWV measurements along the ultrasound scanhead were 2.8 m/sec yielding an elastic modulus of and 28.0kPa from the Moens-Kotewerg equation for a tethered elastic tube. These values are comparable to each other and lower by a factor of about 3 compared to the values before pressure equalization i.e., under normal physiological pressure. Assuming arterial geometry can be determined within an error as large as half of the speckle size (0.1mm), the error in elastic moduli is estimated to be within 20% for the artery sizes to be studied using this method.

**Conclusions:** These preliminary results demonstrate that the arterial elastic modulus can be determined from regional longitudinal PWV data generated by the ultrasound scanhead using pressure equalization and ultrasound speckle tracking. Additional study is underway to explore this method further.

**Acknowledgements:** Work supported in part by NIH grants HL-47401, HL-67647, HL-68658 and a grant from the Renal Research Institute.

074 **COMPUTER AIDED DIAGNOSIS OF BREAST CANCER BASED ON ELASTICITY IMAGES.**

*Tsuyoshi Shiina[1]*, Makoto Yamakawa[1], Ako Itoh[2], Eriko Tohno[2], Ei Ueno[2], Takeshi Matsumura[3], Tsuyoshi Mitake[3].*

[1]Graduate School of Systems and Information Engineering, [2]Graduate School of Human Sciences, University of Tsukuba, Tsukuba, JAPAN; [3]Research & Development Center, Hitachi Medical Corporation, Kashiwa, JAPAN.

**Background:** Conventional sonogram, B-mode image, based on the magnitude of echoes often produces poor contrast between tumor and surrounding tissues. Consequently, the detection of cancerous breast tumors by B-mode images often requires a high degree of skill on the part of the operators. In other words, one must know how to detect an unclear boundary of a tumor and evaluate the smoothness of contour, to understand the intra-tumor texture in the image and subtle differences in brightness. In addition, some artifacts, such as shadow, make the diagnosis more difficult. On the other hand, ultrasonic tissue elasticity imaging can provide novel diagnostic information based on tissue hardness and, consequently, is expected to detect tumor with high contrast and also discriminate benign and malignant disease.

**Methods:** We recently developed commercially based equipment for tissue elasticity imaging and have acquired tissue elasticity images (strain images) as well as B-mode images for 111 cases of beast tumor. In addition, we constituted scores of malignancy by comparing the hypoechoic region of B-mode and elasticity image, which is referred to as *elasticity score* and categorizes patterns of elasticity images into five classes from malignancy to benign. As a result of diagnosis based on the elasticity score, we found that it was possible for non-experienced doctors to attain high precision of diagnosis, that is, sensitivity, specificity and accuracy were 87%, 92% and 90%, respectively, while the accuracy attained by experts based on B-mode image was 88%. It should be noted that even a non-expert could attain a precise diagnosis based on the elasticity score as well as experts since the criteria on the elasticity score is much simpler than conventional B-mode images which requires the skill to recognize many complicated characteristics of the images. This means that the elasticity score is suited to be implemented into the computer-aided diagnosis (CAD) system. In this work, therefore, we tried to develop the CAD system based on the elasticity score. The CAD system extracted characteristics of malignancy from elasticity images based on the elasticity score and categorizes images to five classes by the following procedure. First, the region of tumor in the B-mode image is detected using an adaptive method for boundary detection. Next, by obtaining means and variance of intensity of elasticity image within the tumor region, elasticity images are classified to two major groups, that is, relative benign and malignant groups. Finally, by detecting the extension and pattern of low strain region, the two groups are classified to five classes.

**Results:** The algorithm of the CAD was evaluated by using images for 86 cases of breast tumor such as intraductal carcinoma and fibroadenoma The result categorized by the CAD system showed the high coincidence, that is, 89% with those by experts.

**Conclusions:** These results indicate that the CAD system based on elasticity images is promising as practical means for cancer diagnosis.

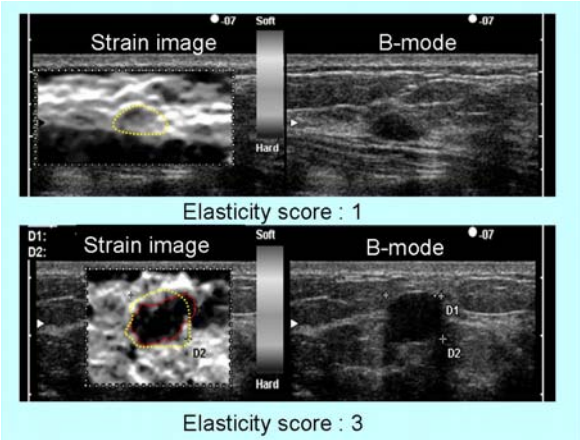


Examples of processed images and results of scoring

* *indicates Presenter*

033 **DIAGNOSIS OF LIVER FIBROSIS IN CHILDREN USING FIBROSCAN®.**

*Laurent Sandrin[1]*, Véronique Miette[1], C Fournier[1], Thierry Lamireau[2], Victor de Lédinghen[3].*
[1]Echosens, 32 rue des Jeuneurs, 75002 Paris, FRANCE; [2]Département de Pédiatrie, Hôpital Pellegrin, CHU Bordeaux, 33076 Bordeaux, FRANCE; [3]Service d'Hépato-Gastroentérologie, Hôpital Haut Lévêque, C.H.U. Bordeaux, 33604 Pessac, FRANCE.

**Aims & Background:** FibroScan® is based on transient elastography. This novel, non-invasive and rapid (<5 min) bedside device is used to assess liver fibrosis by measuring liver stiffness in adult patients. The usefulness of FibroScan® in children with chronic liver disease is unknown. This study aimed to evaluate the feasibility and the accuracy of FibroScan® for the detection of fibrosis and cirrhosis in children with chronic liver disease, in comparison to liver biopsy and to develop a dedicated probe.

**Methods:** 104 consecutive children (49 boys, median age 10.7 years (1 month – 20 years) with chronic liver disease were prospectively included. In 25 cases (24%), a liver biopsy was performed. Liver stiffness measurements were performed with a standard probe including a 3.5 MHz ultrasound transducer or a dedicated probe with a 6 MHz transducer. Stiffness was measured at a depth of between 25 mm to 65 mm on children above 12 years old and between 25 mm to 45 mm on younger children. Fibrosis score was evaluated using the METAVIR scoring system: F0 no fibrosis, F1 fibrosis without septa, F2 few septa, F3 significant fibrosis, F4 cirrhosis. ROC curve analysis was performed.

**Results:** Liver stiffness measurement was possible in 100% of children (children with ascites were excluded since elastic waves do not propagate through liquids). Liver stiffness values ranged from 2.1 to 45.7 kPa. According to histology, fibrosis was F0 F1 in 8 cases, F2 in 4 cases, F3 in 6 cases, and F4 in 7 cases. Area under the ROC curve were respectively 0.91 for $F \geq 2$ and 0.88 for $F = 4$. Performances were significantly improved by using the children-dedicated probe.

**Conclusions:** Liver stiffness measurement by FibroScan® is feasible in children of various ages, including infants under 6 months. FibroScan® is a good non-invasive method for the assessment of liver fibrosis (whatever its cause) and cirrhosis. Its usefulness in the follow-up of children with chronic liver disease should be evaluated, in order to avoid repeated liver biopsies.

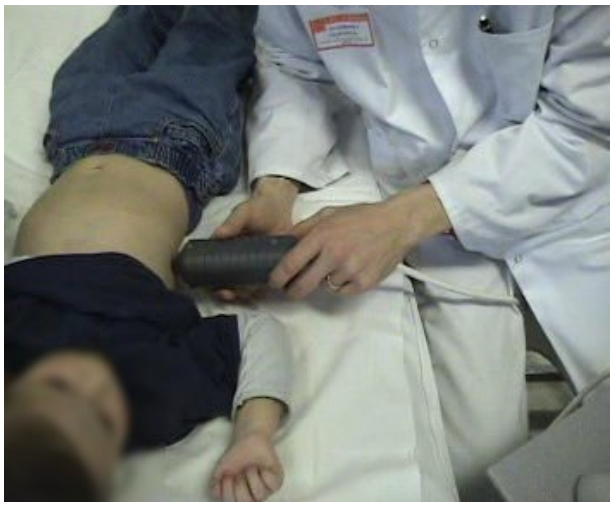

112 **CLINICAL EVALUATION OF THYROID TUMOR WITH REAL-TIME TISSUE ELASTOGRAPHY.**

*K Tanaka[1], N Fukunari[2], H Akasu[1], W Kitagawa[1], K Shimizu[2], K Ito[2], T Mitake[3]*.*
[1]Department of Surgery, Nippon Medical School, Tokyo, JAPAN; [2]Ito Hospital, Tokyo, JAPAN; [3]Hitachi Medical Corporation, Tokyo, JAPAN.

**Aims:** Various practical difficulties exist in realizing an objective technique for visualizing palpable thyroid tumors. In this study, we have explored the feasibility of using *Elastography* technique for the clinical evaluation of thyroid tumors. We will discuss the technique and the clinical outcome of this study.

**Methods:** Sixty cases with nodular lesions (40 papillary thyroid cancers, 8 follicular thyroid cancers, 12 adenomatous goiters, and 5 malignant lymphomas) found by ultrasound B-mode were examined and evaluated with the *Elastography* (EUB-8500, HITACHI, Japan). The results of *Elastography* were compared against the cytology, the cut section, the pathology, and with the images of computed tomography.

**Results:** Using *Elastography*, unique and characteristic images were obtained in every type of thyroid nodular disease. *Elastography* images were classified into 4 types: Pattern 1, light green throughout the inside of the nodule; Pattern 2, light green in the center and blue in the periphery of the nodule; Pattern 3, blue base with mixed colors of light green and red; and Pattern 4, blue in the entire nodule. (Figure 1) Papillary thyroid cancer images mainly showed Pattern 3 or 4, while lymph node metastasis specifically had the images of Pattern 4. Follicular thyroid cancer showed Pattern 2. Adenomatous goiter showed diffuse light green (Pattern 1).

**Conclusions:** *Elastography* provides new information for diagnosing thyroid tumors and helps with deciding therapy. In follicular lesions, it shows distinct differences in tissue elasticity between the peripheral zone and the center. It is possible to see the presence of lymph node metastasis in papillary thyroid cancer, yielding important information for clinical diagnosis. Thus, we believe that *Elastography* will help in creating treatment plans by providing new substantial clinical information.

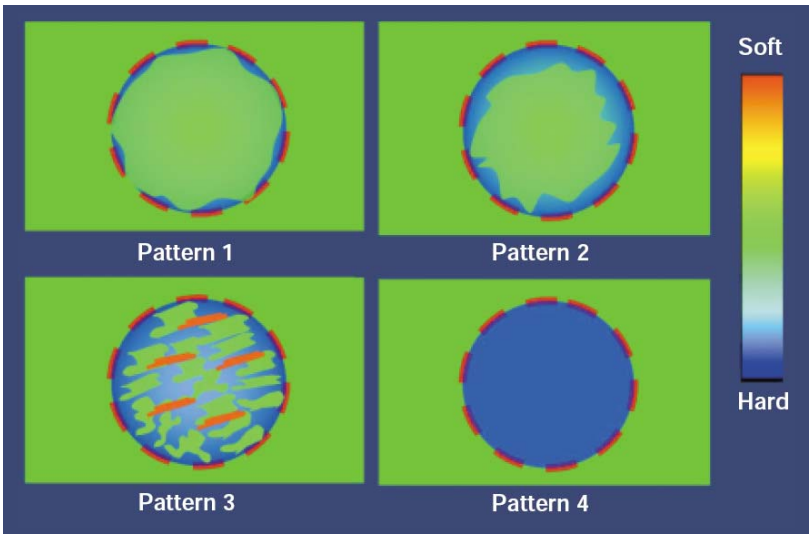


Figure 1: Proposed Clarification of Elastography for Thyroid Tumors

115 **ELASTICITY IMAGING OF 67 CANCERS AND 167 BENIGN BREAST LESIONS SHOWS THAT IT COULD HALVE BIOPSY RATES OF BENIGN LESIONS.**

*William E Svensson[1]*, Dimitri G Amiras[3], Sami Shousha[2], Anand Rattansingh[1], Dupinder Chopra[1], H Dudley Sinnett[3], Tim J Hall[4], Yanning Zhu[5], Joe Malin[6], Carol Lowery[6].*

[1]Radiology, [2]Pathology and [3]Surgery Departments, Charing Cross Hospital, Imperial College School of Medicine, London, England, UK; [4]Medical Physics Department, University of Wisconsin-Madison, Madison, WI, USA; [5]Radiology Department, University of Kansas Medical Center, Kansas City, KS, USA; [6]Siemens Medical Solutions Ultrasound Group, Issaquah, WA, USA.

**Aims:** To evaluate real time elasticity imaging on a clinical ultrasound system in a dedicated symptomatic breast unit and to determine how it to would alter clinical management.

**Background:** *In vitro* and *in vivo* work in recent years has shown that elasticity imaging profiles of benign lesions are smaller than the grayscale appearance and malignant lesions are larger. Though new imaging developments have not reduced the biopsy rate of palpable lesions, they could help to reduce the false positive rate associated with abnormalities found on breast ultrasound examinations particularly in the screening situation.

**Methods:** Real Time Elasticity Imaging (Software from Hall & Zhu of KUMC) was implemented on a Siemens Elegra ultrasound scanner. Breast imaging performed with a VFX 13-5 linear array transducer. Patients attending for routine breast ultrasound in the work up of mammographic or palpable focal breast abnormalities were invited to have breast strain imaging at the end of their ultrasound examination if there was a focal abnormality. The strain images were assessed during the clinic and correlated with subsequent histology or follow up.

**Results:** 234 lesions were assessed and correlated with the subsequent diagnosis; 67 cancers: 5 intermediate (1 radial scars, 3 phylloides, 1 intraductal papilloma) and 162 benign lesions: (103 fibroadenomas, 21 cysts, and 10 inflammatory masses, 6 intramammary lymph nodes, 6 normal breast, 2 gynaecomastia and 14 other lesions (scars, duct ectasia, necrosis, lipoma, sebaceous cyst).

Table 1: Ratio of Elasticity: B-mode.

| Lesion | Larger elasticity than B-mode image | Larger B-mode than elasticity image |
|---|---|---|
| Cancer | 57 | 10 |
| Intermediate | 3 | 2 |
| Benign | 31 | 131 |

Ratio of Elasticity: B-mode >1 indicative of a cancer or intermediate lesion: sensitivity= 83%, specificity = 81%, positive predictive value = 66%, negative predictive value = 92%.

Table 2: Ratio of Elasticity: B-mode to ensure all cancers and intermediate lesions are detected.

| Lesion | Elasticity to B-mode ratio > 0.75 | Elasticity to B-mode ratio < 0.75 |
|---|---|---|
| Cancer | 67 | 0 |
| Intermediate | 5 | 0 |
| Benign | 79 | 83 |

For Cancers and intermediate lesions: Sensitivity = 100%, specificity = 51%, negative predictive value= 100%, positive predictive value equals 48%.

**Conclusions:** The smaller the elasticity image of a lesion, compared with the B-mode size, the greater the likelihood of the lesion being benign. In this study, any lesion with elasticity to B-mode ratio of less than 0.75 was benign. If a ratio of less than 0.75 was used to determine the necessity for biopsy, no cancers would have been missed. In the screening situation, this would halve the number of biopsies of benign lesions (false positive biopsies). As elasticity imaging is a new modality, it is probable that increasing experience with and improvements in elasticity imaging would lead to a further decrease in false positive results than achieved in this study. This modality merits further evaluation in breast ultrasound imaging.

031 **THE ROLE OF ANISOTROPIC ELASTICITY AND VISCOSITY IN SKELETAL MUSCLE.**

*SF Levinson[1]*, S Catheline[2], M Fink[2], RL Ehman[3].*
[1]Rehabilitation Institute of Michigan, Wayne State University, Detroit, MI, USA; [2]Laboratoire Onde et Acoustique, Ecole Supérieure de Physique et de Chimie Industrielles, Paris, FRANCE; [3]Magnetic Resonance Research Laboratory, Mayo Clinic Department of Radiology, Rochester, MN, USA.

**Aims:** We sought to apply elastography to measure anisotropic elasticity and viscosity in skeletal muscle.

**Background:** Although skeletal muscle is known to be anisotropic, little is known about the relationship between anisotropic viscoelasticity and the contractile mechanism. We have previously demonstrated that muscle elasticity is transversely isotropic and increases with contraction [1, 2]. From recent observations, we hypothesize that viscosity is also transversely isotropic and the dominant property in the transverse direction. Anisotropic viscoelastic properties have never previously been measured in human muscle and their relationship to the force of contraction is unknown, as are the potential biomechanical implications.

**Methods:** Supersonic Shear wave Imaging (SSI) involves ultrafast ultrasonic imaging of radiation-force-induced shear waves in tissue. By measuring the speed and attenuation of propagation in different directions, anisotropic moduli can be derived. Using SSI, we calculated elastic and viscous moduli in the biceps brachii of 3 healthy subjects as a function of the applied load. Magnetic Resonance Elastography (MRE) also provides a means of measuring 3D wave propagation. We imaged wave propagation using MRE in the triceps surae of 2 healthy subjects during sustained, controlled contractions.

**Results:** A representative speed of sound map produced from SSI is shown in Figure 1. From the speed of sound data, we noted that the elastic modulus increases uniformly with the applied load, that the axial modulus is roughly 4 times greater than the transverse modulus at rest and that this difference increases dramatically with even modest degrees of contraction. Although the attenuation data was considerably noisier, we were able to ascertain that the transverse viscosity is significantly greater than longitudinal viscosity and that it increases so dramatically with contraction that transverse waves do not propagate at even moderate loads. The data from MRE are more complex and currently being analyzed.

**Conclusions:** Although preliminary, the data obtained using SSI completely support our hypotheses. The degree to which transverse viscosity increases with contraction, however, was unexpected and could have profound implications in our understanding of human biomechanics.

**Acknowledgements:** The authors gratefully acknowledge the support of the University of Rochester School of Medicine and Dentistry, ESPCI and the Mayo Clinic for making this work possible.

**References:**

[1] S. F. Levinson, "Ultrasound propagation in anisotropic soft tissues: the application of linear elastic theory," *Journal of Biomechanics*, vol. 20, pp. 251-60, 1987.
[2] S. F. Levinson, M. Shinagawa, and T. Sato, "Sonoelastic determination of human skeletal muscle elasticity," *Journal of Biomechanics*, vol. 28, pp. 1145-54, 1995.

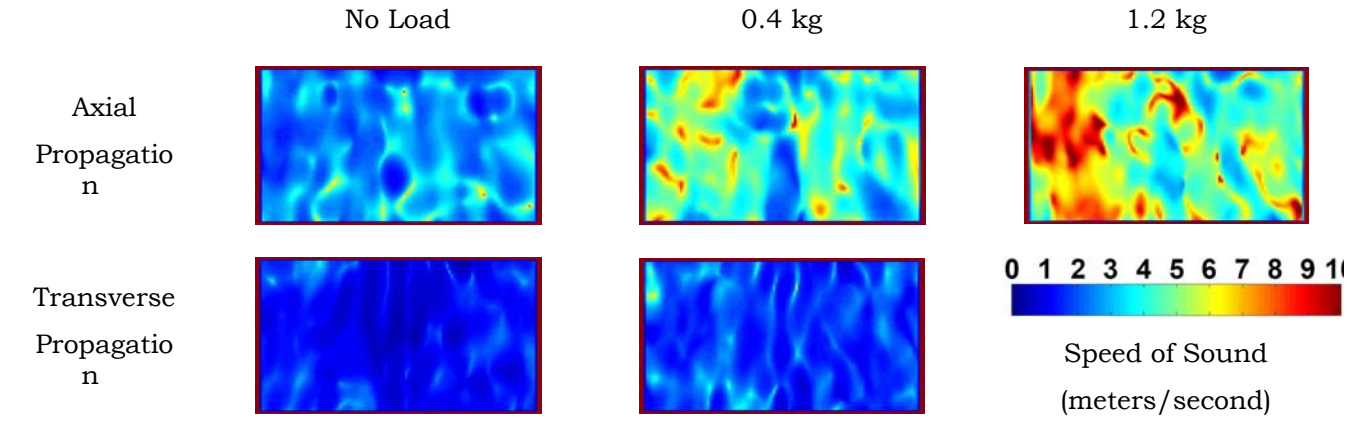


Figure 1: Speed of sound maps of axial and transverse shear wave propagation in the human biceps as a function of the applied load. Viscous attenuation completely dampened transverse propagation as the load exceeded 1 kg.

* *indicates Presenter*

094 **MICROMECHANICAL ANALYSIS OF DENTIN ELASTIC ANISOTROPY.**

*Anil Misra[1]*, Paulette Spencer[2], Orestes Marangos[1], Yong Wang[2], Mary Walker[2], J. Lawrence Katz[1,2].*
[1]University of Missouri-Kansas City, SCE, 350H Flarsheim Hall, 5100 Rockhill Road, Kansas City, MO 64110, USA; [2]University of Missouri-Kansas City, SOD, 650 East 25th Street, Kansas City, MO 64108, USA.

**Aims:** The objectives of this work are: (1) to develop a micromechanical model that relates the anisotropic elastic properties to the microstructure of dentin using a virtual bond idealization, and (2) to study the average force constants and anisotropy parameters utilizing the developed model in order to understand how the dentin elasticity is affected by the presence of water.

**Background:** Resonant ultrasound spectroscopy has been used recently to measure the elastic constants of millimeter sized samples of dry and wet dentin [1]. These measurements indicate that the wet dentin is transversely isotropic, with higher stiffness perpendicular to the tubule direction, while dry dentin is isotropic. A micromechanical analysis of dentin elasticity is performed to understand the fundamental mechanisms that effect dentin elasticity. This micromechanical analysis is based upon the precept that the material stress-strain behavior critically depends upon the underlying mechanisms that occur at scales smaller than the material sample scale.

**Methods:** To accomplish the task of relating the small scale mechanisms to the sample-scale, we consider dentin to be divided into grains whose centroids represent material points. In analogy with atomistic-scale interactions, these grains are viewed as interacting with each other through virtual bonds. These virtual bonds, which are oriented in the different directions of a 3-dimensional space, represent on average how the primary and secondary bonds between various phases contribute to the overall stiffness of the bulk material. Based upon the micromechanical model, closed form expressions of the transverse isotropic stiffness tensor are obtained. These expressions are utilized to compute the stiffness and anisotropy parameters for dry and wet dentin utilizing an optimization method and the resonant ultrasound spectroscopy measurements.

**Results:** Dry dentin anisotropy parameter is found to be zero indicating that dry dentin is isotropic. Wet dentin anisotropy parameter is found to take on negative values indicating that wet dentin is transversely isotropic with a stiffer isotropic plane perpendicular to the tubule direction. The force constants for wet dentin are found to be higher than those of dry dentin.

**Conclusions:** The force constant calculations indicate that the presence of water results in the stiffening of bonds as well as an increase in bond density that contribute to the mechanical stiffness at the sample scale. Moreover, the anisotropy parameter of wet dentin indicates that the bond density becomes higher in the isotropy plane in the presence of water.

**Acknowledgements:** A contribution of the University of Missouri-Kansas City Center for Research on Interfacial Structure and Properties (UMKC-CRISP). This research was supported in part by RO1 DE14392 (PS), K25 DE015281 (YW) from the National Institute of Dental and Craniofacial Research, NIH.

**Reference:**

[1] Kinney JH, Gladden JR, Marshall GW, Marshall SJ, So JH, Maynard, JD. Resonant ultrasound spectroscopy measurements of the elastic constants of human dentin. J. Biomech. 37(4), 437-441 (2004).

095 **CALIBRATING SCANNING ACOUSTIC MICROSCOPY FOR MICROMECHANICAL PROPERTY QUANTIFICATION.**

*Orestes Marangos[1]*, Anil Misra[1], J. Lawrence Katz[1,2], Yong Wang[2], Paulette Spencer[2].*
[1]University of Missouri-Kansas City, SCE, 350H Flarsheim Hall, 5100 Rockhill Road, Kansas City, MO 64110, USA; [2]University of Missouri-Kansas City, SOD, 650 East 25th Street, Kansas City, MO 64108, USA.

**Aims:** In this work, we utilize two methods of calibration for scanning acoustic micrographs: (1) a time domain method; and (2) a frequency domain method.

**Background:** Scanning acoustic microscopy (SAM) has been extensively used for imaging of biological material micromechanical properties by the measurement of the reflection coefficient. However, for biological materials the reflection coefficients vary over a wide range and are often frequency (scale) dependent. Therefore, for any quantification of micromechanical properties, it is important that the scanning acoustic microscope is carefully calibrated.

**Methods:** The time domain method gives an average value of the reflection coefficient over the transducer frequency spectrum whereas the frequency domain method gives reflection coefficients as a function of frequency. Therefore, it is expected that for frequency independent materials, both methods will give very similar reflection coefficients. For frequency dependent materials, the frequency domain method could provide more information as to how the reflection coefficient might vary as function of frequency.

**Results:** Several reference materials with acoustic impedance ranging from ~2 MRayls to 100 MRayls were imaged with SAM using transducers with central frequencies ranging from 30 to 100 MHz. These images were analyzed to generate calibration curves utilizing the above mentioned methods.

**Conclusions:** These calibration curves may be used to quantify the reflection coefficients, acoustic impedance and elastic moduli of biological materials of unknown properties. Examples of these quantifications will be presented.

**Acknowledgements:** A contribution of the University of Missouri-Kansas City Center for Research on Interfacial Structure and Properties (UMKC-CRISP). This research was supported in part by RO1 DE14392 (PS), K25 DE015281 (YW) from the National Institute of Dental and Craniofacial Research, NIH; NIH High-End Instrumentation Grant S10 RR16710 (PS); and R01 HL 69064-01-05 from the National Heart, Lung, Blood Institute (JLK).

** indicates Presenter*

001 **AVERAGE "GRAIN-SIZE" ESTIMATION IN LIQUID OR SOLID CHANNELS.**

*D. Hazony[1], Y. Hazony[2], J. L. Katz[1,3]*.*
[1]Case Western Reserve University, Cleveland, OH, USA; [2]Boston University, Boston, MA, USA; [3]University of Missouri-Kansas City, Kansas City, MO, USA.

**Aims:** To use image processing of acoustic signals in order to estimate the average "grain-size" in liquid or solid channels This presentation is an extension of a conference paper "Average grain-size estimation in polycrystalline channels" J. Acoustic. Soc. Am., No. 4, Pt. 2. p. 2566. Oct. 2004.

**Background:** Of concern is stress pulse propagation in dissipating acoustic media constituted of liquids or solids where the pulse expands as it travels. It will be seen that this expansion may relate to the presence of a very large number of cells ("grains") or liquid clusters. The size of each is a random variable with a defined mean, $g_s$, which may be estimated from the shape changes between the transmitted (echo 1 in the figure below) and received (echo 2) pulses.

**Methods:** We may define a frequency independent attenuation constant with the propagation which is proportional to $g_s$. Both theoretical and experimental results will be given. The process is relatively fast and results are highly reproducible. It is developed by associating – with the channel – a relatively long, cascading and cellular, electrical network model of a known transfer function. The size of each network cell is proscribed by $g_s$ and the model's transfer function approaches the Gaussian shape when the number of cells is increased arbitrarily. It then follows that the transducer input drive must be adjusted to provide a stress pulse closely approximating a modulated Gaussian shape.

**Results:** An example is shown in the figure below for a glycerin channel. The impact of the model and the amelioration of measurement quantization errors will be demonstrated. This procedure also has been applied to measure the average particle size in a powdered compact of hydroxyapatite (HAp) that is used for calibration of scanning acoustic microscope (SAM) images. Using a 20 MHz shear wave transducer a value of 0.2 μm average particle size was obtained.

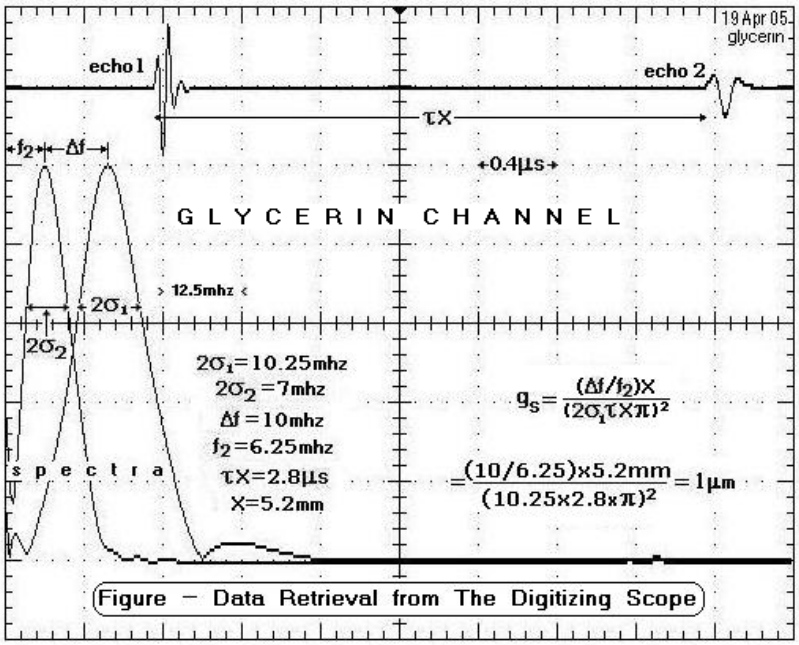

Figure – Data Retrieval from The Digitizing Scope

**Conclusions:** This procedure has a number of potential applications in biomedical research and clinical procedures, as well as in manufacturing processes, e.g. HAp crystallite size and growth in coronary artery disease, mineralite size and growth in bone remodeling during fracture healing and distraction osteogenesis; metallographic, polymer, and ceramic processing, etc.

**Acknowledgements:** Work supported by NIH-NIHLB (DH & JLK).

002 **STUDY OF THE EFFECT OF BOUNDARY CONDITIONS AND INCLUSION'S POSITION ON THE CONTRAST TRANSFER-EFFICIENCY IN ELASTOGRAPHY.**

*D Sosa Cabrera[1,2]*, J Ophir[1,3], T Krouskop[4], A Thitaikumar[1,3], J Ruiz-Alzola[2].*

[1]The University of Texas Medical School, Department of Radiology, Ultrasonics Laboratory, Houston, TX, USA; [2]University of Las Palmas de Gran Canaria, Center for Technology in Medicine, Department of Signals and Communications, Canary Islands, SPAIN; [3]University of Houston, Electrical and Computer Engineering Department, Houston, TX, USA; [4]Baylor College of Medicine, Department of Physical Medicine and Rehabilitation, Houston, TX, USA.

**Introduction:** In classical elasticity, the effects of defects such as holes and cracks on the stress distribution in an elastic medium have been favorite objects for study. The effects of holes drilled in structural members are accounted for by using formulae that reduce the effective dimensions of the remaining material, and have been tabulated for most common geometries [1]. It seems evident that elastographic images of strain are influenced by the size, location relative to the boundaries of the tissue mass, and by the geometry of inclusions.

**Methods:** The Contrast Transfer Efficiency (CTE), η, is defined as the observed strain contrast divided by the true modulus contrast [2]. In the present work, we investigate this efficiency of elastography for true modulus contrast (Ct) ranging from 1.25 to 3. We describe the results of 2-D FEA simulations designed to study how the position of a stiff circular inclusion in an elastic background and the boundary conditions affect the CTE. Six inclusion locations were used with 5 boundary configurations (BC), having a total of 30 cases at 3 levels of Ct, to study how lesion-to-background modulus contrasts were modulated in the corresponding strain images (Figure 1). Later, we studied 3 more positions (positions 7, 8 and 9 in Figure 1) to understand the effect of having an inclusion away from the edge. The unfilled arrowheads indicate the direction in which motion was constrained during displacement of the top surface.

**Results and Discussion:** It was observed that, there is generally a good efficiency of contrast transfer, and there are some cases where such contrast transfer is higher than 1. As expected from previous results [2], the CTE decreases with the modulus contrast. It was observed that the effect of the BC at the left edge on CTE was insignificant when the inclusion was three diameters away from this edge. In Figure 2, we show a strain image showing a partial shadowing of the inclusion due to the BC. Important parameters that affect the contrast transfer were identified as the location of the inclusion, the boundary conditions, and the relation between them.

**Acknowledgement:** Supported by NIH Program Project Grant P01-CA64597, CIFEC Program (Canary Islands' Government), and USIMAG grant (TEC2004-06647-C03-02/TCM) from the Spanish Government.

**References:**

[1] W Young and R Budynas: Roark's Formulas for Stress and Strain, McGraw-Hill, 2002

[2] H Ponnekanti et al: Fundamental Mechanical Limitations on the Visualization of Elasticity Contrast in Elastography, Ultrasound in Med. & Biol. Vol. 21, No 4, pp. 533-543, 1995

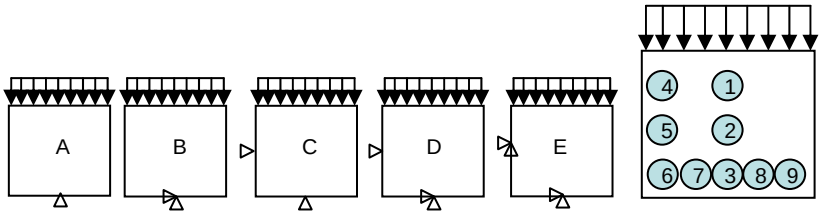


Figure 1: Schemes for the different cases for the boundary conditions and positions of the inclusion.

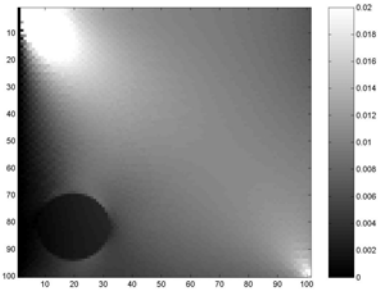

Figure 2: Strain image Pos. 6 Case E.

* *indicates Presenter*

026 ***IN VIVO* MECHANICAL BEHAVIOR OF HUMAN LIVER.**

*Edoardo Mazza[1]*, Alessandro Nava[1], Dieter Hahnloser[2], Wolfram Jochum[3], Michael Bajka[4].*
[1]Mechanical Engineering Department, Swiss Federal Institute of Technology, 8092, Zurich, SWITZERLAND; [2]Visceral and Transplantation Surgery, [3]Pathology, [4]Obstetrics and Gynecology Departments, University Hospital, Zurich, SWITZERLAND.

**Aims:** Characterization of the *in vivo* mechanical behavior of soft human organs is essential for medical applications such as surgery planning, virtual reality surgery training, trauma research, and various diagnostic methods. *In vivo* mechanical testing with well defined kinematic and kinetic boundary conditions provides information for fitting phenomenological constitutive models. In order to gain further understanding of the biomechanical properties of human organs, the parameters of the constitutive models must be linked to histological findings. This paper presents results of *in vivo* mechanical measurements on human liver complemented by histological analysis of biopsies obtained from the testing location.

**Background:** Experiments for the mechanical characterization of the human liver were performed *in vivo*, during open surgery under sterile conditions. Local measurement of the mechanical response of healthy and diseased tissue was undertaken before organ extraction. After extraction, tissue samples were removed and histological exams were carried out. In this way correlations between mechanical parameters and histological findings could be investigated.

**Methods:** Mechanical testing was carried out using the tissue aspiration device, Figure 1. The technique is based upon the pipette aspiration procedure. The device consists of a tube in which the internal pressure can be controlled according to a desired pressure law. The experiment is performed by (1) gently pushing the tube against the tissue to ensure a good initial contact, (2) creating a (time variable) vacuum inside the tube so that the tissue is sucked in through the aspiration hole (diameter of 10 mm). A digital camera records the tissue deformation and a pressure sensor measures the applied pressure. A control system guarantees the repeatability of the same loading conditions for all the experiments performed and therefore allows a direct comparison of the results obtained in different tests. Biopsies were analyzed using standard histological techniques and tissues were classified according to the presence of normal tissue, fibrosis, steatosis, or cancerous tissue.

**Results:** Mechanical parameters were determined from the analysis of tissue's deformation history for given loading conditions. The parameters are related to stiffness and time dependent behavior. Fibrosis of liver tissue leads to significant stiffness enhancement, whereas modest changes are observed in liver tissue with steatosis. Increased stiffness is also seen in cancer tissues, e.g. hepatocellular carcinoma (HCC), with fibrotic tumor stroma, Figure 2.

**Conclusions:** High quality mechanical data were obtained from aspiration experiments during open surgery. These data can be used for fitting of constitutive models and indicate that changes in mechanical properties can be linked to specific pathological modifications of tissue microstructure.

**References:**

[1] Nava, A., Mazza, E., Journal of Technology and Health Care 12 (2004), 269-280.
[2] Mazza, E., Nava, A., Bauer, M. Winter, R. Bajka, M. Holzapfel, G.A., Mechanical properties of the human uterine cervix: an *in vivo* study. Medical Image Analysis, accepted for publication.

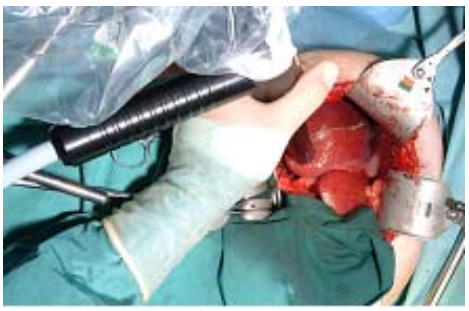

Figure 1: *In vivo* Aspiration Experiment

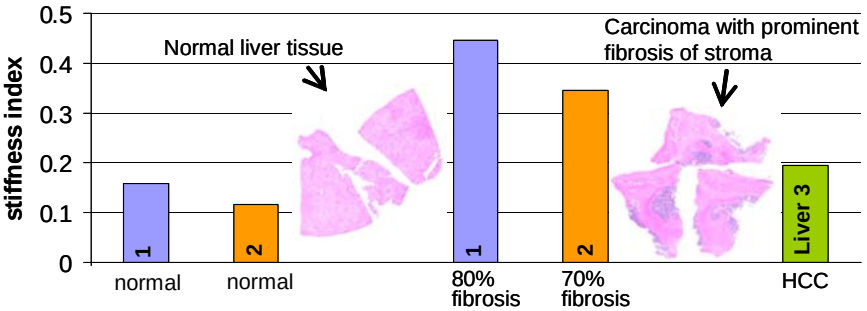


Figure 2: Stiffness Index for Different Samples

027 **MECHANICAL CHARACTERIZATION OF SOFT TISSUE: COMPARISON OF DIFFERENT EXPERIMENTAL TECHNIQUES ON SYNTHETIC MATERIALS.**

*Davide Valtorta[1]*, Marc Hollenstein[1], Alessandro Nava[1], Vincent Luboz[2], Minhua Lu[3], Alex Choi[3], Edoardo Mazza[1], Yongping Zheng[3], Stephane M. Cotin[2].*

[1]ETH Zürich, Swiss Federal Institute of Technology, 8062 Zürich, SWITZERLAND; [2]CIMIT, Simulation Group, Massachusetts General Hospital, Boston, MA, USA; [3]The Hong Kong Polytechnic University, Hong Kong, CHINA.

**Aims:** Accurate mechanical modeling of soft tissue is essential for many applications like medical simulation or surgical planning. Several techniques are currently available for mechanical testing of soft biological tissues. Based on different working principles, strain and frequency ranges, these methods deliver a set of mechanical parameters which can then be used to define constitutive models. The goal of the present work is to propose a system for assessing the reliability of these devices and techniques. Toward this goal, we have created a silicone phantom called TC2. The TC2 has been tested using different devices currently developed in 3 different laboratories. The results, comparing constitutive model parameters determined by each method, are an indicator of the accuracy of each approach.

**Background:** The TC2 is a cylindrical phantom made of silicone gel (Figure 1) with stiffness properties comparable to those of soft biological tissues and showing hyperelastic response up to relatively large deformations. The mechanical properties of the TC2 are stable over time, thus allowing direct comparison of the results obtained in subsequent investigations in different laboratories. Following previous work by Kerdok et al. [1] on a similar phantom, barium markers were embedded inside the cylinder to enable CT measurement of the deformation field in a large strain indentation test.

**Methods:** Independent tests were carried out on the same TC2 phantom: standard uniaxial compression tests [1], shear tests, quasi-static aspiration experiments [2], dynamic torsion tests [3], quasi-static and dynamic indentation (with the device called TeMPeST, [4]), and ultrasonic indentation tests [5]. The large strain indentation experiment has been used as benchmark for the constitutive models obtained from different procedures.

**Results:** Comparison of the experimental results highlighted specific limitations and error sources related to (1) the measurement techniques and (2) the algorithms for material parameter extraction. After analysis of the results, a good agreement was obtained for the material parameters evaluated, the static Young module ranging from 26kPa to 34kPa. Using the constitutive model derived from the experiments, the large strain indentation test has been simulated using FE models (see Figure 2): calculation results agree to a great extent with the experimental forces vs. displacement curve as well as with the deformation field obtained from the CT-scans.

**Conclusions:** This study provides a useful reference for the development of mechanical testing procedures for soft tissue. It also shows that accurate evaluation of mechanical measurements allows definition of reliable constitutive models, which can be used for simulation of large deformation of soft tissue.

**References:**

[1] Kerdok, A.E. et al., Medical Image Analysis 7(2003), 283-291.
[2] Nava, A., Mazza, E., Journal of Technology and Health Care 12 (2004), 269-280.
[3] Valtorta, D., Mazza E., Lecture Notes in Computer Science 3217 (2004), 284-292.
[4] Ottennsmeyer, M.P., Experimental Techniques 26 (2002), 48-50.
[5] Zheng, Y.P., Mak, A.F.T. IEEE Transactions on Biomedical Engineering 43 (1996), 912-918.

Figure 1: TC2 Phantom

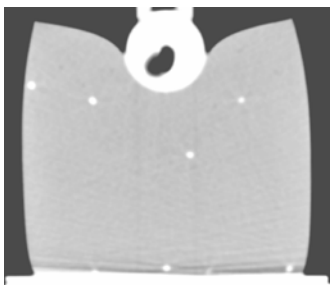

Figure 2: Large Strain Indentation (Real on left; Simulated on right)

* *indicates Presenter*

039 **SHEAR MODULUS RECONSTRUCTION USING ULTRASONICALLY MEASURED STRAIN RATIO.**

*Chikayoshi Sumi*[1]*.

[1]Sophia University, 7-1 Kioicho, Chiyodaku, Tokyo 102-8554, JAPAN.

**Aims:** Our previously developed three methods of shear modulus reconstruction using strain (elongation or compression) ratio [1, 2] are reviewed, and the usefulness of the methods is summarized. Although we have reported the usefulness of the methods for *in vivo* deeply situated tissues such as liver [3], here we focus on the application to *in vivo* breasts.

**Methods:** Method 1 evaluating the strain ratio is useful when the measurement accuracy of the strain is high. However, since tissue having high shear moduli, such as scirrhous carcinoma, often causes singular points/regions, Method 1 interpolates or truncates, using pre-specified upper values, the shear modulus values at singular points/regions, whereas both Methods 2 and 3 realize the regularized implicit-integration using the conjugate gradient method [3]. Specifically, Method 3 carries out regularized implicit-integration only at the singular points/regions while Method 2 caries out throughout ROI (strain ratio is used as initial value). Thus, the smaller number of singular points allows for Method 3's more rapid reconstruction than Method 2. As Method 1, the Method 3 is also useful when the measurement accuracy of strain is high. When evaluating strains at reference regions with a high spatial resolution, reconstructions obtained with Methods 1-3 often become laterally unstable. To cope with this instability, reconstruction of the inverse of the shear modulus obtained by the strain ratio is efficiently low-pass filtered rather than reconstruction of the shear modulus. In this case, implicit-integration (Methods 2 and 3) is performed with respect to the inverse of the shear modulus [2]. Otherwise, when using a homogeneous region as reference such as a block of reference material or fatty tissue, evaluation of strain at reference regions with a low spatial resolution is also effective.

**Results:** A female 59 year old volunteer with a scirrhous carcinoma was supinely positioned. To obtain absolute shear modulus reconstructions, a homogeneous agar phantom with a shear modulus of $1.4\times10^6$ N/m$^2$ was used as the reference. References are taken at the points on the line of 36.1mm depth (reference line) existing in the homogeneous reference. Reconstruction results of the shear modulus and the inverse of the shear modulus are shown in Figure 1 obtained by Method 1 (Methods 2 and 3, omitted).

Lateral instability was coped with by low-pass filtering of the strain ratio and evaluating the strains with a low spatial resolution at the reference line. Although the evaluation of strains with the low spatial resolution yields stable reconstructions with a high spatial resolution (Figures 1f and 1g) compared to low-pass filtering of strain ratio (Figures 1c and 1d), we confirmed through simulations that this yields low quantitative results when reducing artifacts due to 1D reconstruction.

That is, although the quantitativeness of the stiff region and the soft region is improved by setting reference regions to pass through the stress concentration regions and the weak stress regions in front of and behind the regions together with reducing the artifacts occurring at the stress concentration regions and the weak stress regions [2], in such cases reduction of spatial resolution of measured strain is not desirable at the point of quantitativeness.

**Conclusions:** All these methods using strain ratio realizes real-time shear modulus reconstruction. However, we should keep in mind that when the measurement accuracy of strain is not high, Method 2 using, not the strain ratio, but a uniform distribution as an initial value is effective in obtaining stable reconstructions though it takes more iterations, which was confirmed for monitoring of electromagnetic coagulation therapy on *in vivo* liver carcinoma [2].

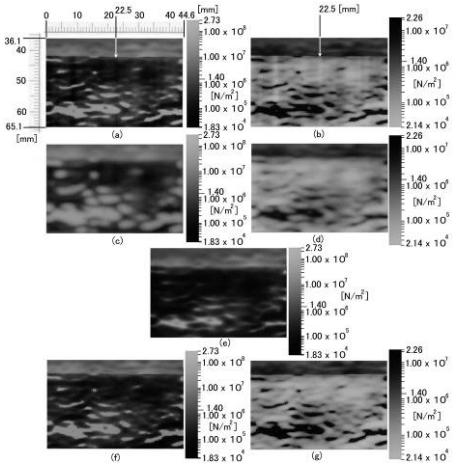

Figure 1: Shear Modulus Reconstructions Obtained by Calculating Strain Ratio (Method 1). (a) Shear modulus. (b) Inverse shear modulus. (c) Low-pass filtered (a). (d) Low-pass filtered (b). (e) Inverse of (d). (f) Shear modulus obtained by using moving-averaged strains at reference line. (g) Inverse shear modulus obtained by using moving-averaged strains at reference line.

**Refereces:**

[1] Sumi, IEICE Trans. Fundamentals, **E78-A**, pp. 1655-1664, 1995.

[2] Sumi, "Usefulness of ultrasonic strain measurement-based shear modulus reconstruction for diagnosis and thermal treatment," IEEE Trans. UFFC, Oct 2005 (in press).

[3] Sumi, IEEE Trans. MI, **17**, 419-428, 1998.

081 **NONINVASIVE INTRAMUSCULAR PRESSURE MEASUREMENTS THROUGH HARMONIC ANALYSIS OF ARTERIAL PULSATIONS.**

*Ted Lynch[1]*, Toshiaki Ueno[2], AD Cutuk[2], JM Wiemann[2], BR Macias[2], Alan R Hargens[2].*
[1]Luna Innovations, Inc., 130 Research Dr., Hampton, VA 23666, USA; [2]University of California San Diego, Dept of Orthopaedics, 350 Dickinson St., San Diego, CA 92103, USA.

**Aims:** A method for the non-invasive assessment of intramuscular pressure (IMP) is developed based on high resolution displacement measurements. The higher harmonics of the displacement waveform are filtered out as IMP increases, providing a means for diagnosing acute compartment syndromes (ACS). ACS is defined as sufficiently high IMP to restrict blood flow in the muscle.

**Background:** The ultrasonic pulsed phase locked loop (PPLL) obtains high resolution displacement waveforms of muscle compartments, the intracranial compartment and vascular walls. The shape of these waveforms is highly correlated to simultaneously obtained pressure waveforms obtained with pressure sensors inserted into the tissue compartment [1]. There is a considerable body of literature [2-11] in which a Windkessel model is applied to the pressure waveform to estimate arterial and intracranial compliance based on the harmonic content of the waveform. Similar analysis of the displacement waveform allows estimation of IMP, and the results have been validated clinically for ACS diagnosis.

**Methods:** ACS is diagnosed with the PPLL by detecting arterial pulsations with micrometer precision. As IMP increases, higher harmonics of the arterial pulsation waveform are filtered out, which is detected by the PPLL. The ratio of the fundamental wave to the second harmonic (FW/H2) is linearly correlated to IMP. Healthy subjects and patients admitted to the UCSD Trauma Center were included in a clinical study used to establish the diagnostic utility of the PPLL for ACS diagnosis.

**Results:** In healthy subjects, the FW/H2 correlated linearly to IMP (R=0.86). As a thigh tourniquet increased IMP from 12 mmHg (+/-2mmHg) to 26mmHg (+/-4mmHg), the FW/H2 increased significantly from 0.65AU (+/-0.05AU) to 1.00AU (+/-0.2AU). FW/H2 further increases at the higher IMP values seen in ACS, with a high of 2.67AU recorded for a patient whose IMP was 60mmHg.

**Conclusions:** The linear correlation of FW/H2 to IMP is demonstrated clinically. Preliminary results indicate that similar algorithms may be employed for the noninvasive measurement of intracranial pressure, and the assessment of cardiovascular disease.

**Acknowledgements:** This work was funded by a Phase II SBIR contract from the Army Research Office.

**References:**

[1] Wiemann JM, et al. "Noninvasive Measurements of Intramuscular Pressure using Ultrasound in a Model Compartment Syndrome." Presentation to the Orthopedic Research Society Annual Conference, 2005.
[2] Brinton TJ, et al. "Arterial compliance by cuff sphygmomanometer: application to hypertension and early changes in subjects at genetic risk" Hypertension 1996 Oct; 28(4):599-603.
[3] Chesney CF, Finkelstein SM and Cohn JN. "Method and instrument to measure vascular impedence." U.S. Patent #6,623,434, 2003.
[4] Chio SS. "Method for diagnosing, monitoring and treating hypertension and other cardiac problems." US Patent #6,540,687.
[5] Molino P, et al. "Beat-to-beat estimation of Windkessel model parameters in conscious rats." Am J Physiol Heart Circ Physiol 274: H171-H177, 1998.
[6] Watts TB and Burrus CS. "Arterial pressure contour analysis for estimating human vascular properties." J Appl Physiol 40: 171-176, 1976.
[7] Daley ML, et al. "An estimated compliance index derived from intracranial pressure recording." Acta Neurochir (2002) [Suppl] 81:183-185.
[8] Daley ML, et al. "Intracranial pressure dynamics: changes of bandwidth as an indicator of cerebrovascular tension." Med Eng & Physics 25 (2003) 679-689.
[9] Lang EW, et al. "Noninvasive intracranial compliance monitoring: Technical note and clinical results." J Neurosurg. 2003 Jan;98(1):214-8.
[10] Michaeli D and Rappaport ZH. "Tissue resonance analysis; a novel method for noninvasive monitoring of intracranial pressure." J Neurosurg. 2002 Jun; 96 (6):1132-7.
[11] Piper IR, et al. "Systems analysis of cerebrovascular pressure transmission: an observational study in head-injured patients." J Neurosurg 1990 Dec;73(6):871-80.

** indicates Presenter*

061 **THE SPATIO-TEMPORAL VARIATION OF THE STRAIN FIELD INSIDE COMPRESSED POROELASTIC MATERIALS.**

*Gearóid P Berry[1]*, Jeffrey C Bamber[1], Nigel L Bush[1], Naomi R Miller[1].*
[1]Institute of Cancer Research, 15 Cotswold Road, Sutton, Surrey, SM2 5NG, England, UK.

**Aims:** To image the spatio-temporal variation of the strain field inside compressed materials containing mobile fluid, and to compare images obtained with analytical and finite element predictions.

**Background:** Soft tissues contain mobile fluid, and this fluid can be encouraged to flow by the application of a compressive displacement to the surface of the tissue [1]. In an attempt to model the effect of this flow on the compression-induced strain field, soft tissue has previously been treated as a poroelastic material [2,3]. Previous preliminary experimental elastographic imaging of the induced strain field in a fluid-rich sample showed time-dependent spatially-varying behaviour that appeared to agree with theoretical predictions [3]. Further experiments, using more samples, were desired to provide statistically valid confirmation of this behaviour.

**Methods:** Using analytical and finite element (FEM) techniques, previous theoretical predictions [2, 3] were further developed and interpreted. Five tofu phantoms, each containing mobile fluid, were subjected to sustained compression, and the time-evolution of the strain field was imaged using elastographic techniques.

**Results:** Analytical and FEM results were in good agreement, providing helpful validation of the modeling software for future use in more general compression problems. The imaged strain field in each phantom was found to be both time-dependent and spatially-varying, and behaved in a manner consistent with both previous predictions of poroelastic theory [2, 3, 4] and those developed in this work. A typical example is shown in Figure 1.

**Conclusions:**
This study provides confidence in our previous experimental results and further insight into how the strain field in soft tissues rich in mobile fluid might behave when the tissue is subjected to sustained compression. Potential applications of importance include the diagnosis of medical conditions such as lymphoedema and malignant tumours.

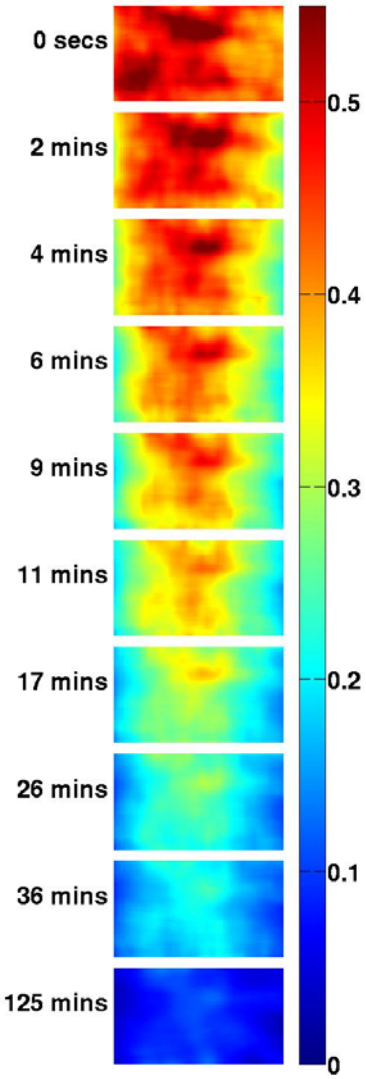


Figure 1: The measured spatio-temporal variation of the lateral-to-axial strain ratio inside a mobile-fluid-rich phantom showing the characteristic retreat with time, of the region of high strain ratio, away from the sample boundaries (centre line = axis of symmetry).

**References:**

[1] Levick JR. An Introduction to Cardiovascular Physiology 4th ed. 2003. ISBN: 0340809213.
[2] Konofagou E, Harrigan TP, Ophir J, Krouskop TA. Poroelastography: imaging the poroelastic properties of tissues. UMB 2001;27(10):1387-1397.
[3] Berry GP, Bamber JC, Miller NR. Towards a model-based poroelastic imaging method. Proc of the 3rd Int. Conf. on the Ultrasonic Measurement and Imaging of Tissue Elasticity 2004:p96.
[4] Biot MA. General Theory of Three-Dimensional Consolidation. J. Applied Physics 1941;12:155-164.

065 **A NEW COMPRESSION METHOD FOR GENERATING POROELASTOGRAMS IN INHERENTLY NOISY APPLICATIONS.**

*Raffaella Righetti[1]*, Jonathan Ophir[1], Brian S. Garra[2], Thomas A. Krouskop[1,3].*
[1]The University of Texas Health Science Center at Houston, 6431 Fannin St., Houston, TX 77030, USA; [2]The University of Vermont College of Medicine, 111 Colchester Av., Burlington, VT 05401, USA; [3]Baylor College of Medicine, One Baylor Plaza, Houston, TX 77030, USA.

**Aim:** To develop a new compression method that allows generation of poroelastograms in inherently noisy environments such as those of clinical interest.

**Background:** Poroelastography requires the acquisition of data over a time interval in order to detect time-dependent changes that occur in poroelastic materials and tissues due to fluid flow. The experimental methodology proposed thus far for phantoms and tissues *in vitro* [1] may not be suitable for monitoring relatively slow time-dependent poroelastic changes in tissue *in vivo*, because of echo decorrelation problems due to uncontrollable motion. To overcome these limitations, we propose a new compression methodology that is more robust in poroelastographic applications *in vivo*.

**Methods:** In this paper, we compare the performance of poroelastography when using the step compression and a new compression scheme. The new compression scheme requires the application of a constant strain rate to the sample and data acquisition during the loading phase. Successively, poroelastograms are generated by continuously moving the reference frame and cross-correlating frames that are equally spaced in time. This allows long acquisition times and also minimizes the decorrelation because of the short inter-frame time interval between the frames that are correlated. Poroelastographic experiments were performed on phantoms and tissues *in vivo* using both methodologies and the two sets of results obtained from the controlled experiments were compared using standard statistical tests.

**Results:** Figure 1 shows the results of the poroelastographic experiments performed on phantoms. The Poisson's ratio elastograms shown in the top row refer to a poroelastogram obtained using a step compression displacement, while the Poisson's ratio elastograms shown in the bottom row refer to a poroelastogram obtained using the new compression scheme. Figure 2 shows the corresponding average Poisson's ratio values (solid curve: step compression; dashed curve: new compression), which were found not to be statistically different. However, in *in vivo* applications, the step method did not allow any meaningful information on the time-dependent poroelastic behavior of the tissues to be collected after 1s. The new compression methodology, instead, retained relatively high correlation between the frames that were used for the generation of the poroelastograms for longer times, thus suggesting the feasibility of using it for monitoring fast (<1s) as well as slow (>1s) tissue time-dependent poroelastic changes.

**Conclusions:** In this paper, we have described a new compression scheme for poroelastography. The new compression method was found to produce similar results to the traditional compression method in controlled phantom experiments, and appeared to be more robust in inherently noisy applications.

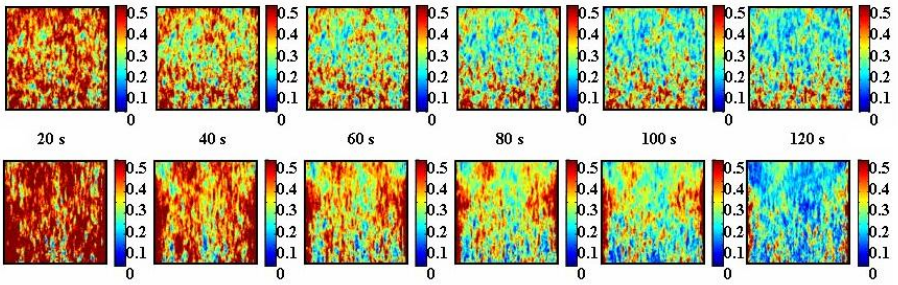


Figure 1

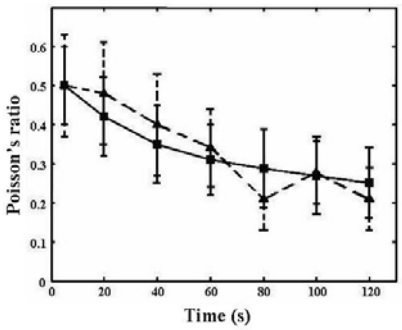


Figure 2

**Acknowledgements:** This work was supported by NCI Program Project PO1-CA64597-12.

**Reference:**

[1] Righetti R, Ophir J, Srinivasan S and Krouskop TA. The feasibility of using elastography for imaging the Poisson's ratio of porous media. Ultrasound Med. Biol. 2004. 30: 215-228.

* *indicates Presenter*

018 **MAXIMUM STRAIN ACCUMULATION FOR *IN VIVO* BREAST TISSUE.**

*AM Sommer[1]*, TJ Hall[1], J Jiang[1].*
[1]Department of Medical Physics, University of Wisconsin – Madison, Madison, WI, USA.

**Background and Aims:** The aim of this study is to determine the maximum amount of tissue deformation that can be tracked accumulatively for *in vivo* breast tissue and study that maximum as a function of the step size for summing multiple deformations. The results for *in vivo* tissue were then compared to that for data from gel phantoms.

**Methods:** Radio frequency (RF) echo data was acquired from a Siemens Elegra with freehand scanning of *in vivo* breast tissue and phantoms. RF-echo fields were dynamically paired with a range of time separations to vary the frame-average strain used to accumulate larger total strains. The displacement field between a reference and deformed RF frame was estimated using a 2-D block-matching technique. The estimated displacement was used to warp the deformed RF-echo field back to the geometry of the reference RF-echo field. Normalized cross correlation between the reference RF field and the motion-compensated deformed RF field was used to measure motion tracking accuracy and compare the various step sizes and to determine the maximum amount of strain that could be accumulated given an acceptable amount of decorrelation.

**Results:** The normalized cross correlation between the reference RF field and the motion-compensated RF field accumulated with frame-average strain step sizes of nominally 0.3%, 0.6%, and 1.2% were compared (Figure 1) with a single large deformation for benign *in vivo* breast tissue. The maximum strain that can be accurately tracked improves significantly by summing multiple smaller strains, but the difference between accumulating 0.3%, 0.6%, and 1.2% strain fields is very small. This data also demonstrates that it is easier to accurately track large deformation in gel phantoms compared to benign and malignant tissue (Figure 2). Tissue motion is significantly more complex than that in phantoms, leading to a large discrepancy between phantom and *in vivo* tissue data. Since malignant tissue is typically much stiffer than benign tissue, significantly more compression of normal tissue is required to achieve the same frame-average strain in a malignant tumor compared to a benign tumor of the same size.

**Conclusions:** Using our current motion tracking algorithm the optimal step size for *in vivo* tissue was found to be nominally 1% frame-average strain. The maximum strain that can be accurately accumulated is limited by the ability of the motion tracking algorithm currently being used. Improving the motion tracking algorithm will decrease the accumulated error and allow for tracking larger tissue deformation accumulatively.

**Acknowledgements:** We are grateful for the support from the USAMRMC (DAMD17-00-1-0596), the NIH (R01-CA100373), the University of Wisconsin and to colleagues at the Mayo Clinic in Rochester, MN, USA, and the Charing Cross Hospital in London, UK, for providing some of the data used in this study.

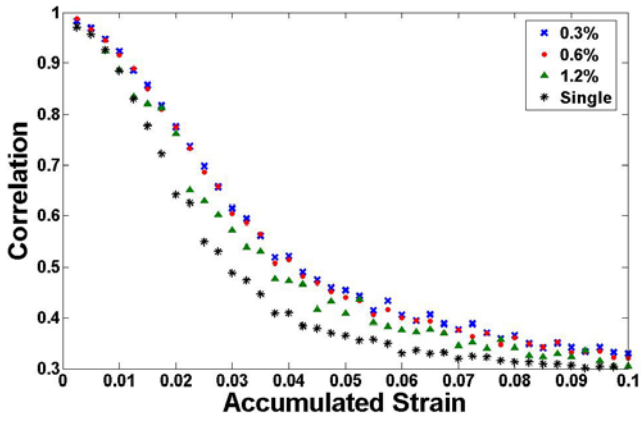


Figure 1

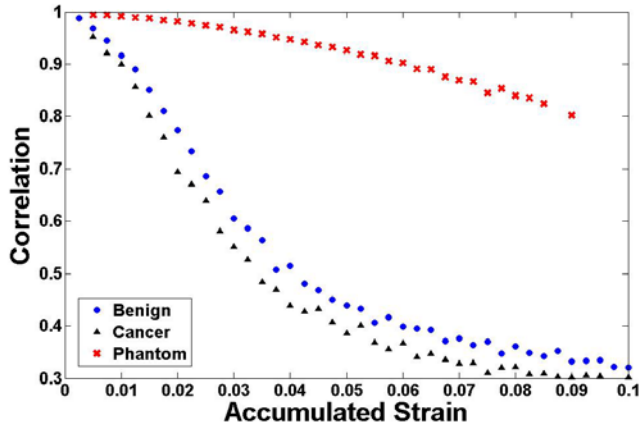


Figure 2

032 **DOPPLER MYOGRAPHY—DETECTING AND IMAGING INTRINSIC MUSCLE SOUNDS.**

*SF Levinson[1]*, H Kanai[2], H Hasegawa[2].*
[1]Rehabilitation Institute of Michigan, Wayne State University, Detroit, MI, USA; [2]Tohoku University, Department of Electronic Engineering, Sendai, JAPAN.

**Aims:** We sought to measure and image intrinsic vibrations that occur with skeletal muscle contraction.

**Background:** It has long been known that muscle fibers vibrate during contraction. These vibrations occur at the resonant frequency of the fibers, which is related to fiber length, tension and elasticity [1, 2]. We have previously demonstrated the ability to use Doppler ultrasound principles to detect propagating heart sounds. The ability to detect skeletal muscle sounds noninvasively could reduce or eliminate the need for needle electromyography (EMG) in neuromuscular diagnosis.

**Methods:** Using surface electrodes and a microphone, we measured surface EMG and phonomyographic (PMG) signals during contractions of the forearm flexor muscles in a single subject. Using an ultrasound transducer coupled to hardware and software previously applied in cardiac experiments, we simultaneously recorded ultrasonic Doppler waveforms from within the contracting muscles. The experimental apparatus is shown in Figure 1.

**Results:** A representative set of waveforms is shown in Figure 2. The Doppler myographic (DMG) signals correlated well with both surface EMG and PMG. Further, it was possible to differentiate between contractions in different digits of the hand with DMG, but not EMG nor PMG.

**Conclusions:** We have demonstrated the feasibility of using Doppler myography to detect the intrinsic sounds of contracting skeletal muscles. Further, we have demonstrated that these sounds can in part be localized without the use of the invasive needles as required for EMG. We anticipate that DMG could become a significant new clinical modality for the diagnosis of neuromuscular disorders.

**Acknowledgements:** The authors gratefully acknowledge the support of the University of Rochester School of Medicine and Dentistry for making this work possible.

**References:**

[1] D. T. Barry, S. R. Geiringer, and R. D. Ball, "Acoustic myography: a noninvasive monitor of motor unit fatigue," *Muscle & Nerve*, vol. 8, pp. 189-94, 1985.
[2] P. A. Dalton and M. J. Stokes, "Frequency of acoustic myography during isometric contraction of fresh and fatigued muscle and during dynamic contractions," *Muscle & Nerve*, vol. 16, pp. 255-61, 1993.

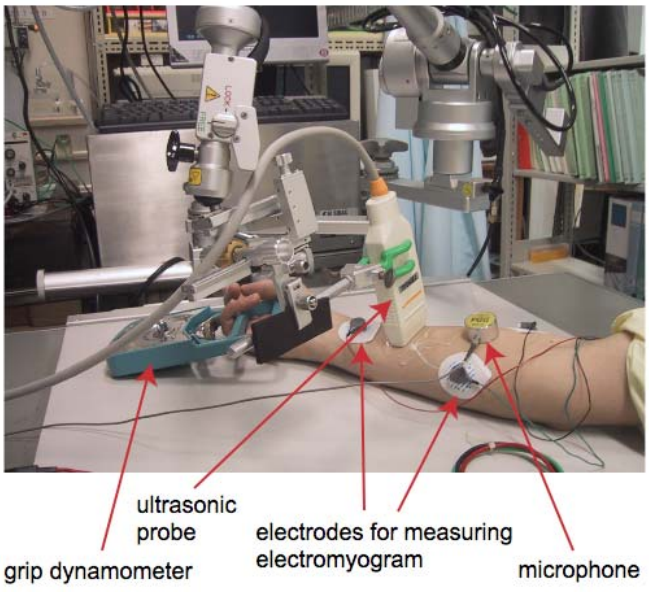


Figure 1: Measurement setup for simultaneous recording of surface EMG, PMG and DMG signals.

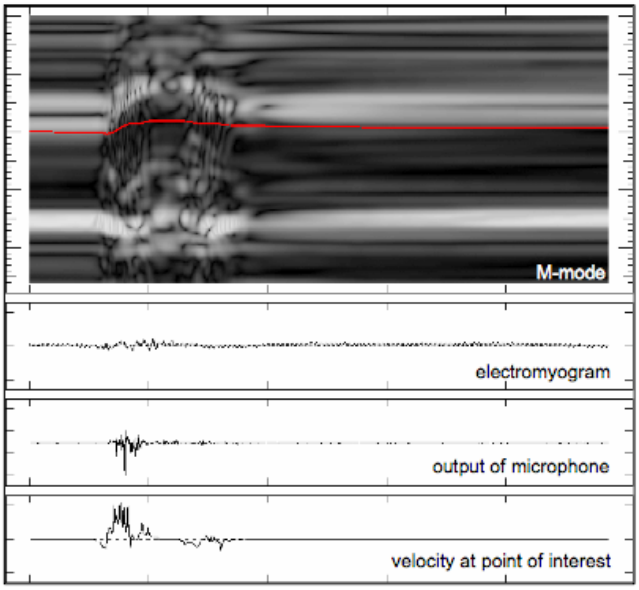


Figure 2: Representative recordings of surface EMG, PMG & DMG during contraction of the forearm flexor muscles.

* *indicates Presenter*

029 **TRANSIENT ULTRASOUND ELASTOGRAPHY USING IMPULSIVE ULTRASOUND RADIATION FORCE.**

*D Melodelima[1], J Bamber[1]*, F Duck[2], S Shipley[2].*
[1]Joint Department of Physics, Royal Marsden NHS Trust and Institute of Cancer Research, Sutton, Surrey, England, UK; [2]Medical Physics Department, Royal United Hospital NHS Trust, Bath, England, UK.

**Aims:** The use of a focused ultrasound transducer to generate impulsive radiation force for strain imaging was investigated to improve breast cancer detection.

**Background:** Alternative imaging methods are needed to improve the effectiveness of breast cancer detection and diagnosis. As a result, the development of imaging systems capable of evaluating the mechanical properties of tissues with high resolution is being carried out by numerous research teams [1-3]. Several groups are studying acoustic radiation force-based imaging modalities [4, 5]. However, to date these have been largely based on the detection, by various means, of signals that are proportional to the displacement induced by radiation force, whereas in pseudo-static elastography generally strain is imaged, as a surrogate for inverse stiffness. The imaging of strain generated by radiation force from a focused ultrasound transducer may be of interest to improve breast cancer detection.

**Methods:** In this study, a focused ultrasound transducer having an f-number of 1.3 was driven at an operating frequency of 1.7 MHz, and was used to apply localised radiation force to a small volume of tissue mimicking phantom. Images were created using a single "pushing" burst at each location, of 8 ms duration. A linear array with a centre frequency of 7.5 MHz was used to obtain echo signals. The focused transducer and the linear array were aligned such that the focus was in the plane of imaging. The time-dependent transient strains resulting from the impulsive radiation force were mapped using a least-squares strain estimator and ultrasound RF correlation-based displacement tracking methods. Gelatine phantoms containing cylindrical stiff inclusions were used.

**Results:** Experimental results demonstrate that strain on the order of 0.04 can be generated and detected with a resolution of about 1 mm. A stiffer region exhibits lower strain than a more compliant region. The instantaneous strain immediately following cessation of the radiation force varies approximately linearly with the Young's modulus of the material. Good agreement was obtained between the size of the inclusion seen macroscopically and measurements made using transient radiation force elastography.

**Conclusions:** Strain imaging using impulsive radiation force offers several advantages. The highly localised and transient strain that is produced by focused and impulsive radiation force may permit the sensing of changes in tissue elastic properties that are difficult to detect with conventional elastography, due to greater independence from boundary conditions and a resulting improved global contrast-to-noise ratio. For example, the characteristic, bi-directional, high strain artefacts due to stress concentration, often seen with static elastography at the tissue-inclusion interface, do not appear using the transient radiation force strain imaging technique. It is also possible to utilize a single pushing burst, strongly focused in two dimensions, that acts as a spatially localised impulse, and to use low frequencies to supply radiation force more efficiently to deeper tissues.

**Acknowledgements:** This work was supported by funding from the UK Department of Health (NEAT D008).

**References:**

[1] Ophir J., Cespedes I., Ponnekanti H., Yazdi Y. and Li X. Elastography: a quantitative method for imaging the elasticity of biological tissues. *Ultrason Imaging* 1991 **13**(2):111-134.
[2] Bercoff J., Tanter M. and Fink M. Supersonic shear imaging: A new technique for soft tissue elasticity mapping. *IEEE Trans Ultrason Ferroelectr Freq Control* 2004b **51**(4):396-409.
[3] Fatemi M. and Greenleaf J. F. An imaging modality based on ultrasound-stimulated acoustic emission. *Proc Natl Acad Sci* 1999 **96**:6603-6608.
[4] Nightingale K. R., Bentley R. and Trahey G. Observations of tissue response to acoustic radiation force: opportunities for imaging. *Ultrason Imaging* 2002 **24**(3):129-138.
[5] Lizzi F., Murator R., Deng C., Ketterling J., Alam S., Mikaelian S. and Kalisz A. Radiation-force technique to monitor lesion during ultrasonic therapy. *Ultrasound Med Biol* 2003 **29**(11):1593-1605.

080 **COMPARATIVE ASSESSMENT OF SPECTRAL AND TEMPORAL BASED ADAPTIVE ELASTOGRAPHIC TECHNIQUES.**

*K Hoyt[1,2], F Forsberg[2]*, CRB Merritt[2], JB Liu[2], J Ophir[3].*
[1]Drexel University, Philadelphia, PA, USA; [2]Thomas Jefferson University, Philadelphia, PA, USA; [3]University of Texas Medical School, Houston, TX, USA.

**Aims:** The objective of this study was to perform an *in vivo* comparative assessment of both spectral- and temporal-based adaptive elastographic techniques.

**Background:** It has been established that due to tissue heterogeneity, adaptive elastographic techniques are better suited for describing strain distributions *in vivo* than their non-adaptive counterparts [1, 2]. Currently, there are two disparate approaches to elastographic imaging, namely, spectral- (incoherent) and temporal-based (coherent). In general, strain estimators using spectral methods are more robust against decorrelation noise sources whereas those derived using temporal methods are more precise.

**Methods:** Stiff hepatic lesions of varying size and depth were induced in swine [3]. A modified HDI 1000 scanner (Philips Medical Systems, Bothell, WA, USA) with a 7.5 MHz linear array was used (either in automated or freehand mode), directly on the surgically exposed surface of the liver with respiration suspended. Following data acquisition, consecutive frames of digitized RF data were windowed (3.0 mm with 80% overlap) and subsequently, used to compute tissue strain using both adaptive spectral [2] and temporal [1] elastographic approaches. Lesions depicted in elastograms were circumscribed and area measurements were computed. A linear regression analysis was used for analyzing lesion measurements against varying doses at constant depth (and vice versa). Automated and freehand results were compared with t-tests. Elastography lesions sizes were compared to corresponding gross pathology. Lastly, comparison of adaptive spectral- and temporal-based elastographic lesion measurements was performed using a 2-sample t-test.

**Results:** A difference was observed in measurement of lesions of varying size but located at constant depth ($p < 0.015$ and $p < 0.001$ for the spectral- and temporal-based elastographic results, respectively). Conversely, same-sized lesions imaged at varying depths resulted in no statistically significant difference when measured from the spectral elastograms ($p > 0.318$). Measurements performed on the same lesions depicted in the temporal elastograms yielded a significant difference ($p = 0.04$) for smaller sized lesions (0.5 ml ethanol injections corresponding to 29 mm2 lesions) located at constant depths, whereas no statistically significant difference ($p = 0.729$) was found for larger lesions located at constant depths. Hence, lesion depth does not appear to influence the corresponding spectral elastogram lesion sizes, whereas adaptive temporal elastography demonstrate a statistically significant difference for smaller-sized lesions. Analysis into the role of scanning technique (automated vs. freehand) concluded that neither the adaptive spectral nor temporal elastographic approaches yielded a statistically significant difference ($p > 0.14$). A regression analysis of lesion sizes depicted in both the spectral or temporal elastograms and the corresponding lesions in the pathology photographs found a statistically significant difference between the image sets ($p < 0.001$). A comparison of congruent adaptive spectral and temporal elastographic lesion measurements concluded that there was no statistically significant difference ($p = 0.48$) between (lesion) data sets.

**Conclusions:** Results indicate that adaptive spectral elastography may be more suited for imaging small and deep sited lesions as compared to adaptive temporal elastographic techniques. This conclusion is predicated on the increased robustness demonstrated by spectral elastographic techniques; an important attribute for elastographic imaging of deep lesions due to the associated increased decorrelation effects.

**Acknowledgements:** This work supported in part by National Institutes of Health (USA) Program Project Grant P01-CA64597.

**References:**

[1] Srinivasan S, Kallel F, Souchon R, Ophir J. An analysis of an adaptive strain estimation technique in elastography. Ultrasonic Imaging 24: 109-118, 2002.
[2] Hoyt K, Forsberg F, Ophir J. Adaptive spectral strain estimation in elastography (abstract). J. Ultrasound Med. 23(6): Supplement, 2005.
[3] Hoyt K, Forsberg F, Merritt CRB, Liu JB, Ophir J. *In vivo* elastographic investigation of ethanol-induced hepatic lesions. Ultrasound Med. Biol. 31(5): 607-612, 2005.

043 **DISPLACEMENT OF A SOLID SPHERE IN A VISCOELASTIC MEDIUM IN RESPONSE TO AN ACOUSTIC RADIATION FORCE: THEORETICAL ANALYSIS AND EXPERIMENTAL VERIFICATION.**

*Salavat R. Aglyamov[1]*, Andrei B. Karpiouk[1], Yurii A. Ilinskii[2], Evgenia A. Zabolotskaya[2], Stanislav Y. Emelianov[1].*

[1]Department of Biomedical Engineering, University of Texas at Austin, Austin, TX 78712, USA; [2]Applied Research Laboratories, The University of Texas at Austin, Austin, TX 78713, USA.

**Aims:** The static displacement and transient motion of a small spherical object (e.g., gas bubble) in response to continuous or pulsed acoustic radiation force depends on the mechanical properties of the surrounding material. The overall goal of our program is to estimate the mechanical properties of the tissue based on the displacements of the gas bubble perturbed by radiation force. The goal of this study was to investigate the dynamic behavior of a rigid sphere in a viscoelastic medium.

**Background:** Methods using acoustic radiation force have been developed to estimate the mechanical properties of tissue. In these approaches, the radiation force of focused ultrasound is used to induce motion in a small volume within the tissue. The magnitude of the radiation force and, therefore, the induced displacement depends primarily on the absorption and reflection of ultrasound. For soft tissues, the absorption has a dominant effect. However, if there is an acoustic inhomogeneity, such as a gas bubble, the reflection of ultrasound may play a more significant role. However, the response depends not only on the viscoelastic properties of the medium but also on the properties of the reflector. Since in many biomedical and clinical applications, the microbubbles are introduced in soft tissue, spherical reflectors are of particular interest. Using a previously developed theoretical model [1], we have performed theoretical, numerical and experimental studies to investigate the dynamic behavior of spherical objects surrounded by a viscoelastic medium.

**Methods:** In theoretical analysis, the viscoelastic medium (Voigt model) was assumed to be isotropic, homogeneous, and incompressible. An impulse or finite duration acoustic radiation force was applied to spherical objects embedded in the medium. Equations describing the displacements of the object were derived using a frequency-domain formalism, and solved analytically or numerically. To verify our theoretical and numerical model, the experiments were performed using the rigid spheres of various diameters (0.3-3.0 mm) and densities embedded into gel-based phantoms of varying viscoelastic properties. The mechanical properties of the gels were estimated independently using load-displacement tests. A 1.5 MHz single-element focused transducer was used to apply the radiation force of desired duration (0.1-5.0 ms). Another single-element focused transducer operating at 25 MHz was used to track the displacements of the sphere every 50 μs. The foci of both transducers were aligned at the position of the sphere, and the displacement of the sphere was measured for up to 40 ms.

**Results:** The results of this study demonstrate good agreement between theoretical predictions and experimental measurements. For short pulses, both gas bubbles and solid spheres continue to move even after the applied force has ended. The delay between the application of radiation force and the displacement reaching the maximum depends strongly on the elasticity of the surrounding tissue, and the size and mass/density of the target. This time delay decreases with increased elasticity of the surrounding tissue, and, in contrast, increases for heavier (higher density) spheres. Maximum displacements are inversely proportional to the Young's modulus of the surrounding material. There are no oscillatory displacements for the relatively light spheres, while the heavier spheres may exhibit a few decaying oscillations. Tissue viscosity dampens the oscillations and reduces the amplitude of the displacement.

**Conclusions:** The developed theoretical model accurately predicts the displacement of the spherical acoustic inhomogeneity in tissue in response to the acoustical radiation force and can thus be used to evaluate mechanical properties of tissue.

**Acknowledgements:** Support in part by National Institutes of Health under grants CA112784 and EB004047 is acknowledged.

**Reference:**

[1] Y.A. Ilinskii, G.D. Meegan, E.A. Zabolotskaya, S.Y. Emelianov (2005). "Gas bubble and solid sphere motion in elastic media in response to applied force," J. Acoust. Soc. Am. 117, 2338–2346.

050 **ELASTOGRAPIC IMAGING OF UTERINE TISSUE.**

*M. A. Hobson[1]*, M. Z. Kiss[1], H. Shi[1], T. Varghese[1,2], M. A. Kliewer[3], J. A. Zagzebski[1] T. J. Hall[1], J. Harter[4], E. M. Hartenbach[5] and E. L. Madsen[1].*

[1]Medical Physics, [2]Biomedical Engineering, [3]Radiology, [4]Pathology, [5]Obstetrics and Gynecology Departments, University of Wisconsin-Madison, 1300 University Avenue, 1530 MSC, Madison, WI 53706, USA.

**Aims:** Leiomyomas (fibroids) and adenomyosis, a condition in which soft endometrial tissue invades the myometrium of the uterus, have similar appearances on conventional ultrasound images. We are investigating whether elastography can aid in differentiation between these two conditions, since the clinical treatments for the two conditions are very different. In addition, clinical differentiation of endometrial cancer from other benign conditions is also of interest.

**Background:** Uterine abnormalities tend to present clinically as dysfunctional uterine bleeding. Causes of irregular vaginal bleeding, especially in post-menopausal women, are often benign endometrial atrophy or hyperplasia (polyps, leiomyomas), although, approximately 10% to 30% of women will be found to have endometrial cancer. For pre-menopausal women, dysfunctional uterine bleeding most often results from benign conditions, such as leiomyomas, endometrial polyps, and adenomyosis. Currently MRI is the only imaging modality capable of distinguishing between these two conditions, leiomyomas and adenomyosis.

**Methods:** Ultrasound elastography was performed on uteri removed via elective hysterectomies. A Siemens Antares with a VFX13-5 transducer was used to acquire radiofrequency data sets, which were post-processed using 2-D block matching and 1- and 2-D cross-correlation analysis to create elastograms. Manual freehand compression using the transducer as the displacement device and stepper motor controlled compressions using a rectangular plate were applied to the excised uterine tissue during the imaging procedures. Following elastographic imaging, rectangular tissue samples were excised from the cervix and the endometrium for dynamic testing on a Bose Enduratec ELF system.

**Results:** Excised uteri from 15 patients have been evaluated. In 8 patients with uterine fibroids, masses identified by the pathologist appeared darker (were stiffer) than the surrounding uterine muscle, In some cases, there is evidence of a softer tissue surrounding the mass, enabling it to be seen more clearly. Elastograms provide more complete visualization of the mass than B-mode images.

**Conclusions:** *In vitro* results support the idea that elastography can play a role in diagnosing the source of postmenopausal bleeding. Fibroids appear stiffer than surrounding muscle tissue; at this time elastographic features of uterine tissue when a diagnosis of adenomyosis has been made are not clear. Strategies for performing *in vivo* elastography have also been developed. Uterine elastography may provide physicians an alternative to MRI.

045 **PVA PROSTATE PHANTOM FOR ULTRASOUND AND MR ELASTOGRAPHY.**

*Walaa Khaled[1]*, Thosten Neumann[1], Joerg Stapf[1], and Helmut Ermert[1].*
[1]Institute of High Frequency Engineering, Ruhr-University, Bochum, GERMANY.

**Aims:** The real time ultrasound elastography system presented in [1] allows the use of elastography in a clinical study for the early detection of prostate cancer during conventional transrectal ultrasound examinations. Since tumors often consist of hard tissue structures, imaging the elastic properties promises to increase the ability to detect prostate cancer. However, in transrectal elastography, the compression is manually induced by the conducting physician, which is operator dependent and leads to unstable image sequences. In this paper, we present a newly designed phantom to help physicians adapt to our real time elastography system.

**Background:** Tissue mimicking phantoms used for elastographic experiments are made mostly from a mixture of agar and gelatin. The solution of agar and gelatin has effectively revealed interesting properties, since gelatin contributes to the elastic character and agar insures stiffness and cohesion [2]. As for the acoustical scattering of such phantoms, it can be adjusted by simply varying the scatterer concentration. The independent control of acoustical and mechanical properties of such phantoms made agar gelatin phantoms attractive for elastographic experiments. However, the disadvantages are the long-term change in geometric and physical properties, and that agar-gelatin phantoms tend to rupture easily under increasing radial stress.

**Methods:** For testing the prostate diagnostic using ultrasound elastography and a rectal probe these phantoms could not simulate the ruggedness and elasticity of the rectal wall. For those reasons, a new material has been tested for this specific application purpose, which has a high breaking strength and is able to emulate the prostate along with structures simulating the rectal wall and the urethra. This material is Poly-Vinyl Alcohol. As a cryogel, it acquires its properties by freeze-thaw cycle processes. Chu et al. [3] have studied this material and found that the acoustical and elastic characteristics of the PVA cryogel are within the range of those of soft tissues. Therefore, for the production of anthropomorphic prostate phantoms with variable realistic elastic, ultrasound and MR properties, we need a set of materials to represent fat, glandular and the perineal membrane. These materials consist of ethyl alcohol in Polyvinyl alcohol with TLC Silica gel 60 H dispersions with different concentrations. Production of molds for making phantoms with geometries suitable for current US and MR prostate elastography with internal structures was achieved including simulated tumors. Some niceties in mechanical properties, like the seminal vesicles, will also be simulated in the phantoms.

**Results and Conclusion:** The variation of the elastic modulus according to thaw and freeze cycles was quantified. Preliminary results established a range of 30± 5.2 kPa – 90.2± 15 kPa for 2-5 freeze-thaw cycles and 7.5% to 10% solution concentration. Different studies of the Young's moduli, the US speeds, US attenuation coefficient, MR $T_1$'s and $T_2$'s are being calculated. The results show that the stress-strain relationship of PVA-phantoms is close to that of a pig tissue, and that the US propagation speed is in the range of (1500m/s -1600m/s). The attenuation values are also promising at 10 MHz.

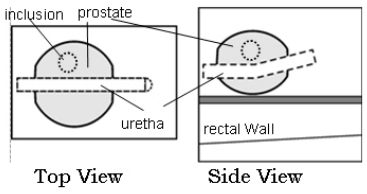


Scheme of the PVA Prostate Phantom

Mold and Phantom

Transrectal Probe and Phantom

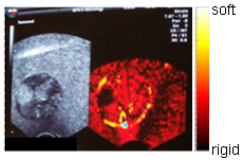


B-Scan Elastography Voluson 730; GE

Images of the Phantom and Results Using US-elastography

**Acknowledgements:** A project of the Ruhr Center of Excellence for Medical Engineering (KMR). Supported by the German Federal Ministry of Education and Research, No. 01 IR A 14 B.

**References:**

[1] Pesavento A, Lorenz A, Ermert H (1999): System for real-time elastography, Electronics Letters, Volume 35, 11, 941-942.
[2] Hall T.J:, Bilgen M., Insana M.F., and Krouskop T.A., Phantom materials for elastography IEEE transactions UFFC 1997, Vol. 44, no. 6, pp. 1355-1364.
[3] Chu K. C. and Rutt B. K., Polyvinyl Alcohol Cryogel: An Ideal Phantom Material for MR studies of Arterial Flow and Elasticity, Magnetic Resonance in Medicine, 1997, Vol. 37, no.2, pp. 314-319.

046 **A NOVEL 3D HAPTIC SENSOR SYSTEM BASED ON ULTRASOUND ELASTOGRAPHY.**

*Walaa Khaled[1]*, Stefan Reichling[2], Otto T. Bruhns[2], Andreas Lorenz[3], Andreas Pesavento[3], Helmut Ermert[1].*
[1]Institute of High Frequency Engineering, [2]Institute of Mechanics, Ruhr-University, Bochum, GERMANY;
[3]LP-IT Innovative Technologies GmbH, Bochum, GERMANY.

**Aims:** A standard screening procedure for the detection of breast, thyroid, prostate, and liver abnormalities is palpation. The pathological state of soft tissues is often correlated with changes in stiffness; however, current medical practice routinely uses sophisticated diagnostic tests through magnetic resonance, computed tomography and ultrasound imaging, which cannot provide direct measure of tissue elasticity.

**Background:** Last year, we presented the concept and first results of the haptic sensor actuator system to visualize mechanical properties of tissue using ultrasonic elastography and electrorheological fluids. Using this system, we reconstruct tissue properties from a real time ultrasound elastography system on a controllable haptic display capable of emulating and differentiating normal and abnormal biological tissue.

**Methods:** Firstly, during the solution of the mechanical forward problem, the biological tissue was modeled as a linear, isotropic, incompressible, elastic medium and a 2-D plane strain state model was used. Furthermore, to develop an inverse elastography reconstruction procedure, finite element simulations were performed for a number of biological tissue object models. The results obtained from finite element analysis were confirmed in the ultrasonic experiments on a set of tissue-like phantoms with known acoustical and mechanical properties. These phantoms were produced using PVA-Materials with different thaw and freeze cycles so that the relative Young's modulus E2/E1 of the inclusions (E2) with the surrounding medium (E1) as a reference is nearly 3 (E1= 30±5kPa, E2=90±15kPa). The RF-data was acquired using a standard ultrasound system (SONOLINE Omnia, Siemens AG, Germany) equipped with a 9 MHz linear array probe and a conventional ADC at a sampling frequency of 50 MHz. The axial displacements were calculated using the fast root-seeking technique [1]. Secondly, we deduce the relative Young's modulus of the sample by solving the inverse problem using two different methods. The first method is a modified direct method based on solving the equations of equilibrium proposed by [2] and modified by the authors. The second method is an iterative method for solving the inverse elasticity problem and is based on recasting the problem as a non-linear optimization problem.

**Results and Conclusion:** The results of an ongoing clinical study on the prostate tumor diagnostic with more than 200 patients show that our real time ultrasound elastography system is able to differentiate hard lumps from soft tissue in a qualitative manner. The data collected with our real time elastography system were also used in the reconstruction approaches which seem promising for an additional quantitative differential diagnosis of lesions in biological tissue. The phantom results show that the iterative approach leads to a relative Young's modulus ratio of about 1.9 (E2~ 57kPa for the inclusion), whereas the direct method results in a ratio of 1.32 (E2~ 40kPa). The feasibility of both methods was also demonstrated using the measured real time ultrasound data from a tissue-like phantom with multiple inclusions and *in vitro* data. The proposed methods were compared with respect to the stability of algorithms using numerical simulations and ultrasound measurements. Based on this comparison, an approach is introduced, which is capable of taking into account large deformations, whereas other existing methods are generally based on the theory of linear elasticity. The images below show the relative Young's modulus in an US experiment and in an FE simulation with noisy input data.

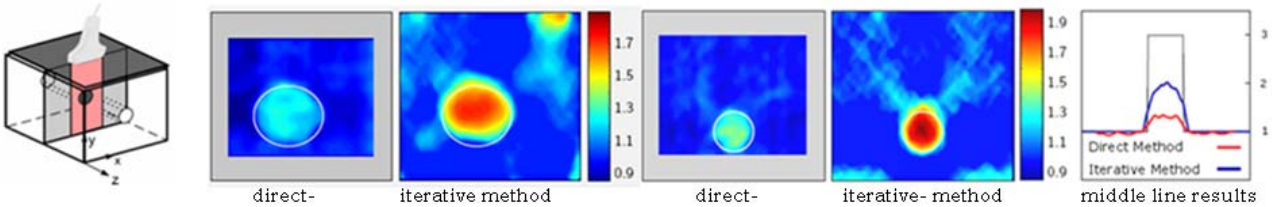


Experiment Scheme Measured Relative E-Modulus US Experiment Simulation Results (Relative E-Modulus) with Noisy Input Data

**Acknowledgements:** A project of the Ruhr Center of Excellence for Medical Engineering (Kompetenzzentrum Medizintechnik Ruhr (KMR), Bochum). Supported by the German Federal Ministry of Education and Research, (BMBF) No. 01 IR A 14 B.

**References:**

[1] Pesavento A, Lorenz A, Ermert H (1999): System for real-time elastography, Electronics Letters, Volume 35, 11, 941-942.
[2] Sumi et. al., IEEE Trans. BME, Vol. 42, 1995, p.193-202.

* *indicates Presenter*

048 **TISSUE MIMICKING MATERIALS AND PHANTOMS FOR ELASTICITY IMAGING.**

*John Beck[1]*, Shriram Sethuraman[1], Srivalleesha Mallidi[1], Andrei B. Karpiouk[1], Salavat R. Aglyamov[1], Stanislav Y. Emelianov[1].*

[1]Department of Biomedical Engineering, The University of Texas at Austin, Austin, TX 78712, USA.

**Aims:** To identify the materials and to develop the procedures for fabrication of sophisticated, durable and time-stable tissue mimicking phantoms of known properties for ultrasound elasticity imaging.

**Background:** Ultrasound elasticity imaging techniques are being developed and improved upon for the use in various biomedical applications. In order to aid in the development of these techniques, it is necessary to produce phantoms which can reliably mimic the properties of human tissue. Before these phantoms can be produced, however, it is also necessary to investigate and to be able to precisely manipulate the properties of the phantom materials. In addition, the properties of the materials must be stable over time, and the phantoms should be easy to produce and have a long shelf-life.

In ultrasound elasticity imaging, the most notable properties of the phantom material are the acoustic and mechanical characteristics. Several materials including gelatin, polyacrylamide gel, plastisol, poly (vinyl alcohol), silicone rubber, etc. have been successfully used to produce tissue phantoms as reported in literature. In this paper, we focus our attention on poly (vinyl alcohol) (PVA) hydrogels because of several unique properties of this material. First, a rich set of parameters (molecular weight and concentration of PVA, number of freeze/thaw cycles, concentration of crosslinking additives, etc.) allows producing hydrated gels of high water content and variable elasticity (Young's modulus). Second, the fabricated hydrogels are easy to produce, nontoxic, stable, durable and have a reasonable shelf-life. Finally, PVA hydrogels can be used in optical, X-ray, ultrasound and NMR (MRI) imaging making these hydrogels attractive for studies of multi-modality imaging techniques.

**Methods:** Aqueous solutions of PVA were prepared by dissolving crystalline granules of PVA in water at 96°C. Once the granules were totally dissolved, the resulting solution was cooled to room temperature and cast into a container of desired shape and size. If left at room temperature, the PVA solution will not crosslink and will remain a liquid. Among mechanical (freeze/thaw cycles), chemical (addition of crosslinking or bonding compounds) and irradiation (e.g., UV light) methods to crosslink PVA solution, freeze/thaw cycles were used exclusively in our experiments. Each cycle consisted of freezing the aqueous solution for 17 hours at 10°C followed by thawing of the sample in water for 7 hours at 25°C. The effect of cycling on polymer strength and the overall stability of mechanical properties of PVA was measured using cylindrical samples subjected to uniaxial load-displacement test. The mechanical properties of hydrogels were also altered using varying (4–10% by weight) concentration of PVA. In all samples, the ultrasound pulse-echo measurements of attenuation and speed of sound were performed to investigate the effect of PVA concentration and number of freeze/thaw cycles on the acoustic properties of the material. Finally, the mass and volume of each sample were also monitored over time.

To produce composite phantoms for elasticity imaging (i.e., layered phantom or phantom with an inclusion), the mechanical structures were contrasted using different number of freeze/thaw cycles. These structures were adhered to each other due to the interpenetration of polymer chains. For ultrasound imaging purposes, the silica particles (0.4-2%) were added to act as ultrasonic scatterers.

**Results:** The attenuation and the speed of sound in PVA hydrogels was measured to be 0.2 dB/cm/MHz (or less) and 1530 m/s, respectively, and did not change appreciably with freeze/thaw cycles or PVA concentration. The mechanical strength of hydrogels was shown to be almost linearly proportional to the PVA concentration. Increasing the number of freeze/thaw cycles increases nonlinearly the mechanical strength of PVA hydrogels. The PVA gels maintained their size, shape, and acoustic and mechanical properties when stored in water at room temperature. The ultrasound and elasticity imaging experiments confirmed that composite PVA-based phantoms maintained their integrity and acoustic/mechanical properties since they were fabricated.

**Conclusions:** The results of this study clearly demonstrate that poly (vinyl alcohol) can be used to produce complex tissue mimicking phantoms with desired acoustic and mechanical properties. The number of freezing and thawing cycles and concentration of aqueous solution of different molecular weight PVA can be manipulated to control properties such as the overall water content and mechanical strength while acoustic properties remain nearly the same. Using PVA, time stable and sturdy composite phantoms with distinct mechanical structures well adhered to each other were produced.

**Acknowledgements:** This research was supported in part by seed grant from The University of Texas Center for Biomedical Engineering.

035 **DEVELOPMENT OF AN *IN VIVO* TISSUE INDENTATION SYSTEM USING AN ELECTROMAGNETIC SPATIAL LOCATING SENSOR.**

*Yongping Zheng[1]*, Minhua Lu[1], Qinghua Huang[1], Winnie Yu[1], Grace H.Y. Lo[1].*
[1]The Hong Kong Polytechnic University, Hong Kong, CHINA.

**Aims:** Indentation tests have been widely used for the assessment of soft tissue stiffness *in vivo*. Its operation resembles the manual palpation using fingers. We have previously developed an ultrasound indentation system with a pen-size ultrasound palpation probe [1]. It has been successfully applied for the assessment of many different soft tissues *in vivo*. However, it requires that the tissue should have a bony substrate to reflect ultrasound echoes. The aim of this study is to develop an indentation system using an electromagnetic spatial locating sensor for the assessment of tissues without body substrate.

**Background:** Quantitative assessment of tissue elasticity *in vivo* is becoming more important recently. The traditional tissue assessment approach using finger palpation is subjective and qualitative. A number of tissue elasticity measurement devices have been developed to provide objective and quantitative assessment. The essential techniques involved are the approaches to measure the tissue deformation and applied load. Hand-held indentation probes are preferred, as they provide more flexible assessment for tissues at various locations.

**Methods:** In this study, we used an electromagnetic spatial locating sensor to measure the tissue deformation. The dimension of the spatial sensor is approximately 5x5x15 $mm^3$. Therefore, it can be attached to a small indentation probe. The applied load is sensed by a strain gauge load cell. A pen-size palpation probe was constructed with the spatial sensor and the load cell. The Young's modulus was extracted from the load-indentation relationship using the equation provided by Hayes et al. [2] and assuming that the thickness is large enough. A series of elastomers with different Young's modulus (ranging from 13.1 to 36.2 kPa) were assessed with both the hand-held indentation system and a Hounsfield material testing machine. Intra- and inter-operator repeatability of the measurement was tested with five operators. The hand-held indentation system was used to measure the effective Young's modulus of the tissues located in the abdominal region *in vivo*. Twenty healthy female subjects with age of 21.1 ± 1.8 years old were recruited for the test.

**Results:** The system was shown to be highly accurate ($R^2$= 0.99) and had good reliability (intra-operator variation = 5.43%, inter-operator variation = 5.99%). The mean effective Young's moduli of the soft tissues surrounding the umbilicus region were approximately 12 kPa.

**Conclusions:** The indentation system based on the electromagnetic spatial sensor is a highly reliable and accurate for the measurement of the tissue stiffness *in vivo*. The system is portable, and the probe is easy to operate. It is particularly suitable for the assessment of those body parts with thick soft tissues, such as breast, waist, abdomen, hip and thigh regions. For the body parts with thin soft tissues covering bony substrates, the tissue thickness plays an important role in extracting the modulus from the load-indentation relationship and should be measured. The ultrasound indentation may play a complementary role, as it is particularly useful for the tissues with bony substrate. In addition, one should be careful that metal objects are avoided near the electromagnetic transmitter or sensor during the measurement.

**Acknowledgements:** This work was partially supported by the Research Grants Council of Hong Kong (PolyU 5245/03E) and The Hong Kong Polytechnic University.

**References:**

[1] Zheng YP and Mak AFT. An Ultrasound Indentation System for Biomechanical Properties Assessment of Soft Tissues In-Vivo. IEEE Trans. Biomed. Eng., 1996; 43: 912-918.
[2] Hayes WC, Keer LM, Herrmann G and Mockros LF. A mathematical analysis for indentation tests of articular cartilage, J. Biomech., 1972; 5: 541-551.

036 **DEVELOPMENT OF A SOFTWARE PLATFORM FOR ULTRASOUND MEASUREMENT OF MOTION AND ELASTICITY (UMME).**

*Yongping Zheng[1]*, Jun Shi[1], Qinghua Huang[1] and Xin Chen[1].*
[1]The Hong Kong Polytechnic University, Hong Kong, CHINA.

**Aims:** Various techniques have been developed by different research groups for ultrasound measurement and imaging of tissue elasticity. Each group uses their own software for the data collection, processing and displaying results. The aim of this project is to develop a software platform which integrates the data collection, processing and displaying results within the same interface and can handle different modes of ultrasound tissue elasticity measurement and imaging.

**Background:** Because of the lack of an available software platform, researchers need to develop their own programs using many different computer languages to acquire ultrasound signals or images, to process the data using various algorithms to extract the motion and elasticity of tissues and, finally, to display the results. It can be imagined that all the groups are using different software interfaces and different data structures. Even within the same group, different investigators may use different custom designed software to solve different problems related to ultrasound elasticity imaging and measurement.

**Methods:** We have developed a software platform, which is designed for multiple purposes to handle various problems related to ultrasound measurement of motion and elasticity (UMME) of tissues. UMME is programmed in Visual C++ and can perform ultrasound signal and image collection from A/D and video capture cards, data processing using various algorithms in both 1D and 2D, and result display.

**Results:** UMME has successfully served as a platform for our techniques of ultrasound elasticity imaging and measurement including ultrasound indentation [1], ultrasound elastomiscroscopy [2, 3], water jet ultrasound indentation [4], ultrasound monitoring of osmosis swelling [5] and sonomyography [6]. Figure 1 shows two typical interfaces. A data structure has been designed for different applications. The software can collect data from A/D and video capturing cards supplied by different companies. The ultrasound signals and images can be simultaneously collected with other variables including force, pressure, angle, vibration, electromyography (EMG), electrocardiography (ECG), etc.

**Conclusions:** It is feasible to use UMME for different modes of ultrasound measurement of tissue motion and elasticity. We expect that other groups may also benefit from this UMME software interface through collaboration. The investigators may focus more on the new problems and algorithms.

**Acknowledgements:** This project is supported by HK RGC (PolyU5245/03E and PolyU 5199/02E).

**References:**

[1] Zheng YP, Mak AFT. Ultrasound indentation. IEEE Trans Biomed Eng 43: 912-918, 1996.
[2] Zheng YP, et al. 1D ultrasound elastomicroscopy. Phys Med Biol 47: 3165-3180, 2002.
[3] Zheng YP, et al. 2D ultrasound elastomicroscopy. Phys Med Biol. 49: 3925-3938, 2004
[4] Lu MH, et al. Water jet ultrasound indentation. Ultrasound Med Biol 31: 817-26, 2005.
[5] Zheng YP, et al. Ultrasound monitoring of cartilage swelling. Ultrasound Med Biol 30: 841-89, 2004.
[6] Zheng YP, et al. Sonomyography. Med Eng Phys. In print, 2005.

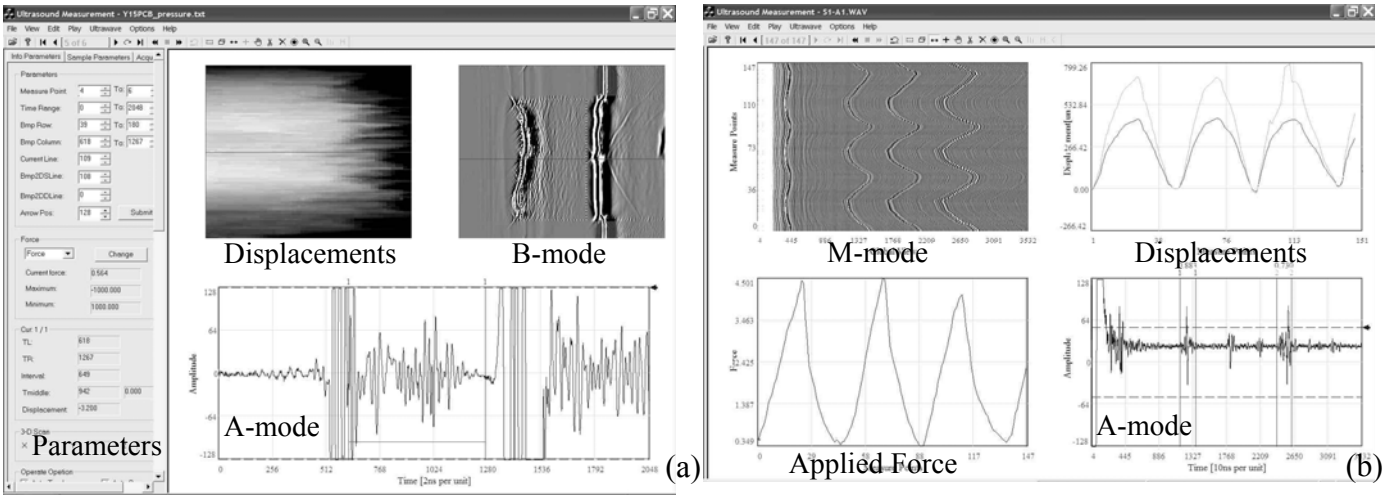


Figure 1: Different Interfaces of UMME. (a) 2D Ultrasound Elastomicroscopy; (b) Ultrasound Indentation

084 **MEASURING STIFFNESS OF BREAST TISSUE *EX-VIVO*.**

*Asif Iqbal[1]*, Tim Frank[1], Donald McLean[1], Alastair Thompson[1], Alfred Cuschieri[1].*
[1]Surgery Technology Group, Division of Surgery and Oncology, Ninewells Hospital and Medical School, University of Dundee, Dundee, DD1 9SY, Scotland, UK.

**Aims:** Breast tumors are known to be harder than normal tissue with palpation. Palpation produces a subjective assessment and, therefore, requires substantial clinical experience. In addition, the qualitative nature of such assessments makes the accumulation of knowledge difficult and imprecise learning. In this study, we present tissue stiffness measurement using a palpating probe.

**Background:** Quantification of tissue stiffness can be done by various mechanical material testing methods. However, indentation testing is probably the non-invasive technique for determining the *in-vivo* and *ex-vivo* mechanical behavior of tissues.

**Methods:** After obtaining ethical clearance and patient permission, we examined fresh mastectomy specimens containing large cancers, excised breast tumors from patients undergoing breast conservation treatment and excised benign lesions before fixation. A hand-held indenter's tip was pressed against the tissue to measure the displacement relative to a cylindrical ring surrounding it. The inner and outer diameters of the ring were 11.5 and 17.5mm, respectively, while the indenting tip was 4.0mm. The probe was comprised of a force transducer and a linear variable displacement transducer.

**Results:** The force-displacement measurement curves on samples of invasive ductal carcinoma, fibroadenoma, medullary carcinoma, fibrocystic breast disease, lobular carcinoma and mucinous carcinoma were plotted in Figure 1. The results indicate not only that the stiffness of benign tissue is different than that of malignant tissue, but also show significant variation in the stiffness of several malignant tumors. Contrary to clinical palpation, the suppleness of mucinous carcinoma is very different than invasive ductal carcinoma.

**Conclusions:** There is demonstrable difference in stiffness of various tumors. This instrument demonstrates the ability of the system to acquire the desired data. Analysis of the results of our initial experiments will be used to make several preliminary observations regarding the characteristics of our measurement system. Our next goal is to develop a detailed look-up table for various tumors at different stages of growth for a clinical assessment system to correlate with corresponding elastographic images. Such a diagnostic test would be particularly useful for breast cancer screening.

**Acknowledgements:** This work is financially supported by the Melville Trust for Care and Cure of Cancer, Tayside University Hospitals Trust (TUHT) and Anonymous Trust grants.

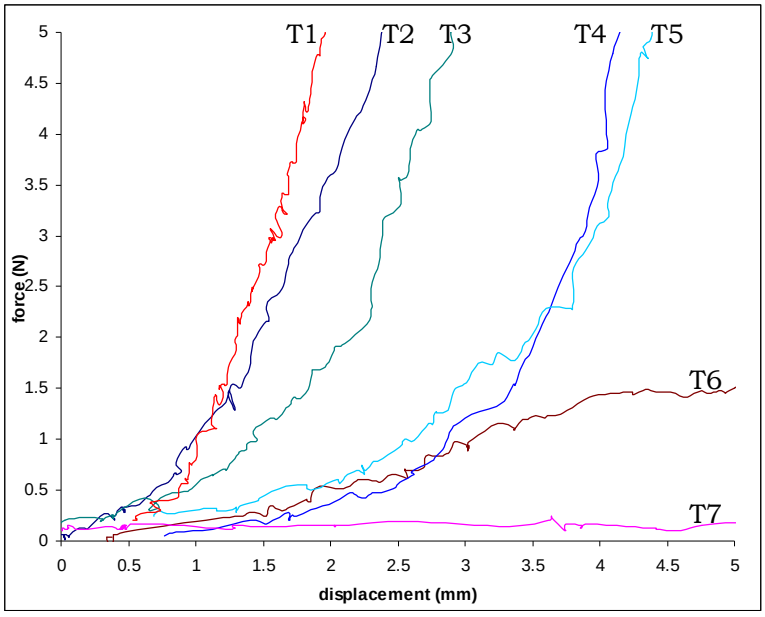


Figure 1: Force-Displacement Curves for Seven Tissue Samples: High Grade Invasive Ductal Carcinoma (T1); Intermediate Grade Invasive Ductal Carcinoma (T2); Fibroadenoma (T3); Fibrocystic Breast Disease (T4); Lobular Carcinoma (T5); Medullary Carcinoma (T6); Mucinous Carcinoma (T7).

Figure 2: Demonstration of the Indentation Test Using the Hand-Held Probe on a Fresh Breast Tissue Sample.

* *indicates Presenter*

098 **2D STRAIN ESTIMATION BASED ON A NEWTON CONSTRAINED MINIMIZATION STRATEGY: APPLICATION TO EXPERIMENTAL DATA.**

*E Brusseau[1], JF Déprez[1]*, G Said[1], O Basset[1].*
[1]CREATIS UMR CNRS 5515 INSERM U630, Lyon, FRANCE.

**Aims:** The aim of this study is the development of an accurate 2D strain estimation technique.

**Background:** Strain estimation is a crucial step in ultrasound elastography since strain fields are directly used for medium interpretation or for reconstruction of mechanical parameters. Thus, it is essential to estimate strains with high accuracy, by considering the 3D tissue motion induced by the physical compression. Because acquired data are 2D ultrasound RF images, we propose beginning with the investigation of a 2D strain estimation numerical model. So far, only a few 2D techniques have been reported.

**Methods:** Recently, we have developed an initial 2D strain estimator [1] that is now improved by the introduction of a Newton constrained minimization strategy. For each 2D RF region, $R_1$, selected in the pre-compression image, ($I_1$), the principle consists in finding its corresponding version, $R_2$, in the post-compression image, ($I_2$), and in estimating its 2D strain. In the axial direction, $R_2$ is supposed to be a time-delayed and scaled replica of $R_1$. The delay, $t_{ax}$, is induced by the accumulation of axial deformations of the regions located between the probe and the region of interest. In the lateral direction, only shifts are considered due to the poor resolution. Locally, after having compensated for $t_{ax}$, the axial scaling factor, $a$, and the lateral shift, $u$, are estimated as the arguments that minimize an objective function, $f$, defined as the opposite of the correlation coefficient between $R_1$ and $R_2$ compensated for $a$ and $u$.

Technique efficiency, and therefore, results accuracy are directly related to the objective function shape, and $f$ may suffer from multiple local minima unless strong constraints are introduced on the variable bounds, defining the admissible domain. The chosen technique is a constrained descent method, that generates a sequence of admissible iterates, until satisfying the Kuhn-Tucker conditions. The descent direction is computed, at each major iteration, by considering the associated quadratic problem. It is calculated as the projection of the Newton direction onto the admissible domain. The descent step is varied to insure fast convergence.

**Results:** The developed technique has been assessed with simulated and experimental data. Two simulated media were created. The first was a 3-layer medium whose middle layer, with Young's modulus (YM) of 50kPa, is twice as soft as the top and bottom layers. The second was a homogeneous cube (YM = 50kPa) with an embedded a harder cylindrical inclusion (YM = 100kPa). Media deformation was computed with FEM software, and corresponding RF ultrasound images were generated with the FIELD II program. The resulting elastograms demonstrate that, in the axial direction, estimated displacement and strain fields are very close to the theoretical ones. In the lateral direction, they are in accordance with the theory, but noisier, due to the poor resolution. Moreover, as the objective function is based on the correlation coefficient between a 2D initial region and its compensated deformed version, this one has been estimated to an average of 0.96. Results have also been obtained with tissue mimicking phantoms. One is a parallelepiped containing a harder cylindrical inclusion, both made of cryogel. This phantom has been subjected to a 3% global deformation. Data were acquired with a 7 MHz central frequency probe and with a 50 MHz sampling frequency. Estimated axial displacement and strain fields are of very good quality with a mean strain of 3.05%, corroborating the experimental conditions. The lateral displacement is noisier, but its significant amplitude demonstrates the necessity of not ignoring it. Finally, the mean correlation coefficient is, in this experimental case, close to 0.9.

**Conclusions:** The proposed technique is robust in regard to the signal decorrelation induced by the lateral motion, resulting in more accurate displacement and strain fields. Future work will deal with *in vitro* and *in vivo* experiments.

**Acknowledgements:** This work has been financially supported by the scientific committee of the INSA-Lyon, France.

**References:**

[1] E. Brusseau, G. Said, J. Fromageau, O. Basset, D. Vray, 2D Strain estimation algorithm – Initial Results, 3rd Int. Conf. on the Ultrasound Measurement and Imaging of Tissue Elasticity, Windermere, Cumbria, United Kingdom, October 17-20, 2004.

083 **STRAIN ESTIMATION WITH PULSE SHAPING.**

*R Souchon[1]*, S Vassant[1], J-C Béra[1], J-Y Chapelon[1].*
[1]INSERM UMR 556, Lyon, FRANCE.

**Aims**: Pulse shaping [1] can theoretically fully restore signal correlation. It consists in compressing the post-compression point spread function (PSF), $p_2$, by a scaling factor $\alpha$ in the time domain:

$$p_2(t) = p_1(\alpha t), \qquad \text{Equation (1)}$$

where $p_1$ is the pre-compression PSF, and $t$ denotes time. Global stretching [2] by a factor $1/\alpha$ is then applied to the received echo signal prior to time delay estimation. For optimal performance, the scaling factor, $\alpha$, is matched to the tissue strain, $\varepsilon$, by the relation:

$$\alpha = (1+\varepsilon)^{-1} \qquad \text{Equation (2)}$$

We investigated the potential of pulse shaping to increase the signal-to-noise ratio (SNRe) in simulated elastograms.

**Background**: In ultrasonic elastography the precision of strain estimates improves with the correlation between the pre- and post-compression echo segments. Unfortunately, the strain to be measured induces signal decorrelation that cannot be fully compensated, even when using adaptive stretching.

**Methods**: We compared the SNRe obtained with and without pulse shaping in 1D simulations of a homogeneous phantom. Simulated RF lines, $s$, were generated by convolving the one-dimensional PSF, $p$, with the scattering function, $m$, of the material (a normal distribution of scatterer amplitudes uniformly distributed). The PSF, $p$, was calculated by convolving the excitation voltage waveform, $u$, by the return-trip impulse response, $h$, of the transducer. A Gaussian impulse response of central frequency, $f_c$, and bandwidth, $B$, was assumed. The process is summarized by Equation (3), where $z$ denotes the distance to the transducer, $c$, the speed of sound, and * is the convolution product :

$$s(t) = u(t) * h(t) * m(t = 2z/c) \qquad \text{Equation (3)}$$

For pulse shaping, the pre-compression excitation waveform, $u_1$, was calculated using Equation (1), yielding: $\alpha\, u_1(\alpha t) * h(\alpha t) = u_2(t) * h(t)$. Note that the impulse response, $h(t)$, must be known to calculate $u_1$. All elastograms were calculated from the gradient of the time delay estimates, using uniform stretching. SNRe was estimated from the mean to standard deviation ratio of strain estimates.

**Results**: Figure 1 shows SNRe vs. strain with and without pulse shaping for $f_c$=6.5 MHz and $B/f_c$=60%. Figure 2 shows what happens for $\varepsilon$=5% in case of an error in the estimate of the bandwidth of the impulse response: SNRe is maximal when the bandwidth of the impulse response, $h(t)$, is properly estimated, but pulse shaping still performs well if fractional bandwidth is only known with ±20% accuracy. Figure 3 shows what happens when the strain estimate, $\varepsilon$, is not exactly equal to tissue strain, $\varepsilon_0$: pulse shaping performs significantly better than stretching alone only within a small range around $\varepsilon_0$.

**Conclusions**: Pulse shaping can significantly improve the SNRe, provided that the scaling factor is accurately chosen and that other causes of decorrelation (SNRs, out of beam motion) are minimized. In practice, it may be necessary to repeat acquisitions while adaptively updating the scaling factor.

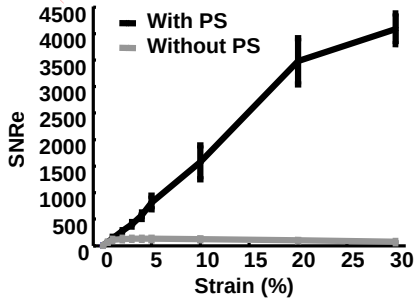


**Figure 1**: SNRe vs strain with and without pulse shaping (PS)

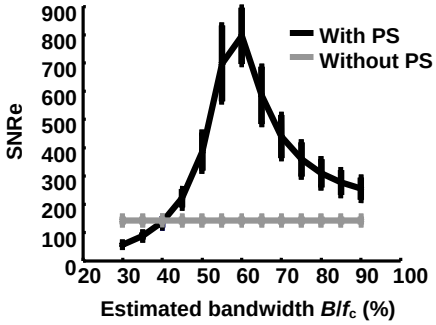


**Figure 2**: Effect on SNRe of an error in transducer bandwidth estimate $B$

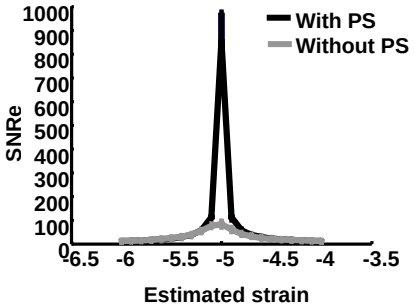


**Figure 3**: Effect on SNRe of an error in strain estimate ε (true strain $\varepsilon_0$=5%)

**Acknowledgements**: This project is supported in part by the National Cancer Institute (NCI) Program Project Grant no. P01-CA64957 to the University of Texas Medical School.

**References**:

[1] Bilgen M, Insana MF. Deformation models and correlation analysis in elastography. J Acoust Soc Am 99 (5), 3212-3224 (1996)
[2] Varghese T, Ophir J. Enhancement of echo-signal correlation in elastography using temporal stretching. IEEE Trans Ultrason Ferroelectr Freq Control 44(1), 173-180 (1997)

** indicates Presenter*

100 **SIGNAL-TO-NOISE RATIO UPPER-BOUND IN SHEAR STRAIN ELASTOGRAMS.**

*A Thitai Kumar[1,2]*, J Ophir[1,2], TA Krouskop[1,3].*
[1]The University of Texas Medical School, Houston, TX, USA;[2]University of Houston, Houston, TX, USA; [3]Baylor College of Medicine, Houston, TX, USA.

**Introduction:** There is only a minimal body of literature relating to images of the shear strains in soft tissues and soft tissue-like materials [1]. The shear strain induced upon the application of axial compression to an inhomogeneous system depends in part on the nature of the bonding between tissue components and their orientation with respect to the axis of normal compression. Therefore, shear strain elastograms (SSE) may provide additional information about the nature of the bonding between tissue components of interest that is not available in current normal strain elastograms. In order to understand the limitations of the SSE, we developed a theoretical upper bound on the signal-to-noise ratio ($SNR_{sse}$) and verified it using simulations and experiments.

**Methods:** Shear strain is estimated elastographically as shown in Equation (1) below.

$$\hat{\varepsilon}_{i,j} = \lim_{\Delta b \to 0, \Delta t \to 0} \frac{1}{2}\left[\frac{\tau^a_{i,j} - \tau^a_{i+1,j}}{\Delta b} + \frac{\tau^l_{i,j} - \tau^l_{i,j+1}}{\Delta t}\right] \qquad \text{Equation (1)}$$

$$\sigma^2_{\hat{\varepsilon}_{i,j}} = \left[\frac{\sigma^2\left(\tau^a_{i,j}\right)}{b\Delta b} + \frac{\sigma^2\left(\tau^l_{i,j}\right)}{T\Delta t}\right] \qquad \text{Equation (2)}$$

Where $\tau^a$ and $\tau^l$ represent the time delay estimate and positional shift estimate along axial and lateral directions respectively, and $\Delta t$ and $\Delta b$ are the shifts in the corresponding directions. The variance of this estimator can be obtained by treating $\tau^a$ and $\tau^l$ as uncorrelated random variables and assuming a linear covariance function for $\tau^a$ components and $\tau^l$ components. The lower bound on the variance is given by Equation (2) in terms of lower bound on axial and lateral delay estimates. The ratio between the applied shear strain and the lower bound on the variance yields SNRsse. Simulated SSE values were obtained from a 40mm x 40mm uniform finite element phantom after subjecting it through steps shown in Figure 1. SNRsse from resulting SSE are studied as a function of the applied shear strain (referred to as the shear strain filter, SSF). Experimental SSE obtained after subjecting a gelatin phantom through the steps shown in Figure 1 was used to create an experimental SSF.

**Results:** The results indicate that the signal-to-noise ratio of shear-strain elastograms improves with increasing shear strain (see Figure 2). It was also observed to improve with improvements in system parameters such as the sonographic signal-to-noise ratio ($SNR_s$), beamwidth, center frequency, and fractional bandwidth.

**Conclusions:** The trend predicted by the theoretical shear strain filter was verified using simulations and experiments and was found to be in reasonable agreement. An important conclusion is that a better quality SSE may be expected for a case where higher shear strains are induced compared to a case where smaller shear strains are induced, for a given axial compression.

**Acknowledgement:** Supported by NIH Program Project P01-CA64597-12 to the University of Texas.

**References:**

[1] Konofagou, E.E., Harrigan, T., and Ophir, J.: Shear strain estimation and lesion mobility assessment in elastography. Ultrasonics, 38, pp 400-404, 2000.

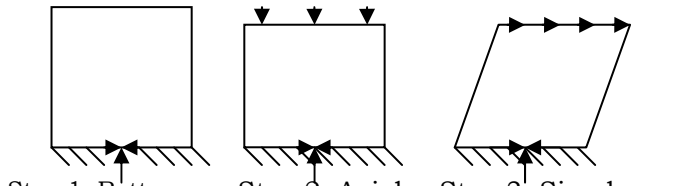


Figure1: Steps Involved in Applying Shear Strain

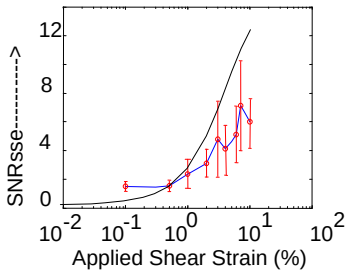


Figure 2: SSF from theory (solid) and simulation (-o-).

041 **REGULARIZATION FOR STRAIN MEASUREMENT AND SHEAR MODULUS RECONSTRUCTION.**

*Chikayoshi Sumi*[1]*.

[1]Sophia University, 7-1 Kioicho, Chiyodaku, Tokyo 102-8554, JAPAN.

**Aims:** We developed multidimensional cross-spectrum phase gradient method, multidimensional autocorrelation method and multidimensional Doppler method. Moreover, we are developing strain measurement-based shear modulus reconstruction methods. We previously reported the effectiveness of regularization for stabilizing these methods, i.e., strain (displacement) measurement method [1] and shear modulus reconstruction method [2]. In this report, we present the regularized results obtained on *in vivo* liver carcinoma which was treated by interstitial microwave coagulation therapy. As penalty terms, $L_2$-norm of target distribution, $L_2$-norm of gradient and the Laplacian of the target distribution are used.

**Methods:** Respective regularization parameter should be determined by echo SNR, correlation coefficient (peak value of cross-correlation function), and ultrasound parameters (frequency, bandwidth). One approach for determining the parameters is utilization of SNR of measured strain evaluated by using mean of strain and lower bound or upper bound of strain variance, e.g., Ziv Zakai Lower Bound (ZZLB) and Strain Filter etc. Thus, these regularization parameters are set at each position (non-uniformly). Furthermore, the regularization parameters for the $L_2$-norm gradient and the Laplacian can be set as different values in each direction of the partial derivative. These can also be evaluated by plural measurements at same positions or different positions [2]. In this report, at the beginning, the correlation coefficient is used to determine the parameters at each position (set at inverse proportional values).

**Results:** The volunteer was a 73-year-old female with carcinoma (diameter = 18mm) located in liver segment 6 [2]. A needle electrode was used having a diameter of 1.6mm [70W, 2.45GHz]. Treatment was carried out for 4 min under abdominal section. During treatment, the ROI was manually compressed with the transducer and echo data frames were successively acquired. The ROI B-mode image during treatment is shown in Figure 1a (7.5 MHz, 29.6mmH41.5mm). 2D cross-spectrum phase gradient method was used (a local region, 0.8mmH1.4mm). The cutoff frequency of the differential filter was 1.02mm$^{-1}$. The reference line was set at depth of 5.7mm (in the liver; value, 1.0) where no blood vessels could be detected.

The non-regularized, and non-uniformly regularized axial strain images are shown in linear gray scale (Figures 1b and 1c), while uniformly regularized, and non-uniformly regularized shear modulus images are in log gray scales where a bright region indicates a relatively soft region and vice versa (Figures 2a and 2b).

The strain images 1c and shear modulus images 2a and 2b are sufficiently regularized ones because peak values of local cross-correlation functions evaluated at the heated region remained low during phase matching (Figure 3: a, before; b, after matching). In other words, measurement accuracy of strains at heated region was not improved by phase matching and remained low although regularization stabilized the measurement. The decorrelation is mainly caused by changes of reflectivity of ultrasound during echo data acquisition (due to generation/fade of bubbles, flow of bubbles, degeneration, congestion etc.). Thus, the measured strain images do not allow effective evaluation of the spatial and temporal changes of the shear modulus. However, from the regularized shear modulus images, particularly from the non-uniformly regularized image 2b, we were able to stably confirm that during treatment the tumor became soft, while a marginal region of several millimeters became considerably stiff.

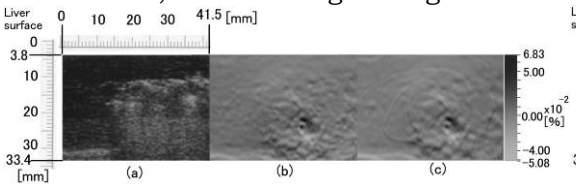


Figure 1

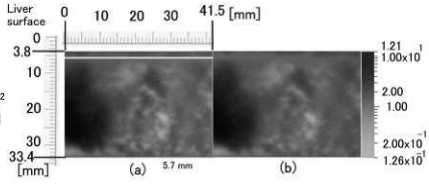


Figure 2

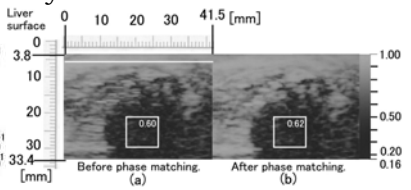


Figure 3

**Conclusions:** Although regularization is effective to stabilize the strain measurement, it does not always improve measurement accuracy, particularly, when correlation coefficients are low in large regions. On the other hand, stabilization by regularization is significantly effective when incorporating information about stress distribution, i.e. when reconstructing shear modulus.

**References:**

[1] Sumi, "Stabilization of tissue displacement vector measurement utilizing ultrasonic cross-spectrum," Technical report of the Japan Society of Ultrasonics in Medicine, **101**, no. 4, pp. 31-41, Dec 2001.

[2] Sumi, "Usefulness of ultrasonic strain measurement-based shear modulus reconstruction for diagnosis and thermal treatment," IEEE Trans UFFC, Oct 2005 (in press).

** indicates Presenter*

107 **2D AND 3D ELASTICITY AND VISCOSITY IMAGING USING NEW RECONSTRUCTION STRATEGIES IN DYNAMIC ELASTOGRAPHY.**

*Jeremy Bercoff[1], Ralph Sinkus[1]*, Mickael Tanter[1], Mathias Fink[1].*
[1]Laboratoire Ondes et Acoustique, ESPCI, 10 rue Vauquelin, 75005, Paris, FRANCE.

**Aims:** Observation of shear-wave propagation in soft tissue is of great interest for the study of tissue viscoelastic properties. Such waves can be generated either by an external vibrator or by an acoustic radiation force and imaged by ultrasound based or MRI techniques. In this work, we investigated two different vibrations modes: monochromatic and transient excitations. New adapted local inversion algorithms are proposed to estimate viscous and elastic parameters of the medium and meet requirements of each mode.

**Methods:** Key parameters influencing the robustness of the algorithms are carefully studied and solutions are proposed. A strategy for decoupling compressional and shear waves by applying the curl operator is investigated. This strategy is shown to be crucial for a correct and quantitative estimation of those parameters in the monochromatic case. In the transient case, it suppresses mode conversion artifacts at lesion boundaries and enhances elasticity and viscosity estimations. Usually assuming local elastic homogeneity, we propose in addition generalized inversion algorithms reconstructing viscoelastic parameters heterogeneously.

**Results:** Studies are validated with 3D finite differences simulations then tested *in vitro* and *in vivo* on female breast using MR based and ultrasound based elastography (the Supersonic Shear imaging technique presented in previous works). Clinical results on carcinomas demonstrate a significant increase in quality and robustness of the developed algorithms compared to classical ones.

097 **AN ANALYTICAL MODEL FOR 3D LONGITUDINAL WAVE PROPAGATION IN A VISCOELASTIC CYLINDER: APPLICATIONS TO MR ELASTOGRAPHY.**

*Geert J. Streekstra[1]*, P. van Horssen[1], D.M.J. van den Berg[1], J.G.G. Dobbe[2], J. Strackee[1].*
[1]Medical Physics, [2]Medical Technological Development Departments, Academic Medical Center, Amsterdam, The NETHERLANDS.

**Introduction:** Viscoelastic properties of tissue are potential indicators for disease, specifically for cancer detection. Accurate measurement of *in vivo* tissue viscoelasticity may help to distinguish between benign and malignant tumors. A modality to measure tissue viscoelasticity is MR Elastography where a 3D displacement field is acquired at several phases of steady state oscillatory motion. Reconstruction of shear viscoelastic properties from the displacement field is established by local inversion of the partial differential equation describing the mechanical wave propagation in tissue.

In MR Elastography equipment, a longitudinal mode of wave excitation is commonly used to allow wave propagation deep into the tissue. Mode conversion due to the presence of boundaries and local inhomogeneities leads to the presence of both dilatational and transverse waves. The transverse wave component is used for the reconstruction of local shear viscoelasticity [1].

The nature of the wave pattern in tissue is dependent on the wave excitation protocol (e.g. longitudinal vs. transverse excitation). We present an analytical model for wave propagation in a viscoelastic cylinder that mimics the principles of excitation and wave propagation in a MR Elastography setting.

**Methods:** In a cylinder, only specific wave patterns (modes) can be present. We consider longitudinal modes that are characterized by a wave number $k_0$ corresponding to longitudinal wave propagation along the cylinder axis (z-axis). In a viscoelastic cylinder, $k_0$ will in general be a complex number. This implies that damping of the modes occur along the cylinder axis.

We developed a method to obtain the modes (i.e. $k_0$ values) present in a viscoelastic cylinder with radius $R$ and complex shear stiffness $\mu=\mu_{re}+i\mu_{im}$. We combined multiple modes to arrive at a 3D wave pattern in the cylinder corresponding to longitudinal excitation at one end of the cylinder.

**Results:** To illustrate the usefulness of our model, we estimated the wave numbers ($k_0$) for a cylinder with a radius of 10cm. The viscoelastic properties are those of kidney at a frequency of 66 Hz [2].

The results reveal that multiple modes are present in a cylinder with viscoelastic properties. Moreover, the $k_0$ values are complex indicating a mode dependent wavelength and damping of the modes (Figure 1). The lowest mode has an extremely large wavelength (in the order of 10km) which corresponds to the "DC component" as observed in MR Elastography image sequences [1].

**Conclusions:** We developed an analytical model of wave propagation in a cylinder that reflects the mechanism of wave propagation in dynamic elastography. The model might be useful to gain insight into the relationship between the wave excitation protocol and the characteristics of the waves or serve as a reference for numerical simulations.

**References:**

[1] Sinkus R, Tanter M, Catheline S, Lorenzen J, Kuhl C, Sondermann E, Fink M. Imaging anisotropic and viscous properties of breast tissue by magnetic resonance-elastography. Magnetic Resonance in Medicine 53 (2): 372-387, 2005.
[2] Nasseri S, Bilston LE, Phan-Thien N. Viscoelastic properties of pig kidney in shear, experimental results and modelling. Rheologica Acta 41 (1-2): 180-192, 2002.

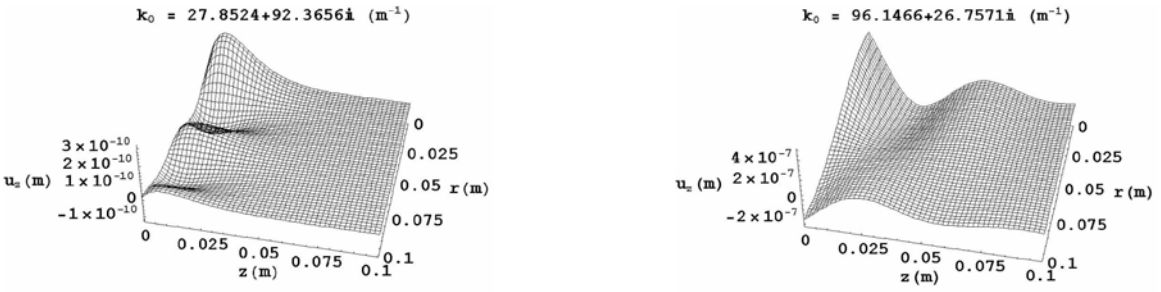


(a) (b)

Figure 1: Wave pattern components in the axis direction (z-axis) of a cylinder with 0.1m radius. (a) mode with large wavelength and high attenuation. (b) mode with small wavelength and low attenuation.

** indicates Presenter*

103 **A BAYESIAN IMAGE RECONSTRUCTION APPROACH FOR MODEL-BASED ELASTOGRAPHY.**

*Marvin M. Doyley[1,3]*, Seshadri Srinivasan[2], Eugen Dimidenko[1], Nirmal Soni[3], Jonathan Ophir[2].*
[1]Dartmouth Medical School, Hanover, NH 03755, USA; [2]Ultrasonics Laboratory, University of Texas Medical School, Houston, TX 77030, USA; [3]Thayer School of Engineering, Dartmouth College, Hanover, NH 03755, USA.

**Aims:** The primary objective of this work is to corroborate the hypothesis that including *a priori* information regarding the mechanical property of the underlying tissue structures and displacement measurement uncertainty will render the inverse elasticity problem a well-posed problem.

**Background:** Quasi-static elastography is an emerging ultrasonic imaging technique that depicts tissue elasticity by visualizing externally or internally induced internal tissue strain. Despite its simplicity and robustness, quasi-static elastographic imaging technique currently endures mechanical artifacts and incomplete contrast recovery when strain images are interpreted as relative stiffness images based on the premise of stress uniformity – an assumption that is valid only for very special cases. Consequently, we are exploring the feasibility of developing quasi-static elastography within the framework of solving the inverse problem – a strategy that holds great promise for improving the elastographic contrast discrimination and contrast recovery. In general, inverse problems are difficult to solve because they are usually ill posed in the original sense of Hadamard, consequently, their solutions are typically non-unique, and small degree of measurement noise often produces erroneous results. To overcome these limitations we have developed a novel inverse reconstruction technique that incorporates *a priori* information procured by employing standard strain imaging methodology in the image reconstruction process via the Bayesian framework.

**Methods:** To evaluate the effect of decorrelation noise and lesion size on the quality of modulus elastograms computed with the Bayesian inversion approach (BA) relative to those computed using three other estimation criteria (the standard least squares estimation criterion (LS), the weighted least squares method (WLS) and the Tikhonov method), we conducted elastographic imaging experiments on elastically inhomogeneous gelatin phantoms. Three performance metrics were employed: contrast recovery, contrast discrimination and spatial resolution.

**Results**. Figure 1 shows representative examples of strain elastograms obtained when elastographic imaging is performed using applied strains of 1.25%, 2% and 4%. The inclusion is discernible in the elastograms at the correct location; however, image quality is compromised noticeably with larger internal strain. In Figure 2, the contrast-to-noise ratio ($CNR_e$) and contrast-transfer efficiency ($CTE_e$) performance metrics are plotted as a function of the percentage of applied strain. The quality of the modulus elastograms decreased significantly when the applied strain exceeded 2%. However, it is apparent from Figure 2a that modulus elastograms computed by employing the Bayesian framework were more tolerant to structural decorrelation noise relative to those computed by employing the standard least squares, the weighted least squares and the Tikhonov estimations criteria. Interestingly, the influence of structural decorrelation noise on our ability to completely recover modulus contrast was small when image reconstruction was performed using the Bayesian reconstruction approach.

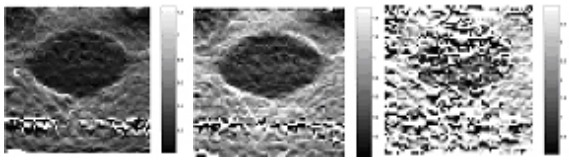

Figure 1: Strain elastograms obtained from a phantom containiing a single 20mm diameter inclusion when elastographic imaging was performed using an applied strain of 1.25%, 2% and 4% respectively.

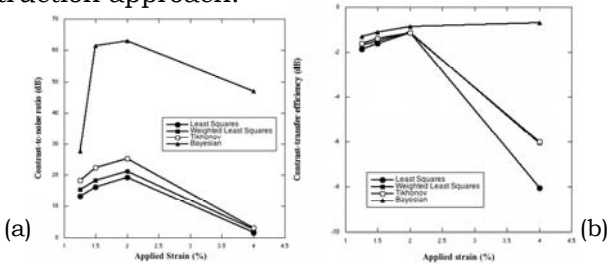


Figure 2: (a) $CNR_e$ and (b) $CTE_e$ performance metrics computed from elastograms reconstructed using four estimation criteria: standard least squares, weighted least squares, Tikhonov method and Bayesian approach.

**Conclusion:** The preliminary results reported in this abstract demonstrate unequivocally that incorporating additional *a priori* information in the modulus image reconstruction process via the Bayesian estimation criterion will render the inverse problem a well-posed problem, thus bolstering its performance particularly when structural decorrelation noise is significant.

077 **IMAGING ANISOTROPIC ELASTICITY USING SUPERSONIC RADIATION FORCE EXCITATION.**

*Jeong-Rock Yoon[1]*, Daniel Renzi[2], Joyce R. McLaughlin[2].*
[1]Clemson University, Clemson, SC 29634-0975, USA; [2]Rensselaer Polytechnic Institute, Troy, NY 12180, USA.

**Aims:** It is important to consider anisotropic tissue models, since some tumors exhibit anisotropy and the structure of fiber orientation may have a correlation with the malignancy of tumor. Based on the multiple supersonic radiation force excitation, we aim to recover two shear moduli and fiber structures in incompressible transversely isotropic tissue model. Our potential application is to distinguish malignancy of tumor.

**Background:** For the isotropic tissue model, a series of uniqueness results for the transient elastography inverse problem have been presented, and a fast stable algorithm to reconstruct the shear stiffness based on arrival time has been suggested [1, 2]. We want to extend this arrival time technique to anisotropic media.

**Methods:** We can generate line sources moving radiation force sources [3]. Observing the SH-polarized shear wave propagation by ultrafast ultrasound scanner [3], we can estimate the arrival times [1, 2]. Assuming the tissue model as incompressible transversely isotropic medium, we derive a nonlinear arrival time equation that relates two shear moduli and fiber orientation with the estimated arrival times. This equation tells that we need at least four measurements, and we show in most cases four measurements are enough to reconstruct the SH-related anisotropic properties.

**Results:** Using four measurements of the SH-wave arrival times (which are generated by supersonic radiation force excitation), we can establish a fourth order polynomial. Solving this polynomial we can find one of the shear moduli and derive an explicit formula for the other shear modulus and fiber orientation. Simulation results are also presented.

**Conclusions:** We show that, in most cases, four SH-wave measurements are enough to reconstruct two shear moduli and fiber direction in incompressible transversely isotropic tissue model. We hope this algorithm can be used to distinguish the malignancy of tumors. In order to recover Young's moduli information (which cannot be recovered in current SH-wave based algorithm), we should look at QS-wave. We are extending our method to QS-wave.

**References:**

[1] J. R. McLaughlin, J. R. Yoon, Unique identifiability of elastic parameters from time dependent interior displacement measurement, Inverse Problems, 20(1):25--45, 2004.
[2] L. Ji, J. R. McLaughlin, D. Renzi, J. R. Yoon, Interior elastodynamics inverse problems: shear wave speed reconstruction in transient elastography, Inverse Problems, 19(6):S1--S29, 2003.
[3] J. Bercoff, M. Tanter, M. Fink, Supersonic shear imaging: a new technique for soft tissue elasticity mapping, IEEE Trans. on Ultra., Ferro., and Freq. Cont., 61(4)396-409, 2004.

113 **FAST INVERSION TECHNIQUES FOR 3D SONOELASTICITY IMAGING.**

*B.B. Guzina[1]*, A.I. Madyarov[1], I. Chikichev[1].*
[1]Univiersity of Minnesota, 500 Pillsbury Drive S.E., Minneapolis, MN, USA.

**Aims:** This paper highlights three recent inversion algorithms for 3D sonoelasticity imaging. The first method, based on non-linear minimization, is shown to perform well provided that the initial "guess" (in terms of lesion geometry and characteristics) is sufficiently close to the true situation. To deal with the latter restriction, two alternative *sampling* inversion algorithms have been proposed that are both computationally effective and robust as they nullify the need for initial guess.

**Background:** Studies have shown that the resolution of elasticity imaging could be enhanced by following the strain or velocity images with a solution to the inverse elasticity problem, e.g. [1]. An efficient and robust solution to the latter ill-posed problem is, however, very much an open question, especially in three dimensions.

**Methods:** Boundary-Only Imaging (BOI): For the 3D sonoelasticity imaging problem, a technique was recently proposed in [2] on the basis of: i) boundary element method, and ii) minimization of the misfit between experiment and elastodynamic theory for a trial obstacle geometry. The key advantage of this approach rests on the fact that BOI avoids costly volume discretization often associated with elastic tomography. Figure 1a illustrates the iterative BOI process of delineating a soft lesion, hidden in a homogeneous tissue ($z$>0), from synthetic measurements.

Topological Derivative Approach (TDA): One recent approach to sonoelastic imaging [3] that does not require global minimization and thus eliminates the need for initial guess is based on the concept of *topological derivative*, originally developed for structural shape optimization [4]. The topological derivative, $T$, furnishes information about the variation of a given cost functional when an infinitesimal lesion is nucleated at a sampling (i.e. trial) point $\boldsymbol{z}$ in the reference (background) tissue. Theory suggests that a finite lesion and its stiffness can both be identified by computing $T(\boldsymbol{z})$ over the prescribed grid of internal sampling points and plotting the resulting $T$-distribution or its associated ("optimal") shear modulus, see Figure 1b.

Linear Sampling Method (LSM): As an alternative to TDA, an effort is undertaken to generate elastograms equivalent to those in Figure 1b by means of LSM. The latter imaging technique, although being the subject of mounting attention in far-field acoustics and electromagnetism (e.g. [5]) has only recently been extended to near-field elastodynamics [6]. Although stemming from a distinct mathematical platform, the elastodynamic LSM is shown to generate images on a point-sampling basis similar to TDA, i.e. without the need for initial guess.

**Results:**

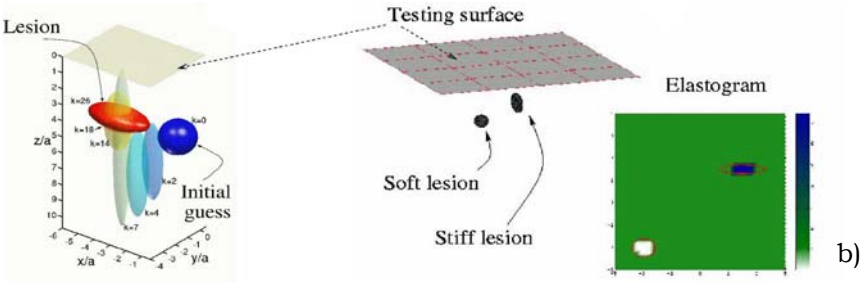


Figure 1: a) Evolution of a trial lesion during BOI minimization (k = iteration number);
b) Shear modulus distribution (horizontal section) obtained using TDA: blue – high modulus, white – low modulus.

**Conclusions:** This paper summarizes three alterative inversion algorithms (BOI, TDA and LSM) for 3D elasticity imaging. The latter two techniques, commonly termed the *sampling methods*, appear to be especially tractable for medical applications owing to their robustness and computational efficiency. For comparative purposes, all three methods are designed to interpret *common* experimental data sets.

**Acknowledgements:** Support of NSF through grant CMS-324348 to B. Guzina is kindly acknowledged.

**References:**

[1] M.M. Doyley, S. Srinivasan, S. Pendergrass, Z. Whu, J. Ophir (2005). *Ultrasnd. Med. Biol.*, **6**, 787-802.
[2] B.B. Guzina, S.F. Nintcheu, M. Bonnet (2003). *Int. J. Solids Struct.*, **40**, 1505-1523.
[3] B.B. Guzina, M. Bonnet (2003). *Quart. J. Mech. Appl. Math.*, **20**, 161-179.
[4] H.A. Eschenauer, V.V. Kobelev, A. Schumacher (1994). *Struct. Optim.*, **8**, 42-51.
[5] D. Colton, J. Coyle and P. Monk (2000). *SIAM Rev.*, **42**, 369-414.
[6] S.F. Nintcheu, B.B. Guzina (2004). *Inv. Problems*, **20**, 713-736.

004 **ULTRASOUND ELASTICITY IMAGING FOR AGING DEEP VENOUS THROMBOSIS IN HUMANS.**

*JM Rubin[1]*, H Xie[1], K Kim[1], WF Weitzel[1], SY Emelianov[2], S Aglyamov[2], TW Wakefield[1], M O'Donnell[1].*
[1]University of Michigan, Ann Arbor, MI, USA; [2]University of Texas at Austin, Austin, TX, USA.

**Aims**: To study the usefulness of ultrasound elasticity imaging for aging deep venous thrombosis (DVT).

**Background:** It is well known that DVTs harden as they age, and the treatment of DVT depends on the age of the thrombi. Given this fact, ultrasound elasticity imaging should be an excellent method to age DVT, and animal studies have confirmed this fact [1, 2]. However, except for case reports [3], the efficacy of elasticity imaging for aging DVT in humans has yet to be shown in a controlled large study.

**Methods:** 57 total DVT patients, 27 patients with chronic DVT, and 30 with acute DVT were evaluated. Chronic DVT subjects had no symptoms and had known thrombi for a year or greater through follow-up examinations on a Greenfield filter protocol. Acute DVT patients had duplex venous ultrasound proven calf or thigh DVTs, and had symptoms or signs of DVT for two weeks or less without a prior history of DVT. Scanning was performed using a 5 MHz linear array scanhead on a Siemens Elegra (Siemens Ultrasound, Issaquah, WA) ultrasound scanner. We performed continuous, freehand external deformation of each thrombus using the scanhead. Strain estimates for the deformation of each thrombus were estimated using a 2D phase-sensitive speckle tracking algorithm. Intrathrombus strains were normalized to the average strain between the skin surface and the back wall of the involved vein. Statistical analyses were performed using a two-tailed T-test assuming unequal variances and ROC analysis.

**Results:** Seven patients were excluded from analysis. Three had acute and four had chronic thrombi. Five were excluded because the overall average deformation was too small (<1%), and two additional chronic subjects were excluded because their thrombi were too small to track, i.e. the thrombi could not be located during retrospective analysis. For the remaining 50 patients, the difference in the mean strains between those with chronic and those with acute DVTs was highly significant ($p < 10^{-9}$). The area under the ROC curve (Az = 0.977 ± 0.018 (std. error)) suggests that the acute and chronic DVT patient populations are well separated.

**Conclusion:** Given the above, it is apparent that ultrasound elasticity imaging can discriminate acute from chronic DVT in humans. This discrimination is important, because the treatment of DVT depends on the thrombus age. The major limitations with the method appear to be small strains and small thrombi that could not be detected in retrospect. Both of these issues would disappear if strains were displayed in realtime during the procedure. Given that realtime strain imaging may be a reality, we believe that elasticity imaging for aging DVT should be close to clinical implementation.

**Acknowledgments:** NIH Grants HL68658, HL67647, HL47401.

**References:**

[1] Emelianov SY, Chen X, O'Donnell M, Knipp B, Myers D, Wakefield TW, Rubin JM. Triplex ultrasound: elasticity imaging to age deep venous thrombosis. UMB 2002;28:757-767.
[2] Xie H, Kim K, Aglyamov SR, Emelianov SY, Chen X, O'Donnell M, Weitzel WF, Wrobleski SK, Myers DD, Wakefield TW, Rubin JM. Staging deep venous thrombosis using ultrasound elasticity imaging: animal model. Ultra Med Biol 2004;30:1385-1396.
[3] Rubin JM, Aglymov SR, Wakefield TW, O'Donnell M, Emelianov SY. Clinical application of ultrasound elasticity imaging for aging DVT - Preliminary Findings. J Ultrasound Med 2003; 22: 443-448.

030 **A NOVEL PERFORMANCE DESCRIPTOR FOR ULTRASONIC STRAIN IMAGING: A PRELIMINARY STUDY.**

*J Jiang[1]*, TJ Hall[1], AM Sommer[1].*
[1]Medical Physics Department, University of Wisconsin-Madison, Madison, WI, USA.

**Background and Aims:** The aim of this study is to differentiate 'good' from 'poor' strain images with a quantitative measure for applications where the 'right answer' is unknown (for example, in vivo tissues). In addition, the strain image quality measure can be used for visual feedback during scanning to assist training and scanning technique optimization. This will lead to improvements in the diagnostic performance of ultrasonic strain imaging.

**Methods:** The proposed performance measure is based on two parameters: accuracy of motion tracking and consistency among consecutive strain fields. The accuracy of motion tracking assesses the reliability of strain images. The consistency among consecutive strain images, in theory, directly reveals the signal quality in strain images if strain signal is coherent but noise is incoherent among successive strain images. A single summary descriptor was obtained by combining these two parameters. Compared to the methods available in the literature (e.g. strain filter [1]), the proposed method has several advantages: (1) no assumptions regarding the signals, underlying motion, or motion tracking algorithms are needed; (2) performance of strain imaging can be assessed for individual cases accurately; (3) the final performance descriptor, a scalar value between zero and one, is quantitative and easy to use. The proposed method has been successfully integrated into our existing program for strain image formation [2].

**Results:** Experiments with tissue-mimicking phantoms and in vivo breast tissue data [3] are reported to demonstrate the proposed method. Preliminary results suggest that the measured performance values matched well with a limited human observer study (three trained physicists, 200 strain images acquired from fibroadenoma and invasive ductal carcinoma). The performance values as a function of frame-average axial strain estimated from in vivo breast data indicated that there is an 'optimal' deformation range (0.8~1.5% frame average strain) under which high quality strain images were likely formed, consistent with previous work.

**Conclusions:** Our results suggested the proposed method can be used to assess the quality of strain images with full automation and the measured performance is consistent with visual perception.

**Acknowledgements:** We are grateful for the support from the USAMRMC (DAMD17-00-1-0596), the NIH (R01-CA100373), and the University of Wisconsin. We are also grateful to colleagues at the Mayo Clinic in Rochester, MN, USA, and the Charing Cross Hospital in London, England, UK for providing some of the data used in this study.

**References:**

[1] T. Varghese and J. Ophir, "Theoretical framework for performance characterization of elastography: the strain filter," IEEE Transactions on UFFC, vol. 44, pp. 164-172, 1997.
[2] Y. Zhu and T. J. Hall, "A modified block matching method for real-time freehand strain imaging," Ultrasonic Imaging, vol. 24, pp. 161-76, 2002.
[3] T. J. Hall, Y. Zhu, and C. S. Spalding, "In vivo real-time freehand palpation imaging," Ultrasound in Medicine & Biology, vol. 29, pp. 427-35, 2003.

111 **A COMPARISON OF REAL-TIME AND POST-PROCESSED ELASTOGRAPHY WITH SURGICAL FINDINGS FOR INTRA-OPERATIVE DETECTION OF BRAIN TUMOURS.**

*A Chakraborty[1]*, JC Bamber[2], NL Dorward[1].*
[1]Department of Neurosurgery, Royal Free Hospital, London, England, UK; [2]Department of Physics, Institute of Cancer Research, Sutton, Surrey, SM2 5PT, England, UK.

**Aims:** We present a study comparing elastographic appearances of brain tumours *in vivo*, produced using both a commercial real-time system and a freehand off-line system, with surgical findings and with appearances on MRI. Elastography was applied to the brain intra-operatively during tumour resection.

**Background:** Detection of the brain tumour interface is essential when resecting brain tumours. Elastography may assist in detecting this interface, but the majority of elastography techniques require off-line processing. For elastography to be useful intra-operatively, images would have to be produced between the time the skull has been removed and the start of tumour removal. Hence, a real-time ultrasound elastography system would be advantageous.

**Methods:** 20 patients were recruited into this study. The Acuvix XQ (Medison, Korea) with the Elastoscan® protocol was used for real-time scanning. The Acuson 128XP scanner with access to RF data was used for generation of off-line elastograms, employing a least squares strain estimator applied to displacement fields obtained using an incremental 2D correlation-based tracking algorithm, as described by Doyley et al [1]. Pre-operative MRI scans were re-sampled in the same plane as the off-line elastograms, employing a StealthStation™ optical tracking system to achieve the required registration between ultrasound and MRI data. Real-time elastography sequences were acquired in approximately the same plane, as best as could be judged visually. Assessment of elastographic contrast and structure was by visual inspection of the images, which were compared with surgical findings that included the relative stiffness of brain compared to tumour and the mechanical properties of the brain tumour interface.

**Results:** It was possible to determine the difference in strain between brain and tumour using both real-time and off-line elastography. Internal tumour structure, such as elastographic heterogeneity, was also seen in both, and correlated with MRI appearances. For real-time, this assessment is an interactive process, involving adjustment of palpation speed and amplitude whilst studying the structures apparent in different frames of the real-time sequence. Areas of high strain correlated with areas of slip using both methods.

**Conclusions:** Real-time elastography can be used intra-operatively when resecting brain tumours. The images produced provide basic strain information analogous to strain information produced using our off-line system, and hold potential for future use in assisting tumour resection.

**References:**

[1] Doyley MM, Bamber JC, Fuechsel F, Bush NL (2001). Ultrasound Med Biol; 27: 1347-1357.

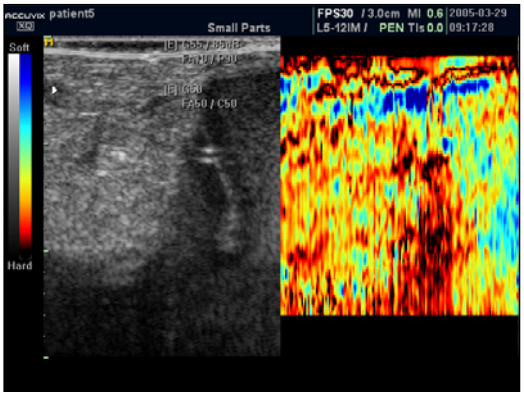


Figure 1: Single frame from a sequence showing a B-scan and associated real-time elastogram. The tumour is stiffer than surrounding brain. There is an area of brain that is stiffer than surrounding brain below the sulcus. It is likely that correlation is poor in this area as slip is occurring above.

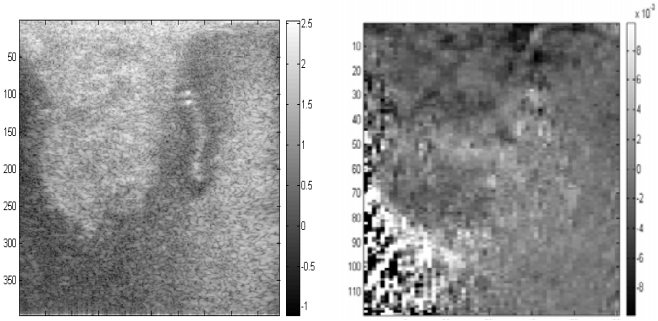

Figure 2: B-mode and off-line elastogram. Tumour has similar or lower strain compared to brain. The strain contrast in the area below the sulcus is less marked than for the real-time image. At surgery a well-developed brain tumour interface was observed, with tumour of a similar stiffness to brain.

* *indicates Presenter*

051 **SOFT TISSUE BIOMECHANCIAL BEHAVIOR DURING ROBOTIC ACUPUNCTURE IN LOW BACK PAIN USING ULTRASOUND ELASTICITY IMAGING.**

*Helene M. Langevin[1]*, Elisa E Konofagou[2], Junru Wu[3], James R. Fox[4] and James C. Iatridis[5].*
[1]Neurology, [3]Physics, [4]Orthopaedics and [5]Engineering Departments, University of Vermont, Burlington, VT, USA; [2]Department of Radiology, Columbia University, New York, NY, USA.

**Aims:** The goal of this study is to examine tissue behavior during acupuncture in the lower back and legs in subjects with Low Back Pain (LBP) compared with subjects without LBP (No-LBP). We hypothesize that needle force and tissue displacement patterns are abnormal in LBP and that these abnormalities are localized to specific locations as predicted by traditional acupuncture theory.

**Background**: The mechanisms of both acupuncture and low back pain are poorly understood. We have previously shown that computer-controlled robotic acupuncture can be successfully used in combination with ultrasound elasticity imaging to quantify soft tissue biomechanical behavior during acupuncture needling [1]. Soft tissue (connective tissue and muscle) pathological abnormalities including fibrosis, atrophy and inflammation may contribute to the pathophysiology of LBP and may cause biomechanical abnormalities that can be detected using these techniques. Thus ultrasound elasticity imaging may reveal important information on both the pathophysiology of LBP and the mechanism of acupuncture.

**Methods:** Ten subjects (5 with LBP and 5 with No-LBP) were tested at the time of abstract submission. We anticipate testing a further 10 subjects by the fall of 2005. All points tested were non-acupuncture points either on acupuncture meridians or off meridians. Each subject received robotic acupuncture needling at four locations: one back point (back Meridian) bilaterally, one point on the right leg (leg Meridian) and one point on the left leg (leg Non-Meridian). The needling procedure consisting of needle insertion at an angle of 20º relative to the ultrasound transducer and to a depth of 0.5 mm beyond the superficial border of muscle (determined by ultrasound prior to needling). After insertion, the needle was rotated (8 uni-directional revolutions at 8 revs-sec) followed by five oscillations (up and down movement) of the needle with an amplitude of 2 mm and at a rate of 5 mm/sec. Needle torque and force were measured during rotation and oscillation respectively. Tissue B-scan ultrasonic imaging was performed with a SystemFive (GE-Vingmed) scanner equipped with a linear array transducer at a frequency of 6.9 MHz. A five second ultrasound cine-loop was acquired during the oscillation sequence at a rate of 13.2 frames/sec. Tissue displacement and strain are estimated using cross-correlation techniques [2].

**Results:** In the subjects tested to date, mean±SE needle torque in the back was 0.23 ± 0.03 mN-m for LBP compared with 0.33 ± 0.06 mN-m for No-LBP. Mean needle force decay rate was 24.2 ± 4.4% over 5 seconds for LBP compared with 10.0 ± 2.3% for No-LBP. Mean±SE tissue displacement in the back was 23.3±2.2μm for LBP vs. 25.2±3.2μm for No-LBP. In the leg, displacement for LBP and No-LBP respectively were 25.7±7.6μm vs. 35.5±7.4μm at meridians and 27.6±2.1μm vs. 28.7±4.1μm at non-meridians. These results suggest that, in LBP, the tissues did not wind as tightly around the needle during rotation (decreased torque) and were slipping past the needle during oscillation (decreased tissue displacement and increased force decay). Preliminary analysis of these data using a mathematical model treating tissue zones (subcutaneous, perimuscular, muscle) as one-dimensional simple harmonic oscillators indicated increased stiffness, decreased damping and decreased needle-tissue coupling time constant in LBP, which could result from abnormal tissue composition and/or architecture. The preliminary observation of a difference between LBP and No-LBP at leg Meridians but not at Non-Meridians also suggests that the abnormal tissue behavior in LBP is not generalized, but rather may be restricted to specific locations.

**Conclusion:** These preliminary results suggest that soft tissue abnormalities may be detectable in LBP using a combination of robotic acupuncture and ultrasound elasticity imaging. These techniques thus may provide biological measurements that could 1) open up a new approach to understanding the mechanisms of both acupuncture and LBP and 2) be used as objective outcome measures in clinical trials.

**Acknowledgements:** Funded by the National Center for Complementary and Alternative Medicine.

**References:**

[1] Langevin HM, Konofagou EE, Badger GJ, Churchill DL, Fox JR, Ophir J, and Garra BS. Tissue displacements during acupuncture using ultrasound elastography techniques. *Ultrasound in Medicine and Biology* 30: 1173-1183, 2004.

[2] Ophir J, Cespedes I, Ponnekanti H, Yazdi Y, and Li X. Elastography: a quantitative method for imaging the elasticity of biological tissues. *Ultrason Imaging* 13: 111-134, 1991.

110 **REALTIME SONOELASTOGRAPHY OF 156 BREAST LESIONS IN A PROSPECTIVE CLINICAL SETTING.**

*S. Weber[1], S. Wojcinski[1], K. Ertan[1], K. Remberger[2], U. Stein[2], R. Ohlinger[3], A. Thomas[4], W. Schmidt[1].*
[1]Department of Gynecology and Obstetrics, [2]Institute for Pathology, University of Saarland, Homburg/Saar, GERMANY; [3]Department of Gynecology and Obstetrics, Ernst-Moritz-Arndt-University, Greifswald, GERMANY; [4]Department of Gynecology and Obstetrics, Charité – CCM, University Berlin, Berlin, GERMANY.

**Aims:** Ongoing technical progress has increased the accuracy of imaging in ultrasound mammography. Using a HITACHI EUB-L54M (50mm, 13-6MHz) and the HITACHI EUB-L53L (92mm, 10-5MHz) transducer, different criteria of dignity can be evaluated for validity. Some diseases, including cancer, can lead to a change of tissue hardness. Therefore, compressibility of a lesion can be used as a criterion. Real-time elasticity imaging is a precise ultrasound technique that can easily be performed with conventional ultrasound probes. Sonoelastography may provide more accurate discrimination of cancers from benign masses because it enables differences in tissue hardness to be detected.

**Methods:** Over a period of 6 months, 156 breast tumors were examined using sonography by two independent examiners. The study was comprised of lesions detected either by mammography, ultrasound or manual palpation. An elastography score consisting of 5 grades has been proposed for the differential diagnosis of breast masses. This elastography score was determined and all images and videos were digitally archived and reviewed by a second examiner without having any other information about the patients. Finally, a biopsy was taken, and the data were then analyzed by previously defined criteria. Diagnostic validity was quantified by means of sensitivity, specificity, positive and negative predictive value, as well as the ODDS-ratio.

**Results:** In total, 135 patients with 156 breast lesions participated in our study. Their mean age was 56 years (16-93 years). 75% of the patients were postmenopausal. The 156 lesions in these patients required biopsy either due to the mammographic, sonographic or clinical appearance. Pathological examination of the material led to the diagnosis of 67 malignant tumors (5 cases of ductal carcinoma *in situ* [DCIS], 2 cases of lobular carcinoma *in situ* [LCIS] and 60 cases of invasive carcinoma) and 89 benign diseases (32 mastopathic lesions, 18 fibroadenoma, 18 cysts, and 21 other findings – fat tissue necrosis, lymph nodes, scars, papilloma, mastitis). A higher elastography score was more frequently associated with malignant tumors. Using the L54 probe SonoElastography as a single method showed only a sensitivity of 64% (CI: 50%-77%) and a specificity of 89% (CI: 83%-95%). The US-BI-RADS classification had a sensitivity of 94% (95% CI: 91%-97%) and a specificity of 99% (CI: 96%-100%). Regarding only those lesions which were difficult to classify in B-mode sonography and therefore were assigned US-BI-RADS 3 or 4, there was no significant advantage in adding SonoElastography as the sensitivity was 55% for the US-BI-RADS 3 lesions and 67% for the US-BI-RADS 4 lesions compared with the overall sensitivity of 64% for SonoElastography.

**Conclusions:** The accuracy of SonoElastography was dependent on the histological subtype of the lesion. As known from pathological examinations, ductal carcinoma, often is the less lobular carcinoma, shows a desmoplastic stroma reaction, a dense cellular reaction with highly cross linked collagenous fibers. The more distinctive this reaction is, the harder the lesion gets. That proposes better results in SonoElastography for ductal carcinoma. This is represented by a higher specificity of 82% for ductal carcinoma, 100% for mixed type ductal/lobular carcinoma versus 64% for all tumors.

075 **NORMAL AND SHEAR ELASTOGRAPHY OF SKIN UNDER SURFACE EXTENSIVE LOADING.**

*Louise Coutts[1], Jeffrey C. Bamber[1]*, Naomi R. Miller[1].*
[1]Institute of Cancer Research, 15 Cotswold Road, Sutton, Surrey, SM2 5NG, England, UK.

**Aims:** Our aim was to evaluate the ability to use ultrasound to produce high resolution *in vivo* images of the stiffness distribution within the skin and investigate the effects of surface extensive loading, of varying direction, on the normal and shear strain generated within normal skin and the underlying tissue layers.

**Background:** The measurement of skin elasticity has the potential to play an important role in the clinical assessment of a range of skin conditions, including acne scars, wounds, skin cancer, radiation fibrosis and lymphoedema, but many of these applications would require measurement of highly local values of elastic properties. Existing methods of assessing skin elasticity, such as measuring overall strain while applying suction, torsion or a uniaxial load to the skin, provide only an overall value of skin stiffness on a scale no smaller than centimetres.

**Methods:** Pseudo-static linear extensive strains of about 20%, large enough for collagen fibre recruitment, were applied to the skin surface on the forearms of 6 normal volunteers whilst measuring the load and acquiring a sequence of ultrasound images using a Sequoia™ 15L8 probe at 14MHz. The small strain (1-2%) between images acquired in sequence allowed two dimensional incremental correlation-based displacement tracking for imaging the total displacement. Least squares strain estimation then formed lateral and axial strain images, using both normal strain and shear strain, for a field of view of about 15mm deep by 40mm wide.

**Results:** At least 9 frame/s were needed to separate the effects of linear elasticity from those of viscous creep. Account also needed to be taken of the limit strain, at which a near linear stress-strain relationship begins. In general, uniform normal strains were seen in the skin, with the strain propagating down into the subcutis, despite the use of surface extensive loads, with a pronounced anisotropy observed as a modulation factor of about two and a periodicity of 90 degrees for the variation of relative stiffness (measured as the ratio of load to strain) with direction of loading. On the other hand, little or no normal strain was generated in underlying muscle. Correspondingly, the extensive (lateral) shear strain was uniformly low in all layers, except for high values at the boundary between subcutaneous fat and muscle.

**Conclusions:** Preliminary conclusions are that the uniformity of strain with depth for normal skin should be helpful in the future, for measuring the effect of lymphoedema and for visualising skin tumours, if they possess stiffness contrast against this background. Care, however, needs to be taken to account for the complex stress-strain characteristics of skin, and for the pronounced anisotropy. This complexity, on the other hand, may contain substantial useful information yet to be taken advantage of.

**Acknowledgements:** This work is supported by funding from the EPSRC.

047 **DIFFERENTIATING MECHANICAL PROPERTIES OF CORNEAL PHANTOMS USING AN ULTRASOUND METHOD.**

*J Liu[1]*, CJ Roberts[1], X He[1].*
[1]The Ohio State University, Columbus, OH, USA.

**Aims:** To detect the differences in mechanical properties of corneal phantoms (i.e., contact lenses) made of different materials using an ultrasound method.

**Background:** Recent studies [1] indicated that variations in corneal biomechanical properties in the normal population may introduce significant error to the measurement of intraocular pressure using Goldmann tonometry – a routine ophthalmic practice for glaucoma diagnosis. There is no method that is currently available for non-invasive measurement of corneal biomechanical properties. We have developed an ultrasound model and system for non-destructive determination of the mechanical properties of cornea-like, thin layer structures. Contact lenses made from different materials were used in this study to verify the sensitivity of our approach in differentiating the mechanical properties of cornea phantoms.

**Methods:** Three types of contact lenses were obtained. They were made of polymethyl methacrylate (PMMA), hydrogel, or hydrogel+silicone. The lenses were immersed in 0.9% saline during ultrasonic measurement. The position of the lenses was controlled by XYZ linear stages and two goniometers to ensure that the ultrasonic beam was centered at the apex of the lens. A broadband ultrasound transducer (20MHz, V316, Panametrics) was used, and driven by a pulser/receiver (5900PR, Panametrics). All reflected signals from the contact lenses were recorded by a 500MHz/8-bit digitizer (Acqiris, DP105). A reference signal was recorded on a Plexiglas block with flat surfaces. The experimental reflection spectra were obtained using Fast Fourier Transformation on experimental data. The theoretical reflection spectra were calculated based on a wave propagation model assuming contact lenses as isotropic materials. An inverse algorithm was constructed to estimate the three physical properties of the contact lenses: density $\rho$, thickness $h$, and longitudinal modulus ($\lambda+2\mu$), using least squares minimization.

**Results:** The experimental spectral curves from different contact lenses had different forms, such as the magnitude and location of minima and maxima (Figure 1). It appeared that the spectra from the PMMA lenses had higher magnitudes in comparison to those from the other two types of lenses. The reconstructed values of the longitudinal modulus were significantly different for lenses made of different materials, while PMMA lenses had the highest longitudinal modulus ($P<0.01$).

**Conclusions:** Our studies on corneal phantoms indicated that the ultrasonic system was sensitive in detecting the differences in the physical properties of cornea-like structures. Further theoretical studies may be needed to model human corneas as anisotropic and viscoelastic materials.

**Acknowledgements:** The authors would like to thank Michael Twa, O.D., M.S., for obtaining contact lens samples, and Xueliang Pan, M.S., for assisting in data analysis. This work is funded by the Ann Ellis Fund from the Columbus Foundation and the Ohio Lions Eye Research Foundation.

**References:**

[1] Liu J, Roberts CJ, Influence of corneal biomechanical properties on intraocular pressure measurement - Quantitative analysis, *Journal of Cataract and Refractive Surgery,* 31 (1): 146-155, 2005.

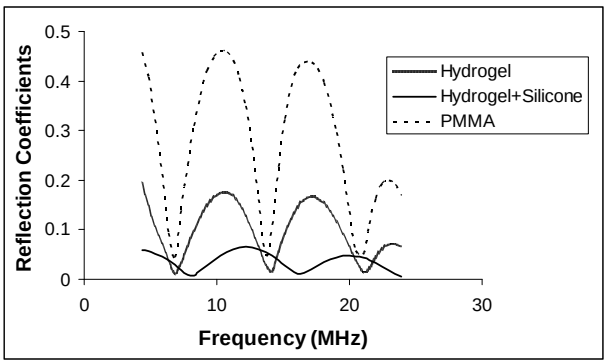


Figure 1: Experimental Spectra of Contact Lenses Made from Different Materials.

010 **ACOUSTOELASTICTY TO BIOLOGICAL TISSUES: MEASUREMENT OF REFLECTION COEFFICIENT CHANGE IN TENDONS UNDER DIFFERENT TENSILE STRAINS.**

*Hirohito Kobayashi[1], Ashish L. Oza[1]*, Ray Vanderby[1].*
[1]Department of Orthopedics and Rehabilitation, University of Wisconsin-Madison, 600 Highland Ave., Madison, WI, USA.

**Aims:** Biological tissues undergo dynamic patterns of physiological stress producing local strains. These strains help maintain the tissues via cell signaling and indicate normal or pathological function. An accurate, non-invasive measurement of strain would then be useful to medical science. Using tendon as a model, the aim of this study was to investigate whether acoustic characteristics of tissues are sufficiently load dependent that they can determine tissue loadings, *in vivo*.

**Background:** Acoustoelasticity (AE) is a theory that describes wave propagation in deformed media. The basis of AE is that acoustic characteristics are stress dependent [1]. A strong correlation between the longitudinal wave velocity and ligament tension has been reported [2] suggesting an AE effect in these tissues. Töyräs et al. similarly showed stress dependence in bovine articular cartilage [3].

**Methods:** In this study, we use reflection coefficients from the surface of tendons under different applied strains to compute tissue strains via AE. The AE formulation below is necessary in order to analyze the load-dependent acoustic properties of these tissues.

$$\varepsilon = \{\frac{[(1+R_0)/(1-R_{0)}]^2}{[(1+R(\varepsilon))/(1-R(\varepsilon))]^2}[\frac{T}{t}]^2\} - 1$$

$\varepsilon$ is tissue strain.
$R_0$ and $T$ are the reflection coefficient and travel time for the unstretched state.
$R(\varepsilon)$ and $t$ are the reflection coefficient and travel time for the stretched state.

Six digital flexor tendons from pigs were collected and placed in the testing machine (MTS 858 BIONIX Test System; 2000 N load cell) containing a hydration bath. Each tendon was held by a specially designed cryogrip and its boney insertion and the bath was filled with phosphate-buffered saline (PBS). An ultrasonic transducer (2.25 MHz) was held perpendicular to the axis of the tendon in the bath. Each tendon was then tested at varying levels of strain. Reflection waves were recorded approximately 4 sec. after the peak strain.

**Results:**

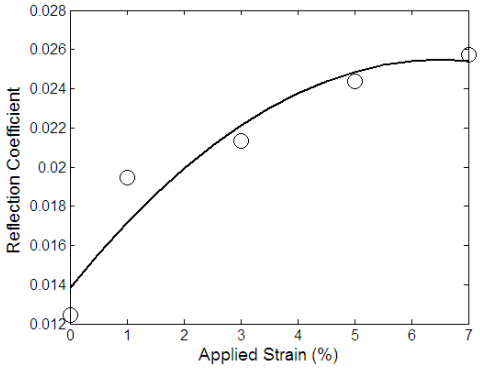


**Figure 1:**
Reflection coefficients from a typical specimen are plotted at different levels of applied strain (grip to grip).
(O): Experimental data points
Solid line: Least squares fit
Results clearly show strain dependence of reflection coefficients.
This behavior (i.e. strong strain dependence) was consistent among all six specimens.

**Conclusions:** This study shows that reflection coefficients of ultrasonic waves off the surface of the tendon change with applied strain. These reflection coefficients, when incorporated into AE analysis, can then be used to compute tissue strains (via the above formula) and transverse stiffness properties of the tissues.

**References:**

[1] Hughes DS and Kelly JL, Phys.Rev. 92, 1145-1149 (1953).
[2] Crisco JJ, et al., J. Biomech. Engr. 120, 321-326 (1998).
[3] Töyräs J, et al., Ultrasound in Medicine & Biology 29(3), 447-454 (2003).

011 **ACOUSTOELASTICTY IN BIOLOGICAL TISSUES: ULTRASOUND WAVE VELOCITY CHANGE IN COMPRESSED TISSUES.**

*Hirohito Kobayashi[1]*, Ashish Oza[1], Michael S. Cooper[2], Ray Vanderby[1].*
[1]Department of Orthopedics and Rehabilitation, University of Wisconsin-Madison, 600 Highland Ave., Madison, WI, USA; [2]Portage Veterinary Clinic, 1803 New Pinery Rd., Portage, WI, USA.

**Aims:** Acoustoelasticity (AE) is a phenomenon that relates alterations of acoustic characteristics in elastic media to deformation. Hence, any analysis regarding wave propagation in a deformed medium should be conducted within the framework of AE. In this study, dilatational wave velocities are measured through compressed biological tissues, and AE is used to identify the mechanical properties of the tissues.

**Background:** The theory of AE was initiated by Hughes and Kelly [1] and has been intensively studied in engineering materials like steel [2], yet it had never been applied to nearly incompressible materials like rubber or biological tissues. Recently, Kobayashi and Vanderby [3] applied AE to nearly incompressible materials like rubber with the introduction of a new strain energy function. Crisco et al. [4] and Töyräs, et al. [5] reported changes of acoustic characteristics in deformed biological tissues, but neither used AE to describe the phenomena. Herein, we investigate the deformation dependence of acoustic dilatational waves in a number of different tumor tissues, indicating the need to use AE theory for analysis.

**Methods:** Sections of different types of biological tissues were placed in a mechanical test system (MTS 858 BIONIX Test System; 5000 N load cell). Target tissues were sandwiched between 2 ultrasonic transducers. Known strains were applied to the tissues and dilatational waves (at 2.25 MHz) from the top to the bottom surface of the tissue were recorded to calculate wave travel time. These data were used to compute the travel velocities.

**Results:**

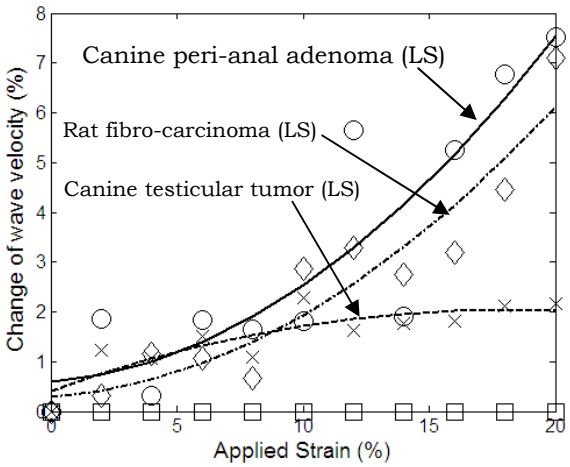


**Figure 1:** Wave velocity changes are plotted as a function of applied engineering strain.
Circle (○): Canine peri-anal adenoma
Cross (H): Canine testicular tumor
Diamond (◊): Rat fibro-carcinoma
Square (□): Poultry breast meat (muscle)

Solid, dash and dash-dot line represents the nonlinear least square fitting (LS) of three different tumors.

Results indicate that the various tumor tissues are substantially strain dependent in their acoustic behavior. In contrast, muscle shows little deformation dependence.

**Discussion and Conclusions:** Except in muscle, acoustic characteristics of all other tissues are clearly dependent on applied strain. Different tissue types show different rate changes in their wave velocities. These patterns may be characteristic of the tumors and may have diagnostic value. The observed strain dependence suggests that AE should be used for analysis. In AE the dilatational wave velocity for this problem setting can be derived as:

$$V_D(e) = \sqrt{\left(\tilde{C}_{11}(e) + t_{11}(e)\right)/\rho}$$

In the above relation, strain dependent stiffness function, applied stress and material density are represented by $\tilde{C}_{11}(e)$, $t_{11}(e)$ and $\rho$ respectively. This relation indicates that the stiffness function for each material can be evaluated from measured velocities, known applied stresses and material density.

**References:**

[1] Hughes, D.S. and Kelly, J.L., Phys. Rev., 92, pp.1145-1149, (1953).
[2] Pao Y. H, Sache W. and Fukuoka H, *Physical Acoustics*, Vol. XVII, Chap.2, (1984).
[3] H. Kobayashi and R. Vanderby, Accepted J. of Applied Mechanics (2005).
[4] J.J. Crsico et al., J. of BioMech. Eng. 120, pp. 321-326, (1998).
[5] J. Töyräs, et al., Ultrasound Med. Bio. , pp.447-454, (2004).

* *indicates Presenter*

034 **NONCONTACT ULTRASOUND INDENTATION SYSTEM FOR ASSESSING BONE-TENDON JUNCTION TISSUES: PRELIMINARY RESULTS.**

*Minhua Lu[1], Yongping Zheng[1]*, Hongbin Lu[2], Qinghua Huang[1], Ling Qin[2].*
[1]Department of Health Technology and Informatics, The Hong Kong Polytechnic University, Hong Kong, CHINA;
[2]Department of Orthopaedics and Traumatology, Chinese University of Hong Kong, Hong Kong, CHINA.

**Aims:** The aim of this study is to use a novel water jet ultrasound indentation system [1] to measure the thickness and stiffness of healing bone-tendon junction (BTJ) of a rabbit model with and without low intensity ultrasound stimulation (LIUS) [2].

**Background:** Many trauma surgeries and reconstructive surgeries involve re-establishment of the BTJ. Experimental and clinical findings show that a direct BTJ repair requires a longer period of immobilization which may be associated a postoperative weak knee. BTJ, such as patellar tendon-patella junction, is characterized with a unique transitional fibrocartilage zone, with calcified fibrocartilage connecting to bone and non-calcified fibrocartilage connecting to tendon. BTJ healing is slow due to the poor regenerative capacity of the fibrocartilage zone between bone and tendon. To enhance the tissue healing, researchers use postoperative mechanical stimulation, such as LIUS, to accelerate the BTJ repair and its restoration of fibrocatilage zone. It is necessary to assess the mechanical property and thickness of the transition zone during the healing process to monitor the formation of a fibrocatilage layer.

**Methods:** Mature female New Zealand White rabbits (18 weeks old) were used for the experiments. One of the rabbit knees was approached and the distal 1/3 of the patella was removed. The patellar tendon was then directly sutured to the proximal patella followed by immobilization for 12 weeks. The opposite knee was served as a control. The ultrasound water indentation system was comprised of a focused high frequency ultrasound transducer, a water beam ejector, and a pressure sensor. The water beam with a diameter of 1.9 mm served as a compressor as well as a medium for ultrasound propagation. The tissue deformation was estimated from the ultrasound echoes reflected from the tissue. During water indentation, the knee joint was fixed with the patella tendon facing up to the water jet perpendicularly. The system then scanned along the patella tendon direction at one pressure level. The scan was repeated under different pressure levels. The variation of the tissue structure and stiffness was obtained by comparing the sequential ultrasound signals collected under different compression levels.

**Results:** Figures 1 and 2 show the thickness and stiffness distributions of the transition zone from patella to tendon of the intact and postoperative samples. There was little formation of new bone of the knee with surgery due to limited time, so only the distal patella and tendon with scars were assessed as the postoperative sample. It was found that, although the thickness of the distal of the patella was not significantly changed, its stiffness decreased. This decrease may be due to the degeneration of the articular cartilage caused by the surgery. The thickness of the tendon increased due to the formation of scar.

**Conclusions:** It is still a challenge to measure the mechanical properties of small specimens. Our ultrasound indentation system using water jet indentation can load on the tissues nondestructively to measure the thickness and stiffness. Preliminary results show its potential to monitor the new formation of cartilage layer during the healing process of BTJ.

**Acknowledgements:** This project was partially supported by the Research Grant Coucil of Hong Kong (PolyU 5245/03E) and The Hong Kong Polytechnic University.

**References:**

[1] Lu MH, et al. Water jet ultrasound indentation. Ultrasound Med Biol 31: 817-26, 2005.
[2] Qin L, et al. Partial patellectomy rabbit model. Med Sci Sports Exer 31:502-6, 1999.

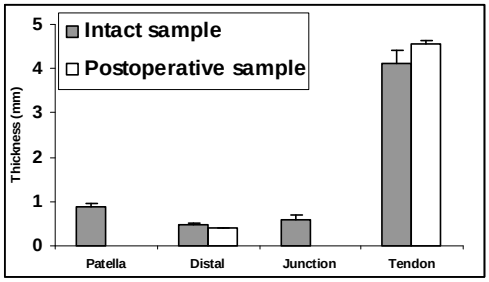


Figure 1: The Thickness Distribution of the BTJ Tissues.

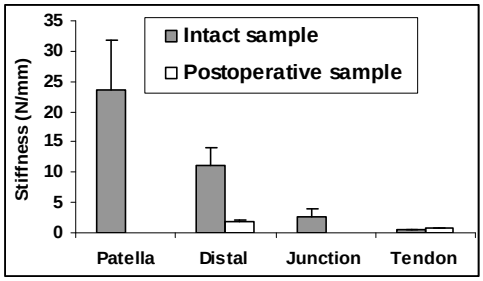


Figure 2: The Stiffness Distribution of the BTJ Tissues.

* *indicates Presenter*

062 **MECHANICAL MEASUREMENT OF ELASTIC PROPERTIES OF BOVINE LIVER AND HUMAN PROSTATE UNDER COMPRESSION.**

*Man Zhang[1]*, Zhe C. Wu[1], Deborah J. Rubens[2], Kevin J. Parker[1].*
[1]Electrical and Computer Engineering, [2]Radiology Departments, University of Rochester, Rochester, NY, USA.

**Aims:** The goal of this study is twofold: first, to establish a reliable and accurate technique for measuring the elastic properties of soft tissues; and second, to compare mechanical measurement results with those obtained from the sonoelastography shear wave interference method.

**Background:** Over the past two decades, ultrasound elasticity imaging has been continuously developed for imaging soft tissue elasticity. However, fundamental knowledge of mechanical properties of soft tissue is lacking. In this study, we proposed the tissue stress-relaxation experiment and the Kelvin-Voigt fractional derivative (KVFD) model to clarify the frequency-dependent elastic properties of bovine liver (normal and high-intensity focused ultrasound (HIFU) ablated) and human prostate (normal and cancer).

**Methods:** Cylindrical samples (10 mm diameter, 8 mm thickness) were acquired from normal and HIFU ablated liver tissues. During the experiment, a 3% compressional strain was applied to measure the stress-relaxation data over 1000 seconds. After that, the stress-relaxation curve of each sample was fit to the KVFD model, in which $\alpha$ and $\eta$ are the two important parameters. Finally, the complex elastic modulus at any frequency was obtained by the Fourier transform of the time domain response. The same procedure was also applied to the human prostate samples. Sonoelastography was used to visualize shear wave interference patterns. Shear wave velocity, and thus shear stiffness can be estimated from those patterns. A piece of fresh bovine liver was placed in between a pair of shear wave sources and the shear wave interference was recorded and analyzed to estimate the liver's shear stiffness.

**Results:** The $\alpha$ ratio and the $\eta$ ratio (Table 1) between the HIFU lesion and the normal liver are about 2:1 and 9:1, respectively. The $\eta$ ratio reflects the stiffness contrast between the two tissues. Figure 1 shows the frequency-dependent elastic properties of three types of liver tissues. The complex elastic modulus slightly increases with frequency. The shear wave interference method estimated that the Young's modulus of a bovine liver sample was 2.7 kPa at 50 Hz while it was 2.9 kPa from the mechanical testing. Shear wave interference experiments at more frequencies are scheduled. We have also tested over 30 samples from 11 different human prostates. For normal prostate samples, we have found that an average value for the elastic constant is 17.5 ± 2.1 kPa at 100 Hz. Cancerous prostate samples were tested as well. In particular, 3 samples were acquired from one gland, each containing 90%, 70% and 0% cancerous tissue, respectively. The stiffness contrasts of these samples are 2.7:2:1.

**Conclusions:** The stress-relaxation test produces repeatable results which fit well to the KVFD model. Sonoelastography shear wave interference method provides preliminary estimation of shear stiffness of the bovine liver, which agrees with the mechanical measurement results. Elastic properties of normal and cancerous human prostates are systematically tested and the preliminary results are provided.

**Acknowledgements:** This study was partly supported by NIH grant 5 RO1 AG016317-05.

| | **η** (kPa sec$^{\alpha}$) | **α** | **$R^2$** |
|---|---|---|---|
| **Normal** *(n=8)* | 7.127 | 0.108 | 0.956 |
| **4' HIFU** *(n=8)* | 66.760 | 0.208 | 0.985 |
| **2' HIFU** *(n=3)* | 27.049 | 0.190 | 0.987 |

Table 1: The parameters of the KVFD model from the curve fitting.

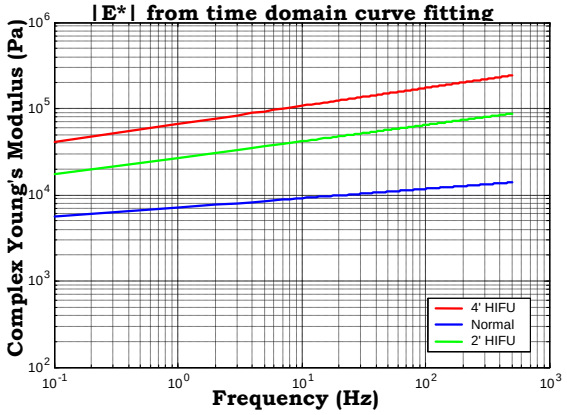


Figure 1: Frequency dependent elastic moduli of bovine liver.

* *indicates Presenter*

069 **VISCOELASTIC AND ULTRASONIC PROPERTIES OF THE UTERUS.**

*M.Z. Kiss*[1]*, *T. Varghese*[1,2], *M.A. Hobson*[1], *M.A. Kliewer*[3], *J. Harter*[4], *E.M. Hartenbach*[5].
[1]Medical Physics, [2]Biomedical Engineering, [3]Radiology, [4]Pathology, [5]Obstetrics and Gynecology Departments, 1300 University Ave., Room 1530, University of Wisconsin-Madison, Madison, WI, USA.

**Aims:** The viscoelastic properties of uterine and cervical tissue have been investigated. Leiomyomas (fibroids) and adenomyosis, a condition where soft endometrial tissue invades the myometrium if the uterus,, have similar appearances on conventional ultrasound images, so the mechanical properties of normal and pathological tissues are of interest in order to develop elastographic methods for differentiating between these two conditions, since the clinical treatments for the two conditions is very different.

**Background:** Dysfunctional uterine bleeding is a common indicator of uterine abnormalities. Benign endometrial atrophy and fibroids are among the common causes, especially in postmenopausal women. However, approximately 10% to 30% of women will be found to have endometrial cancer. Dysfunctional uterine bleeding in premenopausal women is usually the result of benign conditions, such as leiomyomas, endometrial polyps and adenomyosis. However, treatment of each condition is different, so differentiation is clinically important because treatment for the two conditions is very different. Currently MRI is the only imaging modality capable of distinguishing between these two conditions, leiomyomas and adenomyosis.

**Methods:** Uterine and cervical specimens from 14 patients were excised from bulk tissue and cut to a useful geometry (typically rectangular on the order of 10 15×5 mm) and placed in Bose/Enduratec ELF 3220, a dynamic testing device. The complex modulus was determined by applying a periodic strain amplitude of 1 or 2% (with a precompression strain of 1 or 2%, respectively), and a frequency from 0.1 - 100 Hz, and measuring the force response at the load cell. Additionally, tests were conducted where the sample was strained periodically at a frequency of 1Hz at amplitudes ranging from 1 to 10% (at a precompression strain of 2 or 5%). For ultrasonic testing, samples were subjected to simple through transmission tests to determine the ultrasonic attenuation in the frequency range of 5 – 10 MHz using an unfocused broadband transducer with central frequency of 7.5 MHz.

**Results:** Experiments show that the complex modulus for both the cervix and the uterus generally increased with increasing frequency from 25 kPa at 0.1 Hz up to 60 kPa at 100 Hz. The uterus and cervix have similar moduli at low frequencies, and the uterus is slightly stiffer at higher frequencies. The phase of the modulus generally increased from 0.25 to 0.40 over the same frequency range for both the cervix and the uterus. When the age of the patient is considered, it is revealed that the uterine modulus is inversely proportional to age, while the cervix modulus is proportional to age. The ultrasonic attenuation experiments show that the cervix is far more attenuating than the uterus as a function of ultrasound frequency, with the cervix following a power law exponent of 2.1 and the uterus going as 1.6. Attenuation of both the cervix and the uterus also tends to increase with patient age. Uterine fibroids tended to attenuate ultrasound at a rate similar to that of the cervix, but there was no major distinction between the leiomyomas and normal uterus.

**Conclusions:** Characterization of the viscoelastic properties of *in vitro* uterine and cervical specimens may eventually lead to improved elastographic methods of diagnosing certain pathologies. Fibroids tend to be stiffer than surrounding normal tissue, implying that elastographic image contrast may be improved when certain patient attributes are considered, such as age, number of children and history of illness.

**Acknowledgements:** This research is supported in part by NIH grant T32CA09206.

105 **EVALUATION OF ANISOTROPY IN THE NORMAL PLANTAR SOFT TISSUES: SHEAR MODULUS FOR SHEARING DEFORMATION AND COMPRESSIVE DEFORMATION.**

*JB Weaver[1]*, TB Miller[2], MM Doyley[1], PR Perrinez[2], H Wang[2], YY Cheung[1], JS Wrobel[3,4], FE Kennedy[2], KD Paulsen[2].*

[1]Department of Radiology, Dartmouth-Hitchcock Medical Center, Lebanon, NH, USA; [2]Thayer School of Engineering, Dartmouth College, Hanover, NH, USA; [3]VA Medical Center, WRJ, VT, USA; [4]Department of Community and Family Medicine, Dartmouth Medical School, Hanover, NH, USA.

**Introduction:** Magnetic resonance elastography (MRE) [1] is capable of imaging the intrinsic mechanical properties of plantar soft tissues such as the shear modulus (μ) [2] and damping coefficient [3, 4]. The intrinsic mechanical properties of the plantar soft tissues are important in the context of evaluating the weight bearing structures of the foot that are at high risk for ulcers and amputation in diabetic patients. At least three benefits are possible:

a) Following and evaluating the progression of diabetic patho-physiologic deterioration of the weight bearing structures.
b) Optimizing the development of prostheses for deformed diabetic feet that are susceptible to ulceration and amputation at large cost to both the patient and to the health care system.
c) Understanding how the weight bearing structures in the foot function in weight distribution.

The key question we are using MRE to address is: Are the plantar tissues more rigid during shearing deformation or during compressive deformation? The question is relevant to our understanding of how pressures are generated during normal and abnormal gates which is crucial to understanding the formation of ulcers that lead to amputation.

**Methods:** We used steady-state dynamic MRE [1] to measure the μ in the heel fat pad twice in each of three healthy subjects. The two measurements, $\mu_c$ and $\mu_s$, were acquired using different patterns of vibration: moving the plate on which the heel was resting 1) superior-inferior and 2) anterior-posterior. The heel remained fixed in the same position during both acquisitions. The direction of motion as well as the μ was found for all points within the heel. The induced motion is a complicated function of the intrinsic properties of the soft tissue as well as the geometry of the soft tissue and bones. The points which vibrated along the direction of weight bearing in one vibration pattern and in the plane normal to the direction of weight bearing in the other vibration pattern were found. The change in μ at those points represents magnitude of the anisotropy. Two controls were used: the reproducibility of MRE measurements (3.5%) and the variation in μ at points where no change in direction was observed between the two acquisitions. In addition, we imaged gel phantoms to evaluate accuracy and resolution.

**Results:** The MRE μ is accurate to within 10% to 20% and reproducible to 3.5%. In two subjects, aged 26 and 30, the difference between $\mu_c$ and $\mu_s$ was less than that in control points. In the third subject, aged 36, the difference between $\mu_c$ and $\mu_s$ was twice the difference in control points. In two subjects, the mean $\mu_c$ and $\mu_s$ for all control points were significantly different. The effect was probably produced by a change in the pressure applied by the subject between the two acquisitions; in any event the bias was removed from the comparison.

**Conclusions:** MRE can quantitatively image the mechanical properties of plantar soft tissues *in vivo* with excellent accuracy and reproducibility. The shear modulus of normal heel fat pads for deformation perpendicular to the direction of weight bearing is essentially the same as that determined for deformation along the weight bearing axis. However, there is some indication that aging might introduce a difference suggesting that diseases mimicking aging such as diabetes might also introduce differences.

**Acknowledgements:** Supported by R01-DK-063013, R01-NS-33900 and P01-CA-80139.

**References:**

[1] JB Weaver, EEW Van Houten, MI Miga, FE Kennedy, KD Paulsen, Med Phys, 28(8):1620-1628, 2001.
[2] MM Doyley, JB Weaver, EW Van Houten, FE Kennedy, KD Paulsen, Med Phys, 30(4):495-504, 2003.
[3] K.D. Paulsen, E.E.W. Van Houten, M.M. Doyley, J.B. Weaver: IEEE NIBIE, July, p. 157-160, 2002.
[4] R Sinkus, et. al., Mag. Reson. Med. 53:372–387, 2005.

** indicates Presenter*

085 **DIRECT INVERSION METHOD IN SHEAR WAVE SPEED RECONSTRUCTION IN ELASTOGRAPHY.**

*K. Lin[1]*, J. R. McLaughlin[1].*
[1]Rensselaer Polytechnic Institute, Troy, NY, USA.

**Aims:** The goal of this work is to apply and justify stable probabilistically based numerical differentiation schemes in our elastography inverse problem to reconstruct high quality images of tissue stiffness properties in isotropic media and anisotropic media. The data we use are time-dependent displacement data generated in the laboratory of Mathias Fink's group from phantoms. Further investigation is taken in *in vivo* data.

**Background:** Probabilistically based difference schemes to compute numerical derivatives.

**Methods:** Direct Inversion Method based on wave equation in isotropic and anisotropic, linearly elastic media, stable hybridization of averaging scheme and median scheme, and total variation de-noising technique.

**Results:** First order accuracy is achieved by all numerical differentiation schemes in the Gaussian noise case, while the hybrid method shows robustness to extreme noise in data. An image of shear wave speed reconstruction recovers the position and shape of the stiff inclusion in an isotropic phantom accurately. An image of longitudinal shear modulus also recovers the shape and position of the fiber-strengthened transversely isotropic inclusion in anisotropic phantom.

**Conclusions:** We have presented the results of the order of accuracy and stability of probabilistic numerical differentiation methods. A single numerical scheme works well in a specific noise case, while combination of different methods tends to be more accurate and robust to outliers in the case of unknown noise. Application of those methods has produced high quality images that capture the inclusions in phantoms much more accurately compared with standard ultrasound images with the same experimental settings.

**Acknowledgements:** We thank Mathias Fink's group for providing phantom data and Ernest Madsen for building a new anisotropic phantom. We also want to acknowledge discussion with Daniel Renzi, Jeong-Rock Yoon and Jens Klein.

**References:**

[1] Lin Ji, Joyce R. McLaughlin, Daniel Renzi and Jeong-Rock Yoon, "Interior Elastodynamics Inverse Problem: Shear Wave Speed Reconstruction in Transient Elastography", Inverse Problem 19 (2003) S1-S29.
[2] Robert S. Anderssen, Markus Hegland, "For Numerical Differentiation, Dimensionality Can Be a Blessing", Mathematics of Computation, Vol.68, No.227, Pages 1121-1141.
[3] Rudin L I, Osher S and Fatemi E 1992, "Nonlinear Total Variation Based Noise Removal Algorithm", Physica D 60, 259-268.
[4] Stainley Osher, Martin Burger, Donald Goldfrab, Jinjun Xu, and Wotao Yin, "Using Geometry and Iterated Refinement for Inverse Problem (1): Total Variation Based Image Restoration", Journal of Computational Physics, v77, 1988, pp.439-471.
[5] Sandrin L, Tanter M, Catheline S and Fink M 2002, "Shear Modulus Imaging with 2-D Transient Elastography", IEEE Trans. Ultrason. Ferroelectr. Freq. Control, 49, 426-435.
[6] J Bercoff, M Tanter and Mathias Fink, "Supersonic Shear Imaging: A New Technique for Soft Tissue Elasticity Mapping", IEEE Transactions on Ultrasonics, Ferroelectrics, and Frequency Control, Vol.51, No.4, April 2004.
[7] David C. Hoaglin, Frederick Mosteller, John W. Tukey, "Understanding Robust and Exploratory Data Analysis", Wiley, c1983.
[8] James F. Greenleaf, Mostafa Fatemi and Michael Insana, "Selected Methods for Imaging Elastic Properties of Biological Tissues", IEEE Trans. Ultrason. Freq. Control, 49, 1363-1374.

015 **ISSUES IN REAL-TIME ACOUSTIC RADIATION FORCE IMPULSE IMAGING.**

*GE Trahey[1]*, GF Pinton[1], ML Palmeri[1], RR Bouchard[1], JJ Dahl[1].*
[1]Duke University, Durham, NC, USA.

**Aims:** Acoustic Radiation Force Impulse (ARFI) imaging is useful for characterizing localized mechanical properties of tissue [1]. In effort to generate an ARFI imaging system capable of displaying tissue displacement in real-time, several considerations must be addressed in order to improve the frame rate of the ARFI imaging system. The four main issues in ARFI frame rate are patient safety, observation time along a line of sight, number of "push" locations, and processing/flow of data.

**Background:** In ARFI imaging, a localized, long-duration (~30 μs) radiation force (pushing pulse) is used to generate small displacements (1-10 μm) in tissue. The response of tissue is measured using imaging pulses to track these displacements. The pushing pulses used by ARFI imaging generate heat in the tissue as the acoustical wave is absorbed. As the ARFI frame rate increases, so does the amount of heat generated [2]. Tissue heating can be controlled by the amount of observation time (i.e. the length of time for tracking the displacement at a given location), however as this time increases, ARFI frame rate suffers. The size of the field of view (FOV) affects both heating and data acquisition time. Frame rate will also depend on the computational algorithms and data flow.

**Methods:** We propose two methods for improving the frame rate in ARFI imaging without compromising patient safety. These methods include parallel receive beamforming to reduce the number of pushing pulses (and therefore decrease the heat generated in tissue) without decreasing the FOV, and interleaving tracking pulses to decrease the data acquisition time without compromising the observation time. We have created custom beam sequences on a Siemens Antares™ scanner to implement these parallel and interleaved tracking methods in phantom and *ex vivo* experiments and compare with FEM simulations. Simulations were also used to compare the jitter, bias, and computational cost of several displacement tracking algorithms. These tracking methods include normalized cross-correlation, one-dimensional autocorrelation, and two-dimensional autocorrelation.

**Results:** Displacement images produced by parallel tracking ARFI methods were compared to those produced by standard ARFI methods. Displacements varied between the two methods immediately after cessation of the pushing pulse, however, as the shear wave induced by the pushing pulse propagated from the initial pushing position, the displacements became uniform across the parallel beams. Given this delay, the two images appear nearly identical. Interleaving the tracking pulses decreased the amount of time necessary to acquire an ARFI frame. The magnitude of artifacts observed using the interleave method was dependent on the number and spacing of locations for which tracking was interleaved. The artifacts result from shear wave propagation between push locations.

Normalized cross-correlation yielded the least jitter and bias for estimating tissue displacement, however, it required the most computational time. One-dimensional autocorrelation yielded the most jitter and bias for its estimates, but required little computational effort. Two-dimensional autocorrelation showed jitter levels near that of cross-correlation but had greater bias. We present phantom and *ex vivo* ARFI images using parallel receive beamforming, pulse interleaving, and several tracking schemes. We discuss the frame rates achievable using these methods and the resultant tissue heating levels.

**Conclusions:** The proposed tracking methods improve ARFI frame rate without compromising patient safety. Parallel tracking provides near identical results to standard ARFI methods, however, the amount of time necessary for the shear wave to propagate far enough to even the displacement across the parallel tracking beams depends on the stiffness of the tissue and the F/# of the pushing pulse. Interleaving the tracking pulses improves ARFI frame rate, but can introduce image artifacts if the shear waves from adjacent pushing locations overlap during the observation time.

**Acknowledgements:** This work is supported by NIH grants R01- HL075485-02 and R01-EB002132-04. Technical support was provided by Siemens Medical Solutions USA, Inc. in Issaquah, WA.

**References:**

[1] K. Nightingale, M. Soo, R. Nightingale, and G. Trahey, Acoustic radiation force impulse imaging: *In vivo* demonstration of clinical feasibility. Ultrasound Med. Biol., vol. 28, no. 2, pp. 227-235, 2002.
[2] M. Palmeri and K. Nightingale, On the thermal effects associated with radiation force imaging of soft tissue. IEEE Trans. Ultrason., Ferroelect., Freq. Contr., vol. 51, no. 5, pp. 551-565, 2004.

* *indicates Presenter*

073 ***IN VITRO* MEASUREMENT AND IMAGING OF THE STRAIN AT THE BOVINE ACL-BONE INSERTION.**

*Elisa E Konofagou[1]*, Jeff P Spalazzi[1], Simon D Fung-kee-Fung[1], Helen L Lu[1].*
[1]Columbia University, Department of Biomedical Engineering, 1210 Amsterdam Avenue, New York, NY 10027, USA.

**Aims:** The anterior cruciate ligament (ACL) functions as a mechanical stabilizer in the tibiofemoral joint. Over 250,000 Americans each year suffer ACL ruptures and tears, making the ACL the most commonly injured ligament of the knee. A long term goal in tissue engineering has been to regenerate the ACL-bone interface. To this end, an in-depth understanding of the structural and mechanical properties of the transition zone is needed in order to define relevant design parameters.

**Background:** Song et al. [1], using a Finite-Element Modeling (FEM) model of ACL, predicted that stress was transferred from the ligament to bone at the femoral insertion, and the magnitude of the stress was reduced near the tibial insertion compared to the ACL proper. However, experimental determination of the mechanical properties at the interface has been difficult due the small area (<1mm) involved and limited resolution of standard techniques. The current study uses elastography to characterize the functional properties of the interface under applied load.

**Methods:** Three tibiofemoral joints from neonate bovine were mounted on an Instron MTS 858 Bionix Testing System. The ACL was loaded at different strain rates and tested to failure while RF data was acquired at 5 MHz with a Terason (Teratech, Inc.) ultrasound scanner. For both tensile and compression testing, axial elastograms between successive RF frames were generated using cross-correlation and recorrelation techniques using a 3 mm window size and 80% window overlap [2].

**Results:** When the ACL-Bone complex was tested in the tibial alignment on the MTS system, compressive strains were found to dominate at the tibial insertion. Compressive strains were observed in the ligament proper since the transducer was aligned with respect to the insertion during loading. The distribution of tensile and compressive strain varied as a function of strain rate during testing and between loading and unloading. Elastograms were highly repeatable over a multitude of strains applied and across different tissue specimens and clearly indicated that the strain distribution in the ligament is uniform while highly complex throughout the insertions, with both tensile and compressive strains found at the insertion site.

**Conclusions:** The aforementioned results agree with those of prior FEM model predictions [3]. In addition, a narrow band of high tensile strain in the middle of the ACL was detected during tension that is considered to be a softer region of the ACL containing a highly collagenous structure. These preliminary results on ACL geometry and function indicate that elastography can provide important information in understanding the structure and function of both the ACL and the ACL-bone insertion. Ongoing studies focus on in-depth evaluation of the mechanical properties and the structure-function relationship existing at the ACL to bone insertion.

**Acknowledgements:** This study was supported by the Whitaker Foundation.

**References:**

[1] Song Y et al., J. Biomech., 37(3):383-390.
[2] Konofagou E. and Ophir J., Ultras. Med. Biol. 24(8): 1183-1199, 1998.
[3] Matyas et al., J.Biomech., 28(2):147-157, 1995.

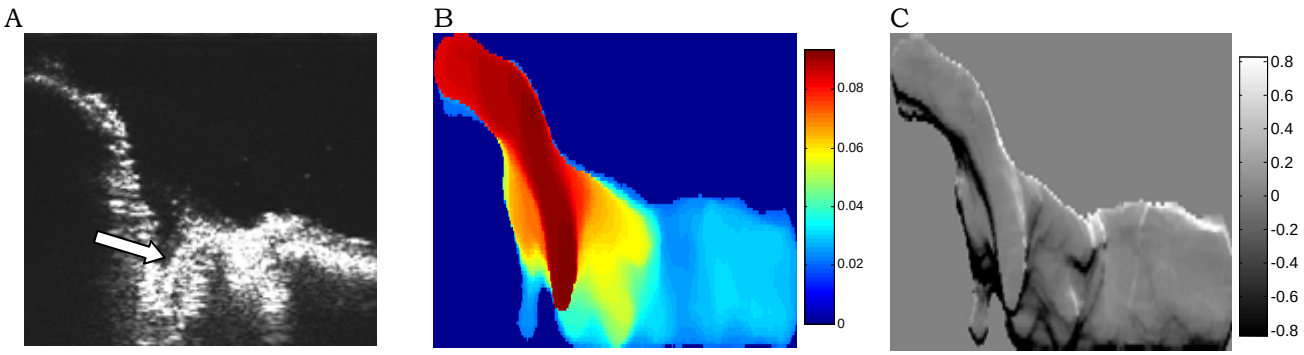


Figure 1: A) A sonogram of the femur (left), the tibia (right) and the ACL-bone insertion (arrow); B) Displacement image (mm) and C) elastogram (%) during stretching of the ACL. Note the 'ridge' formed at the insertion.

096 **FFT ANALYSIS OF THE PERIODIC STRUCTURES IN HAVERSIAN BONE BASED ON SCANNING ACOUSTIC MICROSCOPY (SAM).**

*J. Lawrence Katz[1,2]*, Anil Misra[2], Orestes Marangos[2], Yong Wang[1], Paulette Spencer[1].*
[1]University of Missouri-Kansas City, 3161 SOD, 650 East 25th Street, Kansas City, MO 64108, USA; [2]University of Missouri-Kansas City, SCE, Flarsheim Hall, 5100 Rockhill Road, Kansas City, MO 64110, USA.

**Aims:** To apply fast Fourier transform (FFT) analysis to the pseudo-periodic variations, observed in elastic properties in both haversian (osteonal) and interstitial lamellae in human cortical bone, using scanning acoustic microscopy (SAM) at high frequencies (400-600MHz).

**Background:** Both the Olympus UH3 SAM (Olympus Co., Japan) and the Krämer KSI 2000 SAM (Krämer Scientific Instuments, Germany) have been used to study human femoral cortical bone at 400 and 600 MHz. The Olympus UH3 SAM was used to study specimens of haversian (osteonal) bone from a 60+ male cadaver. The Krämer KSI 2000 SAM was used in a study of both female and male haversian (osteonal) bone as a function of age, (20s, 60s and 70s) at different orientations relative to their femur's long axis. Both the osteonic lamellae and the interstitial lamellae of cortical bone exhibit uniform variations in their elastic properties from lamella to lamella, i.e. the material properties of adjacent lamellae vary systematically from stiff to less stiff. This appears on the SAM images as systematic pseudo periodic variations in gray levels, lighter to darker to lighter and so on, in both the osteonic and interstitial lamellae reflecting the variations in their elastic properties. These pseudo-periodic variations permit the application of fast Fourier transform (FFT) analysis to the SAM images.

**Methods:** Using one of the available math packages, such FFT images have been computed for all the SAM images of interest. Points on the FFT images corresponding to the principal directions of periodicity were then selected for the application of the back FFT analysis. Each back FFT calculation provided the image of the lamellae orientations related to the point used. These back images were then superimposed to reconstruct the FFT counterpart of the original SAM image in each case.

**Results:** The reconstructed image often provided more details than seen on the original SAM image, as it eliminates much of the artifacts imposed on the SAM image by the specimen, e.g. asperities not removed during surface preparation, regions out of the focal plane, preparation cracks, etc. The FFT technique also has provided a rapid method of obtaining average thicknesses of both the osteonal and interstitial lamellae.

**Conclusions:** Application of FFT analysis to SAM measurements of cortical bone properties has provided the means for obtaining more details inherent in the micrographs by eliminating or reducing preparation artifacts. The analysis is now being applied to SAM studies of similar systematic pseudo periodic variations in gray levels observed in human femoral trabecular bone in order to compare lamellar average thicknesses between the two types.

**Acknowledgements:** A contribution of the University of Missouri-Kansas City Center for Research on Interfacial Structure and Properties (UMKC-CRISP). This research was supported in part by RO1 DE14392 (PS), K25 DE015281 (YW) from the National Institute of Dental and Craniofacial Research, NIH, and NIH High-End Instrumentation Grant S10 RR16710 (PS).

* *indicates Presenter*

108 **SHEAR STIFFNESS IDENTIFICATION USING MOVING INTERFERENCE PATTERNS IN SONOELASTOGRAPHY.**

*Joyce R. McLaughlin[1], Daniel Renzi[1]*.*
[1]Rensselaer Polytechnic Institute, Troy, NY, USA.

**Aims:** The target of this work is to produce an image of tissue where the imaging function is a measure of shear stiffness. It is motivated by the fact that shear stiffness is the tissue elastic property that is felt in a palpation exam. Recently two new experiments have been proposed to characterize the elasticity of soft tissue using sonoelastography. In both experiments, a moving interference pattern is observed because of the interactions of the two oscillations at nearby frequencies. The goal of this work is to devise and test algorithms to calculate the shear wave speed, or an imaging functional closely related to the shear wave speed, using the arrival times of the moving interference patterns.

**Background:** Recently two new experiments have been proposed to characterize the elasticity of soft tissue using sonoelastography. The first experiment, the crawling wave experiment, uses two vibration sources oscillating at nearby but different frequencies, each of which create a shear wave that travels through the tissue. The second experiment, the holographic wave experiment, uses one vibration source together with an oscillation of the ultrasound transducers that record the measurements. The vibration source and the transducers are oscillated at nearby but different frequencies. In both experiments:

(1) one component of the vibration amplitude is measured using sonoelastography; and
(2) a moving interference pattern is observed because of the interactions of the two oscillations at nearby frequencies.

By making the two vibration frequencies close enough, the interference pattern can be made to move at a very small fraction of the shear wave speed. This allows the moving interference pattern to be imaged with a high effective frame rate (frame rate divided by interference pattern speed) in real time with a standard Doppler ultrasound machine. In the holographic wave experiment, the shear wave speed can be directly calculated from the moving interference pattern speed, and in the crawling wave experiment, the moving interference pattern speed will be used as an imaging functional for the shear wave speed.

**Methods:** To generate our images, we first derive formulas relating the moving interference pattern speed and the shear wave speed under the assumption that a geometric optics expansion is valid. Then we find the arrival times of the moving interference pattern using a cross-correlation procedure. These arrival times are related to the moving interference pattern speed via a first order nonlinear partial differential equation called the Eikonal equation. The moving interference pattern speed is calculated using an inverse Eikonal solver we have previously developed named the level curve method.

**Results:** We test our algorithm on data obtained from a phantom experiment performed at the University of Rochester Center for Ultrasound. We were able to accurately recover a stiff circular inclusion one centimeter in diameter.

**Conclusions:** We have developed a new algorithm to image the speed of moving interference patterns. This algorithm is composed of two sub-algorithms. The first sub-algorithm finds the arrival times of one of the stripes of the moving interference pattern. The second sub-algorithm takes as input the arrival times found by the first sub-algorithm, and finds the moving interference speed by solving the inverse Eikonal equation using the inverse level curve method for the Arrival Time Algorithm. With data from a crawling wave experiment, a multiple of the speed of the moving interference pattern is used as an imaging functional for the shear stiffness because the relationship between the moving interference pattern speed and the shear stiffness is quite complicated. For the holographic wave experiment, there is a simple linear relationship between the moving interference speed and the shear wave speed, so in that case we image the shear wave speed. We have tested our algorithm with data obtained by Zhe Clark Wu in the laboratory of Kevin Parker, in the Rochester Center for Biomedical Ultrasound at the University of Rochester. They performed both the one and two frequency experiments using a tissue mimicking Zirdine phantom containing a 1cm diameter circular inclusion. We have obtained very good shear stiffness images with both sets of experimental data.

**Acknowledgements:** We would like to thank Zhe Clark Wu and Kevin Parker for providing us with phantom data to test our algorithms.

014 **ASSESSMENT OF MECHANICAL PROPERTIES OF PVA-C WITH FOUR DIFFERENT ELASTOGRAPHIC METHODS.**

*Jean-Luc Gennisson[1]*, Jérémie Fromageau[1], Cédric Schmitt[1], Roch L. Maurice[1], Rosaire Mongrain[2] and Guy Cloutier[1].*

[1]Laboratory of Biorheology and Medical Ultrasonics, University of Montreal Hospital, Pavilion J.A de Sève (Rm Y-1619), 2099 Alexandre de Sève, Montréal, Québec, H2L 2W5, CANADA; [2]Mechanical Engineering Department, McGill University (Rm 369), 817 Sherbrooke Street West, Montréal, Québec, H3A 2K6, CANADA.

**Aims:** In the field of elastography, tissue mimicking phantoms are very useful and essential to establish the validity of a given technique. Usually, these are made of agar, gelatin, or Polyvinyl Alcohol Cryogel (PVA-C). This study is first dedicated to mechanically characterize PVA-C for elastographic applications through two parameters: the Young's modulus ($E$) and the Poisson's ratio ($\nu$). The second purpose is to compare different ultrasound elastographic methods to mechanical indentation instruments, considered to be the gold standard.

**Methods:** The PVA-C mechanical properties were studied as a function of the number of freeze-thaw cycles imposed to the material to control the sample stiffness. The 24h cycles were performed in a temperature controlled chamber. A cycle was constituted of two maximum/minimum thresholds, at +20°C and -20°C during 8h 40min each and two periods of change from the extremes lasting 3h 20min (slope of ±0.2°C/min). The influence of the number of cycles (from 1 to 10 cycles) and of the scatterer concentrations added (Sigmacell particles from 1% to 4%) were investigated. To make the assessment easier, the phantom geometry has been defined as a cylinder of 60mm diameter and of 15mm thick. For each experiment, the speed of sound, speed of shear waves and density were also assessed.

Four different elastographic methods were used: three static elastography techniques based on a scaling factor estimation [1], a Lagrangian estimator (1) [2] and an adapted Lagrangian estimator (2) [3]; and a dynamic method, the transient elastography [4] based on shear wave propagation. Specific inverse problems applied to each method allowed to recover the Young's modulus. The elastographic assessments were compared to mechanical tests, with a commercial (Enduratec, ELF 3200, Minnetonka, MN, USA) and a homemade compression device. For the Enduratec, the tests were done in compression and stretching. All the measurements have been performed under small strain (<20%).

**Results and Conclusion:** As expected, PVA-C phantoms were found to be incompressible ($\nu > 0.4999$) with a Young's modulus very close to those found in biological soft tissues (25kPa < $E$ < 650kPa). A covariance statistical analysis was used to compare each method with the tensile test performed on the Enduratec to confirm that each method is relevant to quantify elastic Young's modulus.

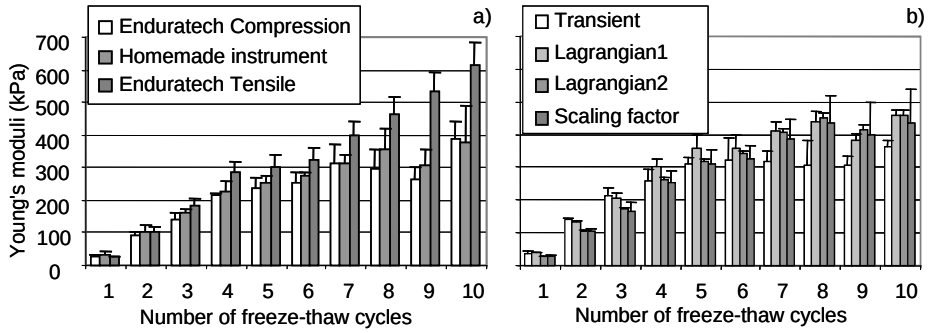


Figure 1: Mean Young's moduli estimated with different methods as a function of the number of freeze-thaw cycles, a) mechanical tests and b) elastographic methods.

**References:**

[1] Fromageau J. *et al.*, "Estimation of Small Time-Scaling Factor using the Hilbert Transform", Submitted to *IEEE-Signal Processing*, 2005.

[2] Maurice R.L. *et al.*, "Lagrangian speckle model and tissue-motion estimation – Theory", *IEEE-Trans. Med. Imag.*, 18(7), pp. 593-603, 1999.

[3] Schmitt C. *et al.*, "Development of non-invasive vascular elastography for carotid artery plaque assessment", *Proc. IEEE-Ultrasonics Symposium*, 2005.

[4] Sandrin L. *et al.*, "Shear elasticity probe for soft tissues with 1D transient elastography.", *IEEE-Trans. Ultra. Ferro. Freq. Cont.*, 49(4), pp. 436-446, 2002.

* *indicates Presenter*

## Lakeway Inn Floor Plan

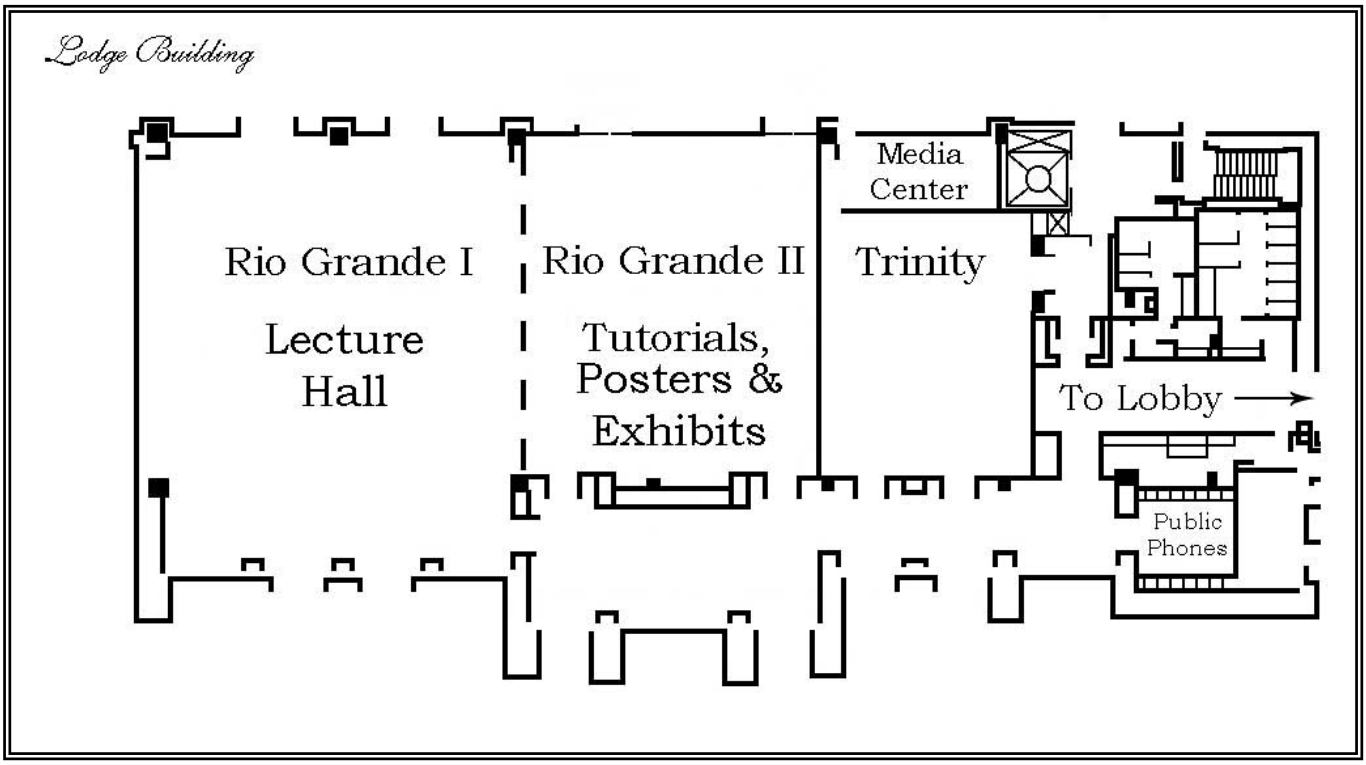

Please Fill Out Both Sides

# Conference Evaluation and Questionnaire

## OVERALL CONFERENCE:

| SCORING: | Very Poor | | Mid | | Excellent |
|---|---|---|---|---|---|
| Overall Conference Evaluation | 1 | 2 | 3 | 4 | 5 |
| Additional comments: | | | | | |
| | | | | | |
| | | | | | |

## SCIENTIFIC PROGRAM

| SCORING: | Very Poor | | Mid | | Excellent |
|---|---|---|---|---|---|
| Quality of the Presentations | 1 | 2 | 3 | 4 | 5 |
| Relevance of Presentations to the Conference's Theme | 1 | 2 | 3 | 4 | 5 |
| Time Allotted for Presentations | 1 | 2 | 3 | 4 | 5 |
| Time Allotted for Discussion | 1 | 2 | 3 | 4 | 5 |
| Poster Session | 1 | 2 | 3 | 4 | 5 |
| Dinner Guest Lecturer | 1 | 2 | 3 | 4 | 5 |
| Tutorials | 1 | 2 | 3 | 4 | 5 |
| Equipment Exhibit | 1 | 2 | 3 | 4 | 5 |
| Student Participation | 1 | 2 | 3 | 4 | 5 |
| Additional comments: | | | | | |
| | | | | | |
| | | | | | |

## CONFERENCE MATERIALS:

| SCORING: | Very Poor | | Mid | | Excellent |
|---|---|---|---|---|---|
| Printed Proceedings Book | 1 | 2 | 3 | 4 | 5 |
| CD Proceedings | 1 | 2 | 3 | 4 | 5 |
| Other Registration Materials | 1 | 2 | 3 | 4 | 5 |
| I would like future abstracts to be expanded up to 2 pages each | | | | Yes | No |
| I would like to submit my full ppt presentation to appear on the Conference website | | | | Yes | No |
| Additional comments: | | | | | |
| | | | | | |
| | | | | | |

## CONFERENCE FACILITIES

| SCORING: | Very Poor | | Mid | | Excellent |
|---|---|---|---|---|---|
| Lecture Hall | 1 | 2 | 3 | 4 | 5 |
| Registration Desk | 1 | 2 | 3 | 4 | 5 |
| Meals: Overall | 1 | 2 | 3 | 4 | 5 |
| Conference Breakfasts and Lunches | 1 | 2 | 3 | 4 | 5 |
| Conference Dinner | 1 | 2 | 3 | 4 | 5 |
| Coffee Breaks | | | | | |
| Opening Reception | 1 | 2 | 3 | 4 | 5 |
| Audio-Visual | 1 | 2 | 3 | 4 | 5 |
| Additional comments: | | | | | |
| | | | | | |

Please Fill Out Both Sides

# Conference Evaluation and Questionnaire

## VENUE AND HOTEL

| SCORING: | Very Poor | | Mid | | Excellent |
|---|---|---|---|---|---|
| Venue – Lake Travis, Austin and Environs | 1 | 2 | 3 | 4 | 5 |
| Would you return to this city? | Yes | | Perhaps | | No |
| Area Attractions | 1 | 2 | 3 | 4 | 5 |
| Hotel: Overall | 1 | 2 | 3 | 4 | 5 |
| Reservations | 1 | 2 | 3 | 4 | 5 |
| Transportation and Accessibility | 1 | 2 | 3 | 4 | 5 |
| Reception and Check – In | 1 | 2 | 3 | 4 | 5 |
| Accommodations | 1 | 2 | 3 | 4 | 5 |
| Facilities | | | | | |
| Parking | 1 | 2 | 3 | 4 | 5 |
| Would you return to this hotel? | Yes | | Perhaps | | No |
| Additional comments: | | | | | |
| | | | | | |
| | | | | | |

## CONFERENCE ADMINISTRATION

| SCORING: | Very Poor | | Mid | | Excellent |
|---|---|---|---|---|---|
| Website | 1 | 2 | 3 | 4 | 5 |
| Registration off-site | 1 | 2 | 3 | 4 | 5 |
| Registration on-site | 1 | 2 | 3 | 4 | 5 |
| Administrative staff | 1 | 2 | 3 | 4 | 5 |
| Correspondence | 1 | 2 | 3 | 4 | 5 |
| Additional comments: | | | | | |
| | | | | | |
| | | | | | |

## GENERAL INFORMATION

| | | | |
|---|---|---|---|
| I am a Returning Delegate | Yes | | No |
| I plan to attend the next conference | Yes | Perhaps | No |
| and present a paper(s) / poster(s) | Yes | Perhaps | No |
| Other(s) from my lab would attend the next conference | Yes | Perhaps | No |
| and he/she / they would present a paper(s) / poster(s) | Yes | Perhaps | No |
| How did you learn of this conference? (Check all that apply) | ☐ Email Announcement | | |
| ☐ Internet | ☐ Website | | |
| ☐ Other | ☐ Colleague | | |
| Tutorial Topic Suggestions for next year: | | | |
| | | | |
| Additional Comments, Improvements or Suggestions: | | | |
| | | | |
| | | | |
| | | | |

If you would be willing to host the Conference in your city, please give your name to the Conference Staff.

**Questions or comments are welcome at any time at <elasticity.conference@uth.tmc.edu>**